Napoleon Enteria
Hazim Awbi
Hiroshi Yoshino *Editors*

Desiccant Heating, Ventilating, and Air-Conditioning Systems

Springer

Desiccant Heating, Ventilating, and Air-Conditioning Systems

Napoleon Enteria · Hazim Awbi
Hiroshi Yoshino
Editors

Desiccant Heating, Ventilating, and Air-Conditioning Systems

Springer

Editors
Napoleon Enteria
Building Research Institute
Tsukuba, Ibaraki
Japan

Hiroshi Yoshino
Tohoku University
Sendai, Miyagi
Japan

Hazim Awbi
University of Reading
Reading, Berkshire
UK

ISBN 978-981-10-3046-8 ISBN 978-981-10-3047-5 (eBook)
DOI 10.1007/978-981-10-3047-5

Library of Congress Control Number: 2016957286

Printed on acid-free paper

This Springer imprint is published by Springer Nature
The registered company is Springer Nature Singapore Pte Ltd.
The registered company address is: 152 Beach Road, #22-06/08 Gateway East, Singapore 189721, Singapore

Preface

The global utilization of the various carbon-based energy resources is increasing as the population increases, urbanization increases, and standard of living improves. This increase of energy utilization is resulting in emission of greenhouse gases and in delicate global energy politics. The building sector is one of the primary consumers of energy sources to provide for the differing energy needs of buildings for their occupants.

The maintenance of a comfortable and healthy indoor environment is one of the main consumers of a building's energy. In a temperate climate, the maintenance of a comfortable indoor environment is very important, particularly during the cold winter season. In a subtemperate climate, the application during both winter and summer seasons is important for providing a thermally comfortable indoor environment. In hot and humid climates such as in the tropics, providing cool, low-humidity indoor air is very important.

A heating, ventilating, and air-conditioning (HVAC) system is needed to provide the required comfortable indoor thermal environment and air quality. This system controls the air temperature by cooling the air during the hot season and heating it during the cold season. The system reduces the air humidity content by cooling the air below the dew point. In addition, the introduction of filtered outdoor air provides for the required air quality and minimizes the buildup of indoor pollutants. The desiccant heating, ventilating, and air-conditioning (DHVAC) system is an alternative that can provide the needed comfortable indoor thermal environment and the required indoor air quality.

The progress of the DHVAC system recently has been rapid as shown in several scientific and engineering papers published annually. Installations in both demonstration and actual buildings in temperate and subtemperate climates and in hot and humid climates such as in tropical regions have been carried out using DHVAC. Experts from around the world were invited to contribute to this book covering fundamental aspects, recent research and development, and actual installation and applications. The editors are grateful for the support of well-known and very busy experts in the field for their contributions to the chapters of this book.

The editors are also thankful to Springer for publishing this book as one of the main contributions to the progress and advancement of DHVAC systems.

The book editors, the chapter contributors, and the publisher are hopeful that as a result of this volume, more fundamental research work, novel design, and practical engineering can be developed further by scientists, researchers, engineers, and graduate students for a more comfortable indoor thermal environment and higher quality indoor air in the most energy-efficient way. We believe this can be accomplished by the practical application of the DHVAC system along with the utilization of available alternative energy sources.

Tsukuba, Japan — Napoleon Enteria
Reading, UK — Hazim Awbi
Sendai, Japan — Hiroshi Yoshino

Contents

About the Editors

Napoleon Enteria is a research specialist of the Building Research Institute, Japan; a visiting researcher at Tohoku University, Japan; and a founder and managing consultant of the Enteria Grün Energietechnik, the Philippines. He was a scientist at the Solar Energy Research Institute of Singapore of the National University of Singapore and a global center of excellence researcher at the Wind Engineering Research Center of the Tokyo Polytechnic University, Japan. His research activities in renewable energy systems, HVAC systems, and building sciences produced several international scientific and engineering papers in books, review journals, research journals, and conference proceedings. He has submitted and presented dozens of technical reports for collaborative projects with research institutes, universities, and companies in several countries and is regularly invited as reviewer for international journals in the field of energy systems, air-handling systems, and building performances. On occasion, he receives invitations to review research funding applications and gives technical and scientific comments on international scientific and engineering activities. He is a Member of the American Society of Mechanical Engineers (ASME), the American Society of Heating, Refrigerating and Air-Conditioning Engineers (ASHRAE), and the International Solar Energy Society (ISES).

Hazim Awbi is a professor emeritus of the University of Reading, United Kingdom, where he was a professor of Building Environmental Science, director of the Technologies of Sustainable Built Environments Centre, and director of the Indoor Environment and Energy Research Group. His research interests are in room air-flow analysis and modeling, computational fluid dynamics, indoor air quality, air distribution systems, low-energy building environmental control systems, heat transfer, and energy storage. He is the author of *Ventilation of Buildings* (Taylor and Francis), editor of *Ventilation Systems—Design and Performance* (Taylor and Francis), editor of the *CIBSE Application Manual 11: Building Performance Modelling*, and coauthor of another four books. He has published more than 160 articles in journals and conference proceedings. Professor Awbi is the chairman of the Building Simulation Group of the Chartered Institution of Building Services Engineers, London.

Hiroshi Yoshino is a professor emeritus of Tohoku University, Japan, where he is currently a president-appointed extraordinary professor. He was the president of the Architectural Institute of Japan (AIJ) from 2013 to 2015. He has been involved in research subjects for building science such as indoor environment and energy conservation, ventilation and indoor air quality, occupants' health and indoor environment, and passive solar system performance. Professor Yoshino is one of the contributors to the reports of the Intergovernmental Panel on Climate Change (IPCC), which was awarded the Nobel Peace Prize in 2007. He is the operating agent at the International Energy Agency's Energy in Buildings and Communities Programme, responsible to the Annex 53 Total Energy Use in Buildings. He is a visiting professor at several universities and professional institutions of international repute and is the author of some 30 book chapters, with more than 200 publications including articles in academic journals and conference proceedings. He has also served as chairman and director of several scholarly societies, conferences, and committees, as well as an editorial board member of international journals. Professor Yoshino has received a number of awards, including those from the AIJ in the area of journal papers in 1992 and the Society of Heating, Air-Conditioning and Sanitary Engineers of Japan (SHASE) Best Papers in 1975, 1992, 1997, 2000, and 2005. He received the Japanese Uichi Inoue Memorial Award from SHASE in 2013, and he is an ASHRAE Fellow.

Chapter 1
Advancement of the Desiccant Heating, Ventilating, and Air-Conditioning (DHVAC) Systems

Napoleon Enteria, Hazim Awbi and Hiroshi Yoshino

Abstract The building sector is one of the largest end-users of primary energy sources. One of the main usages of its energy is for the maintenance of indoor environmental conditions—thermal comfort and air quality. In this regard, the selection, design and installation of the heating, ventilating and air-conditioning systems in buildings and houses are very important when considering the reduction of energy consumption and, at the same time, with the provision of the required comfortable indoor thermal environment and healthy indoor air. The desiccant heating, ventilating and air-conditioning system is one of the alternative heating, ventilating and air-conditioning (HVAC) systems for providing the required indoor thermal environment and air quality. The system can provide the required thermal comfort and air quality by means of controlling the air temperature, humidity, as well as indoor chemical and biological contents. This type of system can utilize diverse sources of energy, which is very important for the optimization of on-site and off-site available alternative energy sources. As the advancement of the desiccant heating, ventilating and air-conditioning system (DHVAC) becomes globally established by the progress in different research deliverables, designs, installations and evaluation methods, it is expected that the system will become one of the most important alternative systems for the maintenance of indoor thermal environment comfort and air quality when considering the reduced reliance on conventional energy usage.

Keywords Air-conditioning systems · Energy efficiency · Indoor environment · Thermal comfort · Air quality · Desiccant materials

N. Enteria (✉)
Building Research Institute, Tsukuba, Japan
e-mail: napoleon@kenken.go.jp; enteria@enteria-ge.com

H. Awbi
University of Reading, Reading, UK

H. Yoshino
Tohoku University, Sendai, Japan

N. Enteria et al. (eds.), *Desiccant Heating, Ventilating, and Air-Conditioning Systems*, DOI 10.1007/978-981-10-3047-5_1

1.1 Introduction

The building sector is one of the primary consumer of energy accounting for 50%, inclusive of commercial and industrial buildings [1]. The building sector energy use is to support electrical appliances, provide thermal comfort, lighting and more. As the global population grows, urbanization increases and as the standard of living rises, it is expected that the energy consumption of the building energy sector will increase [2–4]. A study by York [3] shows that the population size and age structure has an effect on energy consumption, and this will result in increased energy consumption in developing countries as the proportion of the younger population increases. A study by the International Energy Agency [2] predicts that the building sector electrical energy consumption will increase by 119% from 2002 to 2030. In 2006, the residential sector, including agriculture, consumed 56.7% of the electrical energy compared to 44.2% in 1973 [5].

A large part of the energy demand of buildings is used to support the indoor thermal comfort conditions and air quality. In commercial buildings alone, it is almost 50% but varies depending on the location and local climate. There are about 368 million air conditioners and heat pumps installed worldwide [6]. Most of these marketed air conditioners are 90% below 15 kW capacity [7]. As buildings consume a large amount of energy to provide indoor thermal comfort conditions and air quality, it is a challenge of how to reduce the electric energy consumption. In a temperate climate, the peak electric energy consumption occurs in the summertime, shifting the large consumption of building energy to cooling purposes.

The provision of a building's indoor thermal comfort conditions, either through heating or cooling, is done by heat pump systems known as the mechanical vapor compression system. The mechanical vapor compression system's main energy source is electrical energy from the grid line to operate the compressor. The vapor compression system plays a major role in a building's electric energy consumption. In the Middle East, more than 70% of a building's energy consumption is used to support the cooling requirements of buildings [8]. In Europe, 10% of the building sector's energy consumption is used to support the cooling demand [9]. In Hong Kong, 45% of the commercial building energy consumption is for cooling [10]. In Japan, 3% of the building sector energy consumption is for cooling applications [11]. It is expected that in tropical countries which are hot and humid, the demand for energy for cooling and dehumidification is very high [12]. In Singapore alone, more than 60% of an office building's energy consumption is for cooling and ventilation and it is above 30% for a residential house [13].

An alternative heating, ventilating and air-conditioning system which utilizes alternative materials, processes and energy resources can reduce a building's energy consumption [14, 15]. An alternative heating, ventilating and air-conditioning (HVAC) system can be operated with less conventional energy consumption through utilization of alternative energy sources [16]. Several alternative HVAC

systems are being suggested to provide for the cooling of the building [17, 18]. The thermally operated HVAC systems which rely on the direct application of thermal energy are important options for buildings [19]. Such HVAC systems can directly utilize solar energy [20]. The main advantage of these types of system is that its cooling load is in phase with the available solar radiation [21]. Hence, during the summer or during times of higher solar radiation, the amount of the cooling load will also be high and is proportional to the thermal energy that can be collected from the sun.

The thermally operated HVAC systems are achieved by means of applying heat energy for the production of the cooling effect during summer [22] and the direct application of heat energy during the winter by heat exchange with the air. As the main advantage of the thermally operated HVAC systems is the direct application of thermal energy for system operation, low-grade thermal energy can be used to operate the system. In addition, several thermal energy sources can be utilized for the system operation such as waste heat, biomass or others that may be available on-site [23].

1.2 Desiccant-Based HVAC Systems

1.2.1 Desiccant Materials

The sorption process is a surface phenomenon which occurs at the interface of two phases, in which cohesive forces including the Van der Waals forces and hydrogen bonding act between the molecules of all substances irrespective of their state of aggregation and which is called physisorption [24]. The absorption is a chemical process caused by the valence forces called chemisorption [25]. The process of attracting moisture from the air is either by adsorption or by absorption: the adsorption process is a physical process in which the property of the desiccant material or sorbent remains the same, while in the absorption process, upon attracting moisture, the physical characteristic of the desiccant or sorbent material changes. The desiccant or sorbent materials can be either solid or liquid: the solid desiccant and hydrophilic adsorbents are silica gel, activated alumina, zeolites, titanium dioxide and except for calcium chloride which is absorbent. The commercial hydrophobic solid adsorbents are activated carbons, metal oxides, specially developed porous metal hydrides and composite adsorbents [24].

Some desiccant materials are combinations of absorbent and adsorbent so as to enhance their physical properties and sorption capacity, and are called composites [26]. The basic mechanism in the sorption of moisture between the air and the desiccant material is the difference in the water vapor pressure on the surface of the desiccant and of the air. The uptake of moisture from the air to the desiccant is

when the vapor pressure in the air is high; the removal of vapor from the desiccant material is done when the vapor pressure in the air is lower than on the desiccant material. When the vapor pressure is the same both in the air and in the desiccant material, the equilibrium condition is reached and the sorption process is stopped. The only means for making the adsorption process proceed is by using outside forces such as increased air pressure, decreased temperature or by artificial electromotive force [25]. The same procedure is applied for the removal of moisture in the desiccant material which is done in the opposite way.

1.2.2 Sorption Processes

The desiccant heating, ventilating and air-conditioning (DHVAC) system relies on desiccant material in controlling the air moisture content for both air cooling and dehumidification, and for air heating and humidification. The desiccant material reduces the air moisture passing through and by application of evaporative cooling or by other means of air cooling, the supply air becomes cool and dry. On the other hand for purpose of humidifying and heating, the outdoor air becomes humidified and heated by means of solar energy or other thermal sources.

The main advantage of the DHVAC system is the separate handling sensible and latent loads of air. Hence, in the case of a latent load, the desiccant material can be handled through the application of thermal energy. In the case of the sensible load, heat recovery, direct evaporative cooling and other air cooling processes can be applied for summer cooling application. Therefore, for hot and humid air, whose latent load is high, the potential for reduction in the use of conventional energy is possible. In addition, during the winter season, the moisture from the indoor environment can be recovered by using desiccant material by passing the exhaust air over the desiccant material which is utilized to humidify the outdoor air to be supplied in the indoor environment. Heat exchangers utilizing different thermal energy sources can be used to heat up the supply air.

1.2.3 Different System Designs

1.2.3.1 Solid System

The solid-based DHVAC system is primarily based on the use of solid-based desiccant materials in controlling the air moisture content. The sorption mechanism in the solid material is either through absorption or adsorption. Cooling by means of heat recovery, evaporative cooling or other means are used in this type of system.

The design of the system is based on the rotating wheel [27] or fixed bed type as an alternative operation [28]. Application of the encapsulated phase change materials (EPCMs) in the desiccant bed has sometimes been applied. The purpose of this is to absorb the heat of sorption released during the dehumidification process. Based on the study by Rady et al. [29], this approach lowers the temperature of the air passing through it, but its humidity level is higher compared to the pure desiccant. In most cases, the processed air (dehumidified air) is pre-cooled through the rotating heat wheel or by means of heat exchangers that either utilize the cool return air or by using outside air. As the air in most cases is still warm for indoor application, the final cooling of the air is done by means of evaporative cooling and chill cooling.

1.2.3.2 Liquid System

The design of the liquid-based DHVAC system uses the falling film method in the membrane with air passing on its surface [30]. Some designs apply the spray approach to increase the surface area of air-desiccant contact. The design of the air dehumidifier for an isothermal process is based on passing cool air/water at the back of the falling desiccant film [31]. The regeneration of the desiccant material is by a heating process; hence, many designs of the liquid desiccant regenerators are made using solar energy. The cooling of air after the desiccant material is in the same way as in a solid desiccant cooling system. The widely used liquid desiccant materials are lithium chloride, lithium bromide, calcium chloride and glycol-based substances [17]. The application of these materials depends on the cost, operation, and the source of available thermal energy. In addition, some liquid desiccants are corrosive and require proper handling for their application. However, the main advantage of the liquid desiccant is the high moisture removal capacity with the lower regeneration temperature requirement.

1.2.3.3 Hybrid System

There are several designs of the hybrid DHVAC system. Liu et al. [32] presented a dedicated outdoor air system combined with a desiccant wheel. It showed that energy saving is possible as long as there is a source of solar energy and natural gas. The hybrid system is based on either solid or liquid desiccant materials used for the removal of the air moisture content in a vapor compression system used as an air cooler and desiccant regenerator. The main advantage of the hybrid system is the efficient handling of air latent energy and the sensible energy components. In this case, the vapor compression performance is increased since it handles only the air sensible energy part, while the desiccant material handles the air latent energy

part. Hence, with this system, the vapor compression energy consumption is reduced [33].

1.2.4 Applications and Installations

In hot and humid climates, the air temperature and humidity are high. In addition, as daylong dehumidification is needed compared to the other climatic conditions, the cheaper and more available nighttime electric energy (off-peak) can be stored for daytime operation of the system [34]. Enteria et al. [35] shows the applicability of nighttime electric energy storage for daytime utilization. Combining solar energy for air dehumidification with a ground water source for air cooling makes the system utilize natural energy sources such as that used in London [36]. In addition, the design is also applicable for the countries which require heating and humidified indoor air by capturing the moisture of the exhaust air and passing it to the supply air using desiccant material.

The vapor compression system removes the air moisture content by cooling the air below its dew point temperature; however, as the air after cooling it to its dew point temperate becomes very cold, it needs to be reheated before being introduced to the indoor environment. As some regions are very hot and humid all-year-round, the vapor compression system can operate continuously to reduce the outdoor air's very high moisture content. The coupling of the desiccant material with the vapor compression system minimizes the operating condition of the vapor compression system since the desiccant material handles the air latent energy content while the vapor compression system handles the air sensible load [33]. An application of the liquid desiccant HVAC system shows that it can have a performance of 44.5% when applied in a green building [37]. In addition, one of the advantages of the hybrid desiccant HVAC system is its operation in part loads due to the separate handling or air sensible and latent energies [38].

The development and application of the desiccant-based ventilation and air-conditioning system is expanding globally [13, 39]. However, in the hot and humid climate of South and Southeast Asia, South America and Africa, the system is still not fully utilized. Therefore, investigations of the applications of this system in these regions will expand the potential for widening the application of this system. It has been shown that this system has the potential for application in the ventilation and air-conditioning of buildings in hot and humid climates at a high level of energy efficiency [40–42]. The most significant part is the reduction in conventional energy use and lower greenhouse gas emissions for providing human thermal comfort and good air quality in buildings.

1.3 Conclusions

This chapter gives a general introduction of the topics in this book covering the fundamental aspects, design, development and applications of the DHVAC system. It describes the rapid progress in research and development in this area which is taking place in different countries. It also refers to studies that show that this system has a lot of potential for controlling the thermal, chemical and biological components in a building at the same time.

Considering published work, it was shown that most of the research and development and the applications of the system occur in temperate climates. However, more recently, research and installation have taken place in hot and humid climates too. Previously, the system was bulky in size which resulted in difficulties with direct installation in compact spaces such as in small or detached houses. Now, the system is becoming compact and small as demonstrated by the new products. In the old days, the operation of such system was quite complicated which resulted in difficulty in its use by untrained building occupants; however, due to the application of electro-mechanical systems, the operation is now more automated. With the development of desiccant material with higher sorption capability combined with new designs and control mechanisms, it is expected that this system will become more widely used in different commercial buildings and dwellings. The succeeding chapters will show more of the different progress in the desiccant heating, ventilating and air-conditioning systems by different experts around the world who have been working and contributing in this field for some time.

References

1. Zimmermann M, Althaus HJ, Hass A (2005) Benchmarks for sustainable construction a contribution to develop a standard. Energy Buildings 37:1147–1157
2. World Energy Outlook (2004) International Energy Agency. France, Paris
3. York R (2007) Demographic trends and energy consumption in European Union Nations, 1960–2025. Soc Sci Res 36:855–872
4. Solecki WD, Leichenko RM (2006) Urbanization and the metropolitan environment: lessons from New York and Shanghai. Environment 48:8–23
5. Key World Energy Statistics (2008) International Energy Agency. France, Paris
6. Safeguarding the ozone layer and the global climate system: issues related to hydroflouorocarbons and perfluorocarbons. Intergovernmental Panel on Climate Change. https://www.ipcc.ch/report/sroc/. Accessed 26 June 2014
7. Safeguarding the ozone layer and global climate system—Issues related to hydrofluorocarbons and perfluorocarbons. International Panel on Climate Change; ISBN 92-9169-118-6. https://www.ipcc.ch/pdf/special-reports/sroc/sroc_spmts_en.pdf. Accessed 8 Oct 2012
8. El-Dessouky H, Ettouney H, Al-Zeefari A (2004) Performance analysis of two-stage evaporative coolers. Chem Eng J 102:255–266
9. Kolokotroni M, Aronis A (1999) Cooling-energy reduction in air-conditioned offices by using night ventilation. Appl Energy 63:241–253

10. Zain ZM, Taib MN, Baki SMS (2007) Hot and humid climate: prospect for thermal comfort in residential building. Desalination 209:261–268
11. Murakami S, Levine MD, Yoshino H et al (2009) Overview of energy consumption and GHG mitigation technologies in the building sector of Japan. Energy Effic 2:179–194
12. Wong N, Li S (2007) A study of the effectiveness of passive climate control in naturally ventilated residential buildings in Singapore. Build Environ 42:1395–1405
13. Enteria N, Yoshino H, Mochida A (2013) Review of the advances in open-cycle absorption air-conditioning system. Renew Sust Energy Rev 28:265–289
14. Residential and commercial buildings (2007) Climate change mitigation. Intergovernmental panel on climate change. Cambridge University Press, New York
15. IPCC Scoping meeting on renewable energy resources (2008) In: Proceedings, Lubeck, Germany, 20–25 Jan 2008
16. Yu BF, Hu ZB, Liu M et al (2009) Review of research on air-conditioning systems and indoor air quality control for human health. Int J Refrig 32:3–20
17. Grossman G, Johannsen A (1981) Solar cooling and air conditioning. Prog Energy Combust 7:185–228
18. Kim DS, Infante Ferreira CA (2008) Solar refrigeration options—a state—of-the-art review. Int J Refrig 31:3–15
19. Afonso CFA (2006) Recent advances in building air conditioning systems. Appl Therm Eng 26:1961–1971
20. Farber EA (1973) Solar energy, its conversion and utilization. Sol Energy 14:143–252
21. Tabor H (1962) Use of solar energy for cooling purposes. Sol Energy 6:136–142
22. Grossman G (2002) Solar-powered systems for cooling, dehumidification and air-conditioning. Sol Energy 72:53–62
23. Henning HM, Pagano T, Mola S et al (2007) Micro tri-generation system for indoor air conditioning in the Mediterranean climate. Appl Therm Eng 27:2188–2194
24. Srivastava NC, Eames IW (1998) A review of adsorbents and adsorbates in solid-vapour adsorption heat pump systems. Appl Therm Eng 18:707–714
25. Low M (1960) Kinetics of chemisorption of gases on solids. Chem Rev 60:267–312
26. Tokarev M, Gordeeva L, Romannikov V et al (2002) New composite sorbent $CaCl_2$ in mesopores for sorption cooling/heating. Int J Therm Sci 41:470–474
27. Enteria N, Yoshino H, Satake A et al (2010) Experimental heat and mass transfer of the separated and coupled rotating desiccant wheel and heat wheel. Exp Therm Fluid Sci 34:603–615
28. Bongs C, Morgenstern A, Lukito Y et al (2013) Advanced performance of an open desiccant cycle with internal evaporative cooler. Sol Energy 104:103–114
29. Rady MA, Huzayyin AS, Arquis E et al (2009) Study of heat and mass transfer in a dehumidifying desiccant bed with micro-encapsulated phase change materials. Renew Energy 34:718–726
30. Ren CQ, Tu M, Wang HH (2007) An analytical model for heat and mass transfer processes in internally cooled or heated liquid desiccant-air contact units. Int J Heat Mass Trans 50:3545–3555
31. Yin Y, Zhang X, Wang G et al (2008) Experimental study on a new internally cooled/heated dehumidifier/regenerator of liquid desiccant system. Int J Refrig 31:857–866
32. Liu W, Lian Z, Radermacher R et al (2007) Energy consumption analysis on a dedicated outdoor air system with rotary desiccant wheel. Energy 32:1749–1760
33. Enteria N, Mizutani K, Monma Y et al (2011) Experimental evaluation of the new solid desiccant heat pump system in Asia-Pacific climatic conditions. Appl Therm Eng 31:243–257
34. Hammou Z, Lacroix M (2006) A new PCM storage system for managing simultaneous solar and electric energy. Energy Buildings 38:258–265
35. Enteria N, Yoshino H, Satake A et al (2011) Initial operation and performance evaluation of the developed solar thermal and electric desiccant cooling system. Exp Heat Transfer 24:59–87

36. Ampofo F, Maidment G, Missenden J (2006) Review of groundwater cooling systems in London. Appl Therm Eng 26:2055–2062
37. Ma Q, Wang RZ, Dai YJ et al (2006) Performance analysis on a hybrid air-conditioning system of a green building. Energy Buildings 38:447–453
38. Jia CX, Dai YJ, Wu JY et al (2006) Analysis on a hybrid desiccant air-conditioning system. Appl Therm Eng 26:2393–2400
39. Mujahid Rafique M, Gandhidasan P, Rehman S et al (2015) A review on desiccant based evaporative cooling systems. Renew Sust Energy Rev 45:145–159
40. Sekhar SC (2007) A review of ventilation and air-conditioning technologies for energy-efficient healthy buildings in the tropics. ASHRAE Trans 113:426–434
41. Enteria N, Awbi H, Yoshino H (2015) Application of renewable energy sources and new building technologies for the Philippine single family detached house. Int J Energy Environ Eng 6:267–294
42. Enteria N, Yoshino H, Mochida A et al (2012) Performance of solar-desiccant cooling system with silica-gel and titanium dioxide desiccant wheel applied in East Asian climates. Sol Energy 86:1261–1279

Chapter 2
Modeling and Analysis of Desiccant Wheel

Jae Dong Chung

Abstract Desiccant cooling systems have advantages in environmentally friendly operation and separate control of sensible and latent cooling loads, which leads to comfortable indoor air quality. In addition, the desiccant cooling system is a heat-driven cycle and therefore has the ability to use low-grade energy. However, the wide spread use of this technology is not yet possible due to its relatively large size and low system performance. The wheel is the most crucial component of the desiccant cooling system. Therefore, mathematical modeling of the desiccant wheel plays an important role in enhancing the overall system performance. Heat and mass transfer are coupled, and multiple parameters are involved in understanding the complicated phenomena in desiccant wheels. Mathematical models are commonly accepted as an effective method for analyzing the performance of rotary wheels and systems. The models can also be used to guide system operation, interpret experimental results and assist in system design and optimization. Several mathematical models have been constructed and employed to analyze, develop and design desiccant wheels. In this work, a brief review on the mathematical modeling of the desiccant wheel is examined, and some typical issues and results of case studies are discussed.

Keywords Desiccant wheel · Numerical analysis · Parametric study · Optimization · Isotherm

Nomenclature

a	Channel height (m)
A	Area (m^2)
b	Channel width (m)
BP	Rate of outdoor influx

J.D. Chung (✉)
Mechanical Engineering, Sejong University, Seoul 05006, Korea
e-mail: jdchung@sejong.ac.kr

N. Enteria et al. (eds.), *Desiccant Heating, Ventilating, and Air-Conditioning Systems*, DOI 10.1007/978-981-10-3047-5_2

c	Channel wall thickness (m)
c_p	Specific heat of dry air water (J kg^{-1} K^{-1})
COP	Coefficient of performance
D_G	Effective gas phase diffusivity (m^2 s^{-1})
D_h	Hydraulic diameter (m)
D_K	Knudsen diffusivity (m^2 s^{-1})
D_S	Surface diffusivity (m^2 s^{-1})
D_{so}	Pre-exponent constant of surface diffusivity, m^2 s^{-1}
E_a	Activation energy of diffusion, J mol^{-1}
f	Mass fraction of desiccant in the wheel
f_m	Mass fraction of desiccant in the wheel
F_0	Ratio of mean squares of factor i to error
H	Enthalpy (J kg^{-1})
H_{sor}	Heat of adsorption (J kg^{-1})
h	Convective heat transfer coefficient (W m^{-2} K^{-1})
h_m	Mass transfer coefficient (kg m^{-2} s^{-1})
K_y	Gas-side mass transfer coefficient (kg m^2 s)
k	Thermal conductivity (W m^{-1} K^{-1})
L	Channel length (m)
Le	Lewis number
N	Number of experiment
$\dot{m}$	Mass flow rate (kg h^{-1})
MRC	Moisture removal capacity (kg h^{-1})
Nu	Nusselt number, hD_h/k_a
P	Perimeter of flow channel (m)
P, P_s	Pressure, saturated pressure (Pa)
Q	Cooling capacity per unit air flow rate (J kg^{-1})
q^*	Equilibrium water uptake, kg kg^{-1}
r	Radial coordinate
R_u	Universal gas constant, J K^{-1} mol^{-1}
R_v	Gas constant of vapor, JK^{-1} kg^{-1}
R	Separate factor
ST	Sum of square of experiment
t	Time (s)
T	Temperature (°C)
u	Velocity (m s^{-1})
V	Mean square
W	Water content of the desiccant material (kg kg^{-1})
W_{max}	Maximum humidity ration of dry air (kg kg^{-1})
Y	Humidity ratio (kg kg^{-1})
z	Axial coordinate (m)

Greek letters

α	Significance level
α^*	Dimensionless channel area ration, a/b
ε	Performance
ε_d	Wheel effectiveness
φ	Humidity ratio or degree of freedom
γ	Isothermal curve gradient of a linear model
θ	Angular coordinate
ρ	Density (kg m^{-3})
τ	Tortuosity

Subscripts

1, 2, 3	Levels
a	Air
ad	Air in desiccant pore
d	Desiccant
e	Error
h	Hot
H	Constant heat flux
in	Inlet
l	Liquid
out	Outlet
p	Process
r	Regeneration
REC	Regenerative evaporative cooler
SHE	Sensible heat exchanger
T	Constant temperature
v	Vapor
w	Desiccant

2.1 Introduction

The design of heating, ventilating and air-conditioning (HVAC) systems for thermal comfort requires increasing attention, particularly to matters arising from recent regulations and standards for ventilation [1]. Optimum levels of indoor humidity should be desired to be reached and maintained to ensure a comfortable and healthy environment. Desiccant cooling systems have advantages in environmentally friendly operation and separate control of sensible and latent cooling loads, which leads to comfortable indoor air quality. In addition, the desiccant cooling system is

a heat-driven cycle and therefore has the ability to use low-grade energy such as natural gas, waste heat and solar energy.

Desiccant cooling can be used either in a standalone system or a hybrid system coupled with a vapor compression refrigeration-based air-conditioning system or free energy such as solar or industrial waste heat [2]. In hybrid systems, more efficient cooling occurs over a wide range of operating conditions when a vapor compression refrigeration-based air-conditioning system is combined with a desiccant cooling system. This is because in a hybrid system, first the desiccant dehumidifier efficiently removes the moisture from the fresh ventilated air before it enters the conditioned space, and then, the vapor compression system removes only sensible heat from the conditioned space. This type of arrangement removes the requirement of a low dew point temperature of the evaporator cooling coil and subsequently reheating.

Numerous studies have assessed the feasibility of desiccant cooling systems using simulations and experimental methodologies to make them energy-efficient and cost-effective. The reported studies are related to feasibility studies [3–5] performance predictions [6, 7], wheel optimization [8–14] and development of new materials [15–18]

The wide spread use of this technology is not yet possible due to its relatively large size and low system performance. Mittal and Khan [19] evaluated the performance and energy-saving capacity of a desiccant cooling system composed of silica gel bed. Compared to conventional air conditioners where indoor air is completely recycled, the electricity saving is approximately 19%. Advanced desiccant materials and novel system configurations have significant potential to improve performance and reliability. Therefore, improving performance can play a key role in economic feasibility. Further improvements in the energy utilization rate, reductions in cost and size, competitive design and production are the key issues faced by solid desiccant cooling techniques for obtaining more extensive acceptability in the field of space cooling.

The wheel, where an air-to-air heat and mass transfer takes place at a low rotation speed, is the most crucial component of the desiccant cooling system. Therefore, mathematical modeling of the desiccant wheel plays an important role in enhancing the overall system performance. The optimum wheel speed and thickness, and the operating parameters such as the air flow rate, the relative humidity of the inlet air and the regeneration air temperature on the wheel performance have all been examined [11–13, 20–23]. The relationship between the regeneration temperature and the area ratio of the process and regeneration parts has been examined [12]. Most of the studies have investigated balanced flow, i.e., the wheel is split equally between the process and regeneration air flows. It is commonly accepted that as the regeneration temperature decreases, the regeneration section becomes a larger portion of the wheel. According to the manufacturer's catalog, a 1:3 split is generally used at high regeneration temperatures and a 1:1 split is used for low regeneration temperatures. However, it is doubtful that each area ratio effectively covers such a broad temperature range.

The adsorbent properties are also closely linked to enhanced performance. The development of advanced desiccant materials is focused on improving the sorption capacity, the moisture and heat diffusion rates, and the equilibrium isotherms [24]. In addition to the sorption capacity and favorable isotherms, a system performance of these new adsorbents need to be evaluated [17, 18].

From the viewpoint of system performance, the contribution and optimum condition of each component in the desiccant system, such as the regenerative evaporative cooler (REC) and sensible heat exchanger, need to be examined in detail. In addition to the contribution of each system component, the contributions of operating conditions such as outdoor conditions, regenerative temperature and rate of outdoor influx also need to be examined.

Researchers have also developed different cycles to achieve high system performance [9, 13, 25–27]. For each configuration, the evaluation of the contribution of each system component is required to find the optimal configuration.

Heat and mass transfer are coupled, and multiple parameters are involved in understanding the complicated phenomena in desiccant wheels. Mathematical models are commonly accepted as an effective method for analyzing the performance of the rotary wheels and systems. The models can also be used to guide system operation, interpret experimental results and assist in system design and optimization. In this work, a brief review on the mathematical modeling of the desiccant wheel is examined, and some typical issues and results of case studies are discussed.

2.2 Modeling

2.2.1 System Description

Jani et al. [2] made a comparison of various desiccant cooling cycles for air-conditioning and examined the influence of variations in outdoor conditions on the effectiveness of the system. Figure 2.1 shows a typical desiccant cooling system compared with a conventional air-conditioning system using vapor compression refrigeration. In the conventional system, air must be dehumidified by cooling it below its dew point to meet the latent load (② → ⓒ), and reheating is often required (ⓒ → ⑤) to satisfy the sensible heat factor (SHF). This implies very poor energy efficiency, particularly for low SHF, i.e., high latent cooling load. Additionally, a very low temperature can create a cold draft in the air-conditioned space.

In a solid desiccant cooling system, the moisture in the ventilated/recirculated process air is first removed using a rotating desiccant wheel. The temperature of this dried process air is then further lowered to the desired room conditions using of sensible heat exchangers and evaporative cooler. To make the system work continually, the amount of water vapor adsorbed by the rotating desiccant wheel must

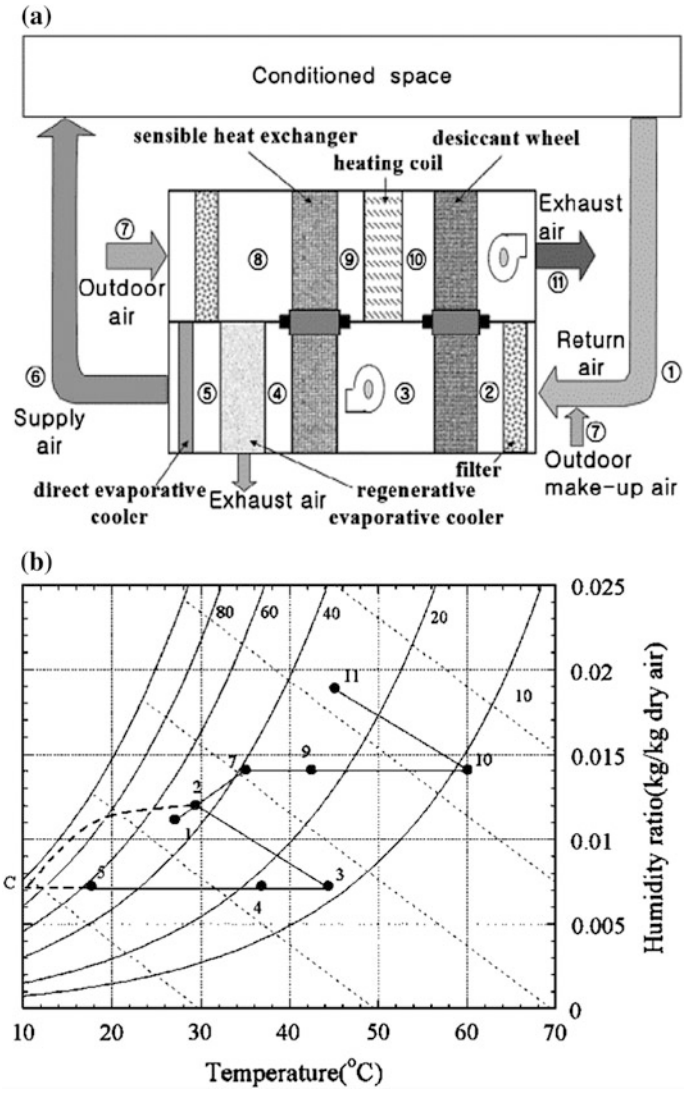

Fig. 2.1 **a** Schematic of a desiccant cooling system and **b** corresponding psychrometric processes compared with a conventional air-conditioning system using vapor compression refrigeration [13]

be removed from the desiccant material so that it can be sufficiently dried, i.e., regenerated to adsorb the water vapor in the next cycle. This is achieved using a rotating cylindrical wheel divided into two sections: the adsorption section and the regeneration section. The desiccant material is heated to regeneration temperature, which is dependent upon the material, i.e., the desiccant used. The energy required for regeneration of the rotary desiccant wheel is supplied through the regeneration heat source, which is either an electrical heater or solar/waste heat.

It is more helpful to understand the physics by expressing the process in the psychrometric chart. The heated and dehumidified supply air exits from the humidification section of the wheel (② → ③). The processed air operates close to an enthalpic process; therefore, the outlet temperature of the processed air will be very high, which reduces the sorption capacity of the desiccant. A sensible heat exchanger (③ → ④) and an evaporative cooler (④ → ⑤) are required to cool the dried processed air before it is introduced into occupied spaces. The sensible heat exchanger acts as a pre-cooler after the desiccant and also as a preheater before the regeneration section, which results in enhanced performance of the whole system.

Regeneration occurs on the other side of the partition where the heated air enters, usually from the opposite direction, and then passes over the desiccant and finally exhausts from the dehumidifier (⑩ → ⑪). The ideal outlets of process and regeneration are the points of intersection between lines of constant relative humidity and enthalpy passing through the inlets of process (②) and regeneration (⑩), respectively.

2.2.2 Mathematical Modeling

The advantages of mathematical models are that it takes less time and cost than experimental methods to predict the performance of a desiccant wheel. Therefore, mathematical models are very convenient to perform parametric research and optimization analysis. In addition, they can predict fundamental physics and surface chemistry of rotary desiccant wheels. Consequently, constructing valid mathematical models for desiccant wheels has become a key subject of many studies.

Mathematical modeling of desiccant wheels is a difficult task because the heat and mass transfer are coupled and too complicated to completely understand. Several mathematical models have been constructed and employed to analyze, develop and design desiccant wheels. Ge et al. [28] reviewed the literature on mathematical models and classified the models according to the modeling types of the heat and mass transfer between the humid air in the air channel and the desiccant wall. The models can be classified into two main categories: (1) gas-side resistance (GSR) model and (2) gas and solid-side resistance (GSSR) model. In the GSR model, heat and mass transfer within the solid desiccant are not taken into account. The governing equations have relatively simple forms with lower accuracy. The GSSR model can be further subdivided into the pseudo-gas-side (PGS) model, the gas and solid-side (GSS) model and the parabolic concentration profile (PCP) model.

GSSR models are higher in precision and more complex compared with GSR models. However, the PGS model requires extensive experimental data to determine the lumped transfer coefficients with different desiccant materials, and its reliability is not good enough. The GSS model also suffers from greater computational effort than the PGS model because of the additional second-order heat and

mass transfer diffusional items. The PCP model also has limitations including the assumption that a parabolic concentration profile for moist concentration exists at all the times in the desiccant particle.

The two-dimensional GSS model was expressed by Charoensupaya and Worek [29].

Conservation of moisture in the process air is expressed as:

$$\frac{\dot{m}_a}{X_m}\left(\frac{1}{u}\frac{\partial Y_a}{\partial t}+\frac{\partial Y_a}{\partial z}\right)=2K_y(Y_d-Y_a) \tag{2.1}$$

Conservation of moisture in the desiccant felt is denoted as:

$$\varepsilon_t\rho_{ad}\frac{\partial Y_d}{\partial t}+(1-\varepsilon_t)\rho_d\frac{\partial W}{\partial t}-D_G\rho_{ad}\frac{\partial^2 Y_d}{\partial r^2}-D_S\rho_d\frac{\partial^2 W}{\partial r^2}=0 \tag{2.2}$$

where D_G and D_S represent the effective gas phase diffusivity and surface diffusivity, respectively.

Conservation of energy within the desiccant felt is represented with the following equation:

$$\varepsilon_t\rho_{ad}\frac{\partial H_{ad}}{\partial t}+(1-\varepsilon_t)\rho_d c_{pd}\frac{\partial T_d}{\partial t}-k_d\frac{\partial^2 T_d}{\partial r^2}=(1-\varepsilon_t)\rho_d H_{sor}\frac{\partial W}{\partial t} \tag{2.3}$$

where the subscript ad represents the air in the desiccant pore.

The rate of energy transfer between the process air and desiccant felt can be expressed as:

$$\frac{\partial H_g}{\partial t}+u\frac{\partial H_g}{\partial z}=\frac{2K_y}{\rho_a\alpha_a}(Y_d(t,x,\alpha_d)-Y_a)\frac{\partial H_g}{\partial Y_a}+\frac{2h}{\rho_a\alpha_a}(T_d(t,x,\alpha_d)-T_a) \tag{2.4}$$

To save computation time, it is desired to take into account the smallest dimension as possible in the model. Because the variation in moisture and temperature is more significant in the axial direction, it is often chosen as main direction for heat and mass transfer when constructing the governing equations. Sphaier and Worek [30] compared one-dimensional and two-dimensional mathematical models for both the solid-side and gas-side resistance and found that the one-dimensional formulation could be used in desiccant wheel applications, whereas a two-dimensional model was needed for an enthalpy wheel when thermal resistance in the desiccant material was high.

Mass transfer kinetics of adsorbent particles from the inter-particle or intra-particle viewpoint is an interesting issue in adsorption physics. The inter-particle mass transfer models include isobaric and non-isobaric models. The isobaric models are over-simplified to completely ignore the inter-particle resistance. Ahn et al. [31] reported that isobaric models are only valid in certain restricted ranges.

Intra-particle mass transfer models include equilibrium, linear driving force (LDF) and solid diffusion models. Solid diffusion models reflect the physical essence of mass transfer in the intra-particle resistance. However, they are complex and difficult to solve; therefore, their application is limited. Therefore, in many cases, simplified models, such as the LDF model or the equilibrium model, are used. The LDF model assumes the uptake profile within the particle as a parabolic function, and the equilibrium model assumes the uptake as a constant. However, there are few discussions on the application range of these simplified intra-particle models even for the equilibrium model, which is obviously incorrect considering that the required equilibrium time is approximately 300 min, which is much longer than a typical cycle time. Hong et al. [32] discussed the validity of the simplified intra-particle models of equilibrium and LDF by comparing them to the solid diffusion model.

Figure 2.2 shows the behavior of the coefficient of performance (COP) according to the non-dimensional diffusion ratio, $t_{\mathrm{cycle}} D/r_{\mathrm{p}}^2$ for each different intra-particle diffusion model. For the entire range of non-dimensional diffusion ratios, the equilibrium model overestimates the performance of the adsorption bed and plays a role in the upper limit of performance. In contrast, the LDF model, which is the most commonly used model to analyze the intra-particle mass transfer kinetics, underestimates the performance of the adsorption bed. The differences between the models become smaller as the non-dimensional diffusion ratio increases. Therefore, the equilibrium model and the LDF model can be used if the non-dimensional diffusion ratio is over a critical value, for example 0.312 for the equilibrium model and 0.228 for the LDF model, with less than 5% relative error from the solid diffusion model. Some other cases of the RD-type silica gel that is frequently used in previous studies [33–35] are provided with their respective non-dimensional diffusion ratios in Fig. 2.2. Note how much the equilibrium and the LDF models distort the performance of the adsorption refrigerator system. The

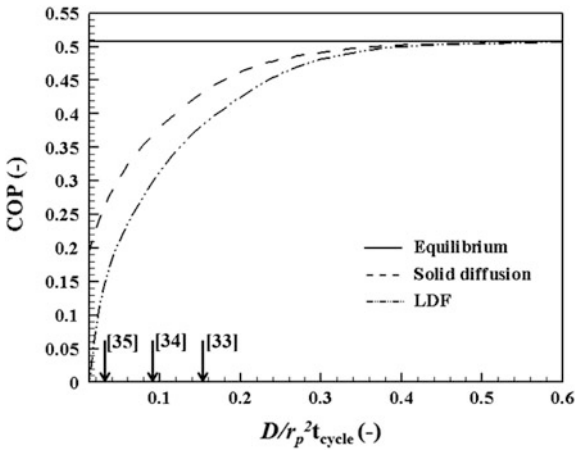

Fig. 2.2 Comparison of the COP of the three different models according to the non-dimensional diffusion ratio [32]

three cases of the typical RD-type silica gel used in the earlier studies [33–35] are overestimated for the equilibrium model by 94.2, 35.0 and 17.7%, respectively, and the earlier studies are underestimated for the LDF model by 45.0, 20.9 and 11.4%, respectively. Therefore, the intra-particle diffusion model should be carefully implemented to avoid seriously distorted results that may occur without serious consideration of the non-dimensional diffusion ratio of the adsorbent.

2.2.3 Chanel Geometrics

Desiccant wheels consist of a frame with a thin layer of desiccant material. The channels of the desiccant wheel frame are fabricated in various structures such as honeycomb, triangular, sinusoidal [36]. Studies have been conducted, mostly on one-dimensional analysis of channel section [37, 38]. However, there has been scanty research interest on channel shape or channel section area. Al-Sharqawi and Lior [39] and Chung et al. [40] introduced a comparative numerical solution of a heat and mass transfer problem in ducts with different cross-sectional geometries such as circular, square and triangular.

Figure 2.3 illustrates the typical channel shapes. Previous studies have identified the hydraulic diameter and Nusselt number for each channel shape. For example, the hydraulic diameter and Nusselt number for a sine-shaped channel (Fig. 2.3) are shown in Eqs. (2.5)–(2.8). The Lewis number for the mass transfer was set at 1 in all cases.

$$D_h/b = (1.0542 - 0.4670\alpha^* - 0.1180\alpha^{*2} + 0.1794\alpha^{*3} - 0.043\alpha^{*4}) \cdot \alpha^* \quad (2.5)$$

$$\mathrm{Nu_T} = 1.1791 \times (1 + 2.7701\alpha^* - 3.1901\alpha^{*2} - 1.9975\alpha^{*3} - 0.4966\alpha^{*4}) \quad (2.6)$$

$$\mathrm{Nu_H} = 1.903 \times (1 + 0.4556\alpha^* + 1.2111\alpha^{*2} - 1.6805\alpha^{*3} + 0.7724\alpha^{*4} - 0.1228\alpha^{*5}) \quad (2.7)$$

$$\mathrm{Nu} = (\mathrm{Nu_T} + \mathrm{Nu_H})/2 \quad (2.8)$$

where $\alpha^* = a/b$, and a, b are the channel height and width, respectively.

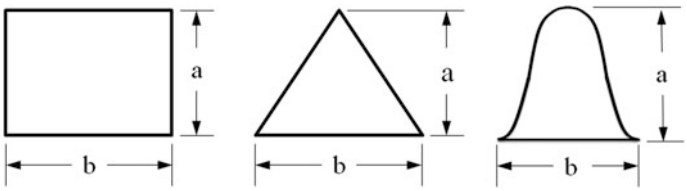

Fig. 2.3 Channel shapes considered in this study

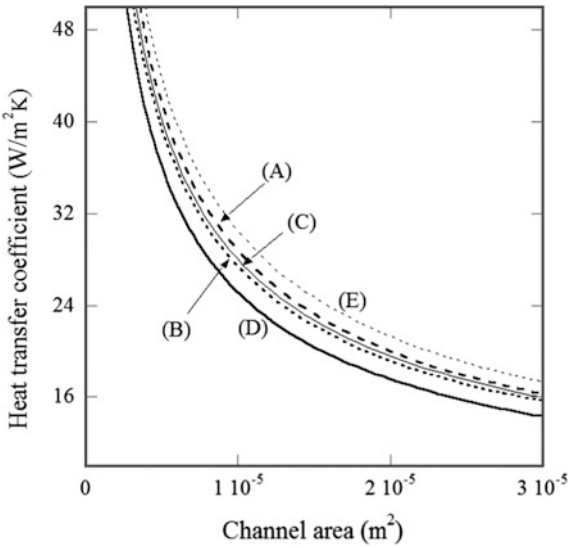

Fig. 2.4 Variation in the heat transfer coefficient according to the channel shape and size [40]

Figure 2.4 shows changes in heat transfer according to the channel shape and section area. (A) indicates a rectangular channel, (B) a triangular channel, (C) a sine-shaped channel (a:b = 1:1), (D) a sine-shaped channel (a:b = 1:2), and (E) a sine-shaped channel (a:b = 2:1). The amount of heat transfer was compared for the desiccant wheel with same channel section area but different channel shape. A triangular channel and a sine-shaped channel have a similar hydraulic diameter and Nusselt number. Conversely, a rectangular channel has a greater hydraulic diameter and Nusselt number and as a result has a larger heat/mass transfer for the same section area. Therefore, a rectangular channel may be more efficient than a triangular or sine-shaped channel. However, the performance of a desiccant wheel cannot be solely judged by the Nusselt number. As Fig. 2.5 shows, the circumference of the unit channel area and the unit desiccant area can also influence the performance of a desiccant wheel. A greater unit-area circumference results in more efficient heat/mass transfer, which explains why a triangular or sine-shaped channel is more efficient than a rectangular channel. [39], who did not included a sine-shaped channel in their study, have also showed that triangular ducts provide higher convective heat and mass transfer and absorb 11 and 42% more water than square and circular ducts, respectively. Gao et al. [37] discussed the effect of the felt thickness and the passage shape on the performance of a desiccant wheel and found that as the thickness of the sorbent increases, the moisture removal capacity (MRC) of the desiccant wheel improves, and a sinusoidal air flow passage was the best shape for greater MRC.

For the same sine-shaped channel, the amount of heat transfer may vary greatly according to the aspect ratio. In the case of (E), the amount of heat transfer was greatest at an aspect ratio of a:b = 2:1.

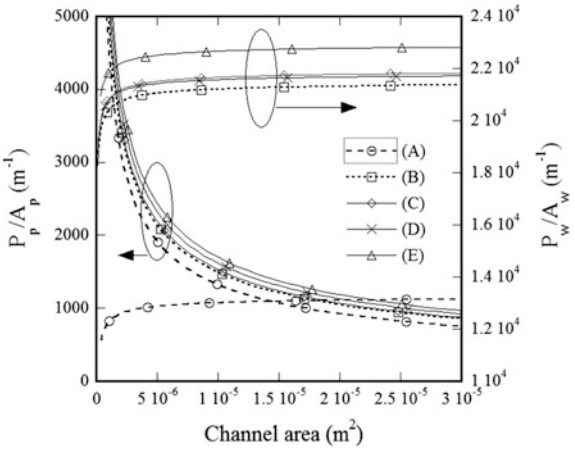

Fig. 2.5 Circumference of the unit channel area and unit desiccant area [40]

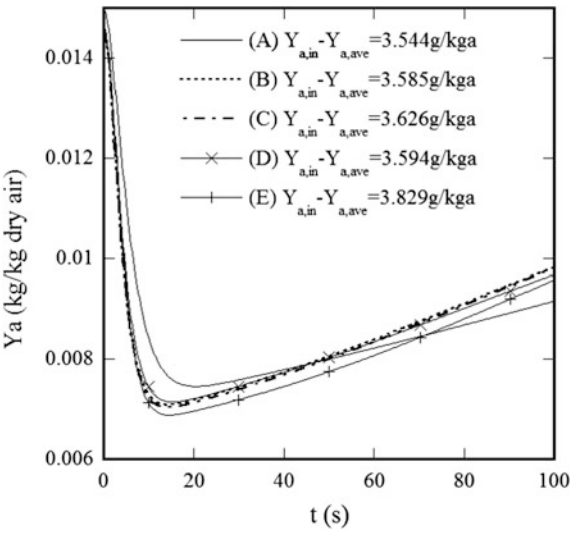

Fig. 2.6 Effect of channel shape on the performance of the desiccant wheel [40]

Figure 2.6 shows the influence of the channel shape corresponding to Fig. 2.4 for the same channel section area. It presents average humidity (Y_a) at the outlet of the dehumidification section according to time. The index of performance, which is the amount of dehumidification or the difference between the humidity at the inlet and the average humidity at the outlet of the dehumidification section ($Y_{a,in} - Y_{a.ave}$), is also included.

To compare the influence of each factor, two additional sets of data were examined and compared to the standard condition: air flow rate, $u_a = 2.0$ m/s; channel section area $= 1 \times 10^{-5}$ m^2; channel wall thickness, $c = 0.15 \times 10^{-3}$ m; channel length, $L = 0.3$ m; mass fraction of the desiccant, $f_m = 0.7$; desiccant

separate factor, $R = 0.1$; maximum water uptake capacity, $W_{max} = 0.4$; dehumidification time, $t_p = 100$ s; and the area ratio of regeneration to the dehumidification section, $t_r/t_p = 0.8$. The silica gel properties were used for ρ, c_p.

A sine-shaped channel with an aspect ratio $a{:}b = 2{:}1$ showed the best excellent dehumidification performance and had the highest heat transfer (Fig. 2.4) and greatest circumference (Fig. 2.5). The most widely used sine-shaped channel with an aspect ratio $a{:}b = 1{:}1$ did not show particularly superb performance compared to the other channel shapes. Specific data are not presented here, but the same trend was observed for different regeneration times (or rotating speed; 50 and 150 s) and an area ratio of 0.9 between the regeneration and the dehumidification section.

The channel section area was set at 0.59×10^{-5} m^2, 1×10^{-5} m^2 and 1.69×10^{-5} m^2 for a widely used sine-shaped channel (dotted line) and a sine-shaped channel with an aspect ratio $a{:}b = 2{:}1$ (solid line), respectively, to measure the humidity distribution and amount of dehumidification at a desiccant wheel outlet (Fig. 2.7). Regardless of the channel shape, both had better performance with a smaller channel section area. For the latter, the amount of dehumidification increased 13.2% when the section area diminished by 1.3^2 times compared to the standard condition (1×10^{-5} m^2). The improvement was much greater than the sine-shaped channel with an aspect ratio $a{:}b = 1{:}1$, which had only a 5.3% increase. The consequent pressure decline does not have a significant impact on the overall cooling system. To improve the performance of a desiccant wheel, it is important to diminish the channel section area.

Variations in wheel size were examined for the mass fraction ($f_m = 0.7/1.3$, 0.7, 0.7×1.3, 0.7×1.5), specific heat ($c_p/1.5$, $c_p/1.3$, c_p, $1.3c_p$), density ($\rho/1.3$, ρ, 1.3ρ, 1.5ρ) and isothermal curve ($R = 0.05$, 0.1, 0.4, 1.0). By

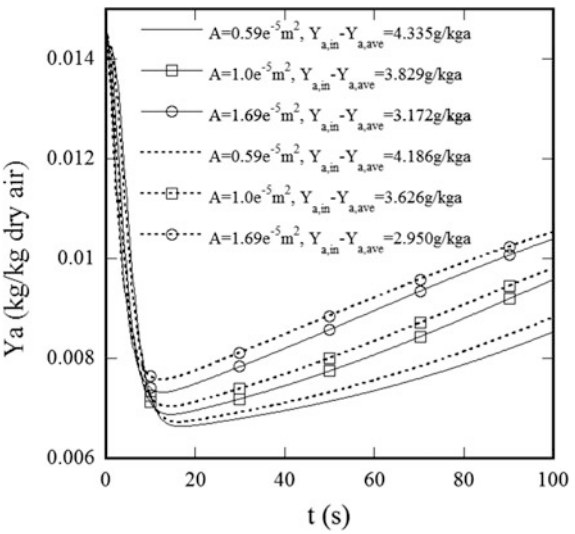

Fig. 2.7 Effect of the channel size on the performance of a desiccant wheel [40]

adjusting the channel shape and section area, the channel length L could be reduced by 43% to yield the same performance under standard conditions. By improving the properties of the desiccant, the size of a desiccant wheel could be reduced by 29%, while maintaining the same dehumidification capacity. When the channel factors and desiccant factors were combined under optimal conditions (sine-shaped channel with an aspect ratio 2:1, channel area 0.59×10^{-5} m^2, desiccant mass $1.3f_m$, specific heat $c_p/1.3$, density 1.3ρ and $R = 0.4$), the size of a desiccant wheel could be reduced by as much as 66% to perform on the same level as under standard conditions (sine-shaped channel with an aspect ratio 1:1, channel area 1×10^{-5} m^2, desiccant mass $0.7f_m$, specific heat c_p, density ρ and $R = 0.1$). The results of the analysis also suggest that the channel section area is the most influential factor that decides the size of a wheel, followed by the separate factor R and the channel shape.

2.2.4 Adsorbent

At present, commercially available desiccants include silica gel, activated alumina, natural and synthetic zeolites, titanium silicate, lithium chloride and synthetic polymers. Silica gel is one of the best performing and commonly investigated materials in desiccant wheels owing to its good long-term stability, minimal hysteresis and availability of data in the literature for comparison and specification. However, it is not a heat-resistant material and therefore is only adequate for low regeneration temperatures.

Zeolites are a common alternative to silica gel because they have widespread chemical uses and can be synthesized according to the application requirements. Conventional zeolites, such as Type A and Type Y, show a typical S-shaped adsorption isotherm, which is ideally suited for dehumidification and drying processes. However, their adsorption isotherm generally has a zone of steepest gradient in the low humidity range, i.e., the minimal amount of adsorbed water vapor is achieved only at extremely low relative humidity. A new generation of zeolites has raised interest both in adsorbent characterization and cooling applications. AQSOA™ (Aqua Sorb Adsorbent) zeolites, recently developed by Mitsubishi Plastics Inc., is an interesting solution to exploit low-grade heat. With this new generation of zeolites, a favorable S-shaped isotherm remains and the steepest gradient zone of the adsorption isotherm is shifted toward higher relative humidity values compared with conventional zeolites such as Type A or Type Y [41]. The experimental results of several studies are available on alternative desiccant materials [42]; however, only a few have investigated the new generation of zeolites [17], and neither a comprehensive nor a model-driven numerical analysis has been carried out on AQSOA zeolite-based desiccant wheels.

The apparently favorable moisture adsorption characteristics of AQSOA are alleged to improve the dehumidification performance of the wheel. However, recent

experimental results [17] showed that silica gel performed as well and sometimes better than the alternative materials over a range of conditions comparing desiccant wheels using silica gel, a super adsorbent polymer and a ferroaluminophosphate (FAM-Z01) zeolite material. It was not clear whether these performance differences were attributed to differences in the desiccant adsorption isotherms or to other material properties. Recently, Hong et al. [18] discussed this issue.

Silica gel has a linear-shaped isotherm, which causes a slow adsorption rate and small adsorption capacity; however, it has some attractive characteristics such as a lower adsorption heat ($\sim$2400 kJ/kg) than zeolites, which reduces the amount of input energy required to remove the heat from the exothermic reactions. FAM-Z01 has a high adsorption rate and a large adsorption capacity due to its S-shaped isotherm, which increases the possibility of it becoming commercially available. Kim et al. [43] developed a hybrid isotherm equation combining both the Henry and Sips equations, from which a comparison of adsorption rates was made between FAM-Z01 and various conventional silica gels (Type-A5BW, Type-RD 2560 and Type-A++). They showed that FAM-Z01 has a larger adsorption capacity than silica gels. The characteristics of FAM-Z01, particularly it isotherm, have been investigated. However, although the isotherm is important to the adsorption capacity, it is only one factor among various parameters that have a complex effect on the system performance. By individually examining the effect of each parameter, the guidelines for developing a new adsorbent can be obtained.

$$q^* = \beta K_{\mathrm{H}}\left(\frac{P}{P_{\mathrm{s}}}\right) + (1-\beta)\frac{q_{\mathrm{m}}\left(K_{\mathrm{S}}\frac{P}{P_{\mathrm{s}}}\right)^{1/n}}{1+\left(K_{\mathrm{S}}\frac{P}{P_{\mathrm{s}}}\right)^{1/n}} \tag{2.9}$$

Equation (2.9) is a combined isotherm equation of both the Henry and Sips equations for FAM-Z01, which was proposed by Kim et al. [43]. The valid range of Eq. (2.9) is 20 °C < T_{b} < 80 °C. The total of nine coefficients that appeared in Eq. (2.9) was obtained using the following equations:

$$K = K_0 \exp\left(-\frac{H_{\mathrm{sor}}}{R_{\mathrm{v}} T_{\mathrm{b}}}\right) \tag{2.10}$$

$$n = A + \frac{B}{T} \tag{2.11}$$

$$\beta = \exp\left(-\alpha\frac{P}{P_{\mathrm{s}}}\right) \tag{2.12}$$

$$\alpha = \kappa_1 + \kappa_2\frac{T}{T_{\mathrm{ref}}} \tag{2.13}$$

Table 2.1 Coefficients used in the FAM-Z01 isotherm equation [18]

Coefficient	Value	Coefficient	Value
$K_{0,H}$	4.717×10^{-3}	$H_{sor,H}$	−8.773
κ_1	9.097	κ_2	−3.569
$K_{0,S}$	6.288×10^{-2}	$H_{sor,S}$	−11.24
A	-7.734×10^{-1}	B	2.732×10^{2}
q_m	2.175×10^{-1}	R^2	0.989

The coefficients used in Eq. (2.9)–(2.13) are shown in Table 2.1. The isotherm equations of the conventional silica gels in the form of the Freundlich or Toth equation are as follows:

Type-RD silica gel [44]

$$q^* = A(T_b)\left(\frac{P}{P_s}\right)^{B(T_b)} \tag{2.14}$$

The simulation results for FAM-Z01 and Type-RD silica gel applied to the fin-tube-type adsorption bed in $0.09 < P/P_s < 0.40$ are shown in Fig. 2.8 and Table 2.2. Kim et al. [43] ascertained that the performance of the adsorption bed is directly proportional to the adsorption rate, but Fig. 2.8a shows that the adsorption chill using FAM-Z01 has only a 2.1% higher Δq_{max}. The COP of the FAM-Z01/water systems is 14.4% lower and 3.87% higher than that of the Type-RD silica gel, respectively.

The performance of the FAM-Z01/water system is expected to be enhanced because of the increased adsorption capacity due to the nature of the S-shaped isotherm. However, the results show a decreased COP compared to the Type-RD silica gel/water system for the same conditions ($0.09 < P/P_s < 0.40$). To examine the cause of the low performance of FAM-Z01, we artificially changed the thermo-physical properties of Type-RD silica gel to match FAM-Z01, one by one,

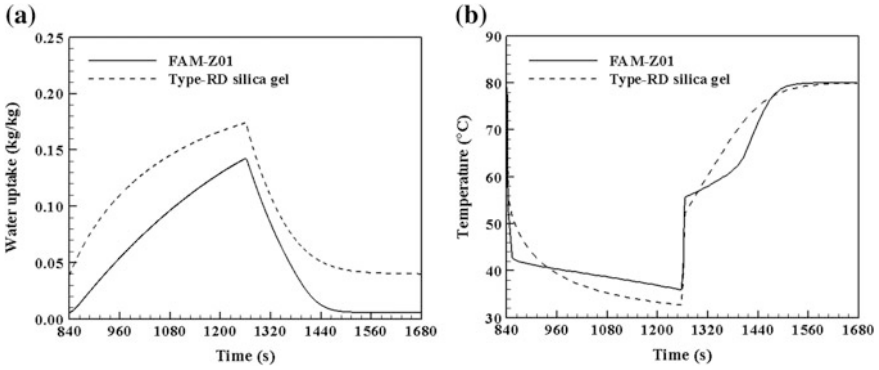

Fig. 2.8 Comparison of the **a** volume-averaged water uptake and **b** volume-averaged bed temperature between FAM-Z01 and Type-RD silica gel [18]

Table 2.2 Performance of each adsorption bed with the FAM-Z01/water and Type-RD silica gel/water systems [18]

	FAM-Z01	Type-RD silica gel
Δq_{max} (kg/kg)	0.1368	0.1340
COP	0.5623	0.6572

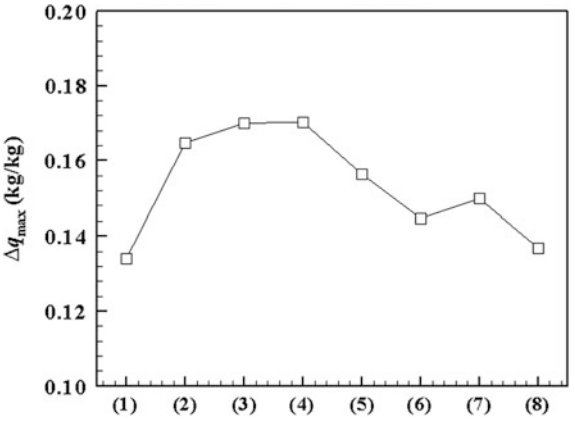

Fig. 2.9 Variation of the Δq_{max} after changing the thermo-physical properties, *2* isotherm, *3* density, *4* specific heat, *5* adsorption heat, *6* thermal conductivity and *7* porosity from *1* Type-RD silica gel to *8* FAM-Z01 [18]

and examined the Δq_{max} and COP. Case (1) on the x-axis in Fig. 2.9 corresponds to Type-RD silica gel. Case (2) represents changing the isotherm property to match FAM-Z01, while keeping the remaining properties of Type-RD silica gel the same. Case (3) represents changing the isotherm and density to match FAM-Z02, while keeping the remaining properties of Type-RD silica gel the same. In the same manner, FAM-Z01's (4) specific heat, (5) adsorption heat, (6) thermal conductivity, (7) porosity and (8) diffusion coefficient were substituted in consecutive order. Finally, case (8) is the result of FAM-Z01. Although case (2)–case (7) are artificial, this strategy provides insight about which property of FAM-Z01 increases or decreases the system performance and the influence each property has on the system performance.

Figure 2.9 and Table 2.3 show the variation of Δq_{max}, according to the changes in the thermo-physical properties one by one, from Type-RD to FAM-Z01. The bigger the Δq_{max}, the larger the cooling energy Q_{eva}. Case (2), where the isotherm of FAM-Z01 was used, has a 22.9% higher Δq_{max} than Case (1), i.e., Type-RD silica gel. This advantage originates from FAM-Z01's S-shaped isotherm. Case (3), where the density of FAM-Z01 was additionally used, has a 3.28% higher Δq_{max} than case (2). The density of FAM-Z01 is lower than Type-RD silica gel. When the density is changed to a low value, the heat transfer capacity is increased; therefore, the mass transfer resistance is reduced. The increased mass transfer capacity causes the adsorption bed to reach the pressure of the evaporator or condenser more rapidly. As a result, the Δq_{max} is increased. Case (4) is the results obtained by the

Table 2.3 Rate of increase in system performance [18]

	Δq_{max} (%)	COP (%)
Case (1)	0	0
Case (2)	+22.9	+4.47
Case (3)	+3.28	−0.58
Case (4)	+0.06	−0.64
Case (5)	−8.11	−16.1
Case (6)	−7.54	−1.00
Case (7)	+3.67	+0.63
Case (8)	−8.74	−0.93

addition of the specific heat of FAM-Z01. The specific heat of FAM-Z01 is lower than the Type-RD silica gel, which results in a lower thermal resistance. The Δq_{max} is increased by the enhanced heat transfer capacity. However, the effect of the specific heat is minor (only a 0.06% increase). The adsorption heat of FAM-Z01 was added to case (5). The adsorption heat indicates the degree of the exothermic and endothermic reactions coming from the phase change in the adsorbate. The larger the adsorption heat, the stronger the reaction, which increases the thermal resistance of the adsorption bed. FAM-Z01 has a 30% larger value of adsorption heat than Type-RD silica gel, which results in an 8.11% decrease in the Δq_{max}. Case (6), with the addition of the thermal conductivity of FAM-Z01, shows a 7.54% lower Δq_{max} than case (5). Thermal conductivity is also proportional to the heat transfer capacity. The lower thermal conductivity of FAM-Z01 decreases Δq_{max}. The porosity of FAM-Z01 was added to case (7). Adsorption occurs by diffusion on the pore surface of the adsorbent (particle); therefore, the adsorption rate is enhanced by large porosity. However, the proportion of vapor with low thermal conductivity is also increased when the porosity is large, which reduces the effective thermal conductivity. The simulation result indicates that the lower porosity of FAM-Z01 increases the Δq_{max} by 3.67%. Case (8) is the case where the diffusion coefficient of FAM-Z01 ($D_{so}/\exp(-E_a/(R_u T_b))$) is added, and finally all the properties of FAM-Z01 are used. The adsorption rate is enhanced as the D_{so} increases and the E_a decreases. Li et al. [45] showed that the diffusion coefficient of FAM-Z01 is lower than Type-RD silica gel. The smaller diffusion coefficient enlarges the intra-particle mass transfer resistance and decreases the Δq_{max} by 8.74%.

In conclusion, the adsorption rate is increased by the S-shaped isotherm, small density, small adsorption heat, large thermal conductivity, small porosity and large diffusion coefficient. Conversely, the characteristics of FAM-Z01, such as large adsorption heat, low thermal conductivity and low diffusion coefficient, are the factors that decrease the adsorption rate.

2.2.5 Isotherm

Inside the porous medium, two phases of water (vapor and adsorbed water) coexist in an equilibrium state, which is characterized by the water vapor–adsorbent sorption isotherm. There are many types of equilibrium adsorption relationships. The relative humidity of the moist air in equilibrium with the adsorbent, ϕ, and the separation factor, R, is used to calculate the water content of the adsorbent, W:

$$W/W_{\max} = \varphi/[R + (1 - R)\varphi] \tag{2.15}$$

Some researchers consider that W is a function of ϕ and the temperature of the moist air in equilibrium with the adsorbent T_{d} can be represented as:

$$W = f(T_{\mathrm{d}}, Y_{\mathrm{d}}) = g(T_{\mathrm{d}}, \varphi) \tag{2.16}$$

Sometimes it is assumed that W is a function of ϕ only, and invariable with the temperature T_{d}:

$$W = f(\varphi) \tag{2.17}$$

In the previous section, we showed that the performance of a desiccant wheel depends on the properties of the adsorbent, but the most influential factor was the isotherm. For the development of a new adsorbent, the isotherm would be one of the targets to find the optimal isotherm shape that leads to maximum dehumidification and explains the reason why the isotherm shape enhances dehumidification on a particular working condition.

From the viewpoint of the regeneration temperature, when the regeneration temperature increases, the wheel operates at a lower mean relative humidity. Therefore, the ideal isotherm is shifted so that the maximum possible moisture gradient occurs over the encountered range of relative humidity. However, it is hard to draw a general conclusion because the ideal isotherm shape varies according to the supply and regeneration air inlet conditions.

In previous studies, a different optimal isotherm shape was reported in each study. Collier et al. [46] found that a general moderately convex isotherm shape gives the best compromise between efficient dehumidification and regeneration processes. However, Zheng et al. [10] found that an isotherm with $R = 0.07$ resulted in the maximum dehumidification performance for Type 1. Dai et al. [11] presented that the desiccant isotherm shape is the most important factor in determining the wave front shapes within the desiccant matrix. They also discussed the effect of the separation factor ($R = 0.01$–1) of the isotherm shape on the regeneration temperature of the desiccant wheel.

2.2.6 Analytic Modeling

Analytic modeling is very important to provide physical insight and a basis for the examination of numerical and experimental results. However, analytic approaches are subject to extensive assumptions; therefore, they cannot explain the complex phenomena involved in coupled heat and mass transfer in desiccant wheels. Most of the previous studies are based on numerical models and analytical studies are scarce. Banks [47, 48] assumed that a desiccant wheel might be represented by the superposition of two heat transfer regenerators driven by combined potentials and presented methods for predicting exit air-conditions. However, intense numerical computation is eventually required due to the nonlinear nature involved in the solutions, which restricts the practical applicability of analytical methods to engineering practices. Lee et al. [49] and Kim et al. [50] presented analytical solutions for the simplified governing equations based on assumption of linear temperature and concentration profiles [49] and uniform heat and mass fluxes [50] at the air-desiccant interface.

Recently, Lee and Kim [51] proposed a simple, yet accurate, integral model and validated the model by comparing with a FDM model and experimental data in the literature. The analysis of the solution revealed that the behavior of a desiccant wheel depends primarily on three dimensionless numbers of the thermal time constant and the Jakob numbers, namely C_r^*, Ja_a and Ja_s. The dimensionless numbers (Ja_a and Ja_s) are the thermodynamic characteristics of an air-desiccant system that deicide the behavior of a desiccant wheel.

2.2.7 Numerical Modeling

Numerical simulation of heat and moisture interactions between the air stream and the particles in a desiccant bed provides useful insight into the dynamics of the bed and its performance characteristics. Assessing the great number of available options and their optimum combinations involved in the design of a desiccant wheel is a time-intensive task when using an experimental approach. Therefore, modeling and numerical simulations are highly effective tools when designing a desiccant wheel because they effectively isolate one variable at a time to examine trends and causes. Different methods of numerical solution have been used by many researchers with different simplified treatments of the fluid and solid domains to predict the behavior of air dehumidifying systems [28].

Figure 2.10 shows the schematic of a desiccant wheel. A desiccant wheel is made by either impregnating a honeycomb-patterned microstructure wheel with a solid desiccant (e.g., silica gel or zeolite), or by coating the same substance on corrugated sheet and rolling it into a wheel. A desiccant rotor contains numerous channels, with a fixed ratio of the regeneration to the dehumidification section. A desiccant section absorbs water, and a slow-revolving desiccant wheel moves the

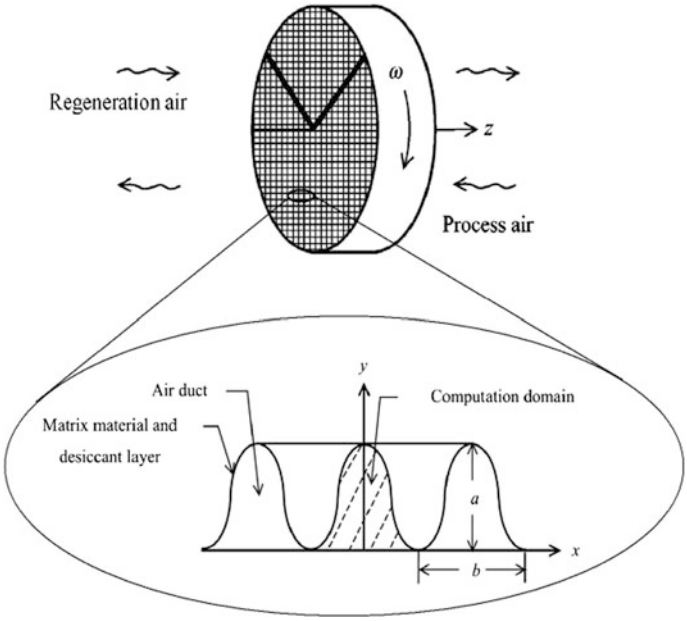

Fig. 2.10 Schematic of a desiccant wheel and the computational domains [22]

section to the high-temperature regeneration section to restore the dehumidifying ability. Then, the desiccant part returns to its initial stage.

Multi-dimensional mathematical models reflecting the effects in radial or circumferential directions can be used to analyze the heat and mass transfer processes comprehensively with improved accuracy. However, the complexity increases simultaneously. Most physical models used in numerical studies of desiccant wheels have been analyzed through 1-D mathematical formulations based on the hypotheses of negligible cross-direction resistance to heat and mass transfer inside the desiccant wall [11, 12, 22, 37, 52–54]. The validity of one-dimensional models is acceptable to relatively thin desiccant walls of the hygroscopic matrix and has been investigated in some studies [30, 55, 56].

Because of the geometric similarity and to avoid prohibitive computation costs, it is reasonable to represent the multiple annular layers of straight slots in the desiccant wheel using a "representative annulus" whose cross-sectional view is presented in Fig. 2.10. In this way, the three cylindrical coordinates (r, θ, z) can reasonably be reduced to a steady two-dimensional (θ, z) or unsteady one-dimensional (t, z) problem. In the present study, the unsteady one-dimensional model (t, z) is chosen for the coupled heat and mass transfer process in the rotary desiccant wheel. The numerical analysis is based on the following assumptions:

(1) The airflow is one-dimensional;
(2) The axial heat conduction and mass diffusion in the fluid are neglected;

(3) There is no leakage of fluid in the desiccant wheel;
(4) All ducts are impermeable and adiabatic;
(5) The thermodynamic properties are constant and uniform; and
(6) The heat and mass transfer coefficient between the airflow and the desiccant wall is constant along the channel.

2.2.7.1 Governing Equations

Based on the above assumptions, the energy and mass conservation equations can be obtained as follows [20, 57].

Mass conservation for the process air:

$$\frac{\partial Y_a}{\partial z} = \frac{h_m P_p}{u_a \rho_a A_p}(Y_d - Y_a) \tag{2.18}$$

where the left-hand and right-hand sides represent the sorbate influx by the fluid flow and the sorbate transfer rate to the felt, respectively. Contrary to the adsorbent, the moisture storage in the air can be neglected.

Energy conservation for the process air:

$$\left(C_{pa} + Y_a C_{pv}\right)\frac{\partial T_a}{\partial z} = \frac{hP_p}{u_a \rho_a A_p}(T_d - T_a) \tag{2.19}$$

where the left-hand side represents the sum of the energy transferred by the fluid flow and decreased by the sorbate transfer to the felt, and the right-hand side represents the conduction heat transfer to the felt. Again, the energy storage in the humid air can be neglected.

Conservation of water content for the absorbent:

$$\frac{\partial W}{\partial t} = \frac{h_m P_d}{\rho_d f_m A_d}(Y_a - Y_d) \tag{2.20}$$

where the left-hand and right-hand sides represent the moisture storage term inside the desiccant and the convective mass transfer between the air and the desiccant, respectively. A mass diffusion within the solid desiccant in the axial direction is neglected.

Conservation of energy for the absorbent:

$$\left(C_{pd} + f_m W C_{pl}\right)\frac{\partial T_a}{\partial t} = \frac{hP_d}{\rho_d A_d}(T_a - T_d) + \frac{h_m H_{sor} P_d}{\rho_d A_d}(Y_a - Y_d) \tag{2.21}$$

where the first term on the left-hand side is the energy transfer by heat conduction and the second term is energy transfer by mass transfer. The first term on the

right-hand side of Eq. (2.21) calculates the convective heat transfer between the solid desiccant and air. The second term on the right-hand side expresses the influence of the adsorption heat.

2.2.7.2 Boundary and Initial Conditions

The above equations are subject to the following boundary and initial conditions, which are easily obtained considering the periodic nature of the desiccant wheel.

For the process section:

$$T_{\mathrm{ap}}(t,0) = T_{\mathrm{ap,in}} \tag{2.22a}$$

$$Y_{\mathrm{ap}}(t,0) = Y_{\mathrm{ap,in}} \tag{2.22b}$$

$$T_{\mathrm{dp}}(0,z) = T_{\mathrm{dr}}(t_{\mathrm{r}}, L-z) \tag{2.22c}$$

$$Y_{\mathrm{dp}}(0,z) = Y_{\mathrm{dr}}(t_{\mathrm{r}}, L-z) \tag{2.22d}$$

For the regeneration section:

$$T_{\mathrm{ar}}(t,0) = T_{\mathrm{ar,in}} \tag{2.23a}$$

$$Y_{\mathrm{ar}}(t,0) = Y_{\mathrm{ar,in}} \tag{2.23b}$$

$$T_{\mathrm{dr}}(0,z) = T_{\mathrm{dp}}\left(t_{\mathrm{p}}, L-z\right) \tag{2.23c}$$

$$Y_{\mathrm{dr}}(0,z) = Y_{\mathrm{dp}}\left(t_{\mathrm{p}}, L-z\right) \tag{2.23d}$$

2.2.7.3 Auxiliary Equations

The governing Eqs. (2.18)–(2.21) have 5 unknowns T_{a}, T_{d}, Y_{a}, Y_{d}, and W. To solve this set of equations, i.e., to close the problem, it is necessary to relate the equilibrium composition Y_{d} to the water content W and temperature of the adsorbent T_{d}. Here, we employ silica gel as the desiccant material; therefore, the water content in the desiccant is governed by the following isotherm [58, 59]:

$$\varphi_{\mathrm{d}} = 0.0078 - 0.0576\,W + 24.2\,W^2 - 124\,W^3 + 204\,W^4 \tag{2.24}$$

where ϕ_{d} is the equilibrium relative humidity over the desiccant with a water content W.

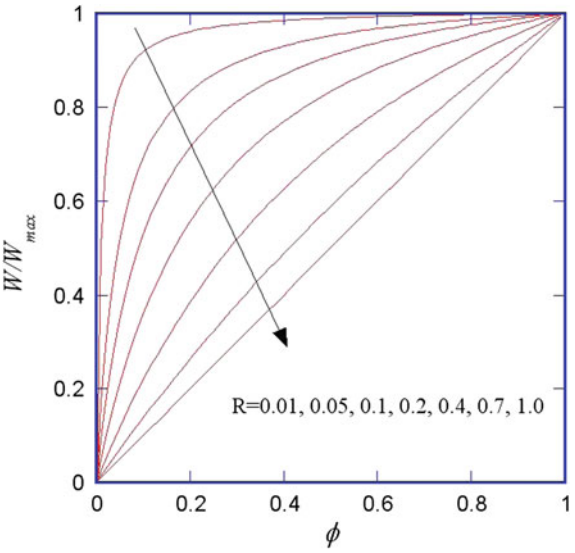

Fig. 2.11 Schematic of the isotherm shape according to the separate factor

Here, we employ another isotherm as follows:

$$\frac{W}{W_{\max}} = \frac{\phi_d}{R + (1-R)\phi_d} \tag{2.25}$$

where ϕ_d is the equilibrium relative humidity over the desiccant with a water content W and R is the separate factor. Figure 2.11 shows the adsorption capacity behavior according to the separate factor. It is obvious to expect a larger adsorption capacity (i.e., a higher wheel performance) for a higher $W_{\max}$. Therefore, we fixed $W_{\max} = 0.4$ and confined our attention to the effect of R on the optimal operation conditions.

The relationship between the humidity ratio and the relative humidity is expressed as:

$$Y_d = \frac{0.622\phi_d P_s}{P - \phi_d P} \tag{2.26}$$

In addition, the values of the adsorption heat H_{sor}, convective transfer coefficient h, thermal conductivity k and moisture diffusivity D_e in the desiccant material are required.

Typical diffusion theory holds that the water vapor molecule has three types of diffusion modes in porous mediums: Fickian diffusion, Knudson diffusion and surface diffusion. Fickian diffusion and Knudsen diffusion occur in series in the pore, and these two diffusions are summarized as the pore diffusion. Moreover, the pore diffusion and the surface diffusion occur in parallel. Fickian diffusion occurs when the mean free path is relatively short compared to the pore size. Knudsen

diffusion is dominant when the mean free path of gas molecules is relatively long compared to the pore size. Pesaran and Mills [60] reported that surface diffusion is a dominant one in moisture transfer in micro-porous silica gel (regular density silica gel). However, for macro-porous silica gel (intermediate density silica gel), both Knudsen diffusion and surface diffusion are important mechanisms. Fickian diffusion can be negligible for silica gel at atmospheric pressure.

The effective diffusivity associated with Knudsen diffusion in a porous desiccant medium can be written as [61]:

$$D_{\mathrm{K,eff}} = 97 r_{\mathrm{v}} \sqrt{\frac{T + 273.15}{R_{\mathrm{v}}}} \frac{\varepsilon_{\mathrm{v}}}{\tau_{\mathrm{v}}} \tag{2.27}$$

The effective diffusivity associated with the surface diffusion of adsorbed water $D_{\mathrm{s,eff}}$ in a porous desiccant medium is directly influenced by the path tortuosity τ and depends on the adsorbate–adsorbent pair. In the present work, the following equation was used [61]:

$$D_{\mathrm{s,eff}} = \frac{D_{\mathrm{s0}}}{\tau_{\mathrm{l}}} \exp\left(\frac{-4.5 \times 10^{-4} H_{\mathrm{sor}}}{b R_{\mathrm{v}} (T + 273.15)}\right) \tag{2.28}$$

where b depends on the type of adsorption bond and D_{s0} is a constant that depends on the adsorbent.

2.2.7.4 Numerical Procedures

The aforementioned governing equations are discretized into finite difference equations by an implicit, forward difference scheme. All the simulations in this paper are performed with a grid of 800 for time and 50 for space. The grid independence has been proved to be valid within a tolerable limit. A cyclic steady state is obtained within 10 iterations with a relative error of 1×10^{-5} which is a root mean square of $\Delta\phi = \left|\left(\phi - \phi^{\mathrm{old}}\right)/\phi\right|$, $\phi = T_{\mathrm{a}}, T_{\mathrm{d}}, Y_{\mathrm{a}}, Y_{\mathrm{d}}$. The relative error of the uptake mass with the release mass is lower than 0.5%.

Simulations have been conducted for a desiccant wheel with a width of 0.2 m and a silica gel wall thickness of 0.15 mm. The geometry of the channels in the wheel shown in Fig. 2.10 is sinusoidal with a width (b) of 3.5 mm and a height (a) of 1.75 mm. The air velocity is 2 m/s in both the adsorption and regeneration period. The convective heat transfer coefficient and hydraulic diameter are expressed in Eqs. (2.5)–(2.8) from the Nusselt number in the sinusoidal-shaped channels [62]. Table 2.4 includes the data for all the properties and geometries employed in the simulations.

Table 2.4 Input data used in the simulations

Channel shape	Sinusoidal
Height, a	1.75×10^{-3} m
Width, b	3.5×10^{-3} m
Wall thickness, c	0.15×10^{-3} m
Wheel length	0.2 m
Facing area	1 m^2
Facing air velocity, u_a	2.0 m s^{-1}
Desiccant material	
Mass fraction of sorbent, f_m	0.7
Capacity, C_{pd}	921 J kg^{-1} K^{-1}
Density, ρ_d	720 kg m^{-3}
Heat of sorption, H_{sor}	2502.68 + $C_{pv}T_a$ kJ kg^{-1}
Air density, ρ_a	1.1614 kg m^{-3}
Capacity, C_{pa}	1007 J $kg^{-1}K^{-1}$
Thermal conductivity, k_a	0.0263 W $m^{-1}K^{-1}$
Water vapor capacity, C_{pv}	1872 J kg^{-1} K^{-1}
Liquid capacity, C_{pl}	4186 J kg^{-1} K^{-1}

2.2.8 Performance Index

The main function of a desiccant wheel is to remove the water vapor from the process air. Therefore, the performance indices represent the dehumidification capacity of the desiccant dehumidifier. There are several performance indices such as moisture removal, relative moisture relative efficiency, effectiveness of the wheel and the dehumidification coefficient of the performance of the wheel.

The primary performance indicator is assessed using the moisture removal capacity (MRC), as described in the ASHRAE proposed national standard method of testing [63]. The MRC quantifies the amount of moisture removed from the processing stream as it passes through the desiccant wheel using the following equation:

$$\mathrm{MRC} = \dot{m}_{\mathrm{p}}\left(Y_{\mathrm{ap,in}} - Y_{\mathrm{ap,out}}\right) \tag{2.29}$$

If the humidity is fixed at the process and regeneration inlets, the behavior of the MRC is usually similar to the effectiveness defined in Eq. (2.30), which is used in other literature [21, 57]. Based on the effectiveness, the best performance is obtained at the lowest adsorption-side outlet humidity, $Y_{\mathrm{ap,out}}$.

$$\varepsilon_{\mathrm{d}} = \frac{Y_{\mathrm{ap.in}} - Y_{\mathrm{ap,out}}}{Y_{\mathrm{ap,in}}} \tag{2.30}$$

In the case of an unbalanced flow, the mass flow rate $\dot{m}_p$ will change according to the ratio of the area of regeneration to dehumidification, A_r/A_p. Therefore, the MRC is more appropriate than ε_d as a performance index of unbalanced flow. At the optimum rotational speed, the MRC reaches a maximum; however, this does not mean a minimum value of $Y_{ap,out}$ because the mass of the moisture removed can become larger not only by decreasing the outlet humidity of the process section, but also by increasing the area of the process section.

2.3 Research Issues and Case Studies

2.3.1 Wheel Speed

The desiccant wheel is the key component of a desiccant cooling system, and the optimum rotation speed is one of the most important factors that can improve the performance of the wheel. The rotation speed should not only be low enough for complete regeneration, but also be high enough to keep the adsorbent far from equilibrium. This conflict yields the optimum rotation speed. The existence of an optimum rotation speed, at which the humidity of the product air becomes minimized, has already been reported [20, 21].

2.3.1.1 Dependence on the Regeneration Temperature and A_r/A_p

For outdoor conditions when $T_{p,in} = 30$ °C and $\phi_{p,in} = 40\%$, Fig. 2.12 shows the variation of the adsorption-side outlet humidity for various wheel speeds

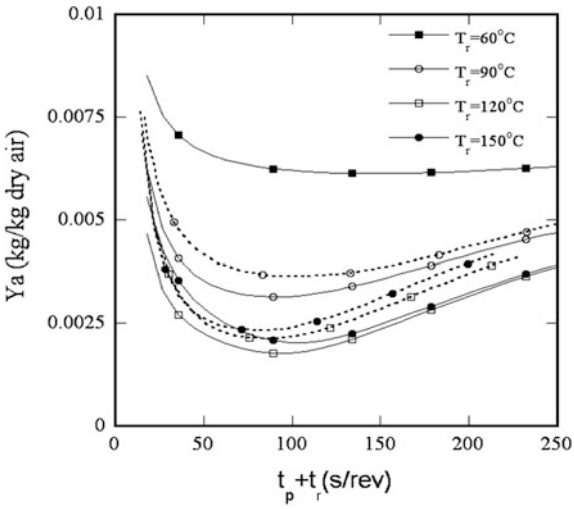

Fig. 2.12 Variations of adsorption-side outlet humidity for various wheel speeds at each regeneration temperature (60, 90, 120 and 150 °C) [12]

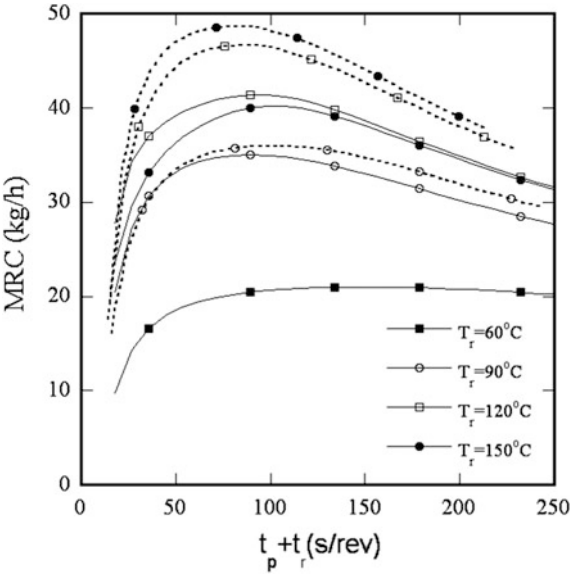

Fig. 2.13 Variations of the MRC for various wheel speeds at each regeneration temperature (60, 90, 120 and 150 °C) [12]

(=3600/($t_p + t_r$) rph) for each regeneration temperature (60, 90, 120 and 150 °C). The optimum area ratio of process to regeneration, A_r/A_p, varies depending on the regeneration temperature, and the resulting optimum A_r/A_p is 0.784, 0.623, 0.521 and 0.424 corresponding to the regeneration temperatures 60, 90, 120 and 150 °C, respectively. The solid lines in Fig. 2.12 show the results for $A_r/A_p = 0.784$, and the dashed lines are for $A_r/A_p = 0.784, 0.623, 0.521$ and 0.424. Note that the optimum value of A_r/A_p is obtained by maximizing the MRC. If the wheel diameter is fixed, the mass of the moisture removed can be increased not only by decreasing the outlet humidity of the process section, but also by increasing the process section area. Therefore, we cannot say that the optimum performance is found at the minimum value of the outlet humidity of the process section if the value of A_r/A_p is the design parameter. Figure 2.13 clearly shows this. If the MRC is chosen as an indicator of wheel performance, the maximum mass of moisture removed is found at the optimum value of A_r/A_p, but in Fig. 2.12, the minimum humidity is found at other values of A_r/A_p.

2.3.1.2 Dependence on the Regeneration Temperature and Outdoor Conditions

The variation of optimum wheel speed as a function of the regeneration temperature and outdoor conditions is shown in Fig. 2.14. For convenience, four outdoor conditions are nominated. Regardless of the outdoor conditions, as the regeneration temperature increases, the optimum wheel speed decreases and then approaches a

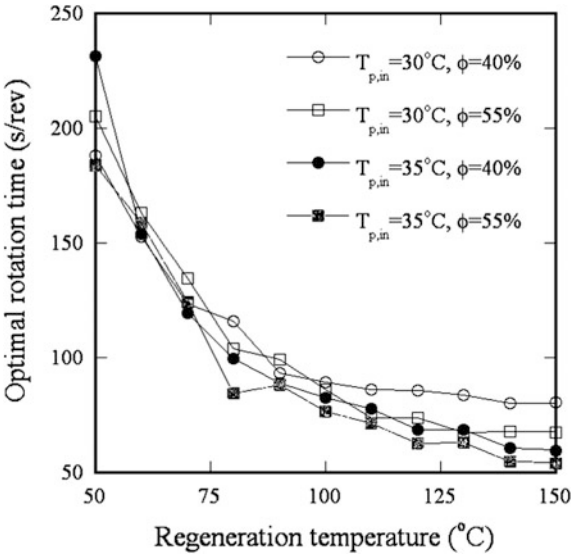

Fig. 2.14 Variations of the optimum wheel speed as a function of the regeneration temperature and outdoor conditions [12]

constant value. At low regeneration temperatures, the optimum speed is not as sensitive to the outdoor conditions compared with high regeneration temperatures. In addition, the optimum wheel speed is dependent on the outdoor humidity. The highest optimum wheel speed is observed for outdoor conditions $T_{p,in} = 30$ °C and $\phi_{p,in} = 40\%$ where the humidity has the smallest value (10.6 g/kga). The optimum wheel speed is almost the same for the outdoor conditions $T_{p,in} = 30$ °C, $\varphi_{p,in} = 55\%$ and $T_{p,in} = 35$ °C, $\varphi_{p,in} = 40\%$. Note that the humidity of these two outdoor conditions is very close (14.6 and 14.1, respectively). The humidity 19.6 g/kgs, which corresponds to the outdoor conditions $T_{p,in} = 35$ °C and $\varphi_{p,in} = 40\%$, results in the lowest optimum wheel speed. For the optimization procedure to maximize the MRC, the IMSL routine ZXMWD is linked to the program to evaluate the wheel performance.

2.3.1.3 Dependence on the Isotherm

Figure 2.15 shows the optimal rotation speed and its dependency on the regeneration temperature and isotherm shape with different values for the separation factor R in Eq. (2.25). Note that the present results differ from earlier studies, which found that the optimum rotating speed was a condition of the fixed regeneration temperature and A_r/A_p. As the regeneration temperature increases, a monotonic decrease in the optimal rotation speed is observed $R > 0.2$, but the behavior is reversed as R becomes less than 0.2. Therefore, the highest optimum rotation speed is found at $R = 0.2$ at low regeneration temperatures, but $R = 0.05$ at high regeneration temperatures. The exceptional behavior of $R = 0.01$ is explained by

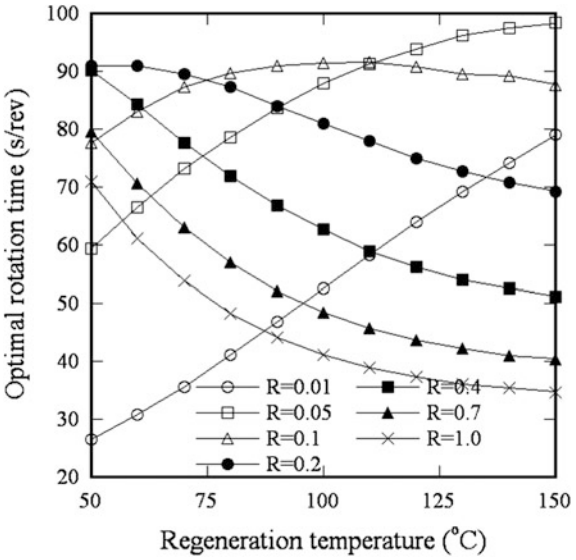

Fig. 2.15 Variations of the optimum rotation speed as a function of the regeneration temperature and isotherm shape [54]

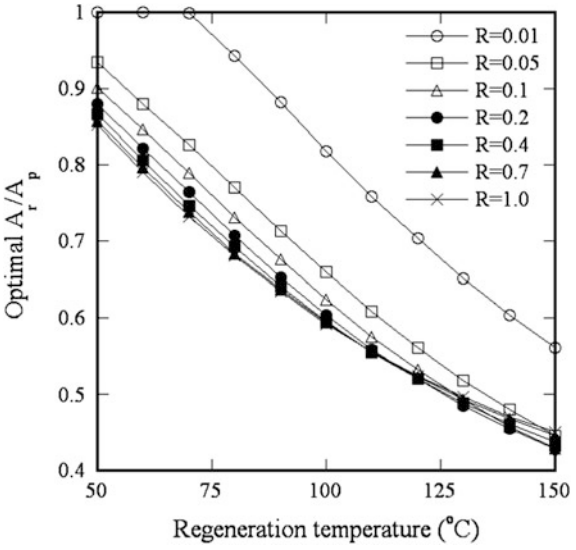

Fig. 2.16 Variations of the optimum value of A_r/A_p as a function of the regeneration temperature and isotherm shape [54]

observing differences in water content of process and regeneration. Note that at low regeneration temperatures, the optimum speed is not as sensitive to the isotherm shape compared with at high regeneration temperatures.

The effect of the value of A_r/A_p on the wheel performance is investigated at different regeneration temperatures and isotherm shapes. Variations in the optimum value of A_r/A_p as a function of the regeneration temperature are shown in Fig. 2.16 for each isotherm shape. The optimum value of A_r/A_p is more sensitive to the

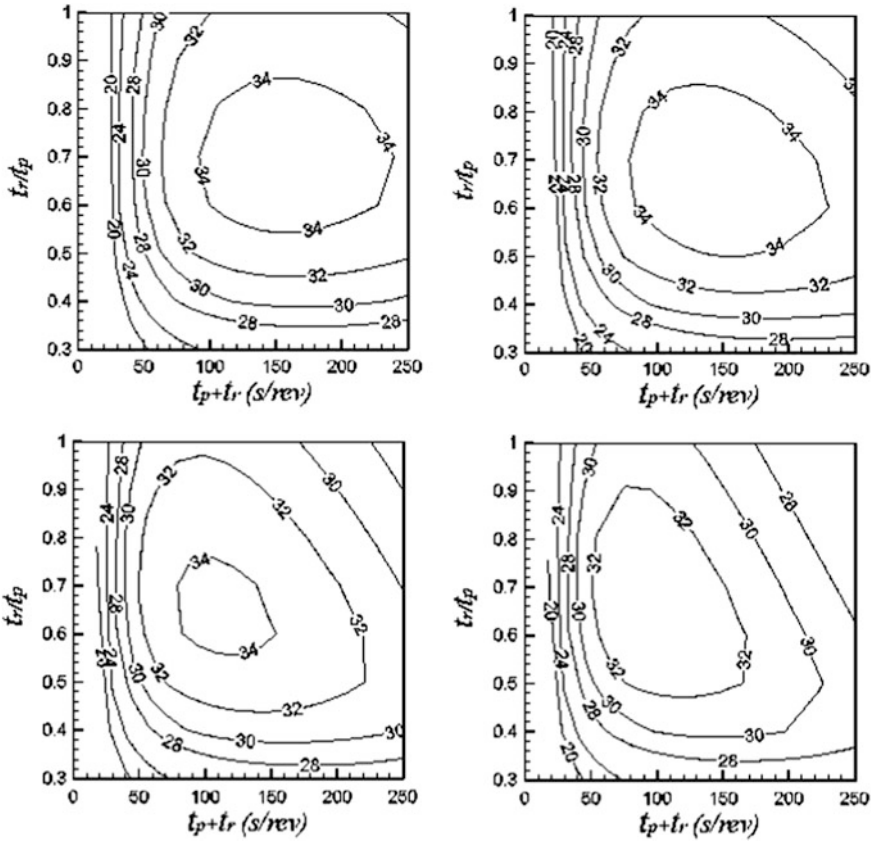

Fig. 2.17 Profiles of the MRC as a function of the optimum rotation speed and A_r/A_p for the isotherm shapes (R = 0.05, 0.1, 0.4, 1.0) and the regeneration temperature $T_{ar,in} = 90$ °C [54]

isotherm shape at low regeneration temperatures than at high regeneration temperatures. The detailed discussion on the dependency of the regeneration temperatures will be given in the following section.

Figure 2.17 shows the profile of the MRC as a function of the optimum rotation speed and A_r/A_p for isotherm shapes ($R = 0.05, 0.1, 0.4,$ and 1.0) and the regeneration temperature $T_{ar,in} = 90$ °C. Note that in contrast to the present work, most of earlier works studied the optimum isotherm shape for a fixed regeneration temperature and A_r/A_p. As shown in Fig. 2.17, the optimal design parameters, here rotating speed and A_r/A_p, are different for each isotherm shape. This means if optimization is conducted on the condition of a fixed rotation speed and A_r/A_p, an incorrect optimum isotherm shape would be found. We expect this is why the earlier works found different optimum isotherm shapes.

The above discussions are based on outdoor conditions of $T_{ap,in} = 30$ °C and $\varphi_{ap,in} = 40\%$, but general dependency on the isotherm shape is the same for other

outdoor conditions such as $T_{ap,in} = 35$ °C, $\varphi_{ap,in} = 40\%$ and $T_{ap,in} = 30$ °C, $\varphi_{ap,in} = 55\%$ and $T_{ap,in} = 35$ °C, $\varphi_{ap,in} = 55\%$.

2.3.2 *Area Ratio of Regeneration to the Dehumidification Section*

As the regeneration temperature decreases, the regeneration section becomes a larger fraction of the wheel. According to the manufacturer's catalog, the 1:3 split is generally used for high regeneration temperatures and a 1:1 split for low regeneration temperatures. However, it is not easy to decide the optimal area ratio of regeneration/dehumidification, which is expected to vary according to not only the regeneration temperature, but also the desiccant isotherm and outdoor conditions. The dependence on the regeneration temperature and isotherm is already discussed in Sect. 2.3.1; therefore, we will focus on the dependence of the optimum value of A_r/A_p on the outdoor conditions for the adsorbent silica gel with the form of the isotherm in Eq. (2.24).

Variations of the optimum value of A_r/A_p as a function of the regeneration temperature are shown in Fig. 2.18 for four different outdoor conditions. We have determined the dependency of A_r/A_p on the outdoor humidity. As the humidity increases, the optimum value of A_r/A_p also increases. The results of Ahmed et al. [23] also show this dependency, but they did not provide any discussion of this issue. The lowest value of A_r/A_p is observed for the outdoor conditions $T_{p,in} = 30$ °C and $\phi_{p,in} = 40\%$, for which the humidity is 10.6 g/kga. The humidities for the

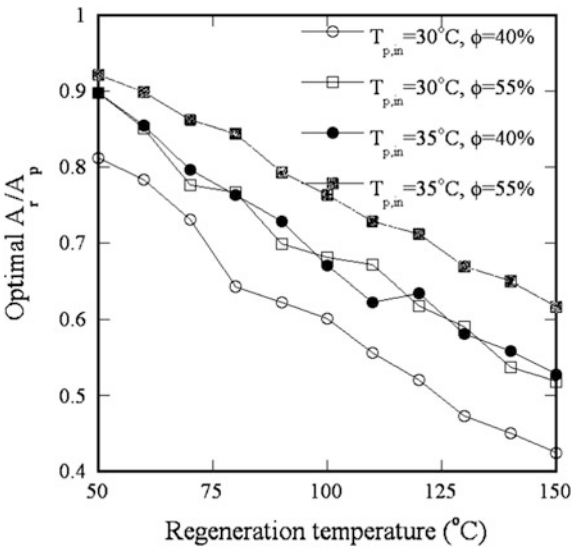

Fig. 2.18 Variations of the optimum value of A_r/A_p as a function of the regeneration temperature and outdoor conditions [12]

outdoor conditions $T_{p,in} = 30$ °C, $\phi_{p,in} = 55\%$ and $T_{p,in} = 35$ °C, $\phi_{p,in} = 40\%$ are almost the same and show similar optimum values of A_r/A_p over the entire range of regeneration temperatures. The outdoor conditions with the highest humidity, i.e., $T_{p,in} = 35$ °C, $\varphi_{p,in} = 40\%$ show the largest optimum value of A_r/A_p.

Ahmed et al. [23] ascertained that the optimum values of A_r/A_p are between 0.7 and 0.9 at $T_{r,in} = 60$ °C and between 0.25 and 0.4 at $T_{r,in} = 90$ °C depending on the inlet humidity. In Fig. 2.18, the optimum values of A_r/A_p are between 0.78 and 0.90 at $T_{r,in} = 60$ °C for the inlet conditions studied, which is similar to the values reported by Ahmed et al. [23]. However, the optimum values of A_r/A_p are between 0.62 and 0.79 for $T_{r,in} = 90$ °C, which shows considerable deviation from the values reported by Ahmed et al. [23]. The relationship between the optimum values of A_r/A_p and regeneration temperature is similar for a different isotherm shape as shown in Fig. 2.16 which covers a full range of isotherm shapes ($0.01 < R < 1.0$).

Considering that $A_r/A_p = 0.33$ is usually used for regeneration temperatures much higher than 90 °C and the regeneration section becomes a larger portion of the wheel as the regeneration temperature decreases, the results of Ahmed et al. [23] seem to under-predict the value of A_r/A_p. Note that in our study, the optimum value of A_r/A_p for $T_{r,in} = 150$ °C is 0.42 for the outdoor conditions $T_{p,in} = 30$ °C and $\phi_{p,in} = 40\%$, which is slightly greater than the value from the manufacturer's catalog (0.33).

Figures 2.19, 2.20, 2.21 and 2.22 show the profiles of the MRC as a function of the optimum wheel speed and A_r/A_p for the regeneration temperatures of 60, 90, 120 and 150 °C and four different outdoor conditions. The optimum behavior, i.e., the maximum MRC, wheel speed and optimum A_r/A_p, is discussed in previous sections, and here the behavior of off-design points is shown. With the sacrifice of a slight decrease in the MRC, the design point can be determined in the range of the wheel speed and A_r/A_p. We can also see that the desiccant wheel is highly effective for dehumidification at high regeneration temperatures [22].

2.3.3 *Sensitivity to Outdoor Weather Conditions*

For the fixed area ratio A_r/A_p, Figs. 2.23, 2.24, 2.25 and 2.26 represent the effect of outdoor conditions ($20\ °C < T < 35\ °C$, $0.005 < Y < 0.025$) on the MRC for the regeneration temperatures of 60, 90, 120 and 150 °C. The performance decreases as the outdoor temperature increases or the outdoor humidity decreases. As the regeneration temperature increases, the effect of the outdoor temperature decreases. In particular, for low values of the outdoor humidity and high regeneration temperatures, the wheel performance is nearly independent of the outdoor temperature.

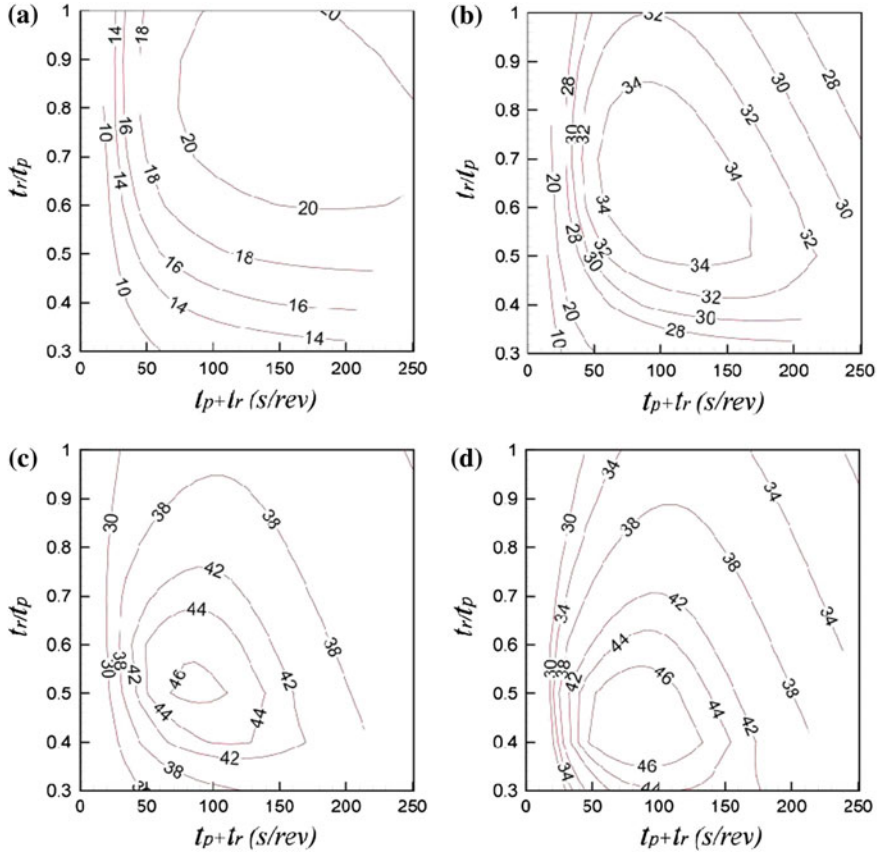

Fig. 2.19 Profiles of the MRC as a function of the optimum wheel speed and A_r/A_p for the outdoor conditions $T_{p,in} = 30$ °C and $\phi_{p,in} = 40\%$; **a** $T_{r,in} = 60$ °C, **b** $T_{r,in} = 90$ °C, **c** $T_{r,in} = 120$ °C and **d** $T_{r,in} = 150$ °C [12]

2.3.4 Isotherm

The separate factor R in Eq. (2.25) reflects the desiccant isotherm shape shown in Fig. 2.11. As R decreases, a larger adsorption capacity is expected even under low humidity. Dai et al. [6] suggested that $R = 0.1$ for a low regeneration temperature ($T_{ar,in} = 78.2$ °C), but should be $R = 0.05$ for a high regeneration temperature ($T_{ar,in} = 120$ °C). On the other hand, Simonson and Besant [64] ascertained that a linear sorption curve, i.e., $R = 1.0$, has the highest effectiveness over a typical range of operation conditions. In our simulation, a higher MRC is expected as R decreases for the range of regeneration temperatures shown in Fig. 2.27. The only exception is $R = 0.01$. This can be explained by examining the water content difference evaluated by the process inlet ($T_{ap,in} = 30$ °C and $\phi_{ap,in} = 40\%$) and the

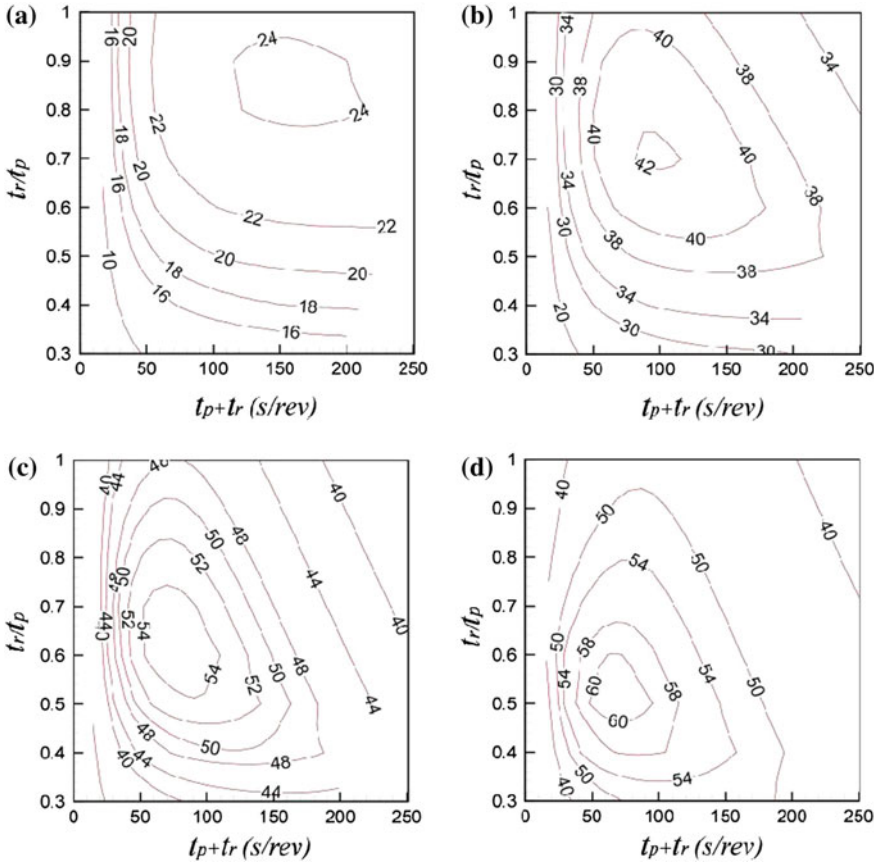

Fig. 2.20 Profiles of the MRC as a function of the optimum wheel speed and A_r/A_p for the outdoor conditions $T_{p,in} = 30$ °C and $\phi_{p,in} = 55\%$; **a** $T_{r,in} = 60$ °C, **b** $T_{r,in} = 90$ °C, **c** $T_{r,in} = 120$ °C and **d** $T_{r,in} = 150$ °C [12]

regeneration inlet ($Y_{ar,in} = Y_{ap,in}$ and varying $T_{ar,in}$) conditions. This value is closely related to the MRC.

The large water content difference in the process and regeneration results has a large potential for moisture transfer, which increases the moisture removal capacity. Figure 2.28 shows a typical example. Figure 2.28a depicts the water content differences evaluated by the process inlet and regeneration inlet conditions of $R = 0.05$ and $R = 0.7$, respectively, in the case of a low regeneration temperature. The water content difference is almost same at $R = 0.7$ and $R = 0.05$. However, when the regeneration temperature is high, the relative humidity at the regeneration inlet decreases compared with low regeneration temperatures, and the water content difference is increased at $R = 0.05$ than at $R = 0.7$ as shown in Fig. 2.28b. Therefore, the isotherm shape of $R = 0.05$ has a higher potential than that of

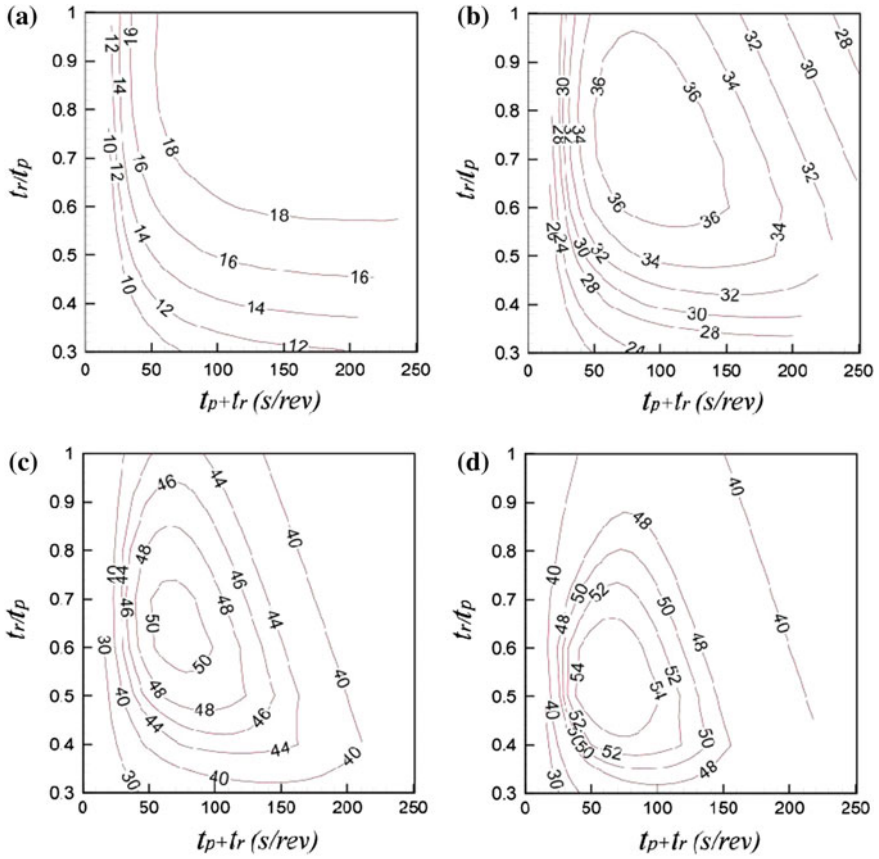

Fig. 2.21 Profiles of the MRC as a function of the optimum wheel speed and A_r/A_p for the outdoor conditions $T_{p,in} = 35$ °C and $\phi_{p,in} = 40\%$; **a** $T_{r,in} = 60$ °C, **b** $T_{r,in} = 90$ °C, **c** $T_{r,in} = 120$ °C and **d** $T_{r,in} = 150$ °C [12]

$R = 0.7$, which suggests that a higher MRC is expected at $R = 0.05$ at high regeneration temperatures. Compared to Fig. 2.27, Fig. 2.29 clearly shows this correlation between the MRC and water content difference.

It should be noted that unlike the present work, earlier works obtained an optimum isotherm shape on the condition of a fixed rotating speed and A_r/A_p for each regeneration temperature. This is why the earlier works found different optimum isotherm shapes. As was found in previous studies, if the same rotation speed and A_r/A_p are used for all R (for example, the optimal values for $R = 1.0$), the adsorption capacity behavior shown in Fig. 2.30 is different from Fig. 2.27. In this case, the highest moisture removal capacity is found at the isotherm shape $R = 0.4$.

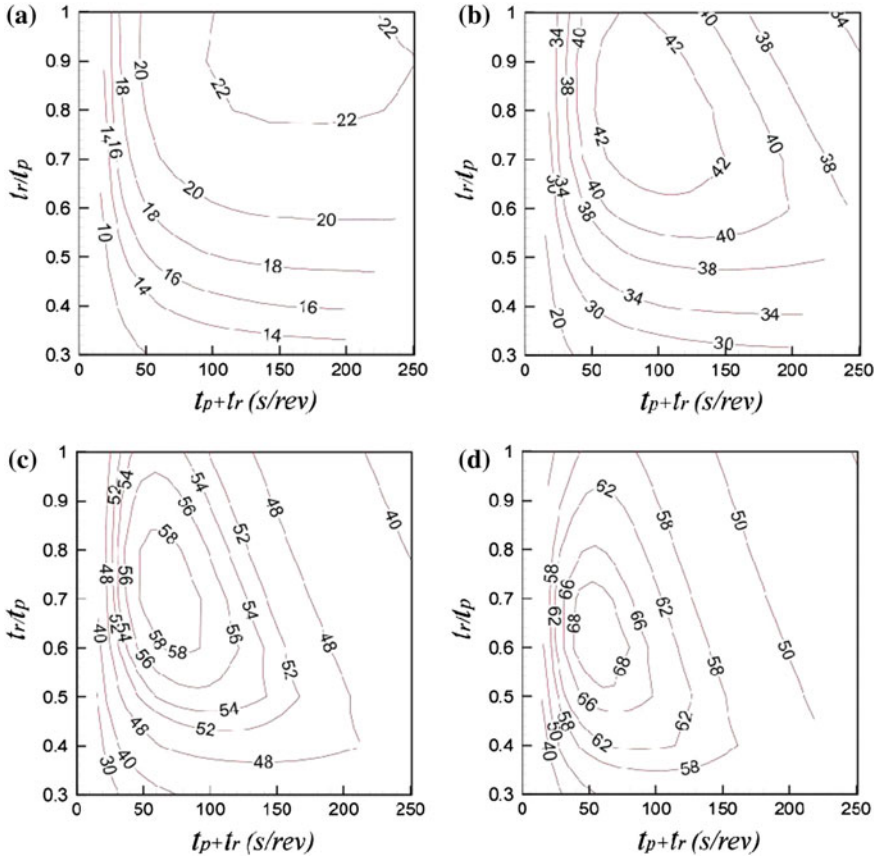

Fig. 2.22 Profiles of the MRC as a function of the optimum wheel speed and A_r/A_p for the outdoor conditions $T_{p,in} = 35$ °C and $\phi_{p,in} = 55\%$; **a** $T_{r,in} = 60$ °C, **b** $T_{r,in} = 90$ °C, **c** $T_{r,in} = 120$ °C and **d** $T_{r,in} = 150$ °C [12]

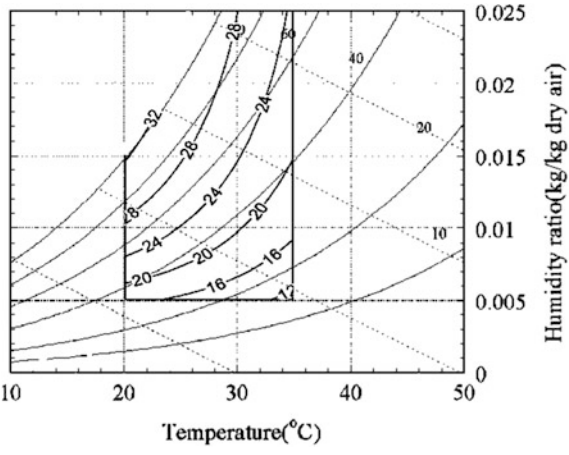

Fig. 2.23 Psychrometric chart representation of the effect of the outdoor conditions on the MRC for $T_{r,in} = 60$ °C [12]

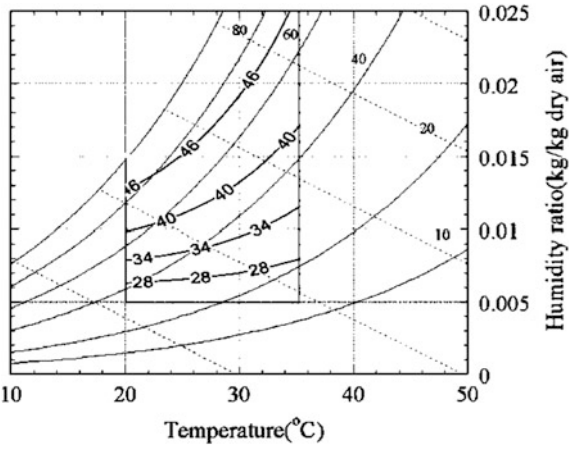

Fig. 2.24 Psychrometric chart representation of the effect of the outdoor conditions on the MRC for $T_{r,in} = 90$ °C [12]

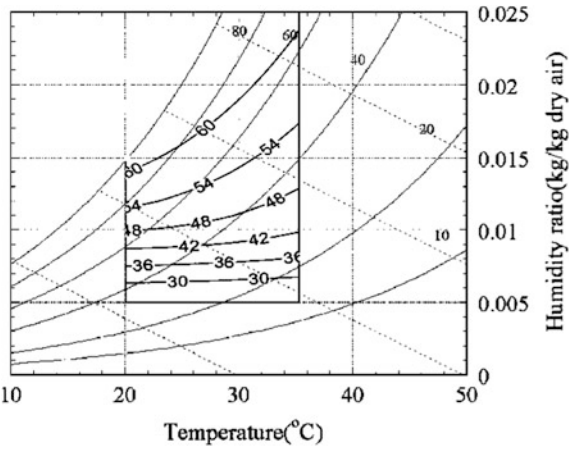

Fig. 2.25 Psychrometric chart representation of the effect of the outdoor conditions on the MRC for $T_{r,in} = 120$ °C [12]

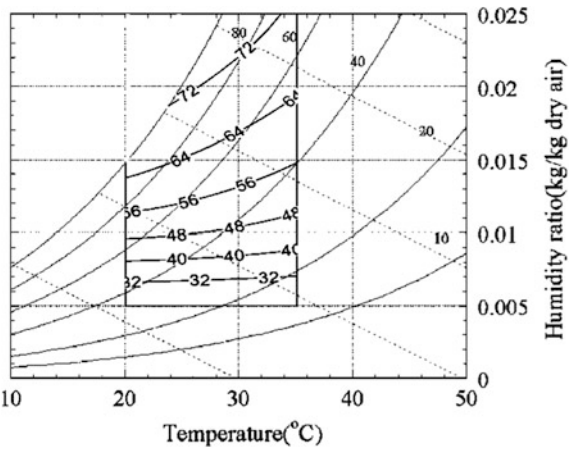

Fig. 2.26 Psychrometric chart representation of the effect of the outdoor conditions on the MRC for $T_{r,in} = 150$ °C [12]

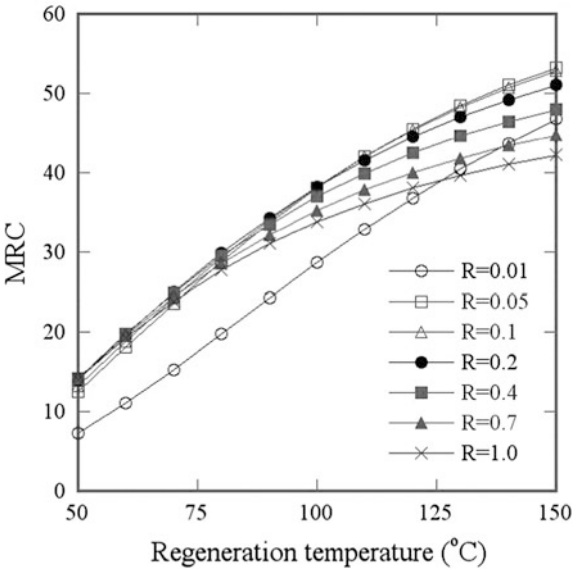

Fig. 2.27 Variations of the MRC for various isotherm shapes and a range of regeneration temperatures from 50 to 150 °C. The MRC is evaluated at the optimal rotation speed and A_r/A_p of each isotherm shape at each regeneration temperature [54]

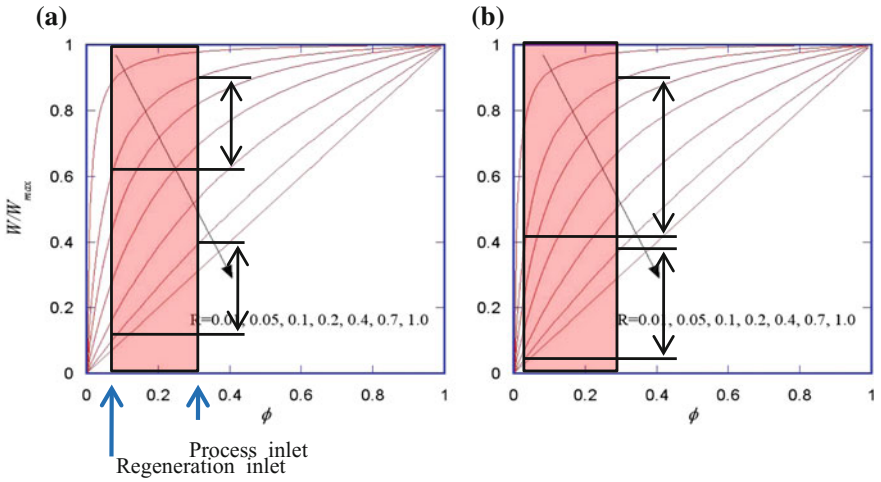

Fig. 2.28 Typical example of water content differences evaluated by the process inlet and regeneration inlet conditions for the isotherm shapes of $R = 0.05$ and $R = 0.7$ at a **a** low regeneration temperature and **b** high regeneration temperature [54]

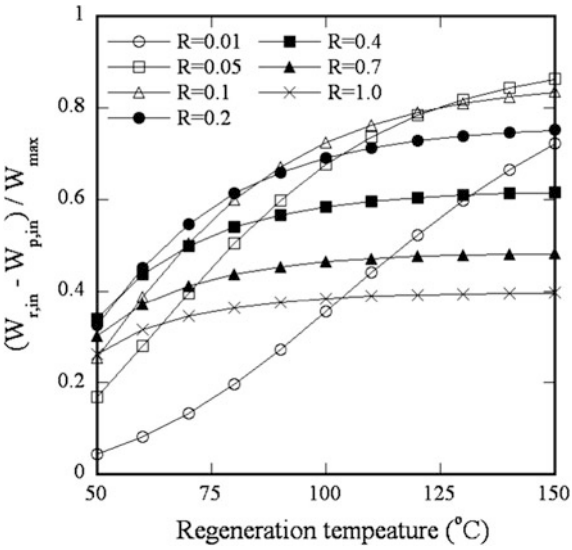

Fig. 2.29 Variations of the water content difference evaluated by the process inlet and regeneration inlet conditions for various isotherm shapes and a range of regeneration temperature from 50 to 150 °C [54]

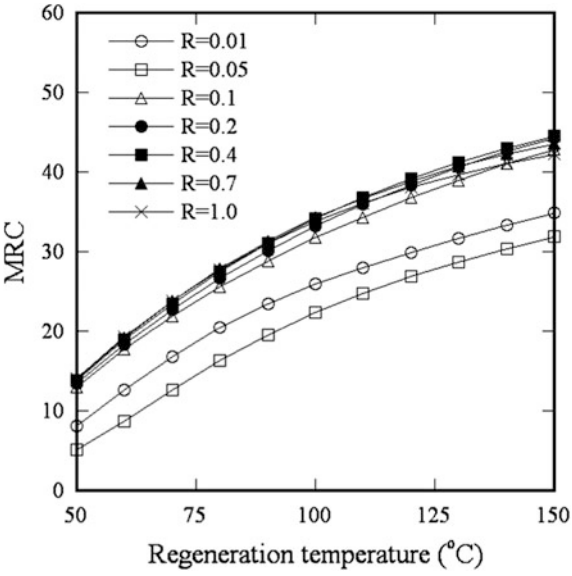

Fig. 2.30 Variations of the MRC for various isotherm shapes and a range of regeneration temperature from 50 to 150 °C. The MRC is evaluated at the optimal rotation speed and A_r/A_p of R = 1.0 at each regeneration temperature [54]

We can also find the sensitivity of the isotherm shape to the design parameters by comparing Figs. 2.15 and 2.16. The variation of optimal rotation speed is much higher than A_r/A_p.

2.3.5 Optimization

The system design of the desiccant cooling system poses a number of questions associated with a single parameter and/or their combinations. These include system components such as the sensible heat exchanger, regenerative evaporative cooler and desiccant wheel, as well as the operating conditions such as the outdoor conditions, regenerative temperature and rate of outdoor influx. The parameters related to the desiccant wheel, such as the wheel speed and the properties of the desiccant material, should be considered.

One of the methods for system optimization is the thermo-economic approach. This exergetic method was applied for the desiccant-evaporative air-conditioning system [65, 66], hybrid system [67, 68] and solar-desiccant air-conditioning system [69]. Enteria et al. [70] compared the different components of exergetic efficiency at the reference conditions of outdoor air.

It is a time-intensive task to examine the contribution of each component of the desiccant system and the contributions of the operating conditions because several parameters are involved in the performance of a desiccant cooling system. Therefore, it is impractical to evaluate each individual case using an exhaustive approach. In the present study, a numerical simulation has been conducted for 11 design parameters with 3 levels. The considered design parameters and its variations (±30% for the properties of the desiccant material and ±10% for the others) are summarized in Table 2.5. It should be noted that the regeneration temperature is set at $T_{10} = 75$, $T_{10} = 60$ °C which is low enough to be acquired from low-density energy resources such as local heating, solar energy and waste heat. The base conditions for the desiccant material are from silica gel. The parameters related to the desiccant material are the mass fraction, heat capacity, density and maximum water uptake. Wheel performance dependency on these parameters is discussed by Chung et al. [40]. Wheel speed is set at 150 s/rev which is near the optimum wheel speed obtained in earlier work [12].

Table 2.5 Base conditions and 3 levels of design parameters employed in the simulations [13]

Factor	Level		
	1 (%)	2 (base condition)	3 (%)
BP	−10	0.3	+10
T_{air} [°C]	−10	35	+10
φ_{air} [%]	−10	40	+10
ε_{SHE} [–]	−10	0.8	+10
ε_{REC} [–]	−10	0.8	+10
T_r [°C]	−30	75	+30
t_p [s]	−30	75	+30
f_d [–]	−30	0.75	+30
$c_{p,d}$ [J kg^{-1}K^{-1}]	−30	921	+30
ρ_d [kg m^{-3}]	−30	720	+30
W_{max} [–]	−30	0.4	+30

Different system configurations have been proposed to achieve high system performance [2]. We confined our interest to only 2 cases in Fig. 2.31. The sensible heat exchanger acts as a pre-cooler after the desiccant and also as a preheater before

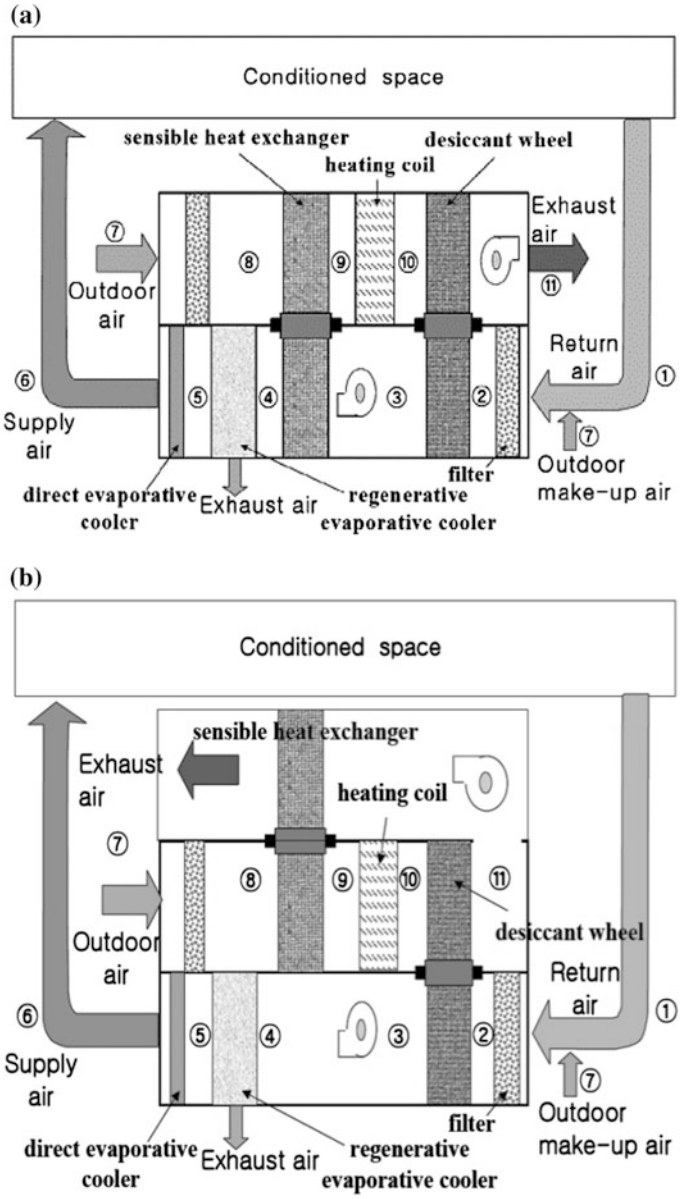

Fig. 2.31 Schematics of the desiccant cooling system in **a** configuration A and **b** configuration B [13]

the regeneration section, which results in enhanced performance of the whole system. Conversely in system configuration B in Fig. 2.31b, the sensible heat exchanger fulfills the role of the preheater before the heating coil, which reduces the required energy for regeneration and results in enhanced performance. The performances of each system are compared. The desired indoor conditions is fixed at $T_1 = 27$ °C and $\phi_1 = 50\%$. The 1:1 split between the regeneration and dehumidification sections of the desiccant wheel is assumed because the present work is focused on low regeneration temperatures.

The cooling performance of the REC can be represented by the cooling effectiveness, which is defined as:

$$\varepsilon_{\mathrm{REC}} = \frac{T_{\mathrm{h,in}} - T_{\mathrm{h,out}}}{T_{\mathrm{h,in}} - D_{\mathrm{h,in}}} \tag{2.31}$$

where $D_{\mathrm{h,in}}$ is the inlet dew point temperature of the process air. It is the lowest outlet temperature that can be achieved in the REC. The base condition for $\varepsilon_{\mathrm{REC}}$ is 0.8.

The performance of the sensible heat exchanger can be evaluated by the following equations:

$$\varepsilon_{\mathrm{SHE}} = \frac{T_9 - T_8}{T_3 - T_8} \quad \text{for system configuration A} \tag{2.32}$$

$$\varepsilon_{\mathrm{SHE}} = \frac{T_9 - T_8}{T_{11} - T_8} \quad \text{for system configuration B} \tag{2.33}$$

The base condition for $\varepsilon_{\mathrm{SHE}}$ is 0.8.

The system performance is the object function for the analysis of variance (ANOVA) and can be evaluated using the amount of cooling capacity per unit air flow rate and/or the COP, which is defined as the ratio of the cooling capacity to the required energy for regeneration.

$$Q = (h_1 - h_6)(1 - BP) \tag{2.34}$$

$$\mathrm{COP} = \frac{Q}{Q_{\mathrm{r}}} \tag{2.35}$$

where the required energy for regeneration is obtained by $Q_{\mathrm{r}} = \dot{m}_{\mathrm{p}}(h_{10} - h_9)\, t_{\mathrm{r}}/t_{\mathrm{p}}$.

The orthogonal array L27 (3^{13}) was adopted for the ANOVA [71] to find the optimal condition for each parameter and give the individual impact ratio of the system performance. The sum of the square is defined as $ST = \sum x_{ij}^2 - (T^2/N)$, where x is the value of the numerical experiment, $T(= \sum x_{ij})$ is the summation of the numerical experiments, and N is the number of numerical experiments. We denote the degree of freedom by ϕ, with the appropriate subscript i (=BP, T_{air}, ϕ_{air}, $\varepsilon_{\mathrm{SHE}}$, $\varepsilon_{\mathrm{REC}}$, T_{r}, t_{p}, f_{d}, $c_{\mathrm{p,d}}$, ρ_{d}, $W_{\max}$), which is defined as the level of factor i minus 1.

The mean square V is obtained by ST/φ. For a given level of significance, if $F_0(= V_i/V_e)$ is greater than the corresponding F-distribution, (i.e., $F(\varphi_i, \varphi_e; \alpha)$), we say that factor i is significant, where α represents the significance level.

If we chose the COP as the indicator of system performance, the results of the ANOVA are summarized in Tables 2.6 and 2.7 for the configurations A and B of the desiccant systems shown in Fig. 2.31. The F_0 values of φ_{air} and ε_{REC} are 3.35 and 2.59, respectively, which is not small enough to be ignored in the case of a significance level of 5%. Therefore, we may consider that the factors φ_{air} and ε_{REC} are also slightly significant. Regardless of the system configuration, the contribution of BP, ε_{SHE} and t_p and the parameters related to the desiccant material such as f_d, $c_{p,d}$, ρ_d and W_{max} are negligible, which may be surprising because it is believed that the desiccant material is one of the dominant factors related to the system performance. Recently, Faust et al. [72] developed a high-powered, SAP-based desiccant that can absorb 4–5 times more water than silica gel or zeolite, which showed clear system performance enhancement. We can conclude that more than ±30% variations of the desiccant material properties are required for the development a new desiccant material to enhance the system performance.

After pooling the contribution of the negligible parameters, the contribution ratio of each factor is re-evaluated. The procedure is summarized in the ANOVA in Tables 2.6 and 2.7, which shows that the factors T_{air}, ϕ_{air}, ε_{REC} and T_r are significant at the 5% level. Note that the values in parentheses are after pooling. The details of the procedure on the ANOVA can be found in Park [71]. The results provide a quantitative estimation of the various design parameters that affect the performance and help to determine the main factors for optimum design of a desiccant cooling system. The regeneration temperature is the most dominant parameter (31.9% for configuration A and 23.9% for system configuration B), and the outdoor conditions play a significant role in the performance of a desiccant cooling system (25.5 and 9% for T_{air} and φ_{air}, respectively, for system configuration A and 20.6 and 8.7% for T_{air} and φ_{air}, respectively, for system configuration B). These results are in line with the results of using the cooling capacity Q as the indicator of system performance. For reference, the results for system configuration A are given in Table 2.8.

If we assume that the errors are normally distributed, the 100(1−α)% confidence interval on the t-distribution is:

$$\bar{y} \pm t\left(\varphi_e; \frac{\alpha}{2}\right)\sqrt{\frac{V_e}{n_e}} \tag{2.36}$$

where φ_e and V_e are the degree of freedom and mean square for error, respectively, and n_e denotes the effective number of replications that can be obtained from the relationship as is calculated as follows:

Table 2.6 ANOVA for system configuration A when the COP is chosen as the indicator of system performance [13]

	BP	T_{air}	φ_{air}	ε_{SHE}	ε_{REC}	T_r	t_p	f_d	$c_{p,d}$	ρ_d	W_{max}	e
Sum of squares	0.01724	0.33964	0.13678	0.00131	0.10569	0.41927	0.01921	0.01930	0.05303	0.00610	0.03354	0.08172(0.23145)
Degree of freedom	2	2	2	2	2	2	2	2	2	2	2	4(18)
Mean square	0.00862	0.16982	0.06839	0.00065	0.05284	0.20964	0.00960	0.00965	0.02652	0.00305	0.01677	0.02043(0.012858)
F_0 (before pooling)	0.42193	8.31197	3.3474	0.03199	2.58648	10.26078	0.47007	0.47226	1.29790	0.14927	0.82081	
F_0 (after pooling)		13.2069	5.31877		4.10972	16.30360						
Contribution ratio		0.255	0.09		0.065	0.319						0.271

Table 2.7 ANOVA for system configuration B when the COP is chosen as the indicator of system performance [13]

	BP	T_{air}	φ_{air}	ε_{SHE}	ε_{REC}	T_r	t_p	f_d	$c_{p,d}$	ρ_d	W_{max}	e
Sum of squares	0.02027	0.28244	0.13621	0.03634	0.22273	0.32192	0.02512	0.00851	0.07827	0.03255	0.02632	0.03591 (0.26329)
Degree of freedom	2	2	2	2	2	2	2	2	2	2	2	4(18)
Mean square	0.01014	0.14122	0.06810	0.01817	0.11136	0.16096	0.01256	0.00426	0.03914	0.01627	0.01316	0.00898 (0.14627)
F_0 (before pooling)	1.12888	15.72880	7.585232	2.023568	12.40336	17.92703	1.39873	0.47391	4.358865	1.812563	1.46586	
F_0 (after pooling)		9.654592	4.6559381		7.613386	11.00390						
Contribution ratio		0.206	0.087		0.158	0.239						0.310

Table 2.8 ANOVA for system configuration A when Q is chosen as the indicator of system performance [13]

	BP	T_{air}	RH_{air}	ε_{SHE}	ε_{REC}	T_{reg}	τ_{pro}	f_d	$c_{p,d}$	ρ_d	W_{max}	e
Sum of squares	8.33292	337.44301	98.83324	5.03098	88.22058	749.5578	8.44539	28.60372	2.39312	14.2557	11.3134	19.22886(97.60410)
Degree of freedom	2	2	2	2	2	2	2	2	2	2	2	4(18)
Mean square	4.1665	168.7215	49.4166	2.5155	44.1103	374.7789	4.2227	14.3019	1.1966	7.1279	5.6567	4.8072(5.42245)
F_0 (before pooling)	0.8667	35.0976	10.2797	0.52327	9.1759	77.9617	0.8784	2.9751	0.2489	1.4827	1.1767	
F_0 (after pooling)		31.1154	9.11334		8.13475	69.1162						
Contribution ratio		0.238	0.064		0.056	0.539						0.103

$$n_e = \frac{n}{\sum \varphi_i + 1} \tag{2.37}$$

The optimum levels of the significant factors in system configuration A that maximize the COP are $T_{air,1}$, $\phi_{air,1}$, $\varepsilon_{REC,3}$ and $T_{r,1}$. Note that the estimated COP at the optimum conditions is 0.9896 within the confidence internal 1.0374 ± 0.1375. The optimum levels of the significant factors in system configuration B are same as system configuration A, and the estimated COP at the optimum conditions is 1.28577, which is also within the confidence internal 1.2042 ± 0.1467.

To focus on the application of a district cooling system to utilize the over-supplied heat in summer season or a solar system using medium-temperature collectors, the regeneration temperature is fixed at a typical value of 75 °C. Additionally, the outdoor conditions are also fixed at $T_7 = 35$ °C and $\varphi_7 = 40\%$, which are the typical summer conditions in Korea. For system configuration A, only the contributions of ε_{REC},t_p,f_d and ρ_d are meaningful. The most dominant parameter is ε_{REC}, whose contribution ratio to the system performance is 32.5%. General trends of the wheel parameters f_d and ρ_d are similar to earlier research by Chung et al. [40]; however, the analysis in Chung et al. [40] is confined to only wheel performance, i.e., the wheel performance is increased as f_d and ρ_d increase.

Contrary to system configuration A, the sensible heat exchanger plays a significant role in system configuration B, whose contribution ratio is estimated to be as high as 16.9%. The impact of the cooling performance of REC is also the most crucial factor in this configuration. This suggests that further research attention on regenerative evaporative cooler should be given to enhance the system performance. In this system configuration, the general trends of the wheel parameters f_d, $c_{p,d}$ and ρ_d are also similar to earlier research by Chung et al. [40].

2.4 Conclusions

Despite the advantage of being an eco-friendly refrigeration system driven by low-grade waste heat and separate control of sensible and latent cooling, widespread use of desiccant cooling systems is impaired by their relatively large size and low system performance. Numerous studies have focused on various aspects of the desiccant system, particularly the desiccant wheel, which is the most crucial component to enhance the system performance.

Mathematical modeling is a convenient approach to performing parametric research and optimization analysis of desiccant wheels with less time and cost than experimental methods. In addition, mathematical modeling can also provide the fundamental physics and intuition to develop new hybrid systems. However, mathematical modeling of desiccant wheels is a difficult task because the heat and mass transfer are coupled and too complicated to completely understand. Several mathematical models have been constructed and employed to analyze, develop and

design desiccant wheels. In this work, a brief review of mathematical modeling for the desiccant wheel is examined, and some typical issues, such as (i) channel geometry, (ii) adsorbent, (iii) isotherm, (iv) wheel speed, (v) regeneration temperature, (vi) area ratio of the regeneration to dehumidification section, (vii) sensitivity to outdoor weather conditions and (viii) optimizing the components of the desiccant system, are examined. The results of the case studies are also discussed.

Although significant advances have been made, in addition to the research issues mentioned above, the issues of newly developed hybrid system and new adsorbents still remain in the reliable and practical application of desiccant systems.

References

1. Mazzei P, Minichiello F, Palma D (2005) HVAC dehumidification systems for thermal comfort: a critical review. Appl Therm Eng 25:677–707. doi:10.1016/j.applthermaleng.2004.07.014
2. Jani DB, Mishra M, Sahoo PK (2016) Solid desiccant air conditioning—a state of the art review. Renew Sustain Energy Rev 60:1451–1469. doi:10.1016/j.rser.2016.03.031
3. Mavroudaki P, Beggs CB, Sleigh PA, Halliday SP (2002) The potential for solar powered single-stage desiccant cooling in southern Europe. Appl Therm Eng 22:1129–1140. doi:10.1016/S1359-4311(02)00034-0
4. Halliday S, Beggs C, Sleigh P (2002) The use of solar desiccant cooling in the UK: a feasibility study. Appl Therm Eng 22:1327–1338. doi:10.1016/S1359-4311(02)00052-2
5. Hong SW, Kwon OK, Chung JD (2016) Application of an embossed plate heat exchanger to adsorption chiller. Int J Refrig 65:142–153. doi:10.1016/j.ijrefrig.2016.02.012
6. Dai Y, Wang R, Zhang H, Yu J (2001) Use of liquid desiccant cooling to improve the performance of vapor compression air conditioning. Appl Therm Eng 21:1185–1202. doi:10.1016/S1359-4311(01)00002-3
7. Mazzei P, Minichiello F, Palma D (2002) Desiccant HVAC systems for commercial buildings. Appl Therm Eng 22:545–560. doi:10.1016/S1359-4311(01)00096-5
8. George OGL, Gerald C, Thomas B (1988) Performance of a solar desiccant cooling system. J Sol Energy Eng 110:165–171
9. Collier RKCB (1991) An analytic investigation of methods for improving the performance of desiccant cooling system. ASME J Sol Energy Sci Eng 113:157–163
10. Zheng W, Worek WM, Novosel D (1995) Performance optimization of rotary dehumidifiers. J Sol Energy Eng 117:40–44
11. Dai YJ, Wang RZ, Zhang HF (2001) Parameter analysis to improve rotary desiccant dehumidification using a mathematical model. Int J Therm Sci 40:400–408. doi:10.1016/S1290-0729(01)01224-8
12. Chung JD, Lee D-YY, Yoon SM (2009) Optimization of desiccant wheel speed and area ratio of regeneration to dehumidification as a function of regeneration temperature. Sol Energy 83:625–635. doi:10.1016/j.solener.2008.10.011
13. Chung JD, Lee DY (2011) Contributions of system components and operating conditions to the performance of desiccant cooling systems. Int J Refrig 34:922–927. doi:10.1016/j.ijrefrig.2011.03.003
14. Kodama A, Hirayama T, Goto M, Hirose T, Critoph RE (2001) The use of psychrometric charts for the optimisation of a thermal swing desiccant wheel. Appl Therm Eng 21:1657–1674. doi:10.1016/S1359-4311(01)00032-1
15. Cui Q, Chen H, Tao G, Yao H (2005) Performance study of new adsorbent for solid desiccant cooling. Energy 30:273–279. doi:10.1016/j.energy.2004.05.006

16. Jia CX, Dai YJ, Wu JY, Wang RZ (2006) Experimental comparison of two honeycombed desiccant wheels fabricated with silica gel and composite desiccant material. Energy Convers Manage 47:2523–2534. doi:10.1016/j.enconman.2005.10.034
17. White SD, Goldsworthy M, Reece R, Spillmann T, Gorur A, Lee DY (2011) Characterization of desiccant wheels with alternative materials at low regeneration temperatures. Int J Refrig 1786–1791
18. Hong SW, Ahn SH, Chung JD, Bae KJ, Cha DA, Kwon OK (2016) Characteristics of FAM-Z01compared to silica gels in the performance of an adsorption bed. Appl Therm Eng 104:24–33. doi:10.1016/j.applthermaleng.2016.05.058
19. Mittal V, Khan BK (2010) Experimental investigation on desiccant air-conditioning system in India. Front Energy Power Eng China 4:161–165. doi:10.1007/s11708-009-0070-5
20. Zheng W, Worek WM (1993) Numerical simulation of combined heat and mass transfer processes in a rotary dehumidifier. Numer Heat Transf Part A Appl 23:211–232. doi:10.1080/10407789308913669
21. Zhang LZ, Niu JL (2002) Performance comparisons of desiccant wheels for air dehumidification and enthalpy recovery. Appl Therm Eng 22:1347–1367. doi:10.1016/S1359-4311(02)00050-9
22. Zhang XJ, Dai YJ, Wang RZ (2003) A simulation study of heat and mass transfer in a honeycombed rotary desiccant dehumidifier. Appl Therm Eng 23:989–1003. doi:10.1016/S1359-4311(03)00047-4
23. Ahmed MHH, Kattab NMM, Fouad M (2005) Evaluation and optimization of solar desiccant wheel performance. Renew Energy 30:305–325. doi:10.1016/j.renene.2004.04.010
24. Liu Y, Wang R (2003) Pore structure of new composite adsorbent SiO2·xH2O·yCaCl2 with high uptake of water from air. Sci China Ser E: Technol Sci 46:551–559. doi:10.1360/02ye0480
25. Maclaine-cross IL (1985) High-performance adiabatic desiccant open-cooling cycles. J Sol Energy Eng 107:102–104
26. Henning HM (2007) Solar assisted air conditioning of buildings—an overview. Appl Therm Eng 27:1734–1749. doi:10.1016/j.applthermaleng.2006.07.021
27. Worek WM, Zheng W, Belding WA, Novosel D, Holeman WD (1991) Simulation of advanced gas-fired desiccant cooling systems. Ashrae Trans 4:609–614
28. Ge TS, Li Y, Wang RZ, Dai YJ (2008) A review of the mathematical models for predicting rotary desiccant wheel. Renew Sustain Energy Rev 12:1485–1528. doi:10.1016/j.rser.2007.01.012
29. Charoensupaya D, Worek WM (1988) Parametric study of an open-cycle adiabatic, solid, desiccant cooling system. Energy 13:739–747. doi:10.1016/0360-5442(88)90106-5
30. Sphaier LA, Worek WM (2006) Comparisons between 2-D and 1-D Formulations of Heat and Mass Transfer in Rotary Regenerators. Numer Heat Transf Part B Fundam 49:223–237. doi:10.1080/10407790500434166
31. Ahn SH, Hong SW, Kwon OK, Chung JD (2013) Validity of inter-particle models for the mass transfer kinetics of a fin tube type adsorption bed. Korea J Air-Conditioning Refrig Eng 25:660–667
32. Hong SW, Ahn SH, Kwon OK, Chung JD (2014) Validity of intra-particle models of mass transfer kinetics in the analysis of a fin-tube type adsorption bed. J Mech Sci Technol 28:1985–1993. doi:10.1007/s12206-014-0347-4
33. Yamamoto E, Katsurayama K, Watanabe F, Matsuda H, Hasatani M (2000) Heat and mass transfer characteristics in adsorption of water vapor for silica gel packed bed adsorber. J Chem Eng Jpn 33:12–18. doi:10.1252/jcej.33.12
34. Watanabe F, Watabe Y, Katsuyama H, Kozuka J, Hasatani M, Marumo C (1993) Heat transfer accompanied by adsorption/desorption of water vapour in adsorption heat pump of packed bed type. Kagaku Kogaku Ronbunshu 19:83–90. doi:10.1252/kakoronbunshu.19.83
35. Li J, Kubota M, Watanabe F, Kobayashi N, Hasatani M (2004) Optimal design of a fin-type silica gel tube module in the silica gel/water adsorption heat pump. J Chem Eng Jpn 37:551–557. doi:10.1252/jcej.37.551

36. Yadav A, Bajpai VK (2011) Optimization of operating parameters of desiccant wheel for rotation speed. Int J Adv Sci Techno 32:109–116
37. Gao Z, Mei VC, Tomlinson JJ (2005) Theoretical analysis of dehumidification process in a desiccant wheel. Heat Mass Transf 41:1033–1042. doi:10.1007/s00231-005-0663-4
38. Zhang LZ, Niu JL (2001) A numerical study of laminar forced convection in sinusoidal ducts with arc lower boundaries under uniform wall temperature. Numer Heat Transf Part A Appl 40:55–72. doi:10.1080/10407780117998
39. Al-Sharqawi HS, Lior N (2008) Effect of flow-duct geometry on solid desiccant dehumidification. Ind Eng Chem Res 47:1569–1585. doi:10.1021/ie0707319
40. Chung DJ, Lee D, Yoon SM (2010) Effect of parameters related to channel and desiccant on the size of desiccant rotor. Int J Air-Conditioning Refrig 18:201–211. doi:10.1142/S2010132510000125
41. Llano-Restrepo M, Mosquera MA (2009) Accurate correlation, thermochemistry, and structural interpretation of equilibrium adsorption isotherms of water vapor in zeolite 3A by means of a generalized statistical thermodynamic adsorption model. Fluid Phase Equilib 283:73–88. doi:10.1016/j.fluid.2009.06.003
42. Eicker U, Schürger U, Köhler M, Ge T, Dai Y, Li H, Wang R (2012) Experimental investigations on desiccant wheels. Appl Therm Eng 42:71–80. doi:10.1016/j.applthermaleng.2012.03.005
43. Kim YD, Thu K, Ng KC (2014) Adsorption characteristics of water vapor on ferroaluminophosphate for desalination cycle. Desalination 344:350–356. doi:10.1016/j.desal.2014.04.009
44. Saha BB, El-Sharkawy II, Chakraborty A, Koyama S (2007) Study on an activated carbon fiber-ethanol adsorption chiller: part I—system description and modelling. Int J Refrig 30:86–95. doi:10.1016/j.ijrefrig.2006.08.004
45. Li A, Bin Ismail A, Thu K, Ng KC, Loh WS (2014) Performance evaluation of a zeolite–water adsorption chiller with entropy analysis of thermodynamic insight. Appl Energy 130:702–711. doi:10.1016/j.apenergy.2014.01.086
46. Collier RK, Cale TS, Lavan Z (1986) Advanced desiccant materials assessment. Final report, February 1985–May 1986. United States
47. Banks PJ (1985) Prediction of heat and mass regenerator performance using nonlinear analogy method: part 2—comparison of methods. J Heat Transf 107:230–238
48. Banks PJ (1985) Prediction of Heat and Mass Regenerator Performance Using Nonlinear Analogy Method: Part 1—Basis. J Heat Transfer 107:222–229
49. Lee G, Lee D-Y, Kim MS (2004) Development of a linearized model and verification of the exact solution for the analysis of a desiccant dehumidifier. J Air-Conditioning Refrig Eng 811–819
50. Kim D, Choi Y, Lee D (2011) Development of a simple analytical model for desiccant wheels-I. Approximate solution of the governing equations. Korean J Air-Conditioning Refrig Eng 23:821–827
51. Lee DY, Kim DS (2014) Analytical modeling of a desiccant wheel. Int J Refrig 42:97–111. doi:10.1016/j.ijrefrig.2014.02.003
52. Cejudo J, Moreno R, Carrillo A (2002) Physical and neural network models of a silica-gel desiccant wheel. Energy Build 34:837–844. doi:10.1016/S0378-7788(02)00100-7
53. Golubovic MN, Worek WM (2004) Influence of elevated pressure on sorption in desiccant wheels. Numer Heat Transf Part A Appl 45:869–886. doi:10.1080/10407780490439068
54. Chung JD, Lee D-Y (2009) Effect of desiccant isotherm on the performance of desiccant wheel. Int J Refrig 32:720–726. doi:10.1016/j.ijrefrig.2009.01.003
55. Ruivo CR, Costa JJ, Figueiredo AR (2006) Analysis of simplifying assumptions for the numerical modeling of the heat and mass transfer in a porous desiccant medium. Numer Heat Transf Part A Appl 49:851–872. doi:10.1080/10407780500483552
56. Ruivo CR, Costa JJ, Figueiredo AR (2008) On the validity of lumped capacitance approaches for the numerical prediction of heat and mass transfer in desiccant airflow systems. Int J Therm Sci 47:282–292. doi:10.1016/j.ijthermalsci.2007.01.032

57. Sphaier LA, Worek WM (2004) Analysis of heat and mass transfer in porous sorbents used in rotary regenerators. Int J Heat Mass Transf 47:3415–3430. doi:10.1016/j.ijheatmasstransfer.2004.01.016
58. Pesaran AA, Mills A (1984) Modeling of solid-side transfer in desiccant particle beds. In: Proceedings of 6th Annual ASME Solar Energy Division Conference. New York
59. Harshe YM, Utikar RP, Ranade VV, Pahwa D (2005) Modeling of rotary desiccant wheels. Chem Eng Technol 28:1473–1479. doi:10.1002/ceat.200500164
60. Pesaran AA, Mills AF (1987) Moisture transport in silica gel packed beds—I. Theoretical study. Int J Heat Mass Transf 30:1037–1049. doi:10.1016/0017-9310(87)90034-2
61. Pesaran AA (1983) Moisture transport in silica gel particle beds. [DESSICANT]. University of California, Los Angeles
62. Kakaç S, Shah RK, Aung W (1987) Handbook of single-phase convective heat transfer. Wiley, New York
63. ASHRAE (1998) Standard 139-1998. Method of testing for rating desiccant dehumidifiers utilizing heat for the regeneration process. ASHARAE, Inc, Atlanta
64. Simonson CJ, Besant RW (1999) Energy wheel effectiveness: part II—correlations. Int J Heat Mass Transf 42:2171–2185. doi:10.1016/S0017-9310(98)00327-5
65. Kanoğlu M, Özdinç Çarpınlıoğlu M, Yıldırım M (2004) Energy and exergy analyses of an experimental open-cycle desiccant cooling system. Appl Therm Eng 24:919–932. doi:10.1016/j.applthermaleng.2003.10.003
66. La D, Li Y, Dai YJ, Ge TS, Wang RZ (2012) Development of a novel rotary desiccant cooling cycle with isothermal dehumidification and regenerative evaporative cooling using thermodynamic analysis method. Energy 44:778–791. doi:10.1016/j.energy.2012.05.016
67. Pons M, Kodama A (2000) Entropic analysis of adsorption open cycles for air conditioning. Part 1: first and second law analyses. Fuel Energy Abstr 41:321. doi:http://dx.doi.org/10.1016/S0140-6701(00)96820-6
68. Hürdoğan E, Buyükalaca O, Hepbasli A, Yılmaz T (2011) Exergetic modeling and experimental performance assessment of a novel desiccant cooling system. Energy Build 43:1489–1498. doi:10.1016/j.enbuild.2011.02.016
69. Enteria N, Yoshino H, Takaki R, Mochida A, Satake A, Yoshie R (2013) Effect of regeneration temperatures in the exergetic performances of the developed desiccant-evaporative air-conditioning system. Int J Refrig 36:2323–2342. doi:10.1016/j.ijrefrig.2013.08.005
70. Enteria N, Yoshino H, Mochida A, Satake A, Takaki R (2015) Exergoeconomic performances of the desiccant-evaporative air-conditioning system at different regeneration and reference temperatures. Int J Refrig 56:81–98. doi:10.1016/j.ijrefrig.2014.11.007
71. Park SH (1996) Robust design and analysis for quality engineering. Chapman & Hall, London
72. Faust S, Guido F, Lee D (2007) Desiccant element and manufacturing method of the same. Korea Patent 0704235

Chapter 3
Simplified Models for the Evaluation of Desiccant Wheels Performance

Stefano De Antonellis and Cesare Maria Joppolo

Abstract At present interest in building HVAC (Heating, Ventilating and Air Conditioning) systems based on a desiccant wheel is increasing, due to the possibility of realizing high-energy-efficiency systems and of integrating renewable energy sources. The design of air handling units based on this technology is quite complex because of the difficulties in predicting the performance of the desiccant wheel, which is the crucial component of the system. In fact, desiccant wheel performance strongly depends on inlet airflow conditions and on the revolution speed. As a consequence, in HVAC systems, practitioners and engineers mainly prefer to adopt conventional cooling and heating coils, which are well-known components. In this context, the purpose of this chapter is to review and analyse the main simplified models available in literature to calculate desiccant wheels performance. Such correlations can be easily used in worksheets or in energy simulation programs, being a useful tool to compare desiccant wheel-based HVAC systems with conventional configurations.

Keywords Desiccant wheel · Correlation · Model · Practitioner · Engineer

Nomenclature

A	Desiccant wheel face area (m^2)
cp	Specific isobaric heat (kJ kg^{-1} K^{-1})
D_W	Desiccant wheel diameter (m)
F_{1-2}	Combined potential
h	Specific enthalpy (kJ kg^{-1})
L_W	Desiccant wheel thickness (m)
MRC	Moisture removal capacity (kg_v h^{-1})
N	Revolution speed (rev h^{-1})

S. De Antonellis (✉) · C.M. Joppolo
Dipartimento di Energia, Politecnico di Milano,
Via Lambruschini, 4, 20156 Milan, Italy
e-mail: stefano.deantonellis@polimi.it

N. Enteria et al. (eds.), *Desiccant Heating, Ventilating, and Air-Conditioning Systems*, DOI 10.1007/978-981-10-3047-5_3

p Pressure (Pa)
T Temperature (°C)
v Face velocity (m s^{-1})
$\dot{V}$ Volumetric flow (m^3 h^{-1})
W_{ads} Adsorption capacity (kg kg^{-1})
X Humidity ratio (kg kg^{-1})

Greek symbols

Δp Pressure drop (Pa)
ρ Density (kg m^{-3})
λ Latent heat of vaporization (kJ kg^{-1})
μ Dynamic viscosity (kg m^{-1} s^{-1})
ϕ $P_v/p_{v,sat}$ (–)
η Effectiveness parameter (–)
Ω Specific mass airflow rate (kg s^{-1} m^{-3})

Subscript

a Air
in Inlet
out Outlet
pro Process
reg Regeneration
sat At saturation
v Water vapour
w Adsorbed water
tot Total

Acronyms

HVAC Heating, Ventilating and Air Conditioning
ID Intermediate Density
RD Regular density

3.1 Introduction

At present interest in building HVAC systems based on a desiccant wheel is increasing, due to the possibility of realizing high-energy-efficiency cooling systems and of integrating renewable energy sources, as clearly discussed in many review papers [1–3]. Such technology can be effectively used in air-conditioning

applications for air dehumidification [4–7] and humidification [8–10] purposes or in the industrial field for product drying [11–15].

The design of air handling units based on this technology is quite complex because of the difficulties in predicting the performance of the desiccant wheel, which is the crucial component of the system [16]. In fact, desiccant wheel performance strongly depends on inlet airflow conditions and on the revolution speed. Many research works deal with the development of detailed desiccant wheels models based on a phenomenological approach [17]. Such models are accurate and particularly suitable for component design and development, but they are not suggested for the simulation of energy systems, due to their high computational load and complexity. Therefore, practical correlations have been developed by several authors [18–25], in order to evaluate desiccant wheel performance through simplified approaches. Anyway, these methods have not been resumed in practical handbooks and their use is mainly delimited to academic personnel working on energy systems simulation.

As a consequence, in HVAC systems practitioners and engineers mainly prefer to adopt conventional cooling and heating coils, which are well-known components. The use of desiccant wheels is considered only in limited cases, requesting direct support to the manufacturer's ore using available commercial tools [17, 26–28].

Based on the aforementioned considerations, in this chapter main simplified models available in literature to calculate desiccant wheels performance are reported and described. A preliminary analysis of desiccant wheels performance and about the influence of working conditions is performed, in order to make practitioners more familiar with such components.

The investigated correlations can be easily used in worksheets or in energy simulation programs, being a useful tool to compare desiccant wheel-based HVAC systems with conventional air handling units.

3.2 Desiccant Wheel Description

A desiccant wheel is a cylindrical rotating device, which is manufactured rolling up sheets of a supporting material impregnated with an adsorbent substance, in order to get many parallel channels with almost a sinusoidal or triangular cross section. Most diffused support materials are paper, aluminium, synthetic fibres or plastic while common adsorbents are silica gel, zeolite and activated alumina.

As shown in Fig. 3.1, the desiccant wheel face area is divided into two parts: two air streams, namely the process and the regeneration flow, pass through the cross-sectional area of the device in counter current arrangement. The ratio between the process and the regeneration airflow face area (A_{pro}/A_{reg}) can be lower, equal or higher than one. The arrangement mainly depends on the regeneration air temperature: the higher the regeneration temperature, the higher A_{pro}/A_{reg}.

Each channel of the device is alternatively crossed by the process and the regeneration airflow: depending on wheel technical specifications and boundary

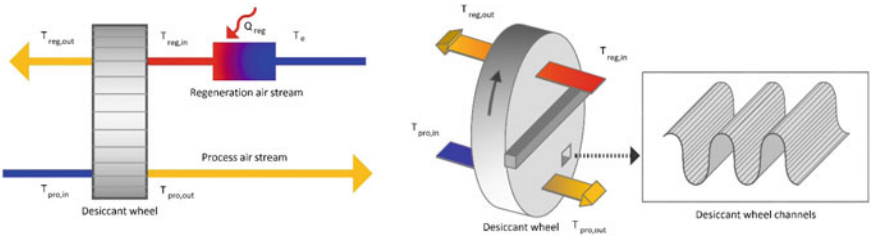

Fig. 3.1 Desiccant wheel scheme

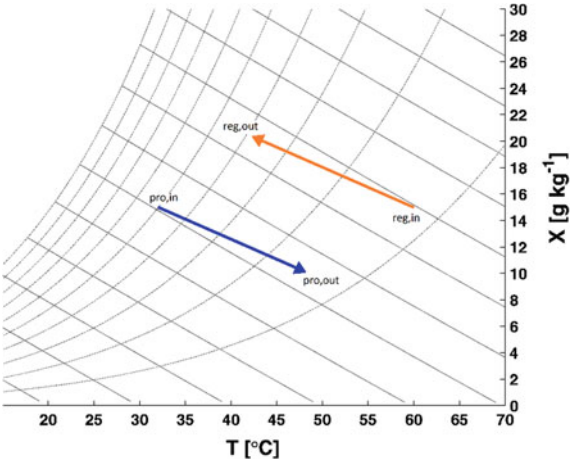

Fig. 3.2 Process and regeneration air transformation in the psychrometric chart

conditions, the wheel is continuously rotated by an electric motor at a revolution speed N generally between 5 and 90 rev h^{-1}.

The process air stream, which is supplied to the building, is dehumidified and heated while the regeneration one, which is used to remove vapour from the desiccant material, is cooled and humidified (Fig. 3.2). The regeneration airflow is generally heated before it crosses the wheel, in order to reduce its relative humidity and to be able to remove water from the sorption material of the device.

Typical desiccant wheel diameter D_W varies between 30 cm and 2 m, while its thickness L_W ranges between 5 and 40 cm. The regeneration air temperature is around 50 °C in case of low temperature configurations, and it increases up to 150–200 °C in conventional direct fired applications.

3.3 Desiccant Wheel Performance

Performance of a specific desiccant wheel strongly depends on operating conditions. In particular, the moisture removal capacity $\left(\mathrm{MRC} = \dot{V}_{\mathrm{pro,in}}\rho_{\mathrm{pro,in}}\left(X_{\mathrm{pro,in}} - X_{\mathrm{pro,out}}\right)\right)$ of the device is directly related to the properties of the sorption material. As shown in

Fig. 3.3, at equilibrium conditions and constant temperature, the higher the air relative humidity (or vapour partial pressure), the higher the capability of the sorption material to adsorb water and vice versa. Each desiccant wheel channel is alternatively in contact with the two air streams. During the process air period, the sorption material increases its water content: the maximum amount of vapour it can adsorb at equilibrium conditions is directly related to the relative humidity and temperature of the inlet process air stream. For instance, according to Fig. 3.3, in case of silica gel RD, $W_{ads,max}$ is equal to 0.35 $kg_w\ kg_{ads}^{-1}$ when $T_{pro,in}$ = 30 °C (temperature of the adsorption isotherm) and $\phi_{pro,in}$ = 70%. Similarly, during the regeneration air period, the lower the air relative humidity, the more effective is the material regeneration and, as a consequence, the dehumidification capacity of the wheel. It is highlighted that the aim of such preliminary and simplified considerations is to provide basic concepts to practitioners, in order to understand desiccant wheel performance and to effectively use the simplified models discussed in this chapter. A detailed analysis of phenomena occurring in a desiccant wheel is not the scope of this work.

As already reported, desiccant wheel dehumidification capacity is significantly influenced by working conditions. In Figs. 3.4, 3.5, 3.6, 3.7, 3.8 and 3.9, it is analysed how each boundary condition affects the outlet process air humidity ratio and temperature. The investigation is performed through a numerical model based on heat and mass transfer equations, previously developed [16] and calibrated [8]. The model reproduces performance of a commercial desiccant wheel made of synthesized metal silicate on inorganic fibre substrate, with D_W = 0.6 m, L_W = 0.2 m and face area split in two equal sections.

The parametric analysis is carried out considering a reference case, characterized by the following conditions:

Equal regeneration and process desiccant wheel area (A_{pro}/A_{reg} = 1). Inlet process airflow conditions equal to $T_{pro,in}$ = 32 °C and $X_{pro,in}$ = 15 g kg^{-1}.

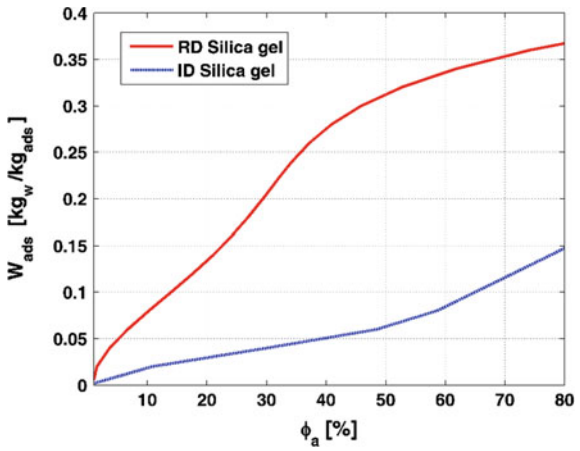

Fig. 3.3 Adsorption isotherm of different sorption materials at 30 °C [29]

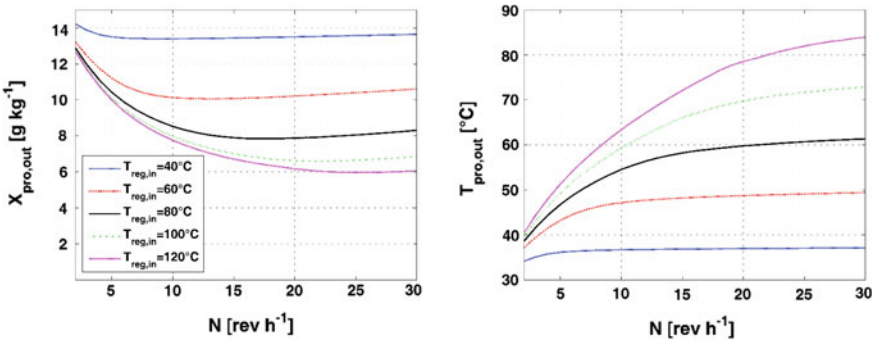

Fig. 3.4 Effect of regeneration air inlet temperature and revolution speed on process air outlet conditions ($T_{pro,in}$ = 32 °C, $X_{pro,in}$ = $X_{reg,in}$ = 15 g kg^{-1}, $v_{pro,in}$ = $v_{reg,in}$ = 2 m s^{-1})

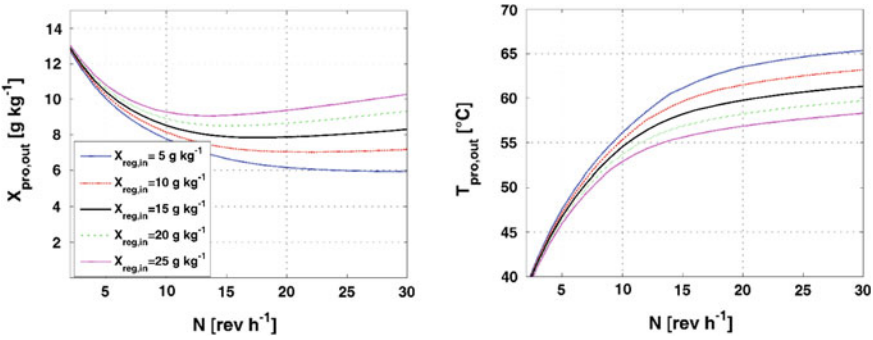

Fig. 3.5 Effect of regeneration air inlet humidity ratio and revolution speed on process air outlet conditions ($T_{pro,in}$ = 32 °C, $T_{reg,in}$ = 80 °C, $X_{pro,in}$ = 15 g kg^{-1}, $v_{pro,in}$ = $v_{reg,in}$ = 2 m s^{-1})

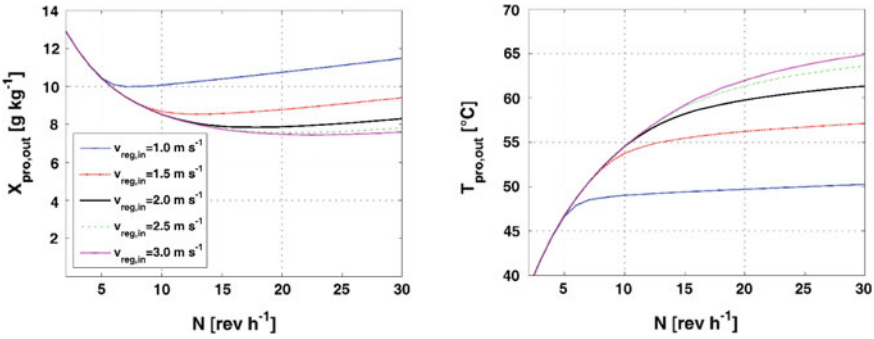

Fig. 3.6 Effect of regeneration air inlet velocity and revolution speed on process air outlet conditions ($T_{pro,in}$ = 32 °C, $T_{reg,in}$ = 80 °C, $X_{pro,in}$ = $X_{reg,in}$ = 15 g kg^{-1}, $v_{pro,in}$ = 2 m s^{-1})

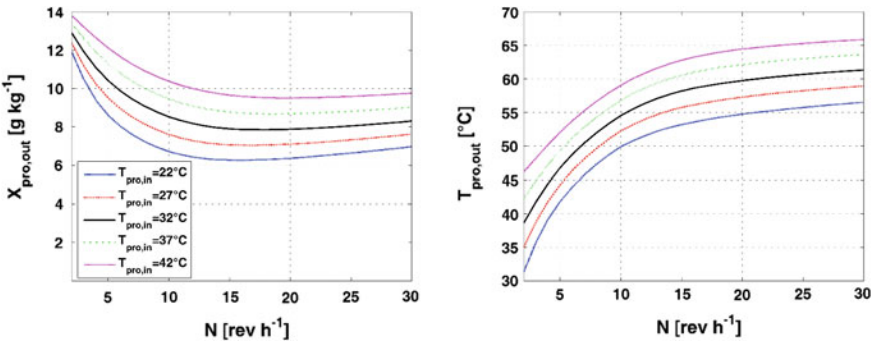

Fig. 3.7 Effect of process air inlet temperature and revolution speed on process air outlet conditions ($T_{reg,in}$ = 80 °C, $X_{pro,in}$ = $X_{reg,in}$ = 15 g kg^{-1}, $v_{pro,in}$ = $v_{reg,in}$ = 2 m s^{-1})

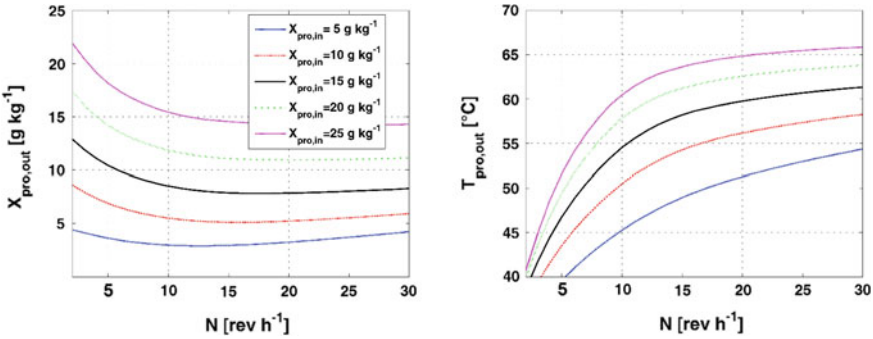

Fig. 3.8 Effect of process air inlet humidity ratio and revolution speed on process air outlet conditions ($T_{pro,in}$ = 32 °C, $T_{reg,in}$ = 80 °C, $X_{reg,in}$ = 15 g kg^{-1}, $v_{pro,in}$ = $v_{reg,in}$ = 2 m s^{-1})

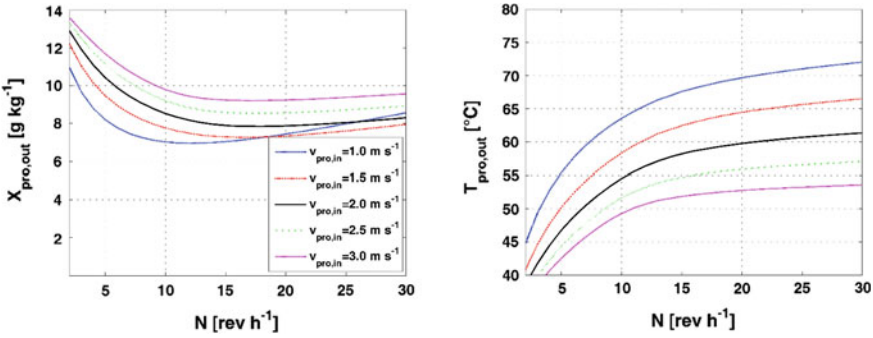

Fig. 3.9 Effect of process air inlet velocity and revolution speed on process air outlet conditions ($T_{pro,in}$ = 32 °C, $T_{reg,in}$ = 80 °C, $X_{pro,in}$ = $X_{reg,in}$ = 15 g kg^{-1}, $v_{reg,in}$ = 2 m s^{-1})

– Inlet regeneration airflow conditions equal to $T_{reg,in}$ = 80 °C and $X_{reg,in}$ = 15 g kg^{-1}.
– Process and regeneration air face velocity equal to $v_{pro,in} = v_{reg,in}$ = 2 m s^{-1}.

Each one of these parameters is independently varied and outlet process air conditions are analysed at different revolution speeds.

Figure 3.4 shows the effect of the variation of the regeneration air temperature on outlet process air humidity ratio and temperature. The higher the regeneration temperature, the higher the dehumidification capacity and, therefore, the lower $X_{pro,out}$. In fact, the regeneration process is more effective (lower inlet air relative humidity) and the sorption material can adsorb more vapour during the process period. In addition, an increase in $T_{reg,in}$ leads to an increase to $T_{pro,out}$ due to higher sensible heat transferred by the wheel matrix and the higher amount of heat of adsorption released in the dehumidification process. Finally, it is highlighted that the higher the $T_{reg,in}$, the higher the optimal revolution speed: in fact, in this case the matrix regeneration is completed faster and each channel should pass to the process period in a shorter time.

Similar effects are shown when $X_{reg,in}$ is varied: in Fig. 3.5, it is put in evidence that the lower the humidity ratio (and therefore the inlet relative humidity at constant temperature), the higher the dehumidification capacity. In this case, an increase in $X_{reg,in}$ leads to an increase in $T_{pro,out}$ mainly due to the higher amount of heat of adsorption released in the dehumidification process, which is more effective.

In Fig. 3.6, the effect of the variation of the regeneration air face velocity is shown. Due to the aforementioned considerations, an increase in $v_{reg,in}$ leads to an increase in the dehumidification capacity, in the outlet process air temperature and in the optimal revolution speed. Anyway, a significant increase in the air velocity (in the investigated case if $v_{reg,in} > 2.5$ m s^{-1}) does not improve the moisture removal from the sorption material and, therefore, the dehumidification capacity of the desiccant wheel.

As shown in Fig. 3.7, if the inlet process air temperature decreases (higher inlet air relative humidity at constant humidity ratio), according to the preliminary analysis and to Fig. 3.2, the dehumidification capacity increases. Consequently, a pre-cooling of the process airflow can be an effective way to increase the dehumidification capacity of the desiccant wheel. Finally, quite obviously it can be stated that an increase in $T_{pro,in}$ leads to an increase in $T_{pro,out}$.

Similarly, in Fig. 3.8 it is shown that if the inlet process air humidity ratio decreases, also the outlet process air humidity ratio decreases. Anyway, a reduction in the inlet process air humidity ratio leads to a lower inlet air relative humidity (at constant temperature) and, therefore, to a decrease in the moisture removal capacity. Both Figs. 3.7 and 3.8 show that the variation of $X_{pro,in}$ and $T_{pro,in}$ slightly affects the optimal revolution speed.

Finally, if the process air velocity is reduced (Fig. 3.9), also the outlet air humidity ratio decreases. It is highlighted that in this case the desiccant wheel revolution speed should be modified and reduced, because the lower process airflow

takes more time to cool the desiccant matrix and, therefore, to start the dehumidification process. Also in this case, as already discussed, the lower $X_{pro,out}$, the higher $T_{pro,out}$.

3.4 Simplified Models of Desiccant Wheels

3.4.1 Input Parameters

As discussed in Sect. 3.3, performance of a specific desiccant wheel depends on inlet process and regeneration air states and on revolution speed. Therefore, assuming that the total pressure is at atmospheric condition (p_{tot} = 101,325 Pa), the following data should be collected to evaluate the performance through the simplified models discussed in this work:

- Inlet process air conditions (for example $v_{pro,in}$, $T_{pro,in}$ and $\phi_{pro,in}$).
- Inlet regeneration air conditions (for example $v_{reg,in}$, $T_{reg,in}$ and $\phi_{reg,in}$).
- Revolution speed (N).

Note that in several models some input data are fixed and therefore they are not required. If inlet states should be provided in terms of specific enthalpy and humidity ratio, the following equations can be adopted:

$$X_a = 0.622 \frac{\phi_a}{\frac{p_{tot}}{p_{v,sat}} - \phi_a} \tag{3.1}$$

where the water vapour saturation pressure can be calculated in this way:

$$p_{v,sat} = e^{23.196 - \frac{3816.44}{T_a + 273.15 - 46.13}} \tag{3.2}$$

and:

$$h_a = (cp_a + X_a cp_v) T_a + \lambda X_a \tag{3.3}$$

where λ = 2501 kJ kg^{-1} is the latent heat of vaporization of water.

The face air velocity of the two streams is:

$$v_{pro,in} = \frac{\dot{V}_{pro,in}}{3600 A_{pro}} \tag{3.4}$$

$$v_{reg,in} = \frac{\dot{V}_{reg,in}}{3600 A_{reg}} \tag{3.5}$$

where $\dot{V}_{pro,in}$ and $\dot{V}_{reg,in}$ are, respectively, the inlet process and regeneration volumetric airflows.

3.4.2 Models Classification

The simplified models to predict desiccant wheel performance can be classified through different approaches, such as the working conditions, the input or output quantities, the technical specifications of the device, etc. In this work, correlations are simply classified referring to the provided output quantities: in particular the following classes of models have been identified:

- Models providing directly $X_{pro,out}$ and $T_{pro,out}$.
- Models providing $h_{pro,out}$ and $\phi_{pro,out}$.
- Models providing the combined potentials of the outlet process air stream, namely $F_{1,pro,out}$ and $F_{2,pro,out}$.

In the first case, the output quantities $X_{pro,out}$ and $T_{pro,out}$ are commonly used by engineers and, therefore, they can be directly used in further calculations or analysis. In the second case, outlet conditions of the process air are based on $h_{pro,out}$ and $\phi_{pro,out}$, which are also well-known parameters for practitioners. $X_{pro,out}$ and $T_{pro,out}$ can be easily determined through a psychrometric chart, tables or by rearranging Eqs. 3.1–3.3.

Instead, in the third case the outlet air condition is provided through two combined potentials $F_{1,a}$ and $F_{2,a}$, introduced by Jurinak [30], that are defined in the following way:

$$F_{1,a} = \frac{-2865}{(T_a + 273.15)^{1.49}} + 4.344\, X_a^{0.8624} \tag{3.6}$$

$$F_{2,a} = \frac{(T_a + 273.15)^{1.49}}{6360} - 1.127\, X_a^{0.07969} \tag{3.7}$$

In order to have useful information about the process air outlet condition, Eqs. 3.6 and 3.7 should be numerically solved in order to get the corresponding values of temperature and humidity ratio. Therefore, the use of the simplified models providing two combined potentials is less practical and simple compared to the other two analysed approaches.

All the models discussed in this work are summarized in Table 3.1. For each correlation, main information is reported, namely literature reference, working range and desiccant wheel specifications. Instead, the detailed description of each model is reported in the next section of the chapter (Sect. 3.4.3).

Table 3.1 Simplified models investigated in the present work

No.	Ref.	Output		Working range								Desiccant wheel			
				$T_{pro,in}$ (°C)	$X_{pro,in}$ (g kg^{-1})	$v_{pro,in}$ (m s^{-1})	$T_{reg,in}$ (°C)	$X_{reg,in}$ (g kg^{-1})	$v_{reg,in}$ (m s^{-1})	N (rev h^{-1})	Balanced flows	D_W (m)	L_W (m)	Desiccant material	A_{pro}/A_{reg} (–)
1	[19]	$X_{pro,out}$	$T_{pro,out}$	20–34	8–15	–	40–60	7–16	–	–	Yes	–	–	Silica gel	–
2	[25]	$X_{pro,out}$	$T_{pro,out}$	17.5–29.5	12–21.5	5.38[a]	34–42.5	13–22.6	5.38[a]	42	Yes	0.55	0.2	Silica gel	1
3	[25]	$X_{pro,out}$	$T_{pro,out}$	17.5–29.5	12–21.5	2.57–5.38[a]	34–42.5	13–22.6	2.57–5.38[a]	42	Yes	0.55	0.2	Silica gel	1
4	[21]	$F_{1,pro,out}$	$F_{2,pro,out}$	24–40	4–14	1.1, 1.8, 2.2[a]	50–80	3–15	1.1, 1.8, 2.2[a]	6	Yes	0.63	0.2	Silica gel	–
5	[24]	$F_{1,pro,out}$	$F_{2,pro,out}$	22.2–38.8	6.4–15.9	1.3	49.8–68.6	6.4–15.9	2	12	Yes	0.60[b]	0.44	Silica Gel	1.5
6	[19]	$\phi_{pro,out}$	$h_{pro,out}$	20–34	8–15	–	40–60	7–16	–	–	Yes	–	–	Silica gel	–
7	[19]	$\phi_{pro,out}$	$h_{pro,out}$	20–34	8–15	–	40–60	7–16	–	–	Yes	–	–	LiCl	–
8	[19]	$\phi_{pro,out}$	$h_{pro,out}$	20–34	8–15	–	40–60	7–16	–	–	Yes	–	–	Silica Gel	–
9	[22]	$\phi_{pro,out}$	$h_{pro,out}$	5–40	5–15	3.6	80–120	5–15	3.6	24	Yes	0.44	0.2	Metal Silicate	1
10	[22]	$\phi_{pro,out}$	$h_{pro,out}$	5–40	5–15	3.6	80–120	5–15	3.6	24	Yes	0.44	0.2	Silica gel	1
11	[31]	$\phi_{pro,out}$	$h_{pro,out}$	30	5.7–15.7	2.0	60–100	5.7–15.7	2.0	–	Yes	–	–	Silica gel	1
12	[31]	$\phi_{pro,out}$	$h_{pro,out}$	30	16	0.79 [a]	60–80	12	0.79[a]	10–60	Yes	0.3	0.1	Silica gel	1
13	[18]	$\phi_{pro,out}$	$h_{pro,out}$	17.6–33.8	9.1–17.4	1.75–2.85	44.4–78.6	8.4–16.3	1.64–2.53	4.9–25.6	No	0.6	0.2	Metal Silicate	1
14	[18]	$\phi_{pro,out}$	$h_{pro,out}$	30,50	5–35	2.0	80,120	5–35	2.0	20	Yes	0.32	–	Zeolite	1
15	[20]	$X_{pro,out}$	$T_{pro,out}$	20–34	8–15	–	40–60	7–16	–	–	No	–	–	Silica gel	–
16	[20]	$X_{pro,out}$	$T_{pro,out}$	20–34	8–15	–	40–60	7–16	–	–	No	–	–	LiCl	–
17	[20]	$X_{pro,out}$	$T_{pro,out}$	20–34	8–15	–	40–60	7–16	–	–	No	–	–	Silica gel	–

[a]Calculated assuming $A_{pro}/A_{reg} = 1$

[b]Net diameter exposed to air streams

3.4.3 Models Description

3.4.3.1 Model 1—Beccali et al. [19]

Model 1 has been introduced by Beccali et al. [19] and is based on silica gel desiccant wheel data directly provided by the manufacturer. Rearranging the original equations proposed by the authors, outlet air conditions can be calculated in the following way:

$$X_{\text{pro,out}} = \left(C_1 X_{\text{pro,in}}^2 + C_2 X_{\text{pro,in}} + C_3\right) T_{\text{pro,in}} + \left(C_4 X_{\text{pro,in}}^2 + C_5 X_{\text{pro,in}} + C_6\right) \quad (3.8)$$

$$T_{\text{pro,out}} = \left(K_1 X_{\text{pro,in}}^2 + K_2 X_{\text{pro,in}} + K_3\right) T_{\text{pro,in}} + \left(K_4 X_{\text{pro,in}}^2 + K_5 X_{\text{pro,in}} + K_6\right) \quad (3.9)$$

where the terms C_{1-6} and K_{1-6} are:

$$C_i = \left(a_i X_{\text{reg,in}}^2 + b_i X_{\text{reg,in}} + c_i\right) X_{\text{pro,in}}^2 + \left(d_i X_{\text{reg,in}}^2 + e_i X_{\text{reg,in}} + f_i\right) X_{\text{pro,in}} + \left(g_i X_{\text{reg,in}}^2 + h_i X_{\text{reg,in}} + i_i\right) \quad (3.10)$$

$$K_i = \left(l_i X_{\text{reg,in}}^2 + m_i X_{\text{reg,in}} + n_i\right) X_{\text{pro,in}}^2 + \left(o_i X_{\text{reg,in}}^2 + p_i X_{\text{reg,in}} + q_i\right) X_{\text{pro,in}} + \left(r_i X_{\text{reg,in}}^2 + s_i X_{\text{reg,in}} + t_i\right) \quad (3.11)$$

The 108 coefficients a_i–t_i are reported in Table 3.2.

3.4.3.2 Model 2—Comino et al. [25]

Comino et al. [25] proposed a first-order model to determine performance of a silica gel desiccant wheel by regression of data obtained from experimental tests. Outlet conditions of process air are calculated in the following way:

$$X_{\text{pro,out}} = \frac{a_0 + \sum_{i=1}^{10} (a_i Y_i)}{1000} \quad (3.12)$$

$$T_{\text{pro,out}} = \frac{b_0 + \sum_{i=1}^{10} (b_i Y_i)}{1000} \quad (3.13)$$

where the terms a_i, b_i and Y_i are reported in Table 3.3.

Table 3.2 Model 1—coefficients to be used in Eqs. 3.10 and 3.11 [19]

i	1	2	3	4	5	6
a_i	−9.81771E−07	2.48646E−05	−0.000155484	2.97891E−06	−0.000770385	0.004898569
b_i	0.000024125	−0.000610844	0.003809656	−0.000735859	0.01901969	−0.1207189
c_i	−0.000142573	0.003601979	−0.0224005	0.004374313	−0.1127932	0.7154694
d_i	0.000120938	−0.003064896	0.01911052	−0.003642969	0.09411271	−0.5966672
e_i	0.002954063	0.0748425	−0.4653281	0.08950781	−2.311069	14.6212
f_i	0.01734688	−0.4383754	2.716457	0.5291188	13.62156	−86.19895
g_i	−0.003395833	0.08619583	−0.5358542	0.10105	−2.610487	16.49429
h_i	0.0825	−2.093475	12.97393	2.47025	63.78412	−401.8073
i_i	−0.4828167	12.22347	−75.36913	14.5702	−374.4862	2362.187
l_i	4.66333E−06	−0.000137699	0.000889096	−0.0001599	0.004608366	−0.02952156
m_i	−0.000122108	0.003660427	−0.02379164	0.00424914	−0.1237906	0.7970592
n_i	0.00075592	−0.02322678	0.1527826	−0.02691875	0.7979418	−5.187328
o_i	−0.000788528	0.02253221	−0.1440601	0.02616227	−0.7356466	4.675441
p_i	0.02103875	−0.6067781	3.896302	−0.7045379	19.94981	−127.2275
q_i	−0.1343869	3.932225	−25.44645	4.561903	−130.5749	838.5968
r_i	0.03264739	−0.9065427	5.741306	−1.055388	29.01258	−182.9765
s_i	−0.8851843	24.70641	−156.8717	28.7686	−794.0862	5018.149
t_i	5.799316	−163.1261	1041.133	−189.9018	5274.441	−33467.1

Table 3.3 Model 2—parameters to be used in Eqs. 3.12 and 3.13 [25]

i	a_i	b_i	Y_i
0	6081.84	−16,707.70	–
1	328.15	144.14	$T_{pro,in}$
2	−400.65	1786.87	$X_{pro,in}$
3	438.02	82.74	$T_{reg,in}$
4	−49.42	505.68	$X_{reg,in}$
5	8.64	−19.08	$T_{pro,in}$ $X_{pro,in}$
6	3.49	3.80	$T_{pro,in}$ $T_{reg,in}$
7	−1.91	2.16	$T_{pro,in}$ $X_{reg,in}$
8	4.62	−6.52	$X_{pro,in}$ $T_{reg,in}$
9	9.73	−13.22	$X_{pro,in}$ $X_{reg,in}$
10	−6.78	−4.24	$T_{reg,in}$ $X_{reg,in}$

3.4.3.3 Model 3—Comino et al. [25]

Model 3 is an improvement of model 2 already proposed by Comino et al. [25]. In this case, the process and regeneration airflows (balanced air streams) can be varied. The model is based on experimental data (silica gel desiccant wheel) and process air outlet conditions can be calculated as:

$$X_{pro,out} = \frac{a_0 + \sum_{i=1}^{15} (a_i Y_i)}{1000} \tag{3.14}$$

$$T_{pro,out} = \frac{b_0 + \sum_{i=1}^{15} (b_i Y_i)}{1000} \tag{3.15}$$

where the terms a_i, b_i and Y_i are reported in Table 3.4. The specific mass airflow rate Ω, which is equal for the process and regeneration air stream (balanced flows), should be within 14.79 and 30.92 kg s^{-1} m^{-3}. It is calculated in this way:

$$\Omega = \Omega_{pro} = \Omega_{reg} = \frac{v_{pro,in}\rho_{pro,in}}{L_W} = \frac{v_{reg,in}\rho_{reg,in}}{L_W} \tag{3.16}$$

where L_W = 0.2 m is the desiccant wheel thickness and ρ is the air density.

3.4.3.4 Model 4—Panaras et al. [21]

Panaras et al. [21] provided correlations based on the combined potentials (Eqs. 3.6 and 3.7) approach initially proposed by Jurinak [30]. In this work, experimental data of a silica gel desiccant wheel are adopted. The outlet process air potentials are calculated from inlet process and regeneration air potentials through Eqs. 3.17 and 3.18:

Table 3.4 Model 3—parameters to be used in Eqs. 3.14 and 3.15 [25]

i	a_i	b_i	Y_i
0	9012.70	−4828.58	–
1	−25.41	−16.01	$T_{pro,in}$
2	23.17	1783.16	$X_{pro,in}$
3	543.06	−189.88	$T_{reg,in}$
4	−291.07	485.12	$X_{reg,in}$
5	−26.53	−337.70	Ω
6	6.38	−7.31	$T_{pro,in}$ $X_{pro,in}$
7	7.34	7.44	$T_{pro,in}$ $T_{reg,in}$
8	−2.36	8.74	$T_{pro,in}$ $X_{reg,in}$
9	8.41	−8.42	$T_{pro,in}$.Ω
10	−0.21	−20.09	$X_{pro,in}$ $T_{reg,in}$
11	4.78	−11.79	$X_{pro,in}$ X_i
12	3.04	6.25	$X_{pro,in}$ Ω
13	−0.51	−4.71	$T_{reg,in}$ $X_{reg,in}$
14	−7.56	14.04	$T_{reg,in}$ Ω
15	3.31	−5.11	$X_{reg,in}$.Ω

$$F_{1,pro,out} = \eta_{F1}\left(F_{1,reg,in} - F_{1,pro,in}\right) + F_{1,pro,in} \tag{3.17}$$

$$F_{2,pro,out} = \eta_{F2}\left(F_{2,reg,in} - F_{2,pro,in}\right) + F_{2,pro,in} \tag{3.18}$$

Depending on the face velocity of the balanced air streams, three pairs η_{F1} and η_{F2} are proposed [21]:

- if $v_{pro,in} = v_{reg,in} = 1.1$ m s^{-1}: $\eta_{F1} = 0.18$ e $\eta_{F2} = 0.72$.
- if $v_{pro,in} = v_{reg,in} = 1.8$ m s^{-1}: $\eta_{F1} = 0.13$ e $\eta_{F2} = 0.66$.
- if $v_{pro,in} = v_{reg,in} = 2.2$ m s^{-1}: $\eta_{F1} = 0.11$ e $\eta_{F2} = 0.67$.

Once $F_{1,pro,out}$ and $F_{2,pro,out}$ are determined, the values of $X_{pro,out}$ and $T_{pro,out}$ should be calculated through Eqs. 3.6 and 3.7.

3.4.3.5 Model 5—Angrisani et al. [24]

In model 5, Angrisani et al. [24] proposed correlations, based on experimental data, to determine performance of a silica gel desiccant wheel at constant and balanced airflows (800 m^3 h^{-1}). The approach is based on the combined potentials proposed by Jurinak [30], as already described for model 4. In this case, the effectiveness pair is $\eta_{F1} = 0.207$ and $\eta_{F2} = 0.717$.

Process air outlet conditions are calculated first through Eqs. 3.17, 3.18 and, then, through Eqs. 3.6 and 3.7.

3.4.3.6 Model 6—Beccali et al. [19]

In model 6, Beccali et al. [19] provided correlations to directly calculate outlet process air relative humidity and enthalpy. Correlations are based on data of a silica gel desiccant wheel directly provided by the manufacturer. Outlet conditions are calculated through Eqs. 3.19 and 3.20 [19]:

$$\phi_{\text{pro,out}} = 0.9428\,\phi_{\text{reg,in}} + 0.0572\,\phi_{\text{pro,in}} \tag{3.19}$$

$$h_{\text{pro,out}} = 0.1312\,h_{\text{reg,in}} + 0.8688\,h_{\text{pro,in}} \tag{3.20}$$

Once $\phi_{\text{pro,out}}$ and $h_{\text{pro,out}}$ are calculated, $X_{\text{pro,out}}$ and $T_{\text{pro,out}}$ can be evaluated through a psychrometric chart or rearranging Eqs. 3.1–3.3.

3.4.3.7 Model 7—Beccali et al. [19]

In model 7, process outlet conditions are calculated through the same approach of model 6. In this case, Beccali et al. [19] proposed correlations to predict performance of a LiCl desiccant wheel, with data provided by the manufacturer. Outlet relative humidity is calculated with Eq. 3.19, while outlet enthalpy through Eq. 3.21 [19]:

$$h_{\text{pro,out}} = 0.1861\,h_{\text{reg,in}} + 0.8139\,h_{\text{pro,in}} \tag{3.21}$$

3.4.3.8 Model 8—Beccali et al. [19]

In model 8, Beccali et al. [19] provided correlations to evaluate performance of a silica gel desiccant wheel through the same approach of models 6 and 7. The desiccant wheel has similar performance compared to the one of model 6: information about differences between the two devices is not reported [19]. Also in this case relative humidity is calculated with Eq. 3.19, while outlet enthalpy is obtained thorough Eq. 3.22 [19]:

$$h_{\text{pro,out}} = 0.1148\,h_{\text{reg,in}} + 0.8852\,h_{\text{pro,in}} - 0.9474 \tag{3.22}$$

3.4.3.9 Model 9—Ruivo et al. [22]

In model 9 proposed by Ruivo et al. [22], a pair of effectiveness parameters based on the quantities ϕ and h is used to calculate desiccant wheel performance. The analysed device is made of metal silicate synthesized on inorganic fibre substrate, and adopted performance data have been extrapolated from manufacturer software. Outlet process air conditions ϕ and h are calculated through Eqs. 3.23 and 3.24:

$$\phi_{\text{pro,out}} = \phi_{\text{pro,in}} - \eta_{\phi}\left(\phi_{\text{pro,in}} - \phi_{\text{reg,in}}\right) \tag{3.23}$$

$$h_{\text{pro,out}} = h_{\text{pro,in}} - \eta_{h}\left(h_{\text{pro,in}} - h_{\text{reg,in}}\right) \tag{3.24}$$

where $\eta_h = 0.147$ and $\eta_\phi = 0.965$.

3.4.3.10 Model 10—Ruivo et al. [22]

In model 10, Ruivo et al. [22] proposed correlations to evaluate performance of a commercial silica gel desiccant wheel, as already described in model 9. Data are provided directly by the manufacturer, and performance is calculated through Eqs. 3.23 and 3.24. In this case $\eta_h = 0.143$ and $\eta_\phi = 0.921$.

3.4.3.11 Model 11—Ruivo et al. [31]

In model 11, the same approach reported for models 9 and 10 is adopted by the authors (Ruivo et al. [31]). In this case, correlations are used to evaluate performance of a silica gel desiccant wheel and experimental data available in literature are used [32]. Outlet air conditions are calculated through Eqs. 3.23 and 3.24 and the following effectiveness pair: $\eta_h = 0.078$ and $\eta_\phi = 0.985$.

3.4.3.12 Model 12—Ruivo et al. [31]

Model 12 is a development of models 9–11: in this case the effect of the variation of the desiccant wheel revolution speed is properly taken into account. Correlations provide outlet process air conditions of a silica gel device, whose experimental data are available in literature [32]. Performance is calculated through Eqs. 3.23 and 3.24, where the effectiveness pair values are not constant but are determined in this way [31]:

$$\eta_h = -0.058096\beta^2 - 0.393058\beta + 0.542448 \tag{3.25}$$

$$\eta_\phi = \alpha\left(-0.365059\beta^2 - 0.052904\beta + 0.937592\right) \tag{3.26}$$

where $\beta = \log(60/N)$ and $\alpha = [(\phi_{\text{pro,in}} - \phi_{\text{reg,in}})/(\phi_{\text{pro,in}} - 0.0536)]^{1/2}$.

3.4.3.13 Model 13—De Antonellis et al. [18]

De Antonellis et al. [18] developed a detailed correlation to predict performance, based on the effectiveness pair η_h and η_ϕ, of a metal silicate desiccant wheel. In this

work, the device has been tested in a wide range of operating conditions and results have been used to develop correlations which take in account the variation of all the inlet air conditions and the revolution speed.

Outlet process air conditions are calculated through Eqs. 3.23 and 3.24. The effectiveness pair values, which are not constant, are determined in this way [18]:

$$\begin{cases} \eta_\phi = \alpha_{\text{vreg}}\alpha_{\text{vpro}}\alpha_T\alpha_X\alpha_N \\ \alpha_{\text{vreg}} = c_1 v_{\text{reg,in}}^2 + c_2 v_{\text{reg,in}} + c_3 \\ \alpha_{\text{vpro}} = c_4 v_{\text{pro,in}}^2 + c_5 v_{\text{pro,in}} + c_6 \\ \alpha_T = c_7 \ln(T_{\text{reg,in}} - T_{\text{pro,in}}) + c_8 \\ \alpha_X = c_9 X_{\text{pro,in}} + c_{10} X_{\text{reg,in}} + 1 \\ \alpha_N = c_{11} N + c_{12} \end{cases} \tag{3.27}$$

$$\begin{cases} \eta_h = \beta_{\text{vreg}}\beta_{\text{vpro}}\beta_T\beta_X\beta_N \\ \beta_{\text{vreg}} = k_1 \left(v_{\text{reg,in}}\right)^{k_2} \\ \beta_{\text{vpro}} = k_3 \left(v_{\text{pro,in}}\right)^{k4} \\ \beta_T = k_5 T_{\text{reg,in}} + k_6 T_{\text{pro,in}} + k_7 \\ \beta_X = k_8 X_{\text{reg,in}} + k_9 X_{\text{pro,in}} + 1 \\ \beta_N = k_{10} N + k_{11} \end{cases} \tag{3.28}$$

The coefficients c_{1-12} and k_{1-11} are reported in Table 3.5.

It is highlighted that in this work a correlation to predict pressure drop across the desiccant wheel is also provided [18]:

$$\Delta p = x_1 \mu_a v_a + x_2 \rho_a v_a^2 \tag{3.29}$$

where $x_1 = 3.77 \times 10^6$, $x_2 = 6.5493$ and μ_a is the dynamic viscosity of air.

3.4.3.14 Model 14—De Antonellis et al. [18]

De Antonellis et al. [18] applied the correlations described in model 13 to evaluate performance of an AQSOA zeolite desiccant wheel. The device has been tested in a previous research work by Intini et al. [33] at balanced and constant airflows, at constant revolution speed and with equal inlet humidity ratio of process and regeneration air streams ($X_{\text{pro,in}} = X_{\text{reg,in}} = X_{\text{in}}$). Therefore, Eqs. 3.27 and 3.28 can be reduced and simplified in the following way [18]:

$$\begin{cases} \eta_\phi = \alpha_T\alpha_X \\ \alpha_T = c_1 \ln(T_{\text{reg,in}} - T_{\text{pro,in}}) + c_2 \\ \alpha_X = c_3 X_{\text{in}} + 1 \end{cases} \tag{3.30}$$

Table 3.5 Coefficients adopted in model 13 (Eqs. 3.27 and 3.28) [18]

c_1	c_2	c_3	c_4	c_5	c_6	c_7	c_8	c_9	c_{10}	c_{11}	c_{12}
−0.003286	0.020519	0.095525	0.008343	−0.04322	0.16501	1.1903	12.331	−4.519	0.80627	0.0030464	4.2846

k_1	k_2	k_3	k_4	k_5	k_6	k_7	k_8	k_9	k_{10}	k_{11}
0.22113	0.23493	0.21763	−0.66335	0.0016778	−0.0056224	1.671	−44.505	27.728	0.13883	4.6438

$$\begin{cases} \eta_h = \beta_T \beta_X \\ \beta_T = k_1 T_{\text{reg,in}} + k_2 T_{\text{pro,in}} + k_3 \\ \beta_X = k_4 X_{\text{in}} + 1 \end{cases} \tag{3.31}$$

where coefficients c_{1-3} and k_{1-4} are summarized in Table 3.6.

Outlet process air conditions are calculated through Eqs. 3.23, 3.24, 3.30 and 3.31.

3.4.3.15 Model 15—Beccali et al. [20]

Beccali et al. [20] proposed an update of the desiccant wheel model previously investigated (model 6 of this work [19]) in order to take into account unbalanced airflow conditions. The model can be used when the process to regeneration volumetric flow ratio is higher than 1. To apply model 15, it is first necessary to calculate outlet process air conditions through model 6 (Eqs. 3.19 and 3.20) assuming process airflow equal to the regeneration air one. Then, in such conditions outlet humidity ratio $X'_{\text{pro,out}}$ and temperature and $T'_{\text{pro,out}}$ should be determined through the psychrometric chart or Eqs. 3.1–3.3. Rearranging the equations proposed by Beccali et al. [20], outlet conditions are finally corrected considering unbalanced flows ($\alpha = V_{\text{pro,in}}/V_{\text{reg,in}}$) in this way:

$$X_{\text{pro,out}} = X_{\text{pro,in}} + \frac{\frac{1}{\alpha}\left(X'_{\text{pro,out}} - X_{\text{pro,in}}\right) - (A\alpha + B)}{(C\alpha + D)} \tag{3.32}$$

$$T_{\text{pro,out}} = T_{\text{pro,in}} + \frac{\frac{1}{\alpha}\left(T'_{\text{pro,out}} - T_{\text{pro,in}}\right) - (E\alpha + F)}{(G\alpha + H)} \tag{3.33}$$

The parameters A–H are summarized in Table 3.7.

It is highlighted that in the work of Beccali et al. [20], the correlations are compared to desiccant wheel data with $\alpha = 1.33$ and $\alpha = 1.66$.

3.4.3.16 Model 16—Beccali et al. [20]

Model 16 is an upgrade of model 7, which takes into account unbalanced airflows. Outlet process air conditions are calculated through the same approach described in Sect. 3.4.3.15 (Eqs. 3.32 and 3.33). In this case, parameters A–H are reported in Table 3.8.

Table 3.6 Coefficients adopted in model 14 (Eqs. 3.30 and 3.31) [18]

c_1	c_2	c_3	
0.099038	0.586	−2.9435	
k_1	k_2	k_3	k_4
0.00058696	−0.00077447	0.16886	−3.9466

Table 3.7 Coefficients adopted in model 15 (Eqs. 3.32 and 3.33) [20]

A	*B*	*C*	*D*	*E*	*F*	*G*	*H*
1.5183	−0.9185	−0.6903	1.5976	3.0621	−1.1643	−0.5745	1.4680

Table 3.8 Coefficients adopted in model 16 (Eqs. 3.32 and 3.33) [20]

A	*B*	*C*	*D*	*E*	*F*	*G*	*H*
−0.0411	0.2426	−0.3540	1.3643	−0.6534	2.2014	−0.2589	1.2061

Table 3.9 Coefficients adopted in model 17 (Eqs. 3.32 and 3.33) [20]

A	*B*	*C*	*D*	*E*	*F*	*G*	*H*
−1.7558	3.2668	−0.4496	1.3526	1.1016	2.8335	−0.5636	1.4794

3.4.3.17 Model 17—Beccali et al. [20]

Model 17 is similar to models 15 and 16: it is an extension of model 8 in order to evaluate performance of such silica gel desiccant wheel at unbalanced airflow conditions. Performance of the device is calculated through Eqs. 3.32, 3.33 and coefficients *A*–*H* are reported in Table 3.9.

3.5 Conclusions

In this chapter book, 17 simplified models to predict outlet process air conditions of desiccant wheels have been resumed and classified. Each of them can be used by engineers and practitioners in order simulate air handling units integrating desiccant wheels and to compare performance with conventional systems. It is highlighted that desiccant wheel properties and working range (Table 3.1) should be properly considered when selecting the model to be used.

In addition, the following criteria can be considered to select the appropriate model:

- In case of basic simulations in a worksheet, simple non-iterative models 1–3 and 6–14 are suggested.
- The variation of the revolution speed can be evaluated only through models 12 and 13.
- High regeneration temperature ($T_{reg,in} \geq 100$ °C) is taken into account only in models 9–11 and 14.
- If it is necessary to control and vary all the input conditions, model 13 should be adopted.

Model outputs should always be carefully evaluated, according to the analysis provided in Sect. 3.3, in order to avoid misleading results.

References

1. Daou K, Wang RZ, Xia ZZ (2006) Desiccant cooling air conditioning: a review. Renew Sust Energy Rev 10(2):55–77. doi:10.1016/j.rser.2004.09.010
2. Ge TS, Dai YJ, Wang RZ (2014) Review on solar powered rotary desiccant wheel cooling system. Renew Sust Energy Rev 39:476–497. doi:10.1016/j.rser.2014.07.121
3. Sultan M, El-Sharkawy II, Miyazaki T, Saha BB, Koyama S (2015) An overview of solid desiccant dehumidification and air conditioning systems. Renew Sust Energy Rev 46:16–29. doi:10.1016/j.rser.2015.02.038
4. Gao W, Worek W, Konduru V, Adensin K (2015) Numerical study on performance of a desiccant cooling system with indirect evaporative cooler. Energy Buildings 86:16–24. doi:10.1016/j.enbuild.2014.09.049
5. O'Kelly M, Walter ME, Rowland JR (2015) Simulated hygrothermal performance of a desiccant-assisted hybrid air/water conditioning system in a mixed humid climate under dynamic load. Energy Buildings 86:45–57. doi:10.1016/j.enbuild.2014.09.068
6. Liu W, Lian Z, Radermacher R, Yao Y (2007) Energy consumption analysis on a dedicated outdoor air system with rotary desiccant wheel. Energy 32(9):1749–1760. doi:10.1016/j.energy.2006.11.012
7. Intini M, De Antonellis S, Joppolo CM, Casalegno A (2015) A trigeneration system based on polymer electrolyte fuel cell and desiccant wheel—part B: overall system design and energy performance analysis. Energy Convers Manage 106:1460–1470. doi:10.1016/j.enconman.2015.10.005
8. De Antonellis S, Intini M, Joppolo CM, Molinaroli L, Romano F (2015) Desiccant wheels for air humidification: an experimental and numerical analysis. Energy Convers Manage 106:355–364. doi:10.1016/j.enconman.2015.09.034
9. La D, Dai Y, Li H, Li Y, Kiplagat JK, Wang RE (2011) Experimental investigation and theoretical analysis of solar heating and humidification system with desiccant rotor. Energy Buildings 43(5):1113–1122. doi:10.1016/j.enbuild.2010.08.006
10. Zeng DQ, Li H, Dai YJ, Xie AX (2014) Numerical analysis and optimization of a solar hybrid one-rotor two-stage desiccant cooling and heating system. Appl Therm Eng 73(1):472–481. doi:10.1016/j.applthermaleng.2014.07.076
11. De Antonellis S, Joppolo CM, Molinaroli L, Pasini A (2012) Simulation and energy efficiency analysis of desiccant wheel systems for drying processes. Energy 37(1):336–345. doi:10.1016/j.energy.2011.11.021
12. Dai YJ, Wang RZ, Xu YX (2002) Study of a solar powered solid adsorption—desiccant cooling system used for grain storage. Renew Energy 25(3):417–430. doi:10.1016/S0960-1481(01)00076-3
13. Wang WC, Calay RK, Chen YK (2011) Experimental study of an energy efficient hybrid system for surface drying. Appl Therm Eng 31(4):425–431. doi:10.1016/j.applthermaleng.2010.09.014
14. Misha S, Mat S, Ruslan MH, Salleh E, Sopian K (2015) Performance of a solar assisted solid desiccant dryer for kenaf core fiber drying under low solar radiation. Sol Energy 112:194–204. doi:10.1016/j.solener.2014.11.029
15. Misha S, Mat S, Ruslan MH, Salleh E, Sopian K (2016) Performance of a solar-assisted solid desiccant dryer for oil palm fronds drying. Sol Energy 132:415–429. doi:10.1016/j.solener.2016.03.041
16. De Antonellis S, Joppolo CM, Molinaroli L (2010) Simulation performance analysis and optimization of desiccant wheels. Energy Buildings 42(9):1386–1393. doi:10.1016/j.enbuild.2010.03.007
17. Ge TS, Li Y, Wang RZ, Dai YJ (2008) A review of the mathematical models for predicting rotary desiccant wheel. Renew Sustain Energy Rev 12(6):1485–1528. doi:10.1016/j.rser.2007.01.012

18. De Antonellis S, Intini M, Joppolo CM (2015) Desiccant wheels effectiveness parameters: correlations based on experimental data. Energy Buildings 103:296–306. doi:10.1016/j.enbuild.2015.06.041
19. Beccali M, Butera F, Guanella R, Adhikari RS (2003) Simplified models for the performance evaluation of desiccant wheel dehumidification. Int J Energy Res 27(1):17–29. doi:10.1002/er.856
20. Beccali M, Adhikari RS, Butera F, Franzitta V (2004) Update on desiccant wheel model. Int J Energy Res 28(12):1043–1049. doi:10.1002/er.1011
21. Panaras G, Mathioulakis E, Belessiotis V, Kyriakis N (2010) Experimental validation of a simplified approach for a desiccant wheel model. Energy Buildings 42(10):1719–1725. doi:10.1016/j.enbuild.2010.05.006
22. Ruivo CR, Angrisani G (2014) The effectiveness method to predict the behaviour of a desiccant wheel: an attempt of experimental validation. Appl Therm Eng 71(2):643–651. doi:10.1016/j.applthermaleng.2013.10.028
23. Ruivo CR, Carrillo-Andrés A, Costa JJ, Domínguez-Muñoz F (2013) A new approach to the effectiveness method for the simulation of desiccant wheels with variable inlet states and airflows rates. Appl Therm Eng 58:670–678. doi:10.1016/j.applthermaleng.2011.12.052
24. Angrisani G, Roselli C, Sasso M (2012) Experimental validation of constant efficiency models for the subsystems of an unconventional desiccant-based air handling unit and investigation of its performance. Appl Therm Eng 33–34(1):100–108. doi:10.1016/j.applthermaleng.2011.09.018
25. Comino F, Adana MRD, Peci F (2016) First and second order simplified models for the performance evaluation of low temperature activated desiccant wheels. Energy Buildings 116:574–582. doi:10.1016/j.enbuild.2016.02.005
26. Novel Aire web site. http://www.novelaire.com/desiccant-wheels-31505.html. Accessed 31 Aug 2016
27. Rotor Source web site. http://www.rotorsource.com/downloads.html. Accessed 31 Aug 2016
28. DRI web site. http://www.drirotors.com/softwares.php. Accessed 31 Aug 2016
29. Pasaran AA, Mils AF (1986) Moisture transport in silica gel packed bed. I theoretical study. Int J Heat Mass Transfer 30:1037–1049. doi:10.1016/0017-9310(87)90034-2
30. Jurinak JJ (1982) Open cycle desiccant cooling—component models and system simulations. Dissertation, University of Wisconsin-Madison
31. Ruivo CR, Costa JJ, Figueiredo AR, Kodama A (2012) Effectiveness parameters for the prediction of the global performance of desiccant wheels—an assessment based on experimental data. Renew Energy 38(1):181–187. doi:10.1016/j.renene.2011.07.023
32. Kuma T, Hirose T, Goto M, Kodama A (1998) Thermally regenerative monolithic rotor dehumidifier for adsorption cooling system. J Sol Energy-T ASME 120(1):45–50
33. Intini M, Goldsworthy M, White S, Joppolo CM (2015) Experimental analysis and numerical modelling of an AQSOA zeolite desiccant wheel. Appl Therm Eng 80(5):20–30. doi:10.1016/j.applthermaleng.2015.01.036

Chapter 4
VENTIREG—A New Approach to Regenerating Heat and Moisture in Dwellings in Cold Countries

Yuri I. Aristov

Abstract In cold countries, a large difference between the indoor and outdoor temperatures (30–60 °C) in winter leads to (a) huge heat losses through a ventilation system, (b) moisture freezing at the systems exit, and (c) great reduction in the indoor humidity and uncomfortable living/working conditions. Therefore, new reliable and efficient solutions are strictly necessary to realize the concept of low (or even zero)-energy building in such climates. This Chapter addresses a new approach (the so-called VENTIREG) recently suggested specifically for cold climates to resolve the mentioned problems. New VENTIREG heat and mass exchangers, developed to realize this method, were tested under climatic conditions of the Western Siberia, Russia. The prototype systems require little maintenance, have a low capital cost, are compact and energy efficient. Technical, economic, and social aspects of this method are briefly discussed.

Keywords Regeneration of heat and moisture · Energy consumption · Heat losses in buildings · Cold climate · Thermal comfort · Ventilation system · VENTIREG · Desiccants · Open adsorption systems

4.1 Energy Consumption in the Building Sector

Nowadays, it is not possible to contemplate our manner of life without modern heating, ventilating, and air-conditioning systems. This is especially true for urban population which is persistently growing for past centuries. At present, more than half of the world's population lives in cities [1]. It is predicted that by 2050 the urban population will reach 70% [2]. Energy efficient buildings are an essential constituent of future sustainable cities. Such buildings have to ensure high levels of comfort and convenience without necessarily sacrificing the standards of living,

Y.I. Aristov (✉)
Boreskov Institute of Catalysis SB RAS,
Lavrentieva Av., 5, 630090 Novosibirs, Russia
e-mail: aristov@catalysis.ru

N. Enteria et al. (eds.), *Desiccant Heating, Ventilating, and Air-Conditioning Systems*, DOI 10.1007/978-981-10-3047-5_4

therefore an input of emerging low-carbon technologies aimed at rational use of thermal energy in dwellings must be decidedly increased [3, 4].

Indeed, at present, a significant part of primary fossil fuels is spent for heating/cooling of buildings, thus greatly contributing to GHG emissions. In Europe, the heat consumption in buildings is responsible for 24% of the total energy consumption of the EU-27 (2008) [5]. Forty-five percentage of total UK final energy consumption for 2012 was for heating purposes; it being known that more than half (24%) was used for domestic heating [6]. The building sector in Canada accounts for about 30% of total GHG emissions [7]. In Germany, the share of households in total final energy consumption in 2011 reaches 25% or 52 Mtoe (million tonnes of oil equivalent), space heating being dominated (72% of the final households energy consumption [8]). In the Russian Federation (RF), 43% of the produced centralized heat or 138 Mtoe is used for buildings [9]. This agrees well with the data of Ref. [10] that Russian residential, public, and commercial buildings in 2005 were responsible for 144.5 Mtoe of final energy use, at that 75% of this heat is consumed in dwellings.

Despite all systematic and active actions that have gone on, heat losses in buildings still remain enormous; hence, there is considerable potential for improving energy efficiency in residential buildings and the related infrastructure. According to the International Energy Agency (IEA), the building sector can reduce energy consumption with an estimated global energy savings of 1509 Mtoe which can possibly mitigate 12.6 Gt (gigatonnes) of CO_2 emissions by 2050 [11]. Technical potential of energy saving in the Russian buildings sector exceeds 68 Mtoe or 47% of the total consumption, the largest potential being evaluated for residential buildings [10]. The major part (67%) of saving can be implemented through the reduction in district heating use for space heating and hot water. About 85% of the technical potential is economically viable, while 72% is market attractive with the 2010 energy prices [10]. Similar estimations are reported in [12]: a technical GHG reduction potential for the Russian building stock by 2030 ranges between 26 and 47% of the national baseline.

4.2 The Structure of Heat Losses in Dwellings

Particular ways of the energy saving in the building sector are dictated by the structure of heat losses in dwellings (Fig. 4.1), which depends on climatic conditions and building types. For instance, the UK has around 26.7 million domestic houses and flats [13], and this building stock is one of the oldest in Europe. As shown in Fig. 4.1b, for average UK dwelling, the main losses due to building fabric are related to heat fluxes through the walls (37%) and windows (19%) together with those associated with air infiltration in ventilation system (18%).

By the end of 2012, the total floor area of dwellings in Russia reached 3.3 billion m^2, 72% being related to urban development [14]. In Russia, the space heating is responsible of 58% of overall energy consumption in residential buildings with

district heating systems which cover c.a. 75% of all dwellings. A small part of dwellings built after 2000 meet acceptable heat efficiency requirements, whereas the majority of older buildings have significantly lower space heating efficiency. The value of Specific Energy Consumption (SEC) for space heating strongly depends on the year of dwelling construction: for buildings erected before 1990, in 1991–2000 and after 2000, the average SEC is estimated as 0.97, 0.55 and 0.38 GJ/m^2/year, respectively [10]. New, and much more severe, standards for thermal protection of buildings were set in 2003 by a new Russian building code (SNiP 23-02-2003 "Thermal Performance of Buildings" [15]). These standards are based on the total number of heating degree days (HDD) for particular climatic zone/city.

Another important factor affecting the heating standards is the dwelling size or the number of storeys. Thermal performance of individual low-rise buildings (1–3

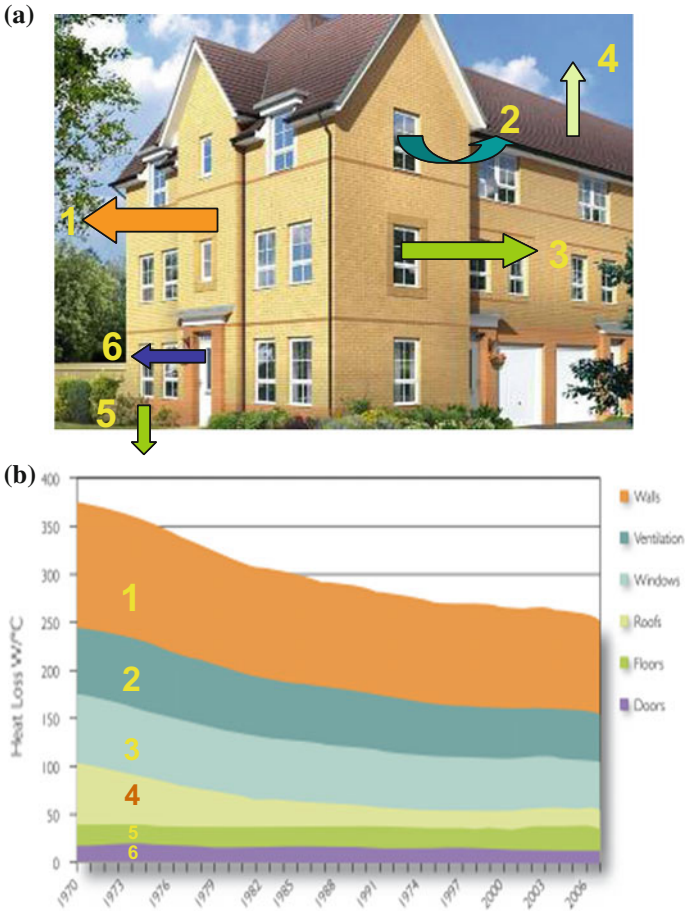

Fig. 4.1 **a** Schematics of heat losses of building, **b** share of heat losses in the average UK building and the whole building stock [16]

storeys) and multi-storied apartment buildings (4–25 storeys) differs essentially: in smaller dwellings, 1 m^2 of heated rooms area is accompanied by 1.7–3.3 m^2 of building fabric area, whereas for larger buildings this ratio is considerably less and varies from 0.6 to 1.3 m^2 [14], which leads to radically lower heat losses through the building constructions (Fig. 4.2). It is interesting to mention that the structure of heat losses in the Russian dwellings erected before 2000 (the left half of Fig. 4.2) is close to that reported for the average building in the UK (Fig. 4.1b).

It can be concluded from Fig. 4.2 that for modern dwellings with better fabric insulation, a portion of the heat losses through ventilation system significantly increases and becomes dominant in high-rise buildings. The same tendency was reported by many researchers (see, e.g., [17, 18]). Therefore, a further improvement in the dwellings thermal efficiency is associated, first of all, with a *decrease in heat losses through ventilation system*. This can be achieved by implementation of traditional and novel technologies of heat recovery in ventilation systems (see, e.g., [17–21]).

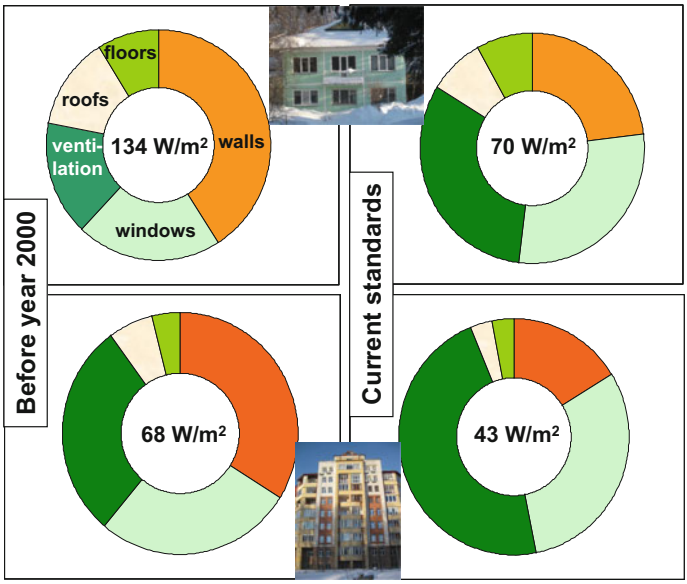

Fig. 4.2 Share of heat losses in individual, two-storied (*top*), and apartment, nine-storied (*bottom*) buildings under climatic conditions of Moscow [16]. *Left* buildings erected before 2000, *right* buildings erected according to the new standards of 2003 [14]. Numbers denote the specific heat losses

4.3 Requirements to Ventilation System in Cold Climates

In this chapter, we briefly consider specific conditions typical for operation of ventilation systems in countries with cold climate.

4.3.1 Heat Recovery

According to the previous studies [14, 17, 20, 21], the heat losses through ventilation system of buildings increase at larger temperature differences between indoor and outdoor air. In cold climates, this difference can often exceed 50 °C. Indeed, Fig. 4.3 clearly demonstrates that in many world's territories the average winter temperature is as low as (−30) to (−45) °C. It is reasonable to assume that these losses correlate with the number of heating degree days $\mathrm{HDD} = H(T_{\mathrm{bas}} - \check{T}_{\mathrm{out}})$, where H is the heating period, T_{bas} is a base indoor temperature (in Russia it is fixed at 20 °C [24]), and $\check{T}_{\mathrm{out}}$ is the outdoor temperature averaged over the heating period (see Table 4.1). In Russia, the heating period $H = H8$ is fixed as a cold season with the mean daily outdoor temperature $T_{\mathrm{out}} \leq 8$ °C. For instance, in Moscow, $H8 = 214$ days and $\mathrm{HDD}\ (T_{\mathrm{out}} \leq 8\ ^{\circ}\mathrm{C}) = \mathrm{HDD8} = 4943$ (°C·day)/year, in Novosibirsk—230 days and 6601 (°C·day)/year, and the average HDD8 in Russia is 5140 (°C·day)/year (Table 4.1).

In other cold countries, the heating period H is calculated in a somewhat different way and the base indoor temperature is fixed lower (16–18 °C) than in Russia. As a result, the so-called HDD10 (an arctic heating degree days below 10 °C) differs from HDD8 as displayed in Table 4.1 for the selected Russian cities. For comparison, the same indicator (in (°C·day)/year) for several European capitals is as follows: London —1860 [25], Helsinki—2601, Oslo—2324, Stockholm—1847, Copenhagen—1311 [14]. Thus, on the largest part of the territory of Russia, the demand for thermal

Table 4.1 Characteristics of heating season in selected Russian cities (the data were taken from [14, 26]) and some useful estimations (see text below)

City	$H8$ (day/year)	$\check{T}_{\mathrm{out}}$ (°C)	HDD8, [(°C·day)/year]	HDD10 [(°C·day)/yr]	$T^{\mathrm{a}}_{\mathrm{min}}$ (°C)	W_{av} (kW)	Q (GJ/year)
Moscow	214	−3.1	4943	2964	−28	1.2	22.2
St. Petersburg	220	−1.8	4796	2750	−26	1.1	21.6
Rostov on Don	171	−0.6	3523	1676	−22	1.0	14.7
Yekaterinburg	230	−6.0	5980	3759	−35	1.3	26.9
Novosibirsk	230	−8.7	6601	4115	−39	1.5	29.7
Yakutsk	256	−20.6	10394	–	−55	2.1	46.8
Khabarovsk	211	−9.3	6182	4425	−31	1.5	27.8

[a]The reference outdoor temperature used for designing the regional heating systems

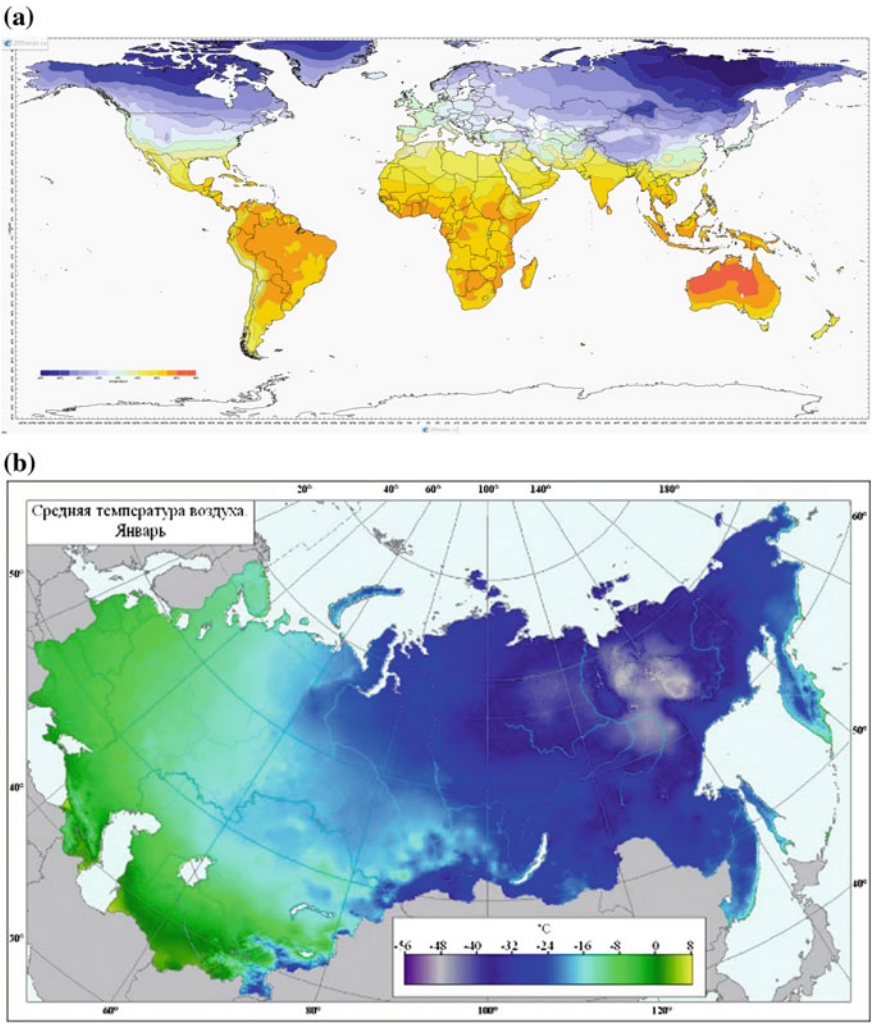

Fig. 4.3 Average air temperature in January in the World [22] (**a**) and territory of the ex-USSR [23] (**b**)

energy needed for space heating is higher than in the Northern Europe. In much the same way, very cold territories are located in the northern parts of Canada and USA (Fig. 4.3), e.g., for Barrow, Alaska HDD10 = 11,055 (°C·day)/year that is similar to Yakutsk, Russia (Table 4.1). One may expect that the most efficient measures to reduce the ventilation heat losses have to be made in the territories with large HDD values.

The data of Table 4.1 allow a brief estimation of the power W_{av} necessary for heating outdoor air up to the base indoor temperature of 20 °C, averaged over the

heating period $H8$. For a reference apartment/house of 100 m^2 total area (or the total volume $V = 300$ m^3) with the air exchange E of 0.5 h^{-1}, this power is $W_{av} = C_p VE\left(T_{bas} - \check{T}_{out}\right)$, where the air-specific heat C_p is assumed constant and equal to 1.25 kJ/(m^3 K). This power is displayed in Table 4.1 together with the annual amount of heat Q necessary for the outdoor air preheating. The annual heat demand only for preheating of outdoor air is larger that the maximum space heating standards established for a low-energy building. For instance, according to the German rules, the latter is 50 kWh/(m^2 year) that corresponds to 18 GJ/year for the reference 100 m^2 house. These estimations clearly demonstrate that recovery of ventilation heat is strictly necessary in cold countries in order to satisfy the standards of energy efficient building and make bills for heating acceptable.

4.3.2 Moisture Recovery

Another problem that appears during cold winter is continuous loosing of moisture through ventilation system [21, 27]. Indeed, the absolute humidity of supplied (outdoor) air d_{out} is extremely low (e.g. ≤0.29 g/m^3 at −30 °C) that results in dramatic reducing the indoor relative humidity (down to 10–20%, Fig. 4.4) in winter season that is far out of the borders of indoor thermal comfort. The indoor RH is also sensitive to the presence of central heating period (Fig. 4.4).

Let us estimate the mass M of water vapour that has to be generated inside the mentioned reference house in order to maintain an acceptable RH of 40% (at $T_{in} = 20$ °C, this corresponds to the indoor absolute humidity $d_{in} = 7.1$ g/m^3) if the outdoor tempera ture is −30 °C: $M = VE(d_{in} - d_{out}) = 1.02$ kg/h. A power of 0.7 kW is required for the forced vapour generation (evaporation) that is ca. a half of the average power spent for air preheating (Table 4.1).

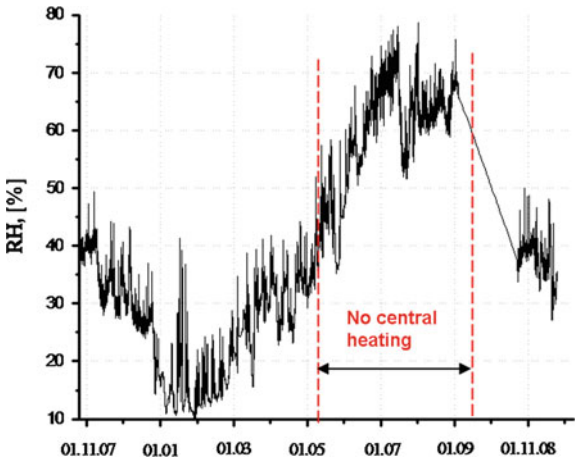

Fig. 4.4 Typical evolution of the indoor relative humidity in a room with natural air infiltration (Novosibirsk, Russia: 55° 02′N, 83° 00′E). The RH data between September 4, 2007, and October 25, 2007, were not recorded

Therefore, in cold countries, it is extremely important to organize not only efficient heat exchange between exhaust and supply air flows, but also a partial exchange of moisture between these flows to maintain the indoor humidity within the comfortable range.

The partial transfer of water vapour from the exhaust flow to the supply one is also necessary in order to avoid a frost formation near the outlet of exhaust air flow of ventilation system. It may happen when outdoor air is cooled below a water freezing temperature [28, 29]. Table 4.2 shows that a dew point of the exhaust air is rather high, and to avoid or at least alleviate a frost formation the absolute humidity of the exhaust air has to be reduced down to 0.2–0.5 g/m^3.

4.3.3 Modern Heat and Moisture Recovery Approaches

As discussed above, for winter season in severe climates (typical for Russia, the Northern Europe, the USA, and Canada), the difference ΔT between indoor and outdoor temperature can reach 50–60 °C or even more that leads to enormous heat losses and freezing of moisture at the system exit. As a result, common heat recovery units integrated in ventilation systems may not be capable to work at these conditions. Moreover, such systems are not able to manage the indoor humidity, which dramatically reduces in winter season that greatly disbalances the indoor heat comfort. Thus, to fill these three main gaps in the current ventilation techniques, the following actions should be performed:

- efficient exchange of heat between the exhaust and supply air fluxes to reduce heat losses,
- reasonable drying of the exhaust air to avoid ice formation at the system exit,
- moisturizing the supply air to provide indoor conditions of human thermal comfort.

There are many technologies suggested and studied for resolving these problems. Here we just briefly survey the current state of the art in this field. The interested reader is referred to appropriate reviews, e.g., Ref. [21] which specifically addresses energy recovery systems in apartment buildings located in cold climate countries using central air handling units. In that review, heat exchangers recovering sensible heat are compared with energy exchangers with recovery of both sensible and latent heat, whereas here we consider only the energy exchangers.

Table 4.2 Dew point of the exhaust air at various RH values and T_{in} = 20 °C

RH (%)	1	2	5	10	20	30	40	60
d_{in} (g/m^3)	0.18	0.36	0.88	1.8	3.6	5.4	7.2	10.8
Dew point (°C)	−34.5	−28	−19	−11	−3	+2	+6	+11

4.3.3.1 Energy wheels

Energy wheels are regenerative exchangers aimed to exchange heat and moisture between supply and exhaust air streams in ventilation systems of buildings (see the fundamentals in Refs. [30, 31]). When humid and warm exhaust air flows through the adsorbent coated wheel in the return section, both moisture and heat taken from this stream are adsorbed and stored in the wheel. Therefore, the frost formation in this section becomes less likely [30]. As the wheel turns, the part, where the sensible and latent energies have been accumulated, appears in the supply section where cold and dry outdoor air takes the stored heat and moisture and becomes more warm and humid. The wheel effectiveness is typically 50–85% for both latent and sensible heat recovery [32] that is sufficient for the majority of applications. These units exhibit a low pressure loss only of 50–200 Pa that is lower than for most of other air-to-air heat exchangers [30].

Some shortcomings are inherent for energy wheels, namely, moving parts that need appropriate maintenance, carryover leakage due to penetration of a small fraction of exhaust air to inlet air that reduces the efficiency and can be a source of odour transfer [33].

4.3.3.2 Membrane energy exchangers

Another solution to resolving the mentioned severe problems is the application of porous polymer membranes partially permeable for moisture. Membrane energy exchangers are a new class of flat plate energy exchangers proposed by Zhang [34], which already has passed away from fundamentals to engineering applications [27, 35, 36].

Such energy exchangers are similar to traditional flat heat exchangers with the difference that the former use polymeric plates permeable for water instead of common metal sheets. Partial transfer of water through the membrane helps in drying the exhaust flux and moisturizing the supply one. The transfer is driven by the gradient of moisture concentration in the streams and depends on the composition, shape, and size of the membrane.

These energy exchangers are simple and reliable. There are no moving parts, and no external heat for regeneration of desiccant is required. However, the problem of odour can still be important because there is a mass transfer through the membrane. Frosting in the membrane, its mechanism and limits also need more theoretical and experimental investigations, because so far the majority of tests have been performed in warm and humid climates, like in Hong Kong [37], rather than in cold and dry ones. At least, paper membranes are expected to be not appropriate for cold climates due to the ice formation on the membranes [21].

Despite significant progress achieved for the past decades in developing energy exchangers for cold climates, some of which have already appeared in the marked, still there is much room for further improving the existing devices and development of new advanced energy exchangers.

4.4 The New Approach to Regeneration of Heat and Moisture in Ventilation System

In this section, we describe a new approach (the so-called VENTIREG) for regenerating heat and moisture in ventilation systems which allows resolution of the problems typical for cold countries, which are discussed above. Several prototypes of VENTIREG units were designed and tested under both laboratory conditions and real climatic conditions of the Western Siberia (Novosibirsk city: 55° 02′N, 83° 00′E).

4.4.1 Description of the Approach

To exchange the sensible heat between the supply (fresh) and outlet (exhaust) air streams, a layer of heat storing material (HSM) is placed closer to the unit exit (1 on Fig. 4.5). A layer of solid desiccant (adsorbent) is located closer to the unit entrance from the room side (2 on Fig. 4.5). It serves as a moisture buffer. The VENTIREG unit operates in two modes:

- outflow mode (Fig. 4.5, upper part): a warm and humid indoor air is blown by an extract fan through the dry adsorbent, which captures and retains the indoor moisture [38]. Dried and warm air enters layer 1 and heats it up. After that, the air flux switches;
- inflow mode (Fig. 4.5, bottom part): a dry and cold outdoor air is blown by a supply fan through the warm layer of HSM and is heated up to temperature T close to that in the room T_{in}, thus recovering the stored heat. Passing through the layer of the humid adsorbent, warm and dry air causes the adsorbed water to be desorbed and brings moisture back to room [38], thus maintaining the indoor moisture balance. Because of the finite heat capacity of layers 1 and 2, the temperature of incoming air is slowly decreasing, and the air flux switches when the difference ($T_{in} - T$) reaches a predetermined value ΔT_0, and so on.

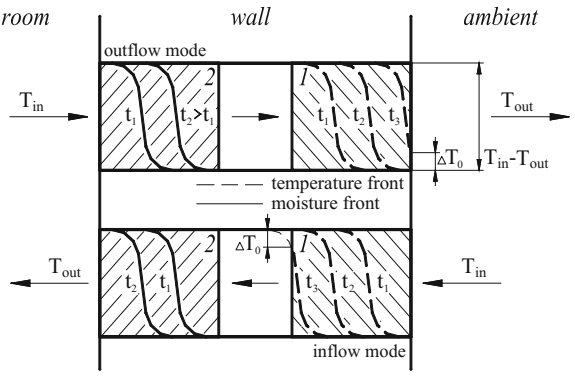

Fig. 4.5 Schematics of the VENTIREG process for simultaneous regeneration of heat and moisture in ventilation system [20]. The temperature and moisture profiles are shown at various times $t_1 < t_2 < t_3$

After a transient period, a steady-state regime is observed with the time interval $\Delta\tau$ (a half cycle time) between the flux switches (see Fig. 4.8). For continuous operation, two similar units should work in the opposite modes (Fig. 4.5).

4.4.2 Selection of Proper Adsorbent

Adsorbent is a key element of the VENTIREG unit. On the one hand, it should have sufficient affinity to water vapour in order to catch moisture and to dry an exhaust air down to a low dew point. On the other hand, it should easily release the retained moisture to a dry air stream without additional heat supply. By now, there is no theoretical prediction what has to be an optimal adsorbent for the VENTIREG units in different climates; however, several commercial desiccants were directly tested for this application [38]. The adsorbents were alumina A1 (γ-Al_2O_3), microporous silica gel of KSM type, and novel composite adsorbents IK-011-1 and IK-011-2. The alumina and silica are common adsorbents used for gas drying [39], whereas IK-011-1 and IK-011-2 consist of alumina and silica, respectively, doped with calcium chloride (12 mass %). The salt was introduced into the alumina pores by "incipient wetness" impregnation from the salt aqueous solution and subsequent drying at 150 °C for 2 h [40]. The salt is highly hygroscopic and can significantly increase both static and dynamic water sorption capacity [40, 41]. Cylindrical grains of alumina and IK-011-1 of 1.8 and 4.5 mm diameter and 6–8 mm length as well as spherical grains of silica of 2–6 mm diameter were used in those experiments.

First, these adsorbents were tested in a flow adsorber under typical conditions of air drying (pressure 5.8 bar, contact time 0.3 s, inlet humidity 17 g/nm^3). The breakthrough curves presented in Fig. 4.6 clearly demonstrate that for all adsorbents tested the dew point of outlet air is lower than –40 °C that makes them potentially applicable not only for air drying, but for the VENTIREG application as well. The water sorption capacity increases in the order IK-011-2 > IK-011-1 > KSM > A1. The breakthrough time for IK-011-1 was 2–2.5 folds longer than for the pure alumina. Hence, the modification of common adsorbents with hygroscopic salts can, indeed, significantly increase the dynamic sorption capacity (for alumina, from 0.14 g/g or 100 g/dm^3 up to 0.35 g/g or 280 g/dm^3). Similar enhancement was observed for mesoporous silica gel KSK modified by $CaCl_2$ (IK-011-2), for which the dynamic sorption capacity was even larger than for IK-011-1 (up to 0.52 g/g or 360 g/dm^3). Unfortunately, this composite sorbent demonstrated lower hydrothermal stability than IK-011-1 [40].

The dynamic sorption capacity of IK-011-1 appeared to reduce from 0.35 to 0.26 g/g for larger adsorbent grains (4.5 mm vs. 1.8 mm diameter). This indicates that intra-grain diffusion of water vapour can be a process that controls the adsorption rate. From this point of view, it is profitable to reduce the grain size; however, it can result in dramatic increasing the hydrodynamic resistance of the

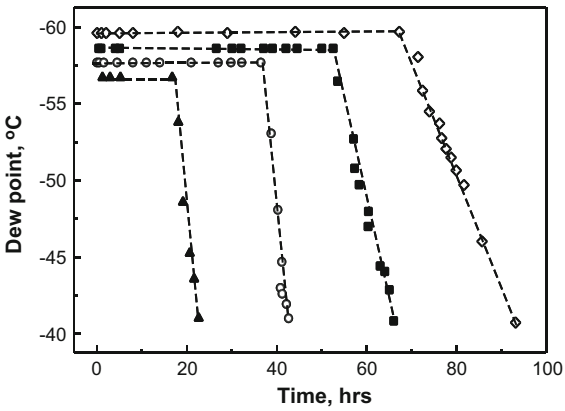

Fig. 4.6 Air dew point at the exit of flow adsorber filled with IK-011-1 (*filled square*) and IK-011-2 (*open diamond*) as well as with common commercial desiccants—silica KSM (*open circle*) and alumina A1 (*filled triangle*) [40]

adsorbent bed (Fig. 4.7), so that the grain size has to be a compromise between these tendencies (tentatively, 2–4 mm).

At the second stage, the three mentioned desiccants were specifically tested under laboratory conditions typical of the VENTIREG process. The experiments were carried out as follows: the adsorbent (ca. 3 kg) was placed into a cylindrical adsorber of 210 mm diameter and 160 mm length. At the adsorption stage, the air at the room temperature and relative humidity $RH = (29.5 \pm 1.5)$ % was passed through the adsorber. After 10 min, a reverse flow of dry air ($RH = 2.3\%$) was supplied at room temperature from the opposite side of the adsorber (desorption stage). The air flux rate was changed from 5.0 to 31.3 m^3/h that corresponded to the contact time 4.0–0.6 s. More experimental details can be found elsewhere [38].

These tests revealed that the commercially produced desiccants can be effectively used as moisture buffers regulating the moisture of the outlet air flow in a wide range. The degree of both air drying and humidification increased in the order

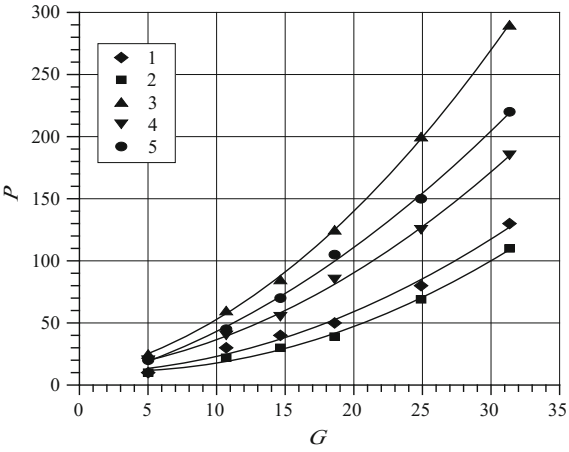

Fig. 4.7 Dependence of the hydrodynamic resistance of adsorbent layer (length 160 mm, diameter 210 mm) on the air flow rate [38]: 1—IK-011-1 (4.5/8 mm); 2—alumina A1 (4.5/8 mm); 3—IK-011-1 (1.8/6 mm); 4—alumina A1 (1.8/6 mm); 5—KSM. *P*, Pa; G, m^3/h

IK-011-1 > KSM > A1 similar to that found for the dynamic water sorption capacity (Fig. 4.6). The use of the IK-011-1 sorbent modified by $CaCl_2$ allows increasing the amount of accumulated moisture by 1.3–1.8 times as compared with the pure alumina. The IK-011-1 absorbs additional amount of water vapour due to the chemical reaction [42]

$$CaCl_2 + nH_2O \Leftrightarrow CaCl_2 * nH_2O \tag{4.1}$$

with the formation of solid hydrates inside the alumina pores (n = 0.33, 1, 2, and 4). Therefore, composite IK-011-1 was selected as the most promising for further testing in the VENTIREG prototypes.

The degree of air drying/humidification depends on the nature of adsorbent, its grain size, the contact time and can reach 0.90–0.98. For example, for IK-011-1 grains (diameter/length = 1.8/6 mm), it reaches 0.98 at the inlet flow rate of 5.0 m^3/h, means, practically all moisture that was introduced into the layer is absorbed by the adsorbent. Even at the flow rate 31.3 m^3/h ($\tau \approx 0.6$ s), the layer absorbs 0.74 of the income moisture. For the pure alumina, these values are 0.75 and 0.62, respectively. For larger grains, the degree of drying appropriately reduces likely due to intra-grain diffusion limitations.

It is interesting that varying the salt nature or/and the salt content one can intently tailor the sorption ability of the composite as discussed in [42]. In particular, smaller salt content can be recommended at larger indoor humidity. Adsorbent optimal for the VENTIREG should exhibit no or little hysteresis which may complicate water desorption. To alleviate the problem of odour and VOC transfer between the income and outcome air streams, the optimal adsorbent has to poorly adsorb these compounds.

4.4.3 Designing and Testing of VENTIREG Prototypes

To study and optimize the heat and moisture recovery, four experimental units with the air flux up to 40 (I), 135 (II, III) and 220 (IV) m^3/h were built and tested (Fig. 4.8). The adsorbers were filled with composite IK-011-1 selected as the best water buffer. The heat storage part was organized as a bed of loose particles of gravel of irregular shape (4–7 mm in size). Units I–III could operate only under intermittent mode because they had only one adsorber. Unit IV was designed for continuous operation and had two “adsorbent—HSM” beds working in opposite modes (Fig. 4.5).

Typical evolution of the air temperature T during cycling operation is displayed in Fig. 4.9 (unit I). The steady-state regime is set after 10–20 min. All the regular tests were performed under this regime. The half cycle time $\Delta\tau$ increases at larger ΔT_0 and longer contact time (or smaller Re-numbers) as shown in Fig. 4.10 plotted for unit III.

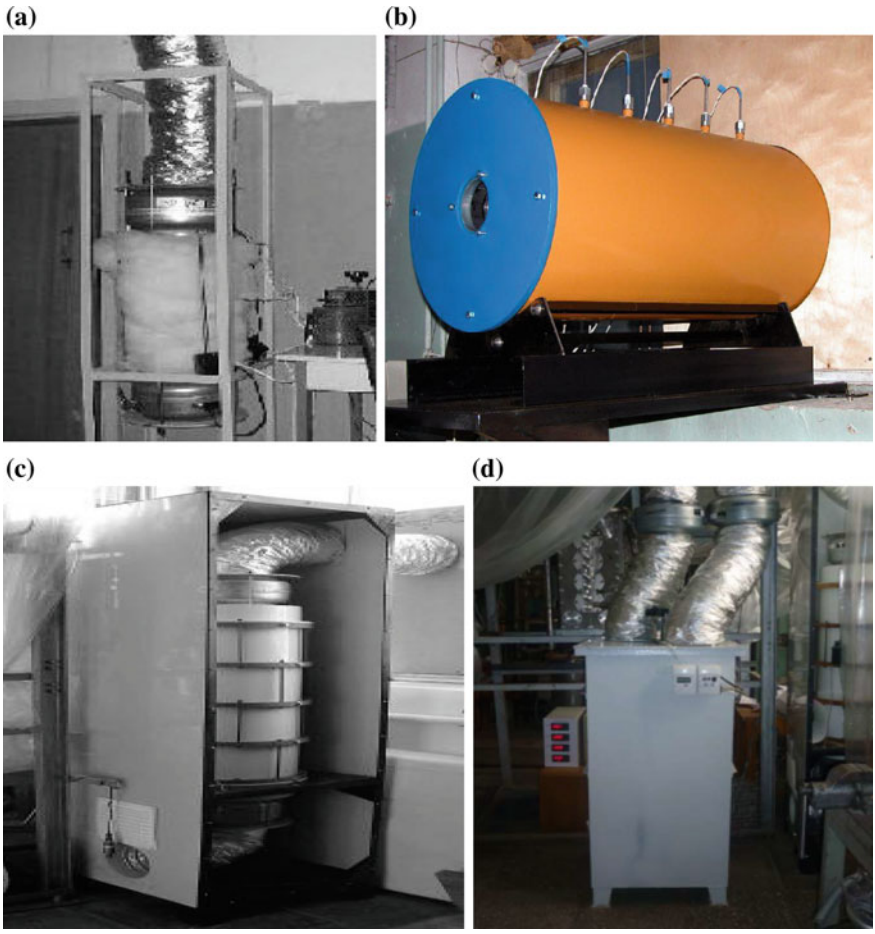

Fig. 4.8 View of VENTIREG units I–IV: the inlet air flow rate up to 40 m^3/h (**a**), 135 m^3/h (**b**, **c**), and 220 m^3/h (**d**)

Figure 4.11 displays typical evolution of the air temperature and absolute humidity as function of time t for cycling (steady state) VENTIREG operation (unit III). During the outflow mode, the indoor air at $T = 20$ °C and $d = 5$ g/m^3 was passed through the adsorbent and HSM. At the beginning of this mode, the air was dried and cooled down to 0.5 g/m^3 and −26 °C, respectively. During this first half of the cycle, the air temperature and humidity were gradually increasing until the temperature reached −18 °C (at $\Delta\tau \approx 580$ s) that was 10 °C higher than the outdoor temperature −28 °C ($\Delta T_o = 10$ °C). Then, the system was switched to the inflow mode: the outdoor air at $T = -28$ °C and $d = 0.35$ g/m^3 was passed through the HSM and adsorbent (see Fig. 4.5). At short times, the air was humidified and heated up to 4.8 g/m^3 and 20 °C. Then, its temperature and humidity were

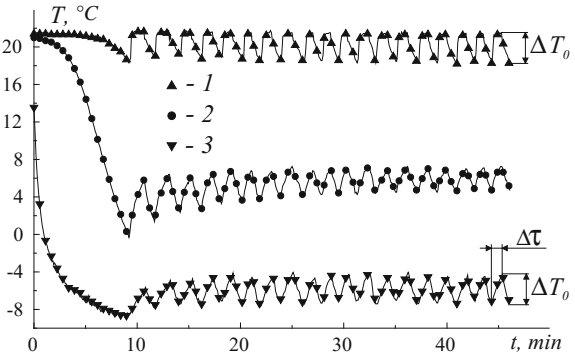

Fig. 4.9 Typical evolution of the air temperature T during cycling operation of unit I (*1* indoor side, *2* between the adsorbent and HSM, *3* outdoor side). T_{in} = 20.5 °C, T_{out} = −8 °C, ΔT_0 = 3 °C

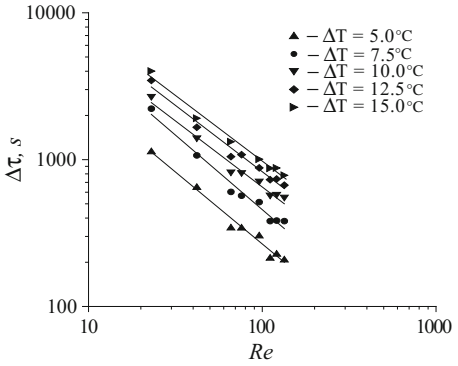

Fig. 4.10 Half cycle time Δτ (s) as a function of the *Re*-number (unit III) [20]

gradually decreasing until the temperature reached 10 °C that was 10 °C lower than the room temperature, and the next cycle was started (Fig. 4.11).

The air fluxes during the inflow and outflow modes were equal, and the data given in Fig. 4.11 allow estimation of the efficiencies of heat regeneration $\theta = S_{ACDE}/S_{ABDE}$ and moisture regeneration $\beta = S_{KMOP}/S_{KLOP}$, where S is the area of appropriate figures. As shown in Fig. 4.11, the θ value is rather large: almost all heat is accumulated during the outflow mode and returned to the room during the inflow mode (only the amount of heat corresponding to area ABC is lost, Fig. 4.11). The heat regeneration degree would be even larger at $\Delta T < 10$ °C.

Unit III was continuously tested under climatic conditions of the Western Siberia (Novosibirsk city: 55° 02′N, 83 °00′E) during a full HDD season of 2005–2006. As the outdoor temperature T_{out} and, hence, the difference $\Delta T_{MAX} = T_{in} - T_{out}$ were not constant during these field tests, it is convenient to present the heat regeneration degree θ as a function of the dimensionless temperature difference $\Delta\tilde{T} = \Delta T_o/\Delta T_{MAX}$ (Fig. 4.12a). The collected data demonstrated that a high heat regeneration efficiency (θ > 0.9) can be readily obtained at $\Delta\tilde{T} \approx 0 \div 0.25$ that is a very common case. The degree of moisture regeneration was lower (Fig. 4.12b).

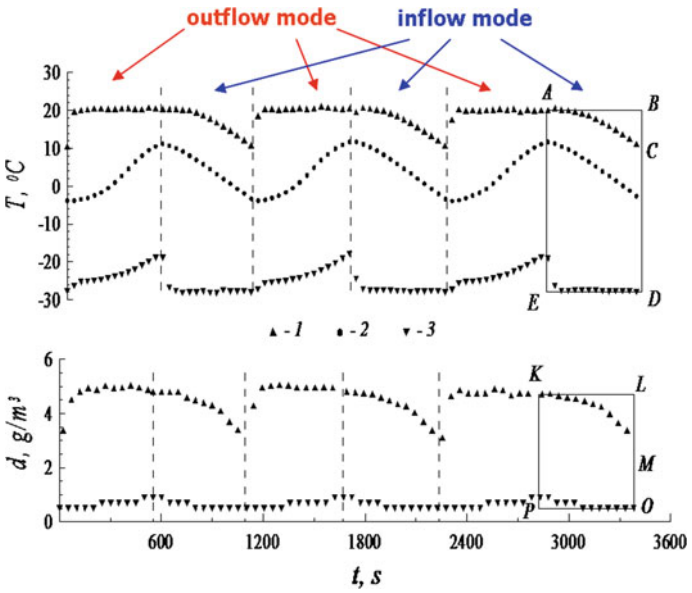

Fig. 4.11 Evolution of the air temperature T and the absolute humidity d as functions of time t during cycling operation of VENTIREG unit III (*1* indoor side, *2* at the middle of the unit, *3* outdoor side). T_{in} = 20 °C, T_{out} = −28 °C, ΔT_0 = 10 °C. Air flux 123 m^3/h

For generalization, it is similarly presented in Fig. 4.12b as a function of dimensionless difference in the absolute humidity $\Delta\tilde{d} = \Delta d/\Delta d_{MAX}$, where Δd is the difference in the absolute humidity at the moment of flux switching, Δd_{MAX} is the maximal difference in the absolute humidity during a particular experiment. Nevertheless, the β values larger than 0.7 were recorded at $\Delta\tilde{d} = 0 \div 0.7$, so that an efficient regeneration of both heat and moisture took place in VENTIREG unit III. It is important that both these efficiencies can be easily and purposefully varied by managing the half cycle time Δτ which depends on ΔT_o and the *Re*-number (Fig. 4.10), and the range of Δτ-variation can be rather wide (3–70 min).

It is somewhat surprising that for unit III the values of both θ and β can be approximated by a unique equation

$$\theta(\beta) = 1 - 0.38 \cdot \Delta\tilde{T}(\Delta\tilde{d}) - 0.12 \cdot \Delta\tilde{T}(\Delta\tilde{d})^2. \tag{4.2}$$

The fact that both θ and β are described by the same equation may indicate a strong coupling of heat and mass transfer processes when a humid air passes through an adsorbent layer [43]. At the same ΔT_o, the efficiency of heat regeneration increases with the rise of ΔT_{MAX} that means the VENTIREG unit operates better at colder climates. Indeed, if ΔT_o = 10 °C, at ΔT_{MAX} = 50 °C, $\Delta\tilde{T}$ = 0.2 and θ ≈ 0.92, at ΔT_{MAX} = 30 °C θ ≈ 0.87, whereas at ΔT_{MAX} = 20 °C the θ value is again lower (0.79), yet very promising for practice.

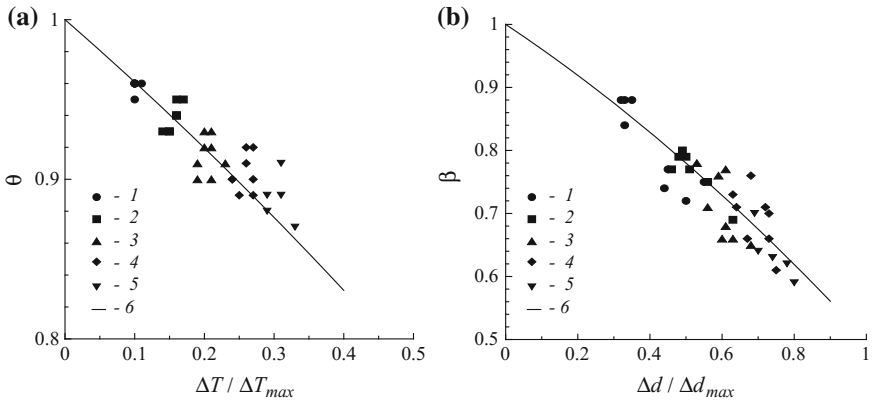

Fig. 4.12 **a** Efficiency of heat regeneration θ as a function of the relative temperature difference $\Delta T_o/\Delta T_{MAX}$; **b** efficiency of moisture regeneration β as a function of the relative difference in the absolute humidity $\Delta d/\Delta d_{MAX}$. ΔT_0 = 5.0 (*1*), 7.5 (*2*), 10.0 (*3*), 12.5 (*4*), 15.0 (*5*) °C; *6* calculated according to Eq. (4.2). Unit III

It is interesting to note that equations similar to Eq. (4.2) were obtained during field tests of VENTIREG units II and IV. This is probably because of the fact that heat and mass transfer processes and the main geometrical proportions [44] of the all three units are similar.

Very important finding of the field tests of VENTIREG units II-IV is that no ice formation inside the units or at the units exit was revealed during the whole winter period. Another finding is a very little maintenance required for the VENTIREG units tested.

4.4.4 Other Aspects of the VENTIREG Technology

Here we consider several issues of further development of the VENTIREG approach, like electricity consumption, scaling-up, as well as economic, hygienic, and social aspects.

Composite sorbent IK-011-1 was found to demonstrate better performance than common desiccants, like silica and alumina, first of all, due to large water sorption capacity and moderate affinity to water vapour. This allows essential minimization of the adsorbent amount and unit size. The reduced amount of adsorbent leads to lower hydrodynamic resistance of the VENTIREG unit as well. As a result, the using of cheap blade-type fans instead of centrifugal ones becomes possible that will give a reduction in the electricity consumption. For instance, unit III consumes for air blowing only 20–40 W of electric power and provides the heating load of 600–1400 W that corresponds to the electrical coefficient of performance as high as 25–35.

The magnification of VENTIREG units from laboratory to larger size may lead to the decrease in the process efficiency with the raise of unit diameter. The scale-up theory shows that this effect is a result of the radial non-uniformity of the velocity distribution in the layer (column) [45, 46]. Application of appropriate mathematical models will permit analysis, optimization, and design of VENTIREG units for heat and moisture recovery in ventilation systems for single room, family house, and large residential buildings. The final aim is to meet the indoor air quality and saving energy standards in such dwellings. Harmonization of the adsorbent with the VENTIREG process is another important goal of future analysis. This analysis is still necessary to realize which adsorbents are optimal for the VENTIREG process in various climatic zones.

Economic impact of the VENTIREG approach is due to the expectation that it reliably supplies fresh air at cost lower than common systems. Estimations [47] based on current performance give for a standard two rooms apartment (47 m^2) in Novosibirsk, Russia, the unit capital cost of about 90–110 Euro, annual saving in operating costs about 40–45 Euro, and a payback period of 2.0–2.6 years. The energy saving is 43–45%. Larger saving can be expected for larger apartments under conditions of Northern Europe, where the cost of electricity, gas, and oil is much higher. Further improvements in the VENTIREG system will make it possible a further increase in the economic impact.

Social impact arises mainly from the fact that the VENTIREG unit provides comfortable and healthy environment in dwellings, which tightly satisfy specified range of human comfort (Fig. 4.13). The final result is the improvement in human living standards.

Thus, the suggested VENTIREG unit exchanges stale, contaminated room air with fresh outdoor air, recovering up to 95% of energy and 70–90% of moisture from the exhaust air and prevents the formation of ice at the unit exit. For countries with a cold climate, this makes it possible to bring in more conditioned fresh air at

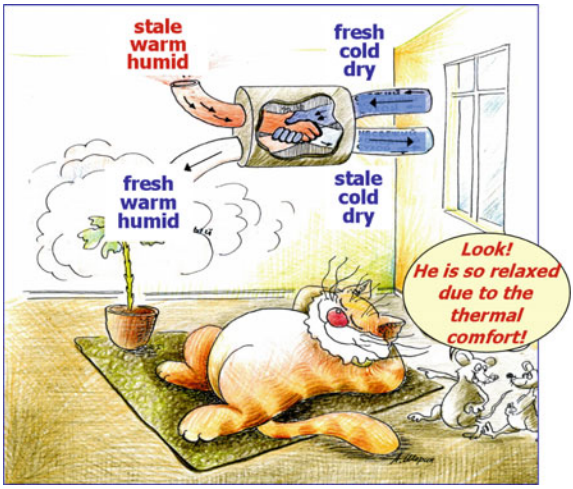

Fig. 4.13 VENTIREG as looked with the eye of the artist (drawn and kindly provided by A. Shorin)

lower cost. The prototype units III and IV supply fresh air at 135–220 m^3/h with effective regeneration of both heat and moisture. This will provide 0.5–1.0 air changes per hour for a typical one family detached house. The unit requires very little maintenance, has a low capital cost, and is compact and energy efficient.

Hygiene is another very important issue. Indeed, the exhausted indoor air may contain various contaminants, including pathogenic bacteria and microbes. Before field testing the VENTIREG units, we had not performed any special precautions against these health hazards. After the field tests during whole winter period, we found no organic contaminations or bacteria growth inside the unit. A possible reason is that no formation of liquid water occurs inside the device during its cyclic operation. Indeed, water caught by the sorbent is stabilized in the form of crystalline hydrates of the salt ($CaCl_2$) according to reaction (4.1). As these hydrates are solid substances, the environment inside the device is not humid; hence, it does not encourage the bacteria formation and growth. Even if some amount of the salt solution forms at high water uptakes, the concentration of the salt in this solution will be larger than 25 wt%. So large salt concentration allows avoiding the bacteria formation and multiplication. This is an essential advantage of the VENTIREG unit over standard ventilating and air-conditioning systems containing liquid water. Future study will show whether this unit requires standard precautions, namely comprehensive epidemiological investigation, periodic cleaning, and inspections for possible bacteria outbreaks as well as appropriate preventive disinfection measures (UV-radiation, ozonation, biochemical treatment, etc.).

References

1. United Nations Population Fund (2012) State of the World population 2011
2. UN-HABITAT (2008) State of the world's cities report 2008–2009: Harmonious cities: http://unhabitat.org/books/state-of-the-worlds-cities-20082009-harmonious-cities-2/. Accessed 25 Aug 2016
3. James P, Magee L, Liam S, Scerri A, Steger M (2015) Urban sustainability in theory and practice: circles of sustainability. Routledge, London
4. Rassia S, Pardalos P (eds) (2015) Cities for smart environmental and energy futures, impacts on architecture and technology. Springer, New York
5. Eurostat (2010) Energy yearly statistics 2008, Publication Office of the European Union
6. DECC (Department of Energy & Climate Change) (2013) Energy consumption in the UK. Overall Energy Consumption Factsheet, Department of Energy & Climate Change. Available from https://www.gov.uk/government/publications/energy-consumption-in-the-uk. Accessed 25 Aug 2016
7. NRC (2006) Operating energy in buildings. http://cn-sbs.cssbi.ca/operating-energy-buildings. Accessed 25 Aug 2016
8. Ziesing HJ, Schlomann B, Rohde C, Eichhammer W, Kleeberger H, Tzscheutschler P (2011) Anwendungsbilanzen für die Endeniergiesek-toren in Deutschland im Jahr 2008. In AG Energiebilanzen beauftragt vom BMWiProjektnummer 40/08
9. Report «On enhancement of energy efficiency of the Russian economy». Arkhangelsk, April 2009. http://www.cenef.ru/file/Report%2025.05.09.pdf. Accessed 25 Aug 2016

10. Bashmakov I, Borisov K, Dzedzichek M, Gritsevich I, Lunin A (2008) Resource of energy efficiency in Russia: scale, costs and benefits. CENEf—Center for Energy Efficiency. Developed for the World Bank, 102 p. http://www.cenef.ru/file/Energy%20balances-final.pdf. Accessed 25 Aug 2016
11. International Energy Agency (2010) Energy technology perspectives 2010: strategies and scenarios to 2050. OECD/IEA, Paris
12. Ürge-Vorsatz D, Novikova A (2008) Potentials and costs of carbon dioxide mitigation in the world's buildings. Ener Pol 36:642–661
13. The Future of Heating: a strategic framework for low carbon heat in the UK, Department of Energy and Climate Change (2012)
14. Filippov SP, Dil'man MD, Ionov MS (2013) The optimum levels of the thermal protection of residential buildings under climatic conditions of Russia. Therm Eng 60:841–851
15. SNiP 23-02-2003, Thermal Performance of Buildings (2004) State Construction Committee of the Russian Federation, The Central Institute for Type Designing, Moscow
16. Aristov YI (2015) Progress in adsorption technologies for low-energy buildings (review). Future Cities Environ 1(10):13p. doi:10.1186/s40984-015-0011-x
17. Liddament MW, Orme M (1998) Energy and ventilation. Appl Therm Eng 18:1101–1109
18. Mardiana-Idayu A, Riffat SB (2012) Review on heat recovery technologies for building applications. Ren Sust Ener Rev 16:1241–1255
19. Riffat SB, Zhao X, Doherty PS (2006) Application of sorption heat recovery systems in heating appliances—feasibility study. Appl Therm Engn 26:46–55
20. Aristov YI, Mezentsev IV, Mukhin VA (2008) A new approach to regenerating heat and moisture in ventilation systems. Energ Build 40:204–208
21. Alonso MJ, Liu P, Mathisen HM, Ge G, Simonson C (2015) Review of heat/energy recovery exchangers for use in ZEBs in cold climate countries. Build Environ 84:228–237
22. http://www.200stran.ru/maps_group28_item304.html. Accessed 25 Aug 2016
23. http://comrade-86.narod.ru/problems/img/rr001.jpeg. Accessed 25 Aug 2016
24. GOST 30494 96 (1999) Residential and Public Buildings: parameters of microclimate for indoor enclosures. State Construction Committee of the Russian Federation. The Central Institute for Type Designing, Moscow
25. http://ukclimateprojections.metoffice.gov.uk/media.jsp?mediaid=87928&filetype=pdf. Accessed 25 Aug 2016
26. www.http://teplo-info.com/. Accessed 5 June 2016
27. Zhang LZ (2012) Progress on heat and moisture recovery with membranes: from fundamentals to engineering applications. Energy Convers Manag 63:173–195
28. Bilodeau S, Brousseau P, Lacroix M, Mercadier Y (1999) Frost formation in rotary heat and moisture exchangers. Int J Heat Mass Transfer 42:2605–2609
29. Simonson CJ, Besant RW (1998) Heat and moisture transfer in energy wheels during sorption, condensation and frosting conditions. ASME J Heat Transf 120(3):699–708
30. Simonson CJ (2007) Heat and energy wheels. Encycl Energy Eng Technol 2
31. Zheng X, Ge TS, Wang RZ (2014) Recent progress on desiccant materials for solid desiccant cooling systems. Energy 74:280–294
32. ASHRAE (2008) ASHRAE handbook HVAC systems and equipment
33. Shah RK, Skiepko T (1999) Influence of leakage distribution on the thermal performance of a rotary regenerator. Appl Therm Eng 19:685–705
34. Zhang LZ, Jiang Y (1999) Heat and mass transfer in a membrane-based energy recovery ventilator. J Membr Sci 163(1):29–38
35. Zhang LZ, Zhang XR, Miao QZ, Pei LX (2012) Selective permeation of moisture and VOCs through polymer membranes used in total heat exchangers for indoor air ventilation. Indoor Air 22:321–330
36. Kistler KR, Cussler EL (2002) Membrane modules for building ventilation. Chem Eng Res Des 80:53–64
37. Zhang LZ, Niu JL (2001) Energy requirements for conditioning fresh air and the long-term savings with a membrane-based energy recovery ventilator in Hong Kong. Energy 26:119–135

38. Aristov YI, Mezentsev IV, Mukhin VA (2005) A study of the moisture exchange under air filtration through an adsorbent layer. J Eng Therm Phys 78:248–255
39. Yang RT (1997) Gas separation by adsorption processes. Imperial College Press, London
40. Aristov YI (2004) Selective water sorbents for air drying: from the lab to the industry. Cat Industry 1:36–41 (in Russian)
41. Aristov YI, Restuccia G, Cacciola G, Parmon VN (2002) A family of new working materials for solid sorption air conditioning systems. Appl Therm Engn 22:191–204
42. Gordeeva LG, Aristov YI (2012) Composites "salt inside porous matrix" for adsorption heat transformation: a current state of the art and new trends. Int J Low Carbon Techn 7:288–302
43. Close DJ, Banks PJ (1972) Coupled equilibrium heat and single adsorbate transfer in fluid flow through a porous medium - I. Predictions for a silica-gel air drier using characteristic charts. Chem Engn Sci 27:1143–1155
44. Aristov YI, Mezentsev IS, Mukhin VA (2004) Method for managing heat and moisture exchange in ventilation system for domestic and office compartments as well as the unit for realizing this method. RF Patent 2,277,205, 14 Dec 2004
45. Boyadijev C (2006) Diffusion models and scale-up. Int J Heat Mass Trans 49:796–799
46. Boyadjiev C, Doichinova M, Popova P, Aristov YI (2006) New approach to regenerate heat and moisture in a ventilation system: modeling. Paper presented at 11th international workshop on transport phenomena in two-phase flow, Bulgaria, Varna, 1–5 Sept 2006
47. Aristov YI, Mezentsev IS, Mukhin VA (2006) New approach to regenerating heat and moisture in ventilation systems. 2. Prototype of real unit. J Engn Thermophys 79:151–157

Chapter 5
Exergetic Performance of the Desiccant Heating, Ventilating, and Air-Conditioning (DHVAC) System

Napoleon Enteria, Hiroshi Yoshino, Rie Takaki, Akashi Mochida, Akira Satake and Ryuichiro Yoshie

Abstract The developed desiccant heating, ventilating and air-conditioning (DHVAC) system was evaluated using the exergetic method under controlled environmental conditions to determine the performances of the whole system and its components. Percentage contributions of exergy destruction of system components at different regeneration temperatures and reference temperatures were determined. Exergy destruction coefficient of different components at different regeneration and reference temperatures was presented. It was shown that exergetic performances varied with respect to the regeneration and reference temperatures. The exergetic performances based on thermal, electric, total exergy input, first definition and second definition efficiencies were shown. Based on the results, reference and regeneration temperatures affected the determination of the system performances and its components. It was shown that air heating coil (AHC), air fans and desiccant wheel (DW) contributed to large percentage of exergy destruction. Hence, the mentioned components should be given attention for further improvement in the system performances.

Keywords Desiccant dehumidification · Evaporative cooling · Air handling system · Exergy analysis

This chapter is an updated version of our paper [1].

N. Enteria (✉)
Building Research Institute, Tsukuba, Japan
e-mail: napoleon@kenken.go.jp; enteria@enteria-ge.com

H. Yoshino · A. Mochida
Tohoku University, Sendai, Japan

R. Takaki
Akita Prefectural University, Akita, Japan

A. Satake
Maeda Corporation, Tokyo, Japan

R. Yoshie
Tokyo Polytechnic University, Atsugi, Japan

N. Enteria et al. (eds.), *Desiccant Heating, Ventilating, and Air-Conditioning Systems*, DOI 10.1007/978-981-10-3047-5_5

Nomenclatures

AHC/HC	Air heating coil
C_p	Specific heat, kJ kg^{-1} K^{-1}
DEC/EC	Direct evaporative cooler
DHVAC	Desiccant heating, ventilating and air-conditioning
DW	Desiccant wheel
D_P	Depletion number
E	End
EA	Exit air
EAF	Exit air fan
HX [1]	Primary heat exchanger (big)
HX [2]	Secondary heat exchanger (small)
h	Enthalpy, kJ kg^{-1}
I_E	Electric current, A
I_{rr}	Irreversibility, kW
L, M, N	Variables
$\dot{m}$	Mass flow rate, kg s^{-1}
OA	Outdoor air
OAF	Outdoor air fan
P	Pressure, Pa
$\dot{Q}$	Heat transfer rate, kW
$\dot{Q}_X$	Input exergy in air heating coil, kW
R	Gas constant, kJ kg^{-1} K^{-1}
RA	Return air
RegT	Regeneration temperature
RT	Reference temperature
$\dot{S}$	Entropy rate, kW K^{-1}
S	Start
SA	Supply air
t	Time, s
T	Temperature, K
$\dot{W}$	Work rate, kW

Greek symbol

ε	Efficiency
ψ	Specific flow exergy, kJ kg^{-1}
ω	Humidity ratio, kg_{Vapor} kg_{Air}^{-1}
Φ	Relative humidity, %

Subscripts

a	Air
Des	Destruction
e	Exit
E_X	Exergy
Gen	Generation
HX	Heat exchanger
i	Inlet
l	Liquid
ma	Moist air
N	Node
o	Outlet
r	Reference condition
Sys	System
v	Vapor
w	Water

5.1 Introduction

Desiccant heating, ventilating and air-conditioning system (DHVAC) is one of the most promising alternatives to the refrigerant-based air-conditioning system [2, 3]. The main advantage of the desiccant-based air-conditioning system is the natural air dehumidification process called sorption process. The typical desiccant air-conditioning system consists of the desiccant wheel (DW), heat wheel and direct evaporative coolers (DECs) installed in the supply and return air (RA) streams [4–7]. Fixed bed [8, 9] and rotating desiccant dehumidifier [6, 10] are the most common desiccant dehumidifiers. However, rotating desiccant dehumidifier (desiccant wheel) is preferable for application due to its simplicity [2].

It is shown that determination of the exergetic performances of any thermal energy system gives more detailed and level playing field in the analysis of the system thermal performances [11]. In fact, there are several researches in the exergetic analyses on renewable energy systems [12, 13], thermal energy systems [14, 15], thermal system components [16], air handling systems [17–20] and buildings [21]. Exergetic analyses for the desiccant-evaporative air-conditioning system [22, 23], hybrid system [24, 25] and solar-desiccant air-conditioning system are studied [26].

In the exergetic evaluation of the desiccant air-conditioning system, it is shown that performances of the system components affected the system performance [27]. It is shown that higher regeneration temperature affected the system performance [28]. Shen and Worek [29] show that there is an optimal regeneration temperature in which the system performance is high. La et al. [23] show that there is trade-off

between the regeneration temperature and the exergy of the supply air (SA) that affects the system performance. This study presented the exergetic evaluation of the developed DHVAC system at different regeneration temperatures using steady-state conditions. The objective of the study is to determine the exergetic performances of the developed system and its components for further improvement also to evaluate the developed system performances in comparison with different desiccant-based air-conditioning systems.

5.2 Experimentation

5.2.1 System Overview

5.2.1.1 System Description

The system consists of the DW, sensible heat exchangers and a DEC. Figure 5.1 shows the developed DHVAC system diagram. In Fig. 5.1, the air from state 1 to state 3 is dehumidified by DW. The air from state 3 is pre-cooled by a sensible heat exchanger (HX [1]) and split into two streams of air (states 4 and 4′). The air from state 4′ is cooled by a DEC. The air of state 4 is sensibly cooled by smaller heat exchanger (HX [2]) from state 4 to state 5. The air at state 5 becomes the SA. The air at state 5 has the same humidity ratio as the processed air at state 3. The air at state 6 is mixed with the RA (state 7) for the preheating of hot air shown at state 9. The hot air at state 9 is heated by the air heating coil (AHC) to become the regeneration air (state 10). The regeneration air at state 10 is used to remove the

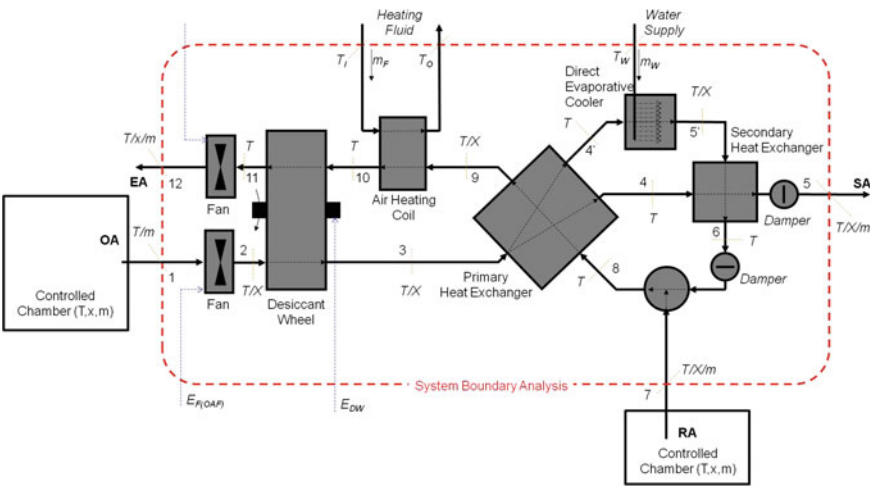

Fig. 5.1 Schematic diagram of the developed DHVAC system

moisture in the DW. The air at state 11 has higher humidity ratio due to regeneration process in the DW. The air at state 11 is exhausted by fan (EAF) to state 12.

5.2.1.2 Components Description

The system uses a honeycomb silica-gel-coated DW with 0.4 m diameter and 0.2 m thickness. The surface areas for air dehumidification side and wheel regeneration side are equal. The installed heat exchangers are cross-flow heat exchanges (sinusoidal flutes). The heat exchangers are made of paper coated with wax to avoid the transfer of moisture. The big heat exchanger (HX [1]) has dimensions of height 0.4 m, width 0.3 m and length 0.3 m. The smaller heat exchanger (HX [2]) has dimensions of height 0.4 m, width 0.15 m, and length 0.15 m. The DEC is a gravity flowing film type made of corrugated paper.

5.2.1.3 System Operation

The system operation is carried on using a controlled chamber (Chamber OA; See Fig. 5.1). The control of the RA conditions (T and x) is done by means of controlled chamber RA. The measurements of the air flow rates (outdoor air (OA), SA, RA and exit air) are determined by means of the orifices in the air duct with pressure difference sensors and temperature sensors. The control of air flow rates (OA, SA, RA and exit air) is done by the air dampers attached to the air ducts. The monitoring and control of the DW rotational speed are through the use of rotational laser sensor attached to the wheel belt. The control of the DEC is done by means of the relative humidity sensor attached at the downstream side (state 5′) through closed-loop control system. The control, monitoring and data gathering of the experimentation are made by means of the sensors attached to the experimental test rig of the desiccant-evaporative cooling system and connected to the personal computer through data logger.

5.2.2 Experimental Setup

5.2.2.1 Assembly

The total experimental setup has two controlled chambers (OA and RA) to control the condition of the air (temperature and humidity) as mentioned above (Sect. 5.2.1.3). Between the two controlled chambers, a working chamber in which the desiccant-evaporative cooling system is located with air ducts is connected (See Fig. 5.1). The air temperatures in the controlled chambers are controlled by the electric heater and air cooler using the heat pump. The heat pump serves also as the dehumidifier for the air, in case air dehumidification is needed. The humidification

process of the air is done through spray-type air humidifier. The operation of the two controlled chambers is meanly accomplished by passing the raw OA to the dehumidifier and cooler/heater device. In case low humidity is needed, dehumidification process operates. However, if the air becomes cool due to dehumidification process, electric heater operates to increase the temperature. In case when higher humidity of air is needed, the raw outside air passes the humidifier. The mixing chamber is installed after the air processing devices to control and homogenize the air prior to supplying it to the working chamber.

5.2.2.2 Instrumentations

All the attached sensors in the developed DHVAC system are evaluated and calibrated in the controlled box prior to their installation. The evaluated and calibrated sensors in the box are the dew point temperature sensors and the thermocouple temperature sensors. Based on the calibration, all the reading is within the specified value given by the manufacturers. Figure 5.1 shows the location and type of the sensors attached to the system. The measurement of the air humidity ratio is done by means of the dew point temperature sensors (±0.5 °C) and dry bulb temperature sensors (fabricated thermocouples). The fabricated thermocouples are from Japanese Industrial Standards (JIS) VT3, O 0.32 mm (±0.5 °C). Proper installations of dew point temperature and thermocouple probes are observed based on our previous experiences [30]. The measurement of the DW rotation is taken by the installed rotational laser sensor attached to the wheel belt. The measurement of air flow rates is taken using the installed orifices with digital pressure difference sensors (±3 Pa). The sensors attached to the DHVAC system are connected to the data logger. The data logger is then connected to the personal computer. In this measurement, the data gathering is made in every 30 s.

5.2.2.3 Cases

In the experimentation, the air conditions for the OA (Point 1) are set at value of 30 °C dry bulb temperature (2% accuracy) and 60% relative humidity (10% accuracy) (16.1 g kg^{-1}). This is the standard summer testing condition in Japan. The RA is set at value of 26 °C dry bulb temperature (1% accuracy) and 55% relative humidity (1% accuracy) (11.6 g kg^{-1}). This is the standard indoor air condition in Japan. The volumetric flow rates for the OA and exit air (EA) are set at 200 m^3 h^{-1}. The volumetric flow rates for the RA and SA are set 100 m^3 h^{-1}. The evaporative water inlet temperature is measured at 21.6 °C average and controlled by water heater to mimic the temperature of supply water pipe. The system is evaluated using the four different regeneration temperatures that can be supported by solar energy or low-temperature thermal energy source from waste heat. The

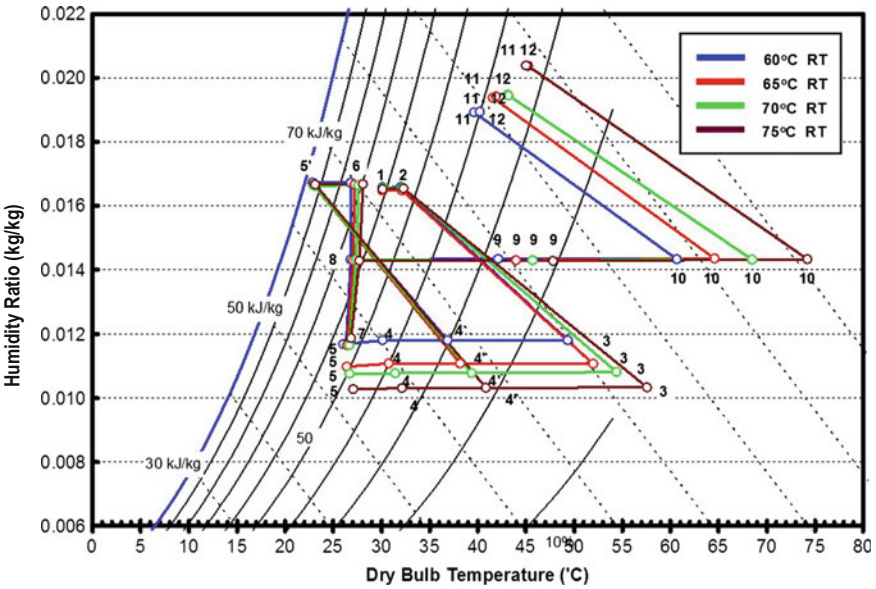

Fig. 5.2 States of air inside the developed DHVAC system in the psychrometric chart for different regeneration temperatures (RT)

Table 5.1 Measured air flow rates for different regeneration temperatures (RT) during the experimental evaluation of the developed DHVAC system

Regeneration temperature (°C)	OA		EA		SA		RA	
	$m^3\ h^{-1}$	$kg\ s^{-1}$	$m^3\ h^{-1}$	$kg\ s^{-1}$	$m^3\ h^{-1}$	$kg\ s^{-1}$	$m^3\ h^{-1}$	$kg\ s^{-1}$
60	201.18	0.0650	205.57	0.0646	94.31	0.0310	92.78	0.0306
65	201.32	0.0650	206.55	0.0646	94.30	0.0310	92.59	0.0305
70	200.65	0.0648	207.01	0.0645	94.27	0.0309	92.71	0.0305
75	200.33	0.0647	207.95	0.0645	94.38	0.0309	92.64	0.0305

regeneration temperatures used in the experimentation are 60, 65, 70 and 75 °C. Figure 5.2 shows the actual states of air inside the DHVAC system. Table 5.1 shows the measured air flow rates for the different regeneration temperatures presented in Fig. 5.2. Table 5.2 shows the values for the specific enthalpy, specific exergy and specific entropy for the different states inside the system for four cases of regeneration temperatures with reference states of 25 °C and 15 g kg^{-1}.

Table 5.2 Air states and equivalent specific enthalpy, specific entropy and specific exergy for different regeneration temperatures (RegT) for the case of 25 °C reference temperatures (RT)

State	Temperature, T (°C)				Humidity ratio, ω (g kg^{-1})				Specific enthalpy, h (kJ/kg)				Specific entropy, s (kJ/kg K)				Specific exergy, ψ (kJ/kg)			
	60 °C	65 °C	70 °C	75 °C	60 °C	65 °C	70 °C	75 °C	60 °C	65 °C	70 °C	75 °C	60 °C	65 °C	70 °C	75 °C	60 °C	65 °C	70 °C	75 °C
Reference	25				0.015				63.37				0.261				–			
1	30.1	30.1	30.2	30.1	0.0166	0.0165	0.0166	0.0165	72.7	72.5	72.7	72.6	0.296	0.295	0.296	0.295	0.056	0.055	0.057	0.055
2	32.0	32.1	32.2	32.3	0.0166	0.0165	0.0166	0.0165	74.7	74.5	74.8	74.8	0.302	0.302	0.303	0.303	0.096	0.097	0.100	0.101
3	49.3	52.0	54.4	57.6	0.0118	0.0111	0.0108	0.0103	80.2	81.1	82.8	84.8	0.306	0.306	0.310	0.315	1.026	1.269	1.498	1.826
4′	36.9	38.2	39.4	40.9	0.0118	0.0111	0.0108	0.0103	67.4	66.9	67.3	67.7	0.265	0.262	0.262	0.262	0.287	0.367	0.436	0.533
4	30.1	30.8	31.4	32.2	0.0118	0.0111	0.0108	0.0103	60.5	59.3	59.2	58.7	0.243	0.237	0.236	0.233	0.095	0.132	0.159	0.198
5′	22.9	22.9	23.0	23.1	0.0167	0.0167	0.0166	0.0167	65.5	65.5	65.5	65.7	0.272	0.272	0.272	0.273	0.021	0.020	0.019	0.018
5	26.0	26.4	26.7	27.1	0.0117	0.0110	0.0107	0.0103	56.0	54.6	54.3	53.5	0.227	0.221	0.219	0.215	0.055	0.083	0.095	0.120
6	26.8	27.2	27.6	28.1	0.0167	0.0167	0.0166	0.0167	69.6	69.9	70.3	70.8	0.286	0.287	0.288	0.290	0.018	0.021	0.024	0.029
7	26.3	26.4	26.7	26.9	0.0117	0.0116	0.0117	0.0119	56.3	56.3	56.6	57.3	0.228	0.228	0.229	0.232	0.056	0.058	0.059	0.053
8	26.8	27.1	27.4	27.7	0.0143	0.0143	0.0143	0.0143	63.5	63.6	64.1	64.3	0.259	0.260	0.261	0.262	0.008	0.010	0.012	0.015
9	42.1	44.0	45.7	47.8	0.0143	0.0143	0.0143	0.0143	79.3	81.1	83.0	85.1	0.311	0.316	0.322	0.329	0.496	0.606	0.716	0.869
10	60.7	64.6	68.5	74.2	0.0143	0.0143	0.0143	0.0143	98.4	102.3	106.5	112.3	0.370	0.381	0.394	0.410	2.060	2.518	3.016	3.823
11	39.6	41.5	43.1	45.2	0.0189	0.0194	0.0194	0.0204	88.6	91.8	93.6	98.2	0.354	0.365	0.371	0.388	0.429	0.545	0.637	0.808
12	40.2	41.9	43.2	45.4	0.0189	0.0194	0.0194	0.0204	89.2	92.2	93.7	98.4	0.356	0.367	0.371	0.389	0.458	0.563	0.643	0.819
Water	21.6	21.7	21.6	21.7	–	–	–	–	90.7	90.8	90.3	90.7	0.319	0.320	0.318	0.320	0.080	0.078	0.083	0.079

5.3 Thermodynamic Analysis

5.3.1 General Formulation

The evaluation of the DHVAC system is based on the governing concept of the laws of thermodynamics. The general formulations for exergy analyses of the thermal system are presented in Eqs. (5.1–5.12) and applied in the DHVAC system of thermodynamic model shown in Fig. 5.1. In these formulations, the reference states are the T_r, Φ_r, ω_r, P_r.

The general mass rate balance for the open system is

$$\sum_{j=1}^{N} \dot{m}_{j,I} - \sum_{i=1}^{M} \dot{m}_{i,O} = \frac{\mathrm{d}m_{\mathrm{Sys}}}{\mathrm{d}t} \tag{5.1}$$

The general energy rate balance for the open system is

$$\sum_{j=1}^{N} \dot{Q}_{j,I} + \sum_{i=1}^{N} \left(\dot{m}_j h_j\right)_I = \sum_{i=1}^{M} \dot{W}_{i,O} + \sum_{i=1}^{M} \left(\dot{m}_i h_i\right)_O \tag{5.2}$$

The general exergy rate balance for the open system is

$$\sum_{j=1}^{N} \left[1 - \left(\frac{T_r}{T_{K,j}}\right)\right] \dot{Q}_{K,j} + \sum_{j=1}^{N} \left(\dot{m}_j \psi_j\right)_I = \sum_{i=1}^{M} \dot{W}_{i,O} - \sum_{i=1}^{M} \left(\dot{m}_i \psi_i\right)_O \tag{5.3}$$

The general entropy generation rate for the open system is

$$\dot{S}_{\mathrm{Gen}} = \sum_{i=1}^{N} \left(\dot{m}_i s_i\right)_O - \sum_{j=1}^{M} \left(\dot{m}_j s_j\right)_I - \sum_{k=1}^{L} \left(\frac{Q_{S,k}}{T_{S,k}}\right) \tag{5.4}$$

The general exergy rate of destruction or the rate of irreversibility is

$$\dot{E}_{X,\mathrm{Dest}} = I_{\mathrm{rr}} = T_r \dot{S}_{\mathrm{Gen}} = \sum_{j=1}^{N} \left(\dot{E}_{x,j}\right)_I - \sum_{i=1}^{M} \left(\dot{E}_{x,i}\right)_O \tag{5.5}$$

The general exergetic efficiency for the open system is

$$\varepsilon_X = \frac{\left[\sum_{i=1}^{M} \dot{W}_{i,O} + \sum_{i=1}^{M} \left(\dot{m}_i \psi_i\right)_O\right]}{\left\langle \sum_{j=1}^{N} \left[1 - \left(\frac{T_r}{T_{K,j}}\right)\right] \dot{Q}_{K,j} + \sum_{j=1}^{N} \left(\dot{m}_j \psi_j\right)_I \right\rangle} = \frac{\sum_{i=1}^{M} \left(\dot{E}_{x,i}\right)_O}{\sum_{j=1}^{N} \left(\dot{E}_{x,j}\right)_I} \tag{5.6}$$

The relative destruction (RD) of exergy for the open system is presented as

$$\mathrm{RD} = \frac{\left(\dot{E}_{X,\mathrm{Dest}}\right)_t}{\sum_{t=1}^{C} \dot{E}_{X,\mathrm{Dest}}} \cdot 100 \tag{5.7}$$

The Van Gool's improvement potential (IP) for the open system is presented as [12]

$$\mathrm{IP} = (1 - \varepsilon_X) \cdot \left(\sum_{j=1}^{N} \left(\dot{E}_{x,j}\right)_I - \sum_{i=1}^{M} \left(\dot{E}_{x,i}\right)_O \right) \tag{5.8}$$

The Van Gool's IP is the maximum possible IP that could be done for any processes through minimization of the exergy destruction or the difference between the inlet exergy and outlet exergy.

The sustainability index (SI) for the open system can be expressed as [31]

$$\mathrm{SI} = \frac{\sum_{j=1}^{N} \left(\dot{E}_{x,j}\right)_I}{\sum_{j=1}^{N} \left(\dot{E}_{x,j}\right)_I - \sum_{i=1}^{M} \left(\dot{E}_{x,i}\right)_O} = \frac{1}{1 - \varepsilon_X} = \frac{1}{D_P} = \frac{\sum_{j=1}^{N} \left(\dot{E}_{x,j}\right)_I}{\sum_{t=1}^{C} \dot{E}_{X,Dest}} \tag{5.9}$$

The SI is an inverse of the depletion number (D_p), which is the relationship between the exergy destruction of the exergy input. When the exergy destruction decreases even with the same exergy input due to the increase in the efficiency, the SI increases. It means that less fuel is consumed particularly when using conventional sources.

The specific flow exergy is

$$\psi = (h - h_\mathrm{r}) - T_\mathrm{r}(s - s_\mathrm{r}) \tag{5.10}$$

The specific exergy of incompressible substance such as water is [19]

$$\psi_\mathrm{w} = C_{\mathrm{P,w}}(T_\mathrm{w} - T_\mathrm{r}) - T_\mathrm{r} C_{\mathrm{P,w}} \ln\left(\frac{T_\mathrm{w}}{T_\mathrm{r}}\right) - R_\mathrm{v} T_\mathrm{r} \ln \varphi_\mathrm{r} \tag{5.11}$$

φ_r is the equivalent relative humidity at reference temperature (T_r) and humidity ratio (ω_r). The specific exergy of moist air is [12]

$$\begin{aligned}\psi_\mathrm{ma} = {} & \left\langle (C_{\mathrm{p,g}} + \omega C_{\mathrm{p,v}}) T_\mathrm{r} \left[\left(\frac{T_\mathrm{ma}}{T_\mathrm{r}}\right) - 1 - \ln\left(\frac{T_\mathrm{ma}}{T_\mathrm{r}}\right) \right] \right\rangle + \left[(1 + 1.607\omega) T_\mathrm{r} \ln\left(\frac{P_\mathrm{ma}}{P_\mathrm{r}}\right) \right] \\ & + R_\mathrm{g} T_\mathrm{r} \left\langle (1 + 1.607\omega) \ln\left[\frac{(1 + 1.607 w_\mathrm{r})}{(1 + 1.7607\omega)}\right] + 1.607 \ln\left(\frac{\omega}{\omega_\mathrm{r}}\right) \right\rangle \end{aligned} \tag{5.12}$$

5.3.2 System Analysis

5.3.2.1 Desiccant Wheel (DW) Exergy Efficiency

$$(\varepsilon_X)_{\mathrm{DW}} = \frac{[\dot{m}_{\mathrm{OA}}(\psi_3 - \psi_2)]}{\left\langle \left(\dot{E}_E\right)_{\mathrm{DW}} + [\dot{m}_{\mathrm{EA}}(\psi_{10} - \psi_{11})] \right\rangle} \tag{5.13}$$

5.3.2.2 Sensible Heat Exchanger (HX [1]/HX [2]) Exergy Efficiency

$$(\varepsilon_X)_{\mathrm{HX}(1)} = \frac{[\dot{m}_{\mathrm{EA}}(\psi_9 - \psi_8)]}{\left\langle \dot{m}_{\mathrm{OA}} \left\{ \psi_3 - \left[\frac{(\psi_{4'} + \psi_4)}{2} \right] \right\} \right\rangle} \tag{5.14}$$

$$(\varepsilon_X)_{\mathrm{HX}(2)} = \frac{[(\dot{m}_{\mathrm{OA}} - \dot{m}_{\mathrm{SA}})(\psi_6 - \psi_{5'})]}{[\dot{m}_{\mathrm{SA}}(\psi_4 - \psi_5)]} \tag{5.15}$$

5.3.2.3 Direct Evaporative Cooler (DEC) Exergy Efficiency

$$(\varepsilon_X)_{\mathrm{EC}} = \frac{[(\dot{m}_{\mathrm{OA}} - \dot{m}_{\mathrm{SA}})\psi_{5'}]}{\langle [\dot{m}_{\mathrm{W}}\psi_{\mathrm{W}}] + [(\dot{m}_{\mathrm{OA}} - \dot{m}_{\mathrm{SA}})\psi_{4'}] \rangle} \tag{5.16}$$

5.3.2.4 Air Heating Coil (AHC) Exergy Efficiency

$$(\varepsilon_X)_{\mathrm{AH}} = \frac{[\dot{m}_{\mathrm{EA}}(\psi_{10} - \psi_9)]}{[\dot{m}_{\mathrm{L}}(\psi_{\mathrm{T}} - \psi_{\mathrm{S}})]} \tag{5.17}$$

5.3.2.5 Air Fan (OAF and EAF) Exergy Efficiency

$$(\varepsilon_X)_{F(\mathrm{OAF})} = \frac{\left[\dot{m}_{F(\mathrm{OAF})}(\psi_2 - \psi_1)\right]}{\left(\dot{E}_E\right)_{F(\mathrm{OAF})}} \tag{5.18}$$

$$(\varepsilon_X)_{F(\mathrm{EAF})} = \frac{\left[\dot{m}_{F(\mathrm{EAF})}(\psi_{12} - \psi_{11})\right]}{\left(\dot{E}_E\right)_{F(\mathrm{EAF})}} \tag{5.19}$$

5.3.2.6 System Exergetic Performances

Electric exergetic coefficient of performance (EE_XCOP):

$$\left[(\varepsilon_X)_{\mathrm{Sys}}\right]_{\mathrm{Electric}} = \frac{[\dot{m}_{\mathrm{SA}}(\psi_1 - \psi_5)]}{\left\langle \left(\dot{E}_{\mathrm{E}}\right)_{\mathrm{DW}} + \left(\dot{E}_{\mathrm{E}}\right)_{F(\mathrm{OAF})} + \left(\dot{E}_{\mathrm{E}}\right)_{F(\mathrm{EAF})} \right\rangle} \tag{5.20}$$

Thermal exergetic coefficient of performance (TE_XCOP):

$$\left[(\varepsilon_X)_{\mathrm{Sys}}\right]_{\mathrm{Thermal}} = \frac{[\dot{m}_{\mathrm{SA}}(\psi_1 - \psi_5)]}{\dot{Q}_X} \tag{5.21}$$

Total exergetic coefficient of performance (SE_XCOP):

$$\left[(\varepsilon_X)_{\mathrm{Sys}}\right]_{\mathrm{Total}} = \frac{[\dot{m}_{\mathrm{SA}}(\psi_1 - \psi_5)]}{\left\langle \dot{Q}_X + \left(\dot{E}_E\right)_{\mathrm{DW}} + \left(\dot{E}_E\right)_{F(\mathrm{OAF})} + \left(\dot{E}\right)_{F(\mathrm{EAF})} + (\dot{m}_{\mathrm{W}}\psi_{\mathrm{W}}) \right\rangle} \tag{5.22}$$

The calculation of thermal exergy delivered to the air heating coil (HC) is based on

$$\dot{Q}_X = \dot{m}_F C_{\mathrm{p}} \left[(T_I - T_O) - T_{\mathrm{r}} \ln\left(\frac{T_I}{T_O}\right) \right] \tag{5.23}$$

5.3.2.7 System Exergetic Efficiencies

The actual thermal coefficient of performance is simply the ratio of the cooling produced to the thermal energy supplied as

$$\mathrm{COP_A} = \frac{\dot{m}_{\mathrm{SA}}(h_1 - h_5)}{\dot{m}_{\mathrm{EA}}(h_{10} - h_9)} \tag{5.24}$$

The Carnot coefficient of performance for any heat-driven air-conditioning system is shown based on the diagram shown in Fig. 5.1.

$$\mathrm{COP_C} = \left(1 - \frac{T_1}{T_{10}}\right)\left(\frac{T_7}{T_1 - T_7}\right) \tag{5.25}$$

The $\mathrm{COP_C}$ is the highest potential of the coefficient of performance for any heat-driven air-conditioning system, which is mostly applied in closed cycles.

The proposed reversible Carnot coefficient of performance for the open-cycle desiccant air-conditioning system is expressed as [27]

$$\mathrm{COP_{Rev}} = \left(1 - \frac{T_c}{T_s}\right)\left(\frac{T_e}{T_c - T_e}\right) \tag{5.26}$$

where T_s, T_e and T_c are equivalent temperatures for the heat source, evaporator and condenser and are expressed based on Fig. 5.1

$$T_s = \frac{h_9 - h_{10}}{s_9 - s_{10}} \tag{5.27}$$

$$T_e = \frac{\dot{m}_{SA}h_5 - \dot{m}_{RA}h_7 + \dot{m}_{W(5\to7)}h_w}{\dot{m}_{SA}s_5 - \dot{m}_{RA}s_7 + \dot{m}_{W(5\to7)}s_w} \tag{5.28}$$

$$T_c = \frac{\dot{m}_{OA}h_1 - \dot{m}_{EA}h_{12} - \left(\dot{m}_{w(5\to7)} + m_{w(4'\to5')}\right)h_w}{\dot{m}_{OA}s_1 - \dot{m}_{EA}s_{12} - \left(\dot{m}_{w(5\to7)} + m_{w(4'\to5')}\right)s_w} \tag{5.29}$$

The exergy efficiency can be expressed as the ratio of the actual coefficient of performance for the thermal-driven air-conditioning system to the reversible coefficient of performance [32]. It is called as the exergy efficiency in the first definition here.

$$(\varepsilon_X)_1 = \frac{\mathrm{COP_A}}{\mathrm{COP_{Rev}}} \tag{5.30}$$

For comparison purposes with different studies in thermal-driven air-conditioning systems, the exergy efficiency is expressed based on the ratio of the cooling produced to the thermal exergy supplied as (exergy efficiency in the second definition) [32].

$$(\varepsilon_X)_2 = \frac{\dot{m}_{SA}(\psi_1 - \psi_5)}{\dot{m}_{EA}(\psi_{10} - \psi_9)} \tag{5.31}$$

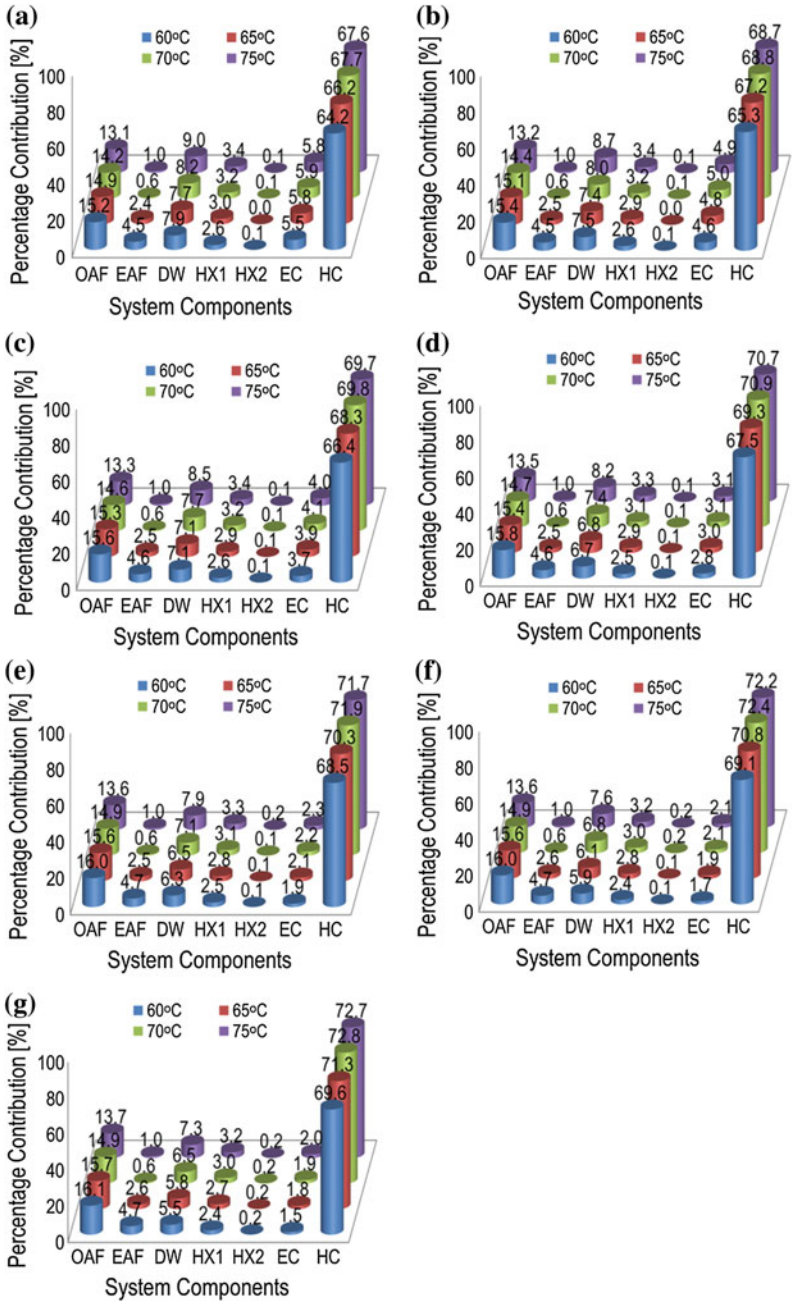

Fig. 5.3 Percentage contribution of exergy destruction for the developed DHVAC system components at different regeneration temperatures (RegT) and reference temperatures (RT): **a** 0 °C RT; **b** 5 °C RT; **c** 10 °C RT; **d** 15 °C RT; **e** 20 °C RT; **f** 25 °C RT, and; **g** 30 °C RT

5.4 Results and Discussion

5.4.1 Exergy Destruction Contribution

Figure 5.3 shows the exergy destruction contribution of the developed DHVAC system at different regeneration temperatures and reference temperatures. The air heating coil (AHC) is contributed to high percentage of the total exergy destruction: the same trend for exergy destruction for the case of Hurdogan et al. [25], which shows that system thermal source and air fans are the main contributors. The destruction contribution is followed by the outdoor air fan (OAF) and then by the DW. As the regeneration temperature increases, the contribution of the AHC to exergy destruction increases. Kodama et al. [28] show that heat source and DW are major sources of exergy destruction (air fans are not considered in their analysis). The exergy destruction contribution of the DW increases as the regeneration temperature increases. The trend for the exergy destruction contributions for the heat exchangers (HX1 and HX2) and direct evaporative cooler (EC) increases as the regeneration temperature increases due to the increase in the components irreversibility. Furthermore, based on the different reference temperatures, it shows the increase in the AHC exergy destruction contribution.

5.4.2 Exergy Destruction Coefficient

Figure 5.4 shows the exergy destruction coefficient for different components of the developed DHVAC system at different regeneration temperatures and reference temperatures. The trend of the exergy destruction coefficient is the same as the exergy destruction contribution presented in Fig. 5.3. The HC has the largest exergy destruction coefficient followed by the OAF and DW. The exergy destruction in the AHC could be lowered by increasing the efficiency of the AHC. La et al. [23] show also that heat source has the largest exergy destruction coefficient. It also shows that when the regeneration temperature increases, the exergy destruction coefficient for the AHC increases due to the increase in heat transfer irreversibility. It is the same for the cases of DW and heat exchangers (HX1 and HX2) and evaporative cooler (EC). On the other hand, when the reference temperature increases, the exergy destruction coefficient for HC increases.

5.4.3 System Performances

Figure 5.5a shows the thermal exergetic coefficient of performance of the system. The thermal exergetic coefficient of performance (TE_XCOP) is varied with the reference temperature, and from 0 to 22 °C, the thermal exergetic performance of

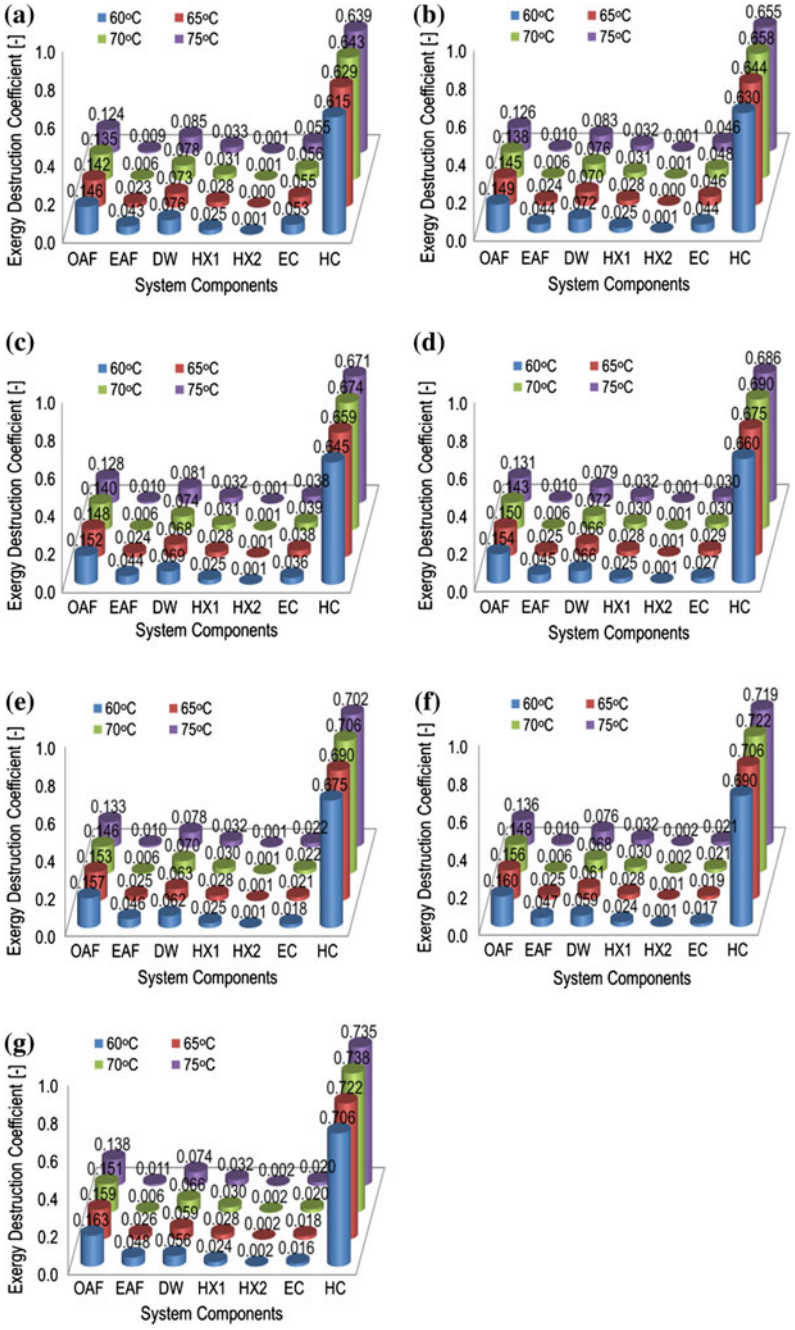

Fig. 5.4 Exergy destruction coefficient for the developed DHVAC system components at different regeneration temperatures (RegT) and reference temperatures (RT): **a** 0 °C RT; **b** 5 °C RT; **c** 10 °C RT; **d** 15 °C RT; **e** 20 °C RT; **f** 25 °C RT, and; **g** 30 °C RT

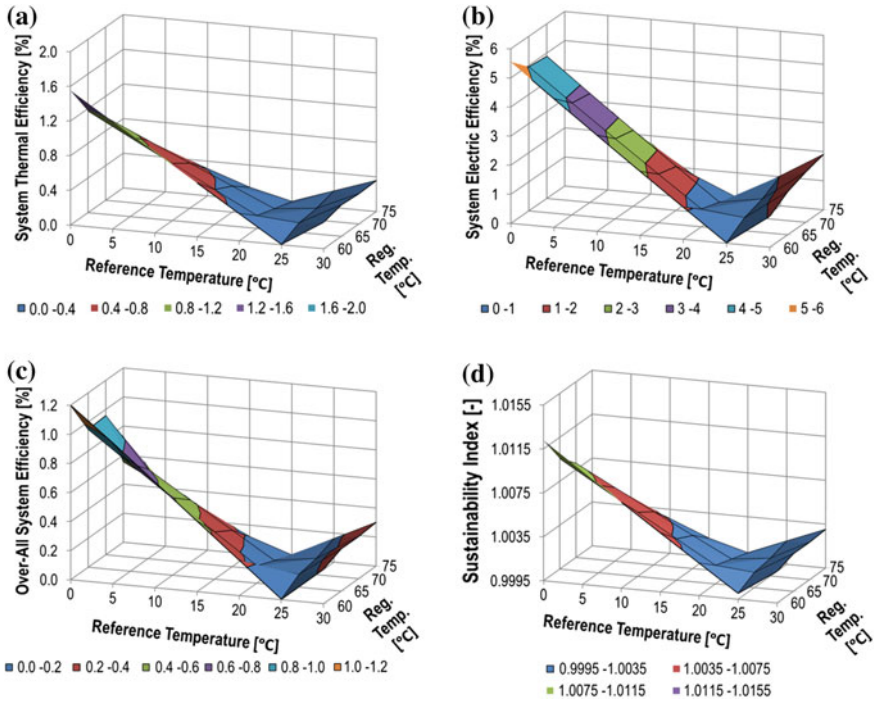

Fig. 5.5 Performances of the developed DHVAC system at different regeneration temperatures (RegT) and reference temperatures (RT): **a** thermal exergetic COP with respect to different reference temperatures (RT) and regeneration temperatures (RegT); **b** electric exergetic COP with respect to different reference temperatures (RT) and regeneration temperatures (RegT); **c** system exergetic COP with respect to different reference temperatures (RT) and regeneration temperatures (RegT); and **d** sustainability index with respect to different reference temperatures (RT) and regeneration temperatures (RegT)

the system decreases, after which the performance increases. However, based on the different regeneration temperatures, from 0 to 22 °C, the thermal exergetic performance of the system decreases as the regeneration temperature increases and suddenly changed from 22 to 30 °C. On the other hand, for the electric exergetic performance presented in Fig. 5.5b, the trend of the electric exergetic coefficient of performance (EE_XCOP) is the same as the thermal exergetic coefficient of performance shown in Fig. 5.5a in terms of reference temperatures. It means that increasing the regeneration temperature also affects the electric consumption of the system due to the increase in system internal frictional losses which resulted in the decrease in the EE_XCOP. On the other hand, the increase in the regeneration temperature results in higher increase in the system thermal exergy destruction due to components irreversibility and results in the decrease in the TE_XCOP as

explained in the different components. Figure 5.5c shows the overall system exergetic coefficient of performance (SE_XCOP). It shows the same trend based on regeneration temperature and reference temperatures. Based on the analysis of each of the three exergetic coefficient of performances (TE_XCOP, EE_XCOP and SE_XCOP), the system performance decreases as the regeneration temperature increases. Furthermore, there is a sudden decrease in the performance from 60 to 65 °C and 70 to 75 °C. Based on Fig. 5.2, the dehumidification and cooling of SA (Point 5) are almost the same for regeneration temperatures of 65 and 70 °C. The SI shows that as the regeneration temperature increases, the SI decreases from 0 to 22 °C and changed from 22 to 30 °C (Fig. 5.5d). The SI is related to exergy efficiency as shown in Eq. (5.9). Hence, from Fig. 5.5c, the overall system exergy efficiency varies as the dead state temperature changes. This is the same trend for the case of the evaporative cooler shown by Caliskan et al. [33].

Figure 5.6a shows the reversible coefficient of performance (COP_{Rev}). It shows that the COP_{Rev} has nothing to do with the reference temperature. As presented, the COP_{Rev} suddenly increases from 60 °C regeneration temperature to 65 °C. The COP_{Rev} then reduces at 70 °C and increases a little at 75 °C. This trend of COP_{Rev} is due to the system dehumidification performance shown in Fig. 5.2. As shown in Fig. 5.2, there is a large increase in the system dehumidification performance from 60 to 65 °C, which resulted in higher increase in COP_{Rev}, and then from 65 to 70 °C, the dehumidification performance is not large even with this same increase in regeneration temperature of 5 °C. In addition, from 70 to 75 °C, the increase is not as large as from 60 to 65 °C; this resulted in lower increase in $COP_{Rev.}$ This trend has little increase in the dehumidification performance of the DW, resulting from the heating of the desiccant material in the dehumidification side due to the heat carry over from the regeneration side to dehumidification side of the DW as observed from our previous studies [30]. The present system has higher COP_{Rev} of 4.20 at regeneration temperature of 65 °C. Lavan et al. [27] got 4.66, while Kanoglu et al. [34] got a COP_{Rev} of 2.63 for double wheel + double evaporative coolers of DHVAC system.

Figure 5.6b shows that the actual coefficient of performance (COP_A) is higher at regeneration temperature of 60 °C and suddenly decreases as the regeneration increases to 75 °C. This trend of decreasing COP_A as the regeneration temperature increases is due to the non-proportional increase in the system cooling capability as the regeneration energy supported to the system increases as the regeneration temperature increases. As the regeneration temperature increases, the heat carry over from the regeneration side of the DW to its dehumidification side increases [30]. The increase in the DW temperature in the dehumidification side hampered the adsorption capacity as the sorption process is the difference of the water vapor pressure between the air and the desiccant surface. Also, the increase in the regeneration temperature increases the exergy of the SA. As shown in Fig. 5.2, the increase in the air temperature after the DW (state 3) is almost linear compared to the increase in the dehumidification capability as the regeneration temperature increases. Kodama et al. [28] show the same trend of result.

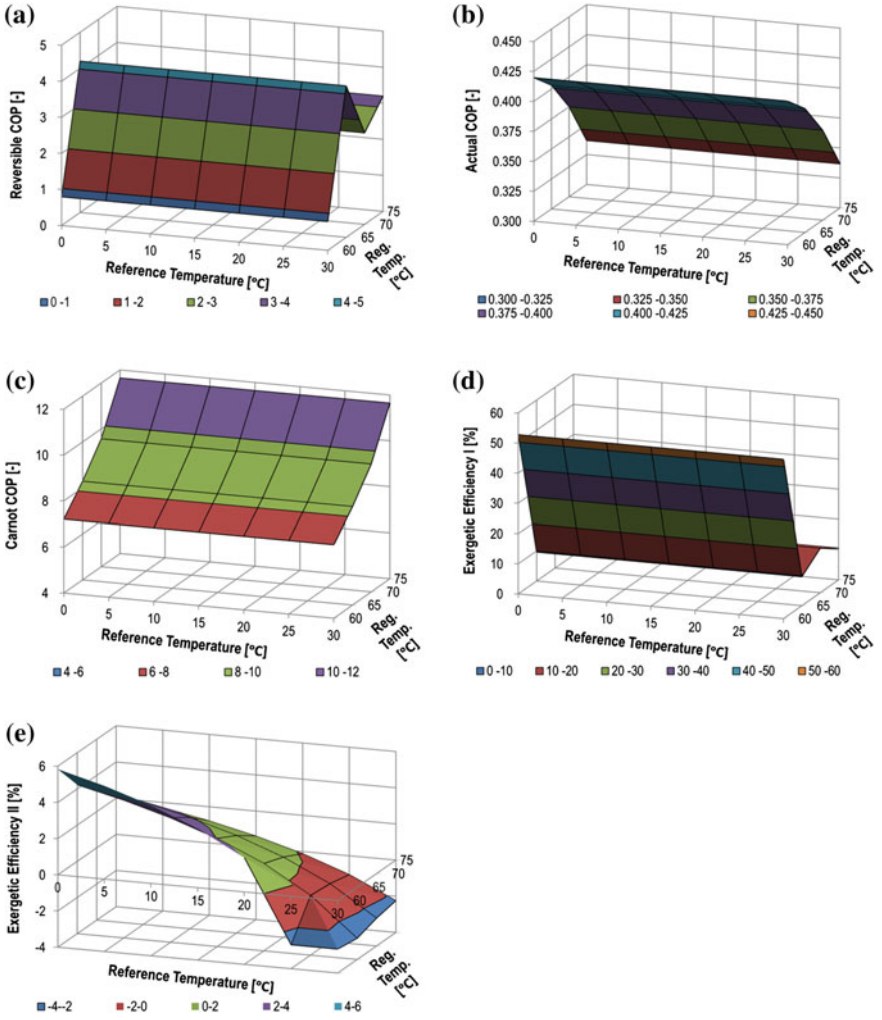

Fig. 5.6 Performances of the developed DHVAC system at different regeneration temperatures (RegT) and reference temperatures (RT): **a** reversible Carnot coefficient of performance $(COP)_{Rev}$ with respect to different reference temperatures (RT) and regeneration temperatures (RegT); **b** actual coefficient of performance $(COP)_{Act}$ with respect to different reference temperatures (RT) and regeneration temperatures (RegT); **c** Carnot coefficient of performance $(COP)_C$ with respect to different reference temperatures (RT) and regeneration temperatures (RegT); **d** Exergetic efficiency I (First Definition); and **e** Exergetic efficiency II (second definition)

Figure 5.6c shows the Carnot coefficient of performance (COP_C), which presents the increasing trend as the regeneration temperature increases. The increasing trend of the COP_C is due to the increase in the regeneration temperature (T_{10}). In addition, as shown in this research, the return temperature (T_7) and the outdoor temperature

(T_7) are held constant. These values of the COP_C are the possible Carnot coefficient of performance of the heat-driven cooling system at closed-cycle equivalent. However, open-cycle DHVAC system is not only for the temperature control but also for the humidity control. Therefore, the actual and the reversible coefficients of performances (COP_A and COP_{Rev}) are different as explained in the above discussions for the COP_A and COP_{Rev}. For comparison purposes, Kanoglu et al. [34] presented a COP_C of 8.74 based on ARI conditions. In this paper, the COP_C at 75 °C is 11.65.

Figure 5.6d shows the exergetic efficiency of first definition (exergetic efficiency I), which shows the decreasing trend as the regeneration temperature increases. The lowest value can be seen in the regeneration temperature of 70 °C, which has also a lower value of $COP_{Rev.}$ It shows that at 60 °C, the exergetic efficiency I is 52.77%, while the lowest is 9.61% at 60 °C. Figure 5.6e shows the decreasing trend of the exergetic efficiency of the second definition (exergetic efficiency II). The negative value of the second definition is due to the increase in the SA exergy upon increase in the reference temperature. The exergetic efficiency of second definition decreases as the regeneration temperature increases due to the smaller increase in the cooling exergy capability of the system even with the increasing regeneration exergy supply to the system. This explanation is the same to the actual coefficient of performance (COP_A). Moreover, the exergetic coefficient of performance of second definition decreases as the reference temperature increases. It means that at higher temperature, the system exergetic performance of second definition is not as efficient as in lower reference temperature due to the reduction in the system cooling exergy produced. Hence, it is expensive and inefficient to operate the system at higher OA temperature than at lower OA temperature.

5.5 Conclusions

This paper showed the exergy evaluation of the developed DHVAC system. The developed system was evaluated based on different regeneration temperatures and reference temperatures in which the system will be subjected to its actual operation.

- AHC, OAF and then DW contributed to high percentage of the total exergy destruction.
- Based on the analysis of each of the three exergetic coefficient of performances (TE_XCOP, EE_XCOP and SE_XCOP), the system performance decreases as the regeneration temperature increases.
- The SI shows that as the regeneration temperature increases, the SI decreases from 0 to 22 °C and changed from 22 to 30 °C (Fig. 5.5d).
- The COP_{Rev} suddenly increases from 60 °C regeneration temperature to 65 °C. The COP_{Rev} then reduces at 70 °C and then increases a little at 75 °C. The trend of COP_{Rev} is due to the system dehumidification performance shown in Fig. 5.2.

- The actual coefficient of performance (COP_A) is higher at regeneration temperature of 60 °C and decreases as the regeneration temperature increases to 75 °C. This trend of decreasing COP_A as the regeneration temperature increases is due to the not proportional increase in the system cooling capability as the regeneration energy supported to the system increases as the regeneration temperature increases.
- The increasing trend of the COP_C as the regeneration temperature increases is due to the increase in the regeneration temperature (T_{10}). In addition, as shown in this research, the return temperature (T_7) and the outdoor temperature (T_7) are held constant.
- The exergetic efficiency of first definition (exergetic efficiency I) shows the decreasing trend as the regeneration temperature increases. The lowest value can be seen in the regeneration temperature of 70 °C, which has also a lower value of $COP_{Rev.}$
- The exergetic efficiency of second definition decreases as the regeneration temperature increases due to the little increase in the cooling exergy capability of the system even with the increasing regeneration exergy supply to the system.

The exergetic evaluation is valuable in the evaluation of the DHVAC system we developed. It shows which components with large destruction of exergy that resulted in lowering of the system exergy efficiencies. AHC, air fans (OAF and EAF) and DW contributed to large percentage of system exergy destruction, resulting in large impact of the reduction in the system performance. Hence, it is important to consider the components with high exergy destruction such as the AHC, air fans and DW for improvement.

It was shown that the system presented in this paper which has one evaporative cooler and two sensible heat exchangers could have better performance compared to the typical double wheels and double evaporative coolers. For comparison purposes, the exergetic efficiency of the liquid DHVAC system is still high (6.8%, the lowest, for the basic system) [34, 35]; however, handling of the liquid desiccant is more complex than solid desiccant. In the case of the solid desiccant, multi-staging will increase the exergetic efficiency from 8.2 to 18.0% [22, 23]. However, multi-staging and making the air flow complex increase the fan power consumption that will affect the system performance when fan exergy input is considered for our case. With respect to the closed-cycle water–LiBr desiccant system, the open system has comparable COP_A at lower regeneration temperature to half-effect and single-effect water–LiBr desiccant system shown by Gebreslassie et al. [36] and Kaushik and Arora [37]. For example, in this paper, the COP_A is 0.42 at 60 °C, while the water–LiBr desiccant system of half effect has 0.458 [36]. However, when converting the closed-cycle water–LiBr system to cool and dehumidify the air, it is expected that the COP_A will be lower. With respect to the closed-cycle, solid desiccant system, the COP_A is lower but could operate at much lower regeneration temperature. For example, at 60 °C temperature, it could have a COP of less than 0.2 [38], which is less than the open-cycle counterpart. Askalany et al. [39] presented some pairs of solid desiccant and refrigerant, which could have higher COP. Hence, application of different types of desiccant-based air-conditioning system depends on the need and specific target. Wang et al. [40] presented important guidelines

of the desiccant-based air-conditioning system. For the case of open-cycle DHVAC system, it offers some advantages for chemical and biological treatments of the SA to the indoor environment [2]. Further investigation through exergoeconomic and exergoenvironmental analyses had been done to deepen the evaluation of the developed DHVAC system [41, 42].

References

1. Enteria N, Yoshino H, Takaki R et al (2013) Effect of regeneration temperatures in the exergetic performances of the developed desiccant-evaporative air-conditioning system. Int J Refrig 36:2323–2342
2. Enteria N, Mizutani K (2011) The role of the thermally activated desiccant cooling technologies in the issue of energy and environment. Renew Sust Energ Rev 15:2095–2122
3. Choudhury B, Saha BB, Chatterjee PK et al (2013) An overview of developments in adsorption refrigeration systems towards a sustainable way of cooling. Appl Energ 104: 554–567
4. Henning HM, Erpenbeck T, Hindenburg C et al (2001) The potential of solar energy use in desiccant cooling cycles. Int J Refrig 24:220–229
5. Panaras G, Mathioulakis E, Belessiotis V (2011) Solid desiccant air-conditioning systems—design parameters. Energy 36:2399–2406
6. Hurdogan E, Buyukalaca O, Yilmaz T et al (2010) Experimental investigation of a novel desiccant cooling system. Energ Buildings 42:2049–2060
7. Bourdoukan P, Wurtz E, Joubert P et al (2008) Potential of solar heat pipe vacuum collectors in the desiccant cooling process: modeling and experimental results. Sol Energy 82:1209–1219
8. Enteria N, Mizutani K, Monma Y et al (2011) Experimental evaluation of the new solid heat pump system in Asia-Pacific climatic conditions. Appl Therm Eng 31:243–257
9. Cho WH, Kato S (2011) Outline of batch type desiccant air-conditioning system and humidification-heating performance. Part 1: Study on development of residential desiccant air-conditioning system and its performance evaluation. Archit Inst Jpn J Environ Eng 75:835–844
10. Finocchiaro P, Beccali M, Nocke B (2012) Advanced solar assisted desiccant and evaporative cooling system equipped with wet heat exchanger. Sol Energy 86:608–618
11. Bejan A (2006) Advanced engineering thermodynamics. Wiley, New Jersey
12. Hepbasli A (2008) A key review on exergetic analysis and assessment of renewable energy resources for a sustainable future. Renew Sust Energ Rev 12:593–661
13. Li H, Yang HX (2010) Energy and exergy analysis of multi-functional solar-assisted heat pump system. Int J Low-Carbon Technol 5:130–136
14. Rosen M (2001) The exergy of stratified thermal energy storages. Sol Energy 71:173–185
15. Kaushik SC, Siva Reddy V, Tyagi SK (2011) Energy and exergy analyses of thermal power plants: a review. Renew Sust Energ Rev 15:1857–1872
16. Fakheri A (2010) Second law analysis of heat exchangers. J Heat Transf 132:1–7
17. Caliskan H, Dincer I, Hepbasli A (2011) Exergetic and sustainability performance comparison of novel and conventional air cooling systems for building applications. Energ Buildings 43:1461–1472
18. Koroneos C, Nanaki E, Xydis G (2010) Solar air conditioning systems and their applicability—an exergy approach. Resour Conserv Recy 55:74–82
19. Marletta L (2010) Air conditioning systems from a 2nd law perspective. Entropy 12:859–877
20. Zhai H, Dai YJ, Wu JY et al (2009) Energy and exergy analyses on a novel hybrid solar heating, cooling and power generation system for remote areas. Appl Energ 86:1395–1404
21. Torio H, Anglotti A, Schmidth D (2009) Exergy analysis of renewable energy-based climatisation systems for buildings: a critical review. Energ Buildings 41:248–271

22. Kanoglu M, Carpinlioglu MO, Yildirim M (2004) Energy and exergy analyses of an experimental open-cycle desiccant cooling system. Appl Therm Eng 24:919–932
23. La D, Li Y, Dai YJ (2012) Development of a novel rotary desiccant cooling cycle with isothermal dehumidification and regenerative cooling using thermodynamic analysis method. Energy 44:778–791
24. Pons M, Kodama A (2000) Entropic analysis of adsorption open cycles for air conditioning. Part 1: first and second law analyses. Int J Energ Res 24:251–262
25. Hurdogan E, Buyukalaca O, Hepbasli A (2011) Exergetic modeling and experimental performance assessment of a novel desiccant cooling. Energ Buildings 43:1489–1498
26. Enteria N, Yoshino H, Mochida A (2013) First and second law analysis of the developed solar-desiccant cooling system. Energ Buildings 60:239–251
27. Lavan Z, Monnier JB, Worek WM (1982) Second law analysis of desiccant cooling systems. J Sol Energy Eng 104:229–236
28. Kodama A, Jin W, Goto M (2000) Entropic analysis of adsorption open cycles for air conditioning. Part 2: Interpretation of experimental data. Int J Energ Res 24:263–278
29. Shen CM, Worek WM (1996) The second-law analysis of a recirculation cycle desiccant cooling system: cosorption of water vapor and carbon dioxide. Atmos Environ 30:1429–1435
30. Enteria N, Yoshino H, Satake A (2010) Experimental heat and mass transfer of the separated and coupled rotating desiccant wheel and heat wheel. Exp Therm Fluid Sci 34:603–615
31. Rosen MA, Dincer I, Kanoglu M (2008) Role of exergy in increasing efficiency and sustainability and reducing environmental impact. Energ Policy 36:128–137
32. Dincer I, Rosen M (2013) Exergy: energy, environment and sustainable development. Elsevier, UK
33. Caliskan H, Hepbasli A, Dincer I et al (2011) Thermodynamic performance assessment of a novel air cooling cycle: Maisotsenko cycle. Int J Refrig 34:980–990
34. Kanoglu M, Bolatturk A, Altuntop N (2007) Effect of ambient conditions on the first and second law performance of an open desiccant cooling process. Renew Energ 32:931–946
35. Xiong ZQ, Dai YJ, Wang RZ (2010) Development of a novel two-stage liquid desiccant dehumidification system assisted by $CaCl_2$ solution using exergy analysis method. Appl Energ 87:1495–1504
36. Gebreslassie BH, Medrano M, Boer D (2010) Exergy analysis of multi-effect water-LiBr absorption systems: from half to triple effect. Renew Energ 35:1773–1782
37. Kaushik SC, Arora A (2009) Energy and exergy analysis of single effect and series flow double effect water-lithium bromide absorption refrigeration systems. Int J Refrig 32:1247–1258
38. Luo HL, Dai YJ, Wang RZ (2006) Experimental investigation of a solar adsorption chiller used for grain depot cooling. Appl Therm Eng 26:1218–1225
39. Askalany AA, Salem M, Ismael IM (2013) An overview on adsorption pairs for cooling. Renew Sust Energ Rev 19:565–572
40. Wang RZ, Ge TS, Chen CJ (2009) Solar sorption systems for residential applications: options and guidelines. Int J Refrig 32:638–660
41. Enteria N, Yoshino H, Mochida A et al (2015) Exergoeconomic evaluation of desiccant-evaporative air-conditioning system at different regeneration and reference temperatures. Int J Refrig 56:81–98
42. Enteria N, Yoshino Y, Satake A (2016) Exergoenvironmental evaluation of the desiccant air-conditioning system subjected to different regeneration temperatures. Int J Refrig Air-Cond. doi: http://dx.doi.org/10.1142/S2010132516500231

Chapter 6
Heat and Mass Transfer Performance Evaluation and Advanced Liquid Desiccant Air-Conditioning Systems

Yonggao Yin, Tingting Chen and Xiaosong Zhang

Abstract In recent years, liquid desiccant air-conditioning systems have attracted much attention for its prominent potential of energy saving. In such systems, dehumidifiers/regenerators are the core components where heat and mass transfer occurs. The heat and mass transfer coefficients determine the accuracy of mathematical model which were used to design the dehumidifiers/regenerators. So, in this paper, the methods to obtain heat and mass transfer coefficients are evaluated theoretically. In order to enhance the mass transfer process, the internally cooled/heated dehumidifier/regenerator is designed and investigated experimentally and theoretically. Further, several advanced liquid desiccant air-conditioning systems are also introduced. Results show that the proposed equivalent integral mean method has high accuracy in calculating the coupled heat and mass transfer coefficients. Unlike Lewis number which was often assumed as one for describing heat and mass transfer between air and water, the defined *Le* factor may deviate appreciably from one in the heat and mass transfer process between air and liquid desiccant. The internally heated regenerators help to develop zero-carryover gas–liquid contactors because of much higher performance than adiabatic regenerators under low solution flow rate. It also helps to reduce energy consumption because of the high regeneration thermal efficiency, which indicates that the internally heated regenerators are promising and deserve much more renovation and application.

Keywords Liquid desiccant · Heat and mass transfer coefficient · *Le* factor · Internally cooled/heated · Regeneration thermal efficiency · Hybrid air-conditioning

List of Symbols

A	Mass transfer area, m^2
C_{ps}	Specific heat capacity of solution, kJ/kg °C
C_{pa}	Specific heat capacity of humid air, kJ/kg °C

Y. Yin (✉) · T. Chen · X. Zhang
School of Energy and Environment, Southeast University, Sipailou Road, Nanjing 210096, China
e-mail: y.yin@seu.edu.cn

N. Enteria et al. (eds.), *Desiccant Heating, Ventilating, and Air-Conditioning Systems*, DOI 10.1007/978-981-10-3047-5_6

C_{pw} Specific heat capacity of water, kJ/kg °C
H Height along solution flow direction, m
h_a Enthalpy of humid air, kJ/kg
h_e Enthalpy of air in equilibrium with solution, kJ/kg
h_d Mass transfer coefficient, kg/m^2 s
h_c Heat transfer coefficient between air and solution, kW/m^2 °C
h_{cw} Heat transfer coefficient between water and solution, kW/m^2 °C
h_s Enthalpy of liquid desiccant, kJ/kg
G_a Air flow rate, m^3/s
M_a Air mass flow rate, kg/s
M_s Solution mass flow rate, kg/s
M_w Water mass flow rate, kg/s
M_r Moisture evaporation rate, g/s
k_d Mass transfer coefficient, m/s
r Vaporization heat of water, kJ/kg
r_0 Vaporization heat of water at 0 °C, kJ/kg
t_a Air temperature, °C
t_s Solution temperature, °C
t_w Water temperature, °C
v_a Air velocity, m/s
w_a Air humidity ratio, g/kg
w_e Air humidity ratio in equilibrium with solution, g/kg
X_s Concentration in salt
i Inlet
o Outlet

6.1 Scientific Evaluation of the Coupled Heat and Mass Transfer Coefficients Based on Experimental Data

This part aims to set a foundation to design dehumidifiers/regenerators. Firstly, as a basis for design, mathematical models for heat and mass transfer between air and liquid desiccants are introduced. In commonly used mathematical models, heat and mass transfer coefficients are critical to determine the prediction accuracy. So, secondly, different calculation methods of heat and mass transfer coefficients are provided and compared. Lastly, combining with experimental data and the mathematical model, heat and mass transfer coefficients are presented to give guidance and reference to relevant engineers and designers.

6.1.1 Mathematical Model for Heat and Mass Transfer Between Air and Liquid Desiccant

Generally three kinds of models have been widely used to describe the heat and mass transfer process between air and liquid desiccants. The complex differential equation model [1] is usually used in laminar flow where mass, energy and momentum conservation are applied. Thus, much computational effort must be consumed to obtain concentration, temperature and velocity profiles. On the contrary, the effectiveness model [2, 3] is simplest and with low computational cost. But only outlet parameters can be obtained using the effectiveness model. The profiles in dehumidifiers/regenerators are not available. Another disadvantage is the low accuracy compared with other models. The finite difference model arouses much more attention due to suitable accuracy and computational cost. *NTU-Le* model is a finite difference model and has been used by many investigators [3–5]. In this chapter, *NTU-Le* model is employed so it is simply introduced here.

In the *NTU-Le* model, assumptions are made as follows: (1) The desiccant solution can wet the packing material or falling film plates completely; (2) the liquid side resistance is ignored because of very thin film thickness; (3) physical parameters in the control volume are uniform; and (4) diffusion and conduction along the flow direction is ignored. Taking parallel flow as an example, according to mass and energy conversion in the control volume shown in Fig. 6.1, the following equations are obtained, respectively:

$$M_{\mathrm{a}}\mathrm{d}w_{\mathrm{a}} + \mathrm{d}M_{\mathrm{s}} = 0 \tag{6.1}$$

$$\mathrm{d}(M_{\mathrm{s}}X_{\mathrm{s}}) = 0 \tag{6.2}$$

$$M_{\mathrm{a}}\mathrm{d}h_{\mathrm{a}} + \mathrm{d}(M_{\mathrm{s}}h_{\mathrm{s}}) = 0 \tag{6.3}$$

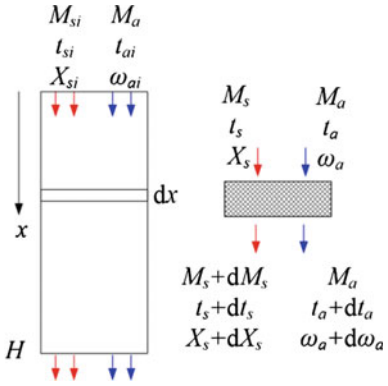

Fig. 6.1 Control volume of parallel flow

where

$$h_a = C_{pa} t_a + r_0 \tag{6.4}$$

$$h_s = C_{ps} t_s \tag{6.5}$$

In addition, the mass and energy transfer between the air and liquid desiccant can be expressed by:

$$M_a \mathrm{d}w_a = h_d (w_e - w_a) \mathrm{d}A \tag{6.6}$$

$$M_a \mathrm{d}h_a = h_d r (w_e - w_a) \mathrm{d}A + h_c (t_s - t_a) \mathrm{d}A \tag{6.7}$$

Substitute Eq. (6.4) into Eq. (6.7), the following equation can be obtained:

$$M_a \mathrm{d}t_a = h_d Le (t_s - t_a) \mathrm{d}A \tag{6.8}$$

where *Le* factor relates heat transfer with mass transfer and can be written as

$$Le = \frac{h_c}{C_{pa} h_d} \tag{6.9}$$

Sometimes, for convenience, h_d is replaced by dimensionless number, *NTU*, which is defined as:

$$NTU = \frac{h_d A}{M_a} \tag{6.10}$$

From equations above, there are five variables (M_s, t_s, X_s, t_a, w_a) and five differential equations totally. With the boundary conditions of inlet parameters (M_{si}, t_{si}, X_{si}, t_{ai}, w_{ai}) and heat and mass transfer coefficients, the outlet parameters (M_{so}, t_{so}, X_{so}, t_{ao}, w_{ao}) can be calculated. The temperature and humidity distribution in the dehumidifier/regenerator can also be achieved.

6.1.2 Methods to Calculate Heat and Mass Transfer Coefficients

As mentioned before, the magnitude of heat and mass transfer coefficients dominates in prediction accuracy. This has significant effects on the design of gas–liquid contactors. Taking the design of packed tower as an example, with the target moisture removal/evaporation rate, the packing size is decided by the coupled heat and mass transfer coefficients when the thermal and flow conditions are given. On the one hand, if the coupled heat and mass transfer coefficients in the mathematical model are set higher than the real value, the designed packing size will be larger,

causing higher initial cost as well as bigger occupied space. On the other hand, if the coupled heat and mass transfer coefficients are set lower than the real value, the designed packing size will be smaller, resulting in failing to meet the demand of dehumidification/regeneration. This implies that the heat and mass transfer coefficients are the key parameters affecting economy, flexibility and availability.

So far, mainly three methods are applied to obtain heat or mass transfer coefficient in the open literature. The first is arithmetic mean method [6, 7] in which the mass transfer coefficient (h_d) is calculated by the following equation:

$$h_d = \frac{M_a(w_{ai} - w_{ao})}{A(w_{av} - w_{ei})} \tag{6.11}$$

where

$$w_{av} = \frac{w_{ai} + w_{ao}}{2} \tag{6.12}$$

In the arithmetic mean method, only the inlet and outlet air humidity ratios are used. This corresponds to the linear distribution of humidity ratio in dehumidifiers/regenerators, which is apparently inconsistent with the real condition. The second method is logarithmic mean method [3, 8]. In the pure sensible heat transfer process, since the temperature difference between the wall and fluid is linear to the temperature change of the fluid within a control volume, heat transfer coefficient can be achieved with high accuracy by logarithmic mean temperature difference method. The formula for parallel flow is as follows:

$$h_c = \frac{M_a C_{pa}(t_{ai} - w_{ao})}{A\Delta t_a} \tag{6.13}$$

where

$$\Delta t_a = \frac{(t_{ai} - t_{si}) - (t_{ao} - t_{so})}{\ln[(t_{ai} - t_{si})/(t_{ao} - t_{so})]} \tag{6.14}$$

Further, logarithmic mean humidity difference method is used to calculate mass transfer coefficient by analogy with the sensible heat transfer. In this method, mass transfer coefficient for parallel flow is:

$$h_d = \frac{M_a(w_{ai} - w_{ao})}{A\Delta w_a} \tag{6.15}$$

where

$$\Delta w_a = \frac{(w_{ai} - w_{ei}) - (w_{ao} - w_{eo})}{\ln[(w_{ai} - w_{ei})/(w_{ao} - w_{eo})]} \tag{6.16}$$

In addition, based on the assumption that *Le* factor (*Le*) equals one, logarithmic mean enthalpy difference method defines mass transfer coefficient in parallel flow as:

$$h_{\mathrm{d}} = \frac{M_{\mathrm{a}}(h_{\mathrm{ai}} - h_{\mathrm{ao}})}{A\Delta h_{\mathrm{a}}} \tag{6.17}$$

where

$$\Delta h_{\mathrm{a}} = \frac{(h_{\mathrm{ai}} - h_{\mathrm{ei}}) - (h_{\mathrm{ao}} - h_{\mathrm{eo}})}{\ln[(h_{\mathrm{ai}} - h_{\mathrm{ei}})/(h_{\mathrm{ao}} - h_{\mathrm{eo}})]} \tag{6.18}$$

The third method is integral mean method, where the temperature and humidity distribution in dehumidifiers/regenerators must be known and the expressions of coupled heat and mass transfer coefficients are defined as follows:

$$h_{\mathrm{d}} = \frac{M_{\mathrm{a}}(w_{\mathrm{ai}} - w_{\mathrm{ao}})H}{A\int_0^H (w_{\mathrm{ax}} - w_{\mathrm{ex}})\mathrm{d}x} \tag{6.19}$$

$$h_{\mathrm{c}} = \frac{M_{\mathrm{a}}C_{\mathrm{pa}}(t_{\mathrm{ai}} - t_{\mathrm{ao}})H}{A\int_0^H (t_{\mathrm{ax}} - t_{\mathrm{sx}})\mathrm{d}x} \tag{6.20}$$

Considering the accuracy level and application range, in the following passage, only logarithmic mean method (temperature and humidity difference) and integral mean method are analyzed and compared.

6.1.3 *Conventional Logarithmic Mean Method Versus the Method Considering Local Distribution*

6.1.3.1 Calculation Procedures

The integral mean method is perfectly accurate but in fact it is difficult to obtain the real temperature and humidity distribution by measurement. This makes the integral method unavailable. Yin and Zhang [4] proposed a method to solve the problem. The temperature and humidity distribution was obtained by mathematical model combined with experimental data. Simultaneously, the coupled heat and mass transfer coefficients were calculated by Newton secant method. The results can be regarded as that from the integral mean method. So, in the next passage, the method presented by Yin et al. is called equivalent integral mean method. Formulas of the logarithmic mean method have been described in detail. In this part, we focus on the equivalent integral mean method. The equivalent method is on the basis of *NTU-Le* model elaborated in Sect. 6.1.2.

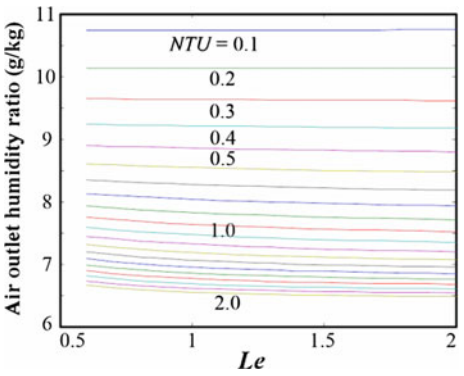

Fig. 6.2 Effect of *Le* factor on air outlet humidity ratio under different *NTU*s

Figure 6.2 shows the air outlet humidity ratio variation under different h_d and *Le* with the constant inlet parameters. In the figure, h_d is replaced by the dimensionless quantity of *NTU*.

It seems that the air outlet humidity ratio shows weak sensitivity to the magnitude of *Le* factor. For dehumidification, when *Le* increases from 0.6 to 2, the air outlet humidity decreases slightly. Especially for the condition that *NTU* is less than 0.5, almost no change happens to the air outlet humidity ratio. Therefore, the air outlet humidity ratio is almost only related with the mass transfer coefficient and it can be expressed by:

$$w_{ao} = f_1(M_a, t_{ai}, w_{ai}, M_s, t_s, X_s, A, h_d) \tag{6.21}$$

Similarly, with a certain h_d, the air outlet temperature is determined by *Le* factor. Thus, according to inlet parameters of air and solution and outlet parameters of air measured by experiment, the coupled heat and mass transfer coefficients can be determined in return. The detailed steps of the calculation for coupled heat and mass transfer coefficients are as follows:

(1) The outlet air humidity ratio (w_{ao}), temperature (t_{ao}), the inlet parameters of air and liquid desiccant solution (M_a, t_{ai}, w_{ai}, M_{si}, t_{si}, X_{si}) as well as heat and mass transfer area (A) are obtained from experiments;
(2) Assume two different groups of h_d and *Le*, namely h_{d1}, Le_1, h_{d2}, Le_2, then substitute h_{d1}, Le_1 and other inlet parameters into *NTU-Le* model aforementioned to calculate a group of outlet parameters (w_{ao1}, t_{ao1}); similarly, use h_{d2} and Le_2 to calculate another group of outlet parameters (w_{ao2}, t_{ao2});
(3) Obtain a new h_{d3} using the Newton segment method shown in Fig. 6.3a since w_{ao} is the function of h_d under constant operation conditions; calculate a new Le_3 using the same method in Fig. 6.3b; combine h_{d3} with Le_3 to get w_{ao3} and t_{ao3};
(4) Repeat step (3) until the computed outlet air humidity ratio and temperature meet the deviation requirement compared with the experimental values (w_{ao}, t_{ao}).

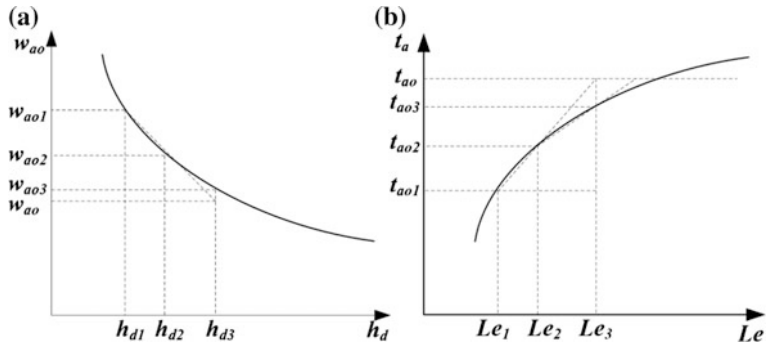

Fig. 6.3 Newton segment method to calculate h_d and Le: **a** h_d; **b** Le

6.1.3.2 Evaluation Accuracy Comparison

In air dehumidification or desiccant regeneration, the heat and mass transfers are complex and interact with each other. On the one hand, the heat transfer occurs due to the temperature difference between air and liquid desiccant. The desiccant temperature changes accordingly, causing the vapor pressure variation at the solution surface. This makes the mass transfer potential change and affects the mass transfer. On the other hand, the mass transfer between air and liquid desiccant occurs due to the vapor pressure difference, accompanying the release of latent heat, which changes the air and desiccant temperatures. Thus, the heat transfer potential changes and the heat transfer are affected in return. Under this condition, the existing methods to obtain heat and mass transfer coefficients may be unreasonable because some methods are derived only considering the single potential change. Hence, this part theoretically investigates and compares the evaluation accuracy of the (equivalent) integral mean method and the logarithmic mean method. In the following passage, two types of conditions are analyzed according to liquid-to-air flow ratio (R_m).

The first condition is that the mass flow rate of the liquid desiccant is much higher than that of the air. It could be assumed that the state of liquid desiccant does not change during the heat and mass transfer process. All parameters of the liquid desiccant (T_s, X_s, M_s) can be thought as constant along the falling film direction. Hence, Eqs. (6.6) and (6.8) can be written as, respectively:

$$dw_a = \frac{NTU(w_{ei} - w_a)}{H} dx \tag{6.22}$$

$$dt_a = \frac{NTU \cdot Le(t_{si} - t_a)}{H} dx \tag{6.23}$$

Integrating Eqs. (6.22) and (6.23) along the height gives the air parameters in the dehumidifier/regenerator:

$$w_{ax} = w_{ei} + (w_{ai} - w_{ei}) \exp\left(\frac{-NTU}{H} x\right) \tag{6.24}$$

$$t_{ax} = t_{si} + (t_{ai} - t_{si}) \exp\left(\frac{-NTU \cdot Le}{H} x\right) \tag{6.25}$$

At the air outlet, x equals H and w_{ax} equal w_{ao}. It is easy to get from Eqs. (6.24) and (6.10):

$$h_d = \frac{M_a \cdot \ln((w_{ai} - w_{ei})/(w_{ao} - w_{eo}))}{A} \tag{6.26}$$

This is in accord with the result from Eq. (6.15) using logarithmic mean humidity difference method. Similarly, from Eq. (6.25):

$$h_c = \frac{M_a \cdot C_{pa} \cdot \ln((t_{ai} - t_{si})/(t_{ao} - t_{so}))}{A} \tag{6.27}$$

The result is also the same with that from Eq. (6.13) using logarithmic mean temperature difference method.

Above theoretical analysis shows that the logarithmic mean method is exactly accurate regardless of calculating h_d or h_c when the liquid-to-air flow ratio is infinite.

The second condition is that the mass flow rate of the air can be comparable with the liquid desiccant, which is close to the actual application conditions. Since the temperature and humidity of the air and liquid desiccant change together, the parameters in dehumidifier/regenerator can't be achieved directly using the integral method. So, the equivalent integral mean method described in Sect. 6.1.3.1 is employed to calculate h_d and h_c. The calculated values by the equivalent integral and logarithmic mean methods are compared with the actual values. The methods of precision verification are introduced as follows.

The actual values of h_d and Le are assumed as 12 g/m^2 s and 1, respectively. Under the given inlet parameters of air and desiccant, the outlet parameters can be derived by combining mathematical model and the assumed h_d and Le. After that, the h_{d1} and Le_1 can be obtained by the equivalent integral mean method and h_{d2} and Le_2 can be obtained by the logarithmic mean method. Further, applicability of the calculation methods used for coupled heat and mass transfer processes can be studied.

Lithium bromide aqueous solution is used as liquid desiccant, and the packed tower is used as dehumidifier. The packing is 0.5 m in height, 0.5 m in width and 0.5 m in length. In addition, the specific surface area is set as 396 m^2/m^3. Figures 6.4 and 6.5 show the accuracy of the equivalent integral mean method and

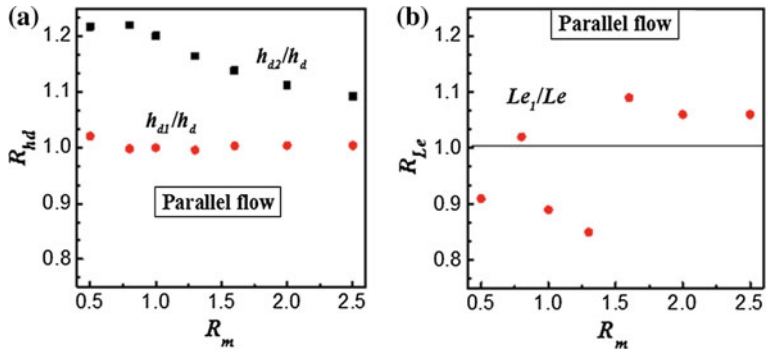

Fig. 6.4 Accuracy of two methods under high latent load for parallel flow: **a** h_d; **b** *Le*

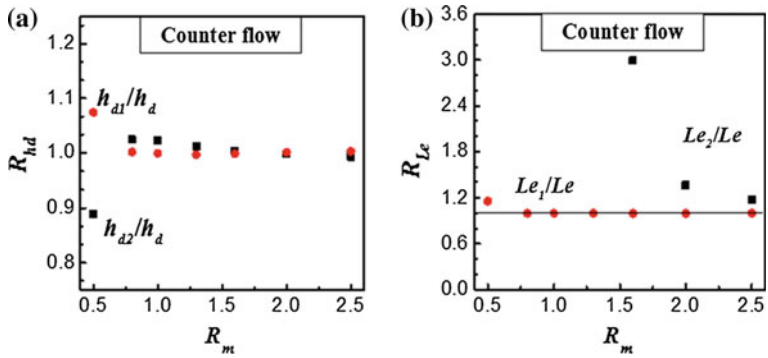

Fig. 6.5 Accuracy of two methods under high latent load for counterflow: **a** h_d; **b** *Le*

logarithmic mean method under high latent load. The inlet parameters for parallel-flow pattern are listed in Table 6.1. In order to compare the deviation between the calculated values and the actual values, the ratios of h_{d1} to h_d, h_{d2} to h_d, Le_1 to *Le* and Le_2 to *Le* are depicted in Fig. 6.4. The ratio of h_{d1} to h_d is close to 1, which means the mass transfer coefficient calculated by the equivalent integral mean method is almost the same with the actual value. And the ratio of h_{d2} to h_d shows a downward trend with an increase in the liquid-to-air flow ratio (R_m). The average absolute deviation of h_{d1} is about 0.5%, while the average absolute deviation of h_{d2} is about 9.5%. As to the calculation of heat transfer coefficient, only the equivalent integral mean method can be used because the air temperature and the

Table 6.1 Inlet parameters under high latent load

Variable	M_a (m/s)	R_m	t_a (°C)	t_s (°C)	w_a (g/kg)	X_s
R_m	0.333	0.5–2.5	34	22	26.9	0.5

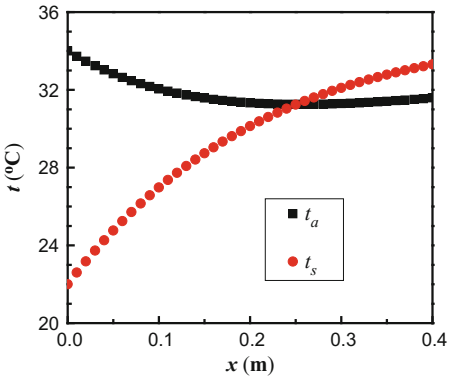

Fig. 6.6 Temperature distribution along solution flow direction

desiccant temperature intersect as illustrated in Fig. 6.6. This results in the meaninglessness of the logarithmic operation. Therefore, no data points about Le_2 appear in Fig. 6.4b. The average absolute deviation of Le_1 is about 8.3%. For the counterflow pattern, the equivalent integral mean method also has higher accuracy than the logarithmic mean method especially calculating heat transfer coefficients. However, it seems that the advantage of equivalent integral mean method is depressed compared with the parallel-flow pattern. When the liquid-to-air flow ratio is more than 6.5, mass transfer coefficients calculated by two methods are almost the same and the heat transfer coefficient can also be calculated by logarithmic mean temperature method. It should be noted that the equivalent integral mean method performs well to calculate the heat transfer coefficient while the logarithmic mean temperature method performs badly even fails.

Figures 6.7 and 6.8 show the accuracy of the equivalent integral mean method and logarithmic mean method under low latent load. The inlet parameters are listed in Table 6.2 and the packing size changes to 0.4 m in height, 0.4 m in width and

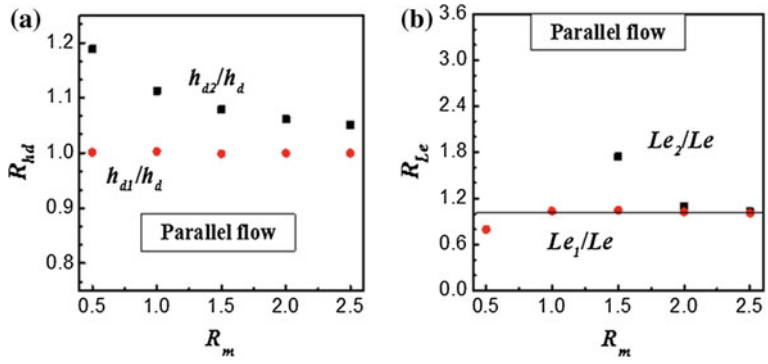

Fig. 6.7 Accuracy of two methods under low latent load for parallel flow: **a** h_d; **b** Le

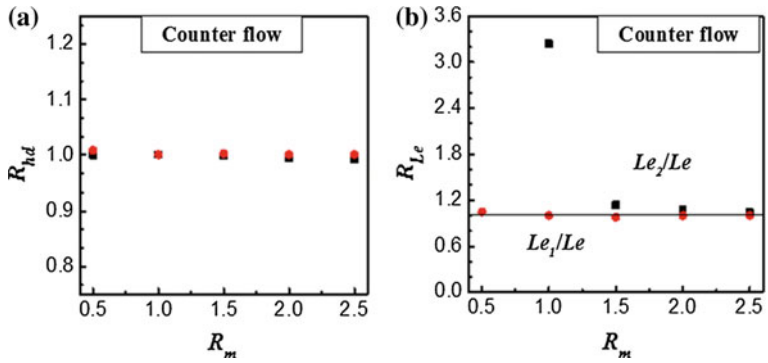

Fig. 6.8 Accuracy of two methods under low latent load for counterflow: **a** h_d; **b** Le

Table 6.2 Inlet parameters under low latent load

Variable	M_a (m/s)	R_m	t_a (°C)	t_s (°C)	w_a (g/kg)	X_s
R_m	0.333	0.5–2.5	30.3	22	15.3	0.5

0.4 m in length. In the parallel-flow pattern, the equivalent integral mean method shows good performance with the deviation of 0.1% for h_{d1} and the deviation of 6.6% for Le_1. The accuracy of the logarithmic mean method improves, which can be mainly reflected by two aspects. One is the higher calculation precision of h_{d2} than that under high latent load. The other is the higher availability for calculating heat transfer coefficients. In the counterflow pattern, two methods are exactly accurate to obtain the mass transfer coefficients with the deviation within 0.3% from the actual values. When the liquid-to-air flow ratio is more than 2.0, the logarithmic mean method can be used to calculate heat transfer coefficients with high accuracy.

According to discussions above, the equivalent integral mean method is an effective method to obtain the coupled heat and mass transfer coefficients regardless of the inlet conditions. However, the accuracy of the logarithmic mean method heavily depends on the inlet conditions. The inlet desiccant temperature is usually lower than the inlet air temperature to realize dehumidification. Under the high latent load, it is probable that the outlet desiccant temperature is higher than the outlet air temperature because of the release of vaporization heat during the dehumidification process. This is due to the most vaporization heat entering the desiccant solution. Under this case, the logarithmic mean method fails to calculate the heat transfer coefficient. This problem can be alleviated with an increase in the liquid-to-air flow ratio which helps depress the temperature increase.

6.1.4 *Experimental Study on the Coupled Heat and Mass Transfer Coefficients*

In this section, the equivalent integral mean method is used to obtain the coupled heat and mass transfer coefficients during experiments. The steps to calculate heat and mass transfer coefficients combining the mathematical model and experimental data have been described in Sect. 6.1.3.1. Effects of the inlet parameters on the coupled heat and mass transfer coefficients are investigated, and reliable experimental data are also provided.

6.1.4.1 Empirical Values for Packed Towers

Extensive dehumidification experiments were conducted to provide reliable reference data using a cross-flow packed tower dehumidifier. Lithium chloride aqueous solution and structured Munters Celdek were used as liquid desiccant and packing, respectively. The packing with the specific area of 396 m^2/m^3 is 0.5 m in height, 0.5 m in length and 0.2 m in width. When one variable is analyzed, the other variables are kept constant. Inlet conditions of air and solution are listed in Table 6.3.

Figure 6.9 shows mass transfer coefficient and *Le* factor under different air velocities during dehumidification. As air velocity increases from 0.22 to 0.71 m/s, the mass transfer coefficients increases linearly from 3.1 to 9 g/(m^2 s), and *Le* factor changes slightly between 6.3 and 6.9. So, the heat transfer coefficient also increases with the air flow rate. This can be explained by the lower heat and mass transfer resistances under higher air velocity.

Table 6.3 Inlet parameters of experimental data in cross-flow

Variable	v_a (m/s)	M_s (kg/s)	t_a (°C)	t_s (°C)	w_a (g/kg)	X_s
v_a	0.22–0.71	0.06	28.1–28.3	30.5–30.8	8.38–8.4	0.35
w_a	0.47	0.085	24.7	30	10–16	0.365

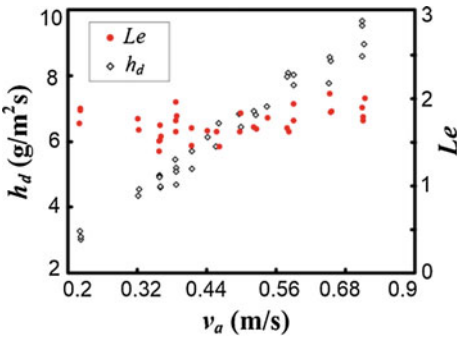

Fig. 6.9 Effect of air velocity for cross-flow during dehumidification [4]

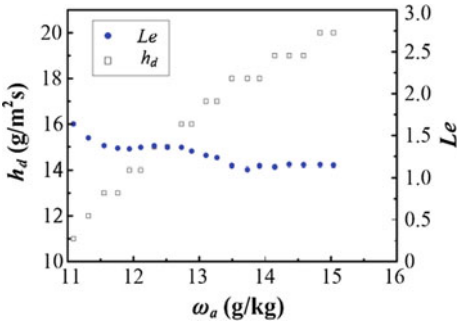

Fig. 6.10 Effect of air humidity ratio in cross-flow during dehumidification [4]

Figure 6.10 shows mass transfer coefficient and *Le* factor under different air humidity ratios. The higher inlet air humidity ratio promotes the mass transfer coefficient significantly. In Fig. 6.9, the inlet air humidity ratio is only about 8 g/kg. Thus, the mass transfer coefficient maintains at a low level less than 10 g/m^{2}s. In Fig. 6.10, the mass transfer coefficient is as high as 20 g/m^{2}s when the inlet air humidity ratio is about 15 g/kg. Due to stable *Le* factor and significant increase in the mass transfer coefficient, the heat transfer coefficient also rises with the air humidity ratio.

6.1.4.2 Empirical Values for Falling Film Columns

Experiments were also carried out using a flat-plate falling film dehumidifier depicted in Fig. 6.11. The lithium bromide aqueous solution from the distributor was divided into four pieces and flows vertically along four flat plates, respectively. To wet the surface completely, each flat plate was covered by gauze sheet and the

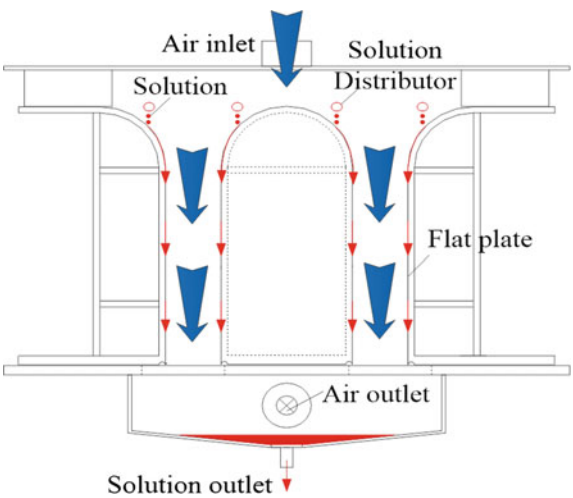

Fig. 6.11 Flat-plate falling film equipment

Table 6.4 Inlet parameters of experimental data in parallel flow

Variable	v_a (m/s)	M_s (kg/s)	t_a (°C)	t_s (°C)	w_a (g/kg)	X_s
v_a	0.78–6.63	0.025	26.6	30.5–30.8	14.3–14.5	0.547–0.556
M_s	0.98	0.023–0.043	26.5	28.4–30.7	14.8–15.0	0.497–0.505

total wetted area was 3 m^2. The liquid desiccant was brought into contact with the air from the top of the dehumidifier and heat and mass transfer occurs accordingly. Inlet conditions of air and solution are listed in Table 6.4.

Figure 6.12 demonstrates the effect of air velocity on the mass transfer coefficient and *Le*. When air velocity changes from 0.78 to 6.63 m/s, the mass transfer coefficient increases from 9.5 to 13.7 g/m^2 s. In addition, *Le* factor shows an upward trend with the air velocity more than 0.9 m/s. Therefore, the heat transfer coefficient also increases due to the obvious increase in h_d and *Le*.

Figure 6.13 demonstrates the effect of the solution flow rate on the mass transfer coefficient and *Le*. The increase in the solution flow rate enhances the mass transfer coefficient at first but further increase hardly contributes. Similar to the air velocity, the increase of the solution velocity also strengthens the interface turbulence, resulting in lower mass transfer resistance. As the solution mass flow rate increases, *Le* fluctuates around 0.6.

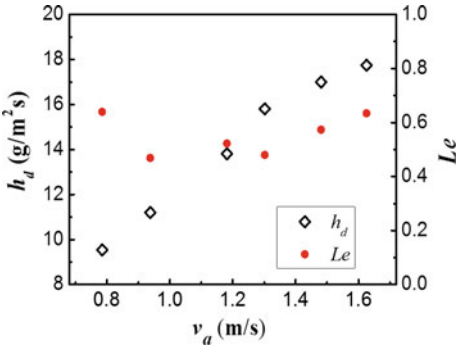

Fig. 6.12 Effect of air velocity for parallel flow during dehumidification

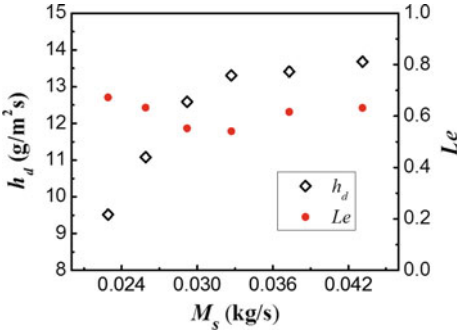

Fig. 6.13 Effect of solution flow rate for parallel flow during dehumidification

The results from experiments show that different from conventional Lewis number, the defined *Le* factor in this chapter is not always close to 1. But for experiments in this chapter, the *Le* factor changes not distinctly when only one variable changes. So, the *Le* factor should be selected carefully based on pertinent experimental data. Moreover, when the humidity ratio is about 15 g/kg, the mass transfer coefficients are mostly within the range between 10 and 20 g/m^2s. In order to obtain accurate heat and mass transfer coefficients, reasonable methods considering local distribution are recommended.

6.2 Efficient Equipment for Liquid Desiccant Dehumidification/Regeneration

This part aims to highlight the optimum design of the dehumidifier/regenerator used in liquid desiccant air-conditioning systems. The performance enhancement is discussed experimentally and theoretically.

Dehumidifiers/regenerators are the core equipment in liquid desiccant air-conditioning systems, where air and the liquid desiccant contact and as a result heat and mass transfer occurs. Adiabatic packed towers are the commonly used configuration of gas–liquid contactors for the merit of simplicity. However, during dehumidification process, the solution temperature rises significantly due to the release of latent heat from the condensed vapor in dehumidified air. This causes the reduction of mass transfer potential since the vapor pressure at the solution surface increases. Therefore, the dehumidification performance declines obviously. Similarly, during regeneration process, the solution temperature will decrease significantly because of the absorption of the latent heat, leading to poor regeneration performance. Two methods have been put into use to solve the problem. One method is increasing the solution flow rate to maintain lower temperature in dehumidifiers and higher temperature in regenerators. The other method is using cooling sources to remove latent heat during dehumidification and using heating sources to provide latent heat during regeneration. The former method often causes severe droplet carryover inevitably, which makes pipes and devices corroded and may pose a potential threat to air quality. So the latter method has received much attention [9–15].

Here, a novel internally cooled/heated dehumidifier/regenerator was designed and experimentally tested. Further, the mathematical model for internally cooled/heated dehumidifier/regenerator was developed and verified using experimental data. Based on the model, the performance of the internally heated regenerators under different conditions was theoretically analyzed and compared with the adiabatic regenerators.

6.2.1 *Experimental Test of a Internally Cooled/Heated Dehumidifier/Regenerator*

6.2.1.1 Structure of the Internally Cooled/Heated Dehumidifier/Regenerator

In the adiabatic gas–liquid contactors, the release and absorption of the latent heat obviously changes the desiccant temperature during humidification/regeneration, leading to poor mass transfer performance. To solve the problem, a plate-fin heat exchanger (PFHE) was designed [16]. The structure of the PFHE is shown in Fig. 6.14a, b. A unit of PFHE consists of seven parallel water channels and six solution/air channels intermingled with each other. All channels are 298 mm in length. The water channel is 3 mm in width, while the solution/air channel is 12 mm in width. In addition, the height of the PFHE unit is 100 mm. In order to provide more contacting area for desiccant solution and air, between two neighboring plates, there are three layers of fins with the distance of 4 mm side-by-side intercrossing.

As depicted in Fig. 6.14c, the internally cooled dehumidifier or internally heated regenerator is composed by six identical units of PFHE stacking up along the vertical direction. For the convenience of installation, two neighboring PFHEs have opposite water inlet sides. Therefore, three PFHEs have their inlet/outlet on one side and the remaining PFHEs have their inlet/outlet on the other side. The desiccant solution from the top of the dehumidifier/regenerator is distributed evenly over the fins and flows countercurrently relative to the air from the bottom. For dehumidification, cooling water entering the water channels flows horizontally and removes

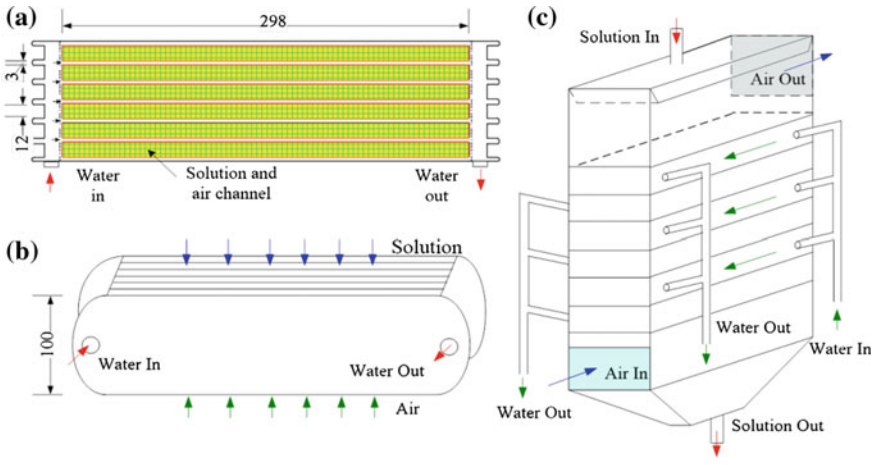

Fig. 6.14 Structures of PFHE and dehumidifier/regenerator: **a** top view of the plate-fin heat exchanger; **b** schematic diagram of the plate-fin heat exchanger; **c** structure of the whole dehumidifier/regenerator [16]

vaporization heat to maintain low solution temperature during the dehumidification process, producing high mass transfer potential. For regeneration, heating water is transported into the water channels and provides vaporization heat to maintain high solution temperature as well as high mass transfer potential. If no water is used, the dehumidifier/regenerator becomes adiabatic.

6.2.1.2 Experimental Test and Performance Comparison

In order to test the performance of the designed internally cooled/heated dehumidifier/regenerator, pertinent experiments were conducted using lithium chloride aqueous solution as liquid desiccant. A comparative study was also conducted between the adiabatic and the internally cooled/heated dehumidifier/regenerator. The humidity ratio difference is taken as a performance index. On the one hand, the humidity ratio difference can represent moisture removal/evaporation rate with the constant air flow rate. On the other hand, it reflects the processed air outlet humidity ratio, which is critical for dehumidification requirement in comfort air-conditioning systems. In this section, the humidity ratio difference for dehumidification is defined as:

$$\Delta w_a = w_{ai} - w_{ao} \tag{6.28}$$

And the humidity ratio difference for regeneration is defined as:

$$\Delta w_a = w_{ao} - w_{ai} \tag{6.29}$$

As known to us, the air velocity has a remarkable impact on the heat and mass transfer coefficient [13, 14]. Besides, the solution temperature significantly affects the partial vapor pressure at the solution surface, which determines the mass transfer potential in some degree. Thus, the effects of air velocity and solution temperature on the performance index were investigated. In addition, the effect of cooling water temperature was also discussed for internally cooled dehumidifier.

As to dehumidification, inlet conditions of air, solution and cooling water are shown in Table 6.5.

Figure 6.15 shows humidity ratio difference under different air velocities for the internally cooled and adiabatic dehumidifier, respectively. When the air velocity increases, the humidity ratio difference firstly increases linearly and afterward stays

Table 6.5 Inlet parameters for the internally cooled dehumidifier during experiments

Variable	v_a (m/s)	M_s (kg/s)	M_w (kg/s)	t_a (°C)	t_s (°C)	t_w (°C)	w_a (g/kg)	X_s
v_a	6.49–3	0.1036	0.151	30.9	25.3	24	10.6	0.386
t_s	2.84	0.1036	0.151	30.5	20.4–36.6	22	13.4	0.377
	2.84	0.1036	0.151	30.9	23.6–28.9	22	12.6	0.388
t_w	3.36	0.1036	0.151	30.3	27.0	19–25	12.6	0.387

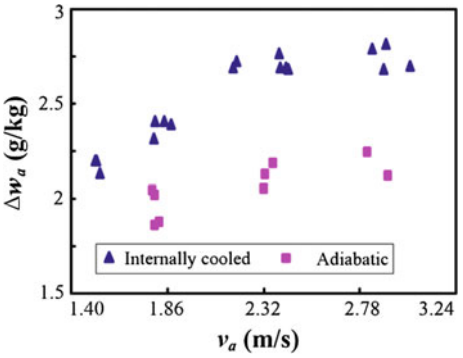

Fig. 6.15 Effect of air velocity on the humidity ratio difference for dehumidification [16]

almost constant. Both the internally cooled dehumidifier and the adiabatic dehumidifier have the same trend but with the different magnitude of humidity ratio difference. The humidity ratio difference of the internally cooled dehumidifier is 0.5 g/kg larger than that of the adiabatic dehumidifier on average. Compared with the adiabatic dehumidifier, performance of the internally cooled dehumidifier is improved by about 25%. This is because the cooling water effectively carries away the vaporization heat and keeps the solution temperature low, producing higher overall vapor pressure difference between air and desiccant in internally cooled dehumidifier. The appeared significant increase in the humidity ratio difference can be attributed to the mass transfer coefficient, which increases more quickly than the air flow rate under higher air velocity. The reason for the almost constant trend later is that the increase in the mass transfer coefficient is close to the increase in the air flow rate when the air velocity is high enough. If the air velocity increases further, the air flow rate may increase more rapidly than the mass transfer coefficient, resulting in the drop of humidity ratio difference.

Two group experiments were conducted to study the effect of solution temperature on the humidity ratio difference for two types of dehumidifiers. As illustrated in Fig. 6.16, the humidity ratio difference shows an obvious downward trend with the increase in the solution temperature. The performance of the internally cooled

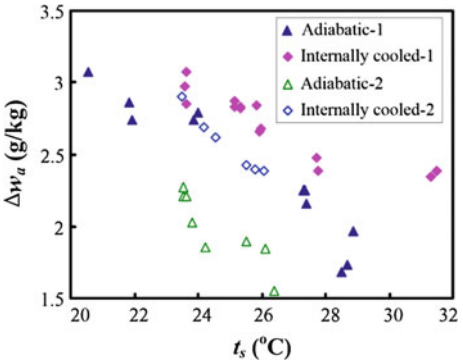

Fig. 6.16 Effect of solution temperature on the humidity ratio difference for dehumidification [16]

dehumidifier is better than that of the adiabatic dehumidifier in terms of the humidity ratio difference. In order to disclose effects of the solution temperature on the humidity ratio difference accurately, the mass transfer coefficient between the processed air and solution is calculated by the following equation according to the literature [15]:

$$k_{\mathrm{d}} = \frac{G_{\mathrm{a}}(w_{\mathrm{ai}} - w_{\mathrm{ao}})}{A(w_{\mathrm{ai}} - w_{\mathrm{ei}})} \tag{6.30}$$

where k_{d} is different from aforementioned h_{d} but can also reflect the mass transfer process.

From Fig. 6.17, the mass transfer coefficient decreases with the solution temperature. This means that the reduction of the humidity ratio difference is because of not only the bigger vapor pressure at the solution surface but also the smaller mass transfer coefficient the high solution temperature brings. The overall solution temperature in the internally cooled dehumidifier is lower than that in the adiabatic dehumidifier. So, it is clear that the humidity ratio difference of the internally cooled dehumidifier is higher than that of the adiabatic dehumidifier.

Since no cooling water is used in the adiabatic dehumidifier, the humidity ratio difference stays constant when the cooling water temperature changes. Under this condition, the adiabatic dehumidifier is not analyzed. Figure 6.18 presents the effect of cooling water temperature in the internally cooled dehumidifier. As the cooling water temperature varies from 19 to 25 °C, the humidity ratio difference declines. The overall solution temperature variation accounts for this phenomenon.

As to regeneration, inlet conditions of air, solution and heating water are shown in Table 6.6.

Figure 6.19 shows the effect of the air velocity on the performance of internally heated regenerator and the adiabatic regenerator. The humidity ratio difference of the internally heated regenerator is much higher than that of the adiabatic regenerator. The average deviation is about 3 g/kg. Compared with the adiabatic dehumidifier, performance of the internally heated regenerator is improved by about 33%. This can be explained as follows. In the adiabatic regenerator, the vapor pressure at the solution surface is higher than that of the scavenging air. So the

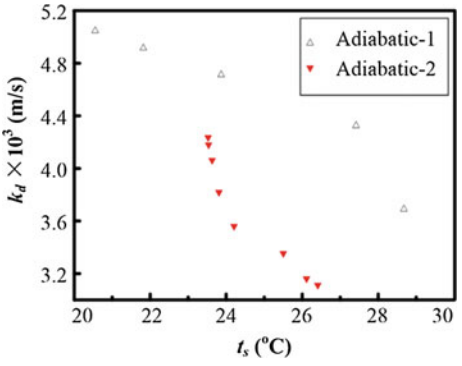

Fig. 6.17 Mass transfer coefficients under different solution temperatures for dehumidification

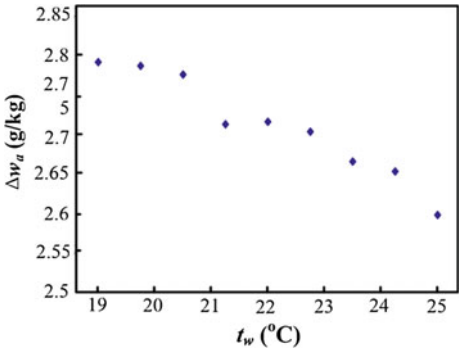

Fig. 6.18 Effect of water temperature on the humidity ratio difference for dehumidification [16]

Table 6.6 Inlet parameters for the internally heated regenerator during experiments

Variable	v_a (m/s)	M_s (kg/s)	M_w (kg/s)	t_a (°C)	t_s (°C)	t_w (°C)	w_a (g/kg)	X_s
v_a	6.68–3.59	0.1	0.14	26.5	70.0	70	16.5	0.380
t_s	2.42	0.1	0.14	26.7	62.0–73.0	72	16.3	0.360

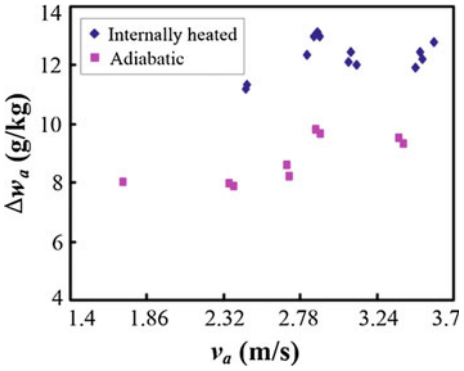

Fig. 6.19 Effect of air velocity on the humidity ratio difference for regeneration [16]

moisture transfers from the desiccant solution to the air, accompanying the absorption of vaporization heat, which mainly comes from the sensible heat of desiccant solution. Hence, the temperature of the desiccant solution decreases dramatically and regeneration performance decays. However, in the internally heated regenerator, the heating water enters the regenerator and provides the desiccant solution with sensible heat-by-heat transfer. During regeneration process, the solution can stay high temperature and the regeneration performance can be enhanced accordingly. With the increase in the air velocity, the humidity ratio difference also increases for both internally heated and adiabatic regenerators. This should be explained from two aspects. The first is that the higher air velocity helps to increase the mass transfer coefficient for stronger turbulent fluctuation. The second is that the regeneration air can be carried away rapidly. As a result, the mass transfer potential is maintained relatively high.

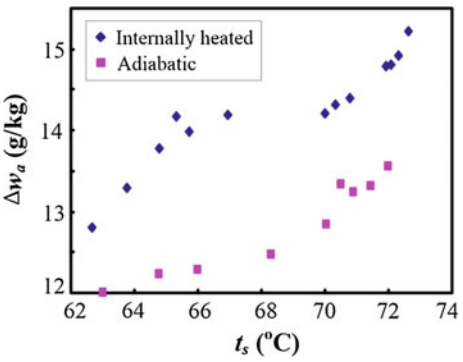

Fig. 6.20 Effect of solution temperature on the humidity ratio difference for regeneration [16]

The effect of the solution temperature for regeneration is shown in Fig. 6.20. During experiments, the solution temperature varies from 62 to 73 °C by regulating the electric heater with a temperature controller. It can be seen that the humidity ratio difference of the internally heated regenerator is much more than that of the adiabatic regenerator especially for the solution temperature among 65–69 °C. Moreover, both internally heated and adiabatic regenerators show upward trend in the humidity ratio difference. This may be due to higher vapor pressure difference between liquid desiccant and air with an increase in the solution temperature.

The above analysis experimentally verified the excellent superiority of the internally cooled/heated dehumidifier/regenerator by comparison with the adiabatic dehumidifier/regenerator. The cooling water helps to keep the low temperature of desiccant solution during dehumidification, and the heating water helps to keep the high temperature of desiccant solution during regeneration, which promotes mass transfer. With good dehumidification/regeneration performance, the internally cooled/heated dehumidifier/regenerator can also be made smaller in terms of the size. It indicates that the internally cooled/heated dehumidifier/regenerator is a promising alternative to the adiabatic dehumidifier/regenerator.

For the liquid desiccant air-conditioning system, the desiccant regeneration determines the system economy because the regeneration process consumes much energy. Therefore, the internally heated regenerator was further discussed theoretically.

6.2.2 Modeling and Performance Simulation of a Internally Heated Regenerator

6.2.2.1 Mathematical Model and Verification

In order to simulate the heat and mass transfer process for internally heated regenerator under different operation conditions, a simple mathematical model was set up.

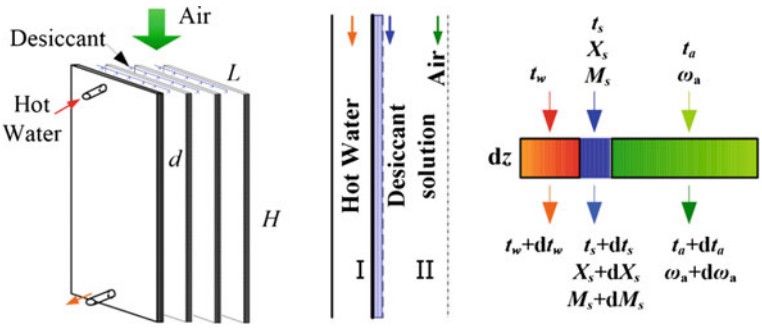

Fig. 6.21 Regenerator structure and control volume

The internally heated regenerator in Fig. 6.21 had two types of channels including one type of hot water channels (channel I) and the other type of air and desiccant channels (channel II). If the hot water was not inactivated, the regenerator was an adiabatic regenerator. Fins were equipped between two plates in the air and desiccant channels to expend the heat and mass transfer area for air and liquid desiccant. The internally heated regenerator was 300 mm in length (L), 1000 mm in height (H). Besides, the channel II was 24 mm in width, and the extended coefficient of the area of the fin in the regenerator (β) was 4.

The finite difference model is used, and the control volume is also shown in Fig. 6.21. In the control volume, heat and mass transfer happens between three types of fluids. Firstly, heat and mass transfer happens between the air and desiccant. According to Refs. [11, 17], the change of air temperature and humidity ratio can be expressed as follows:

$$\mathrm{d}t_\mathrm{a} = \frac{2h_\mathrm{c}(t_\mathrm{s} - t_\mathrm{a})L\beta}{M_\mathrm{a}C_\mathrm{pa}}\mathrm{d}z \tag{6.31}$$

$$\mathrm{d}w_\mathrm{a} = \frac{2h_\mathrm{d}(w_\mathrm{e} - w_\mathrm{a})L\beta}{M_\mathrm{a}}\mathrm{d}z \tag{6.32}$$

Secondly, heat transfer also happens between liquid desiccant and air. Temperature of the desiccant solution changes due to heat transfer with the air and hot water, which can be expressed by:

$$\mathrm{d}t_\mathrm{s} = -\frac{M_\mathrm{a}\cdot\mathrm{d}h_\mathrm{a} + M_\mathrm{w}C_\mathrm{pw}\cdot\mathrm{d}t_\mathrm{w} + M_\mathrm{a}\cdot C_\mathrm{ps}\cdot t_\mathrm{s}\cdot\mathrm{d}w_\mathrm{a}}{C_\mathrm{ps}M_\mathrm{s}} \tag{6.33}$$

Due to the evaporation of the water in the solution, the mass flow rate and the concentration of the desiccant also change, which can be determined by following equations:

$$dX_s = \frac{M_a \cdot dw_a}{M_s + M_a \cdot dw_a} X_s \tag{6.34}$$

$$dM_s = -M_a \cdot dw_a \tag{6.35}$$

According to the energy balance, temperature change of the hot water can be calculated as follows:

$$dt_w = \frac{h_{cw}(t_s - t_w)L}{C_{pw}M_w} dz \tag{6.36}$$

In addition, the dimensionless correlation of mass transfer coefficient is derived based on the experiments aforementioned. It is written as:

$$Sh_a = 25.8154 t_s^{-3.36} Re_a^{1.55} Sc_a^{0.33} \tag{6.37}$$

Based on the mathematical model and the dimensionless correlation, the outlet air temperature, humidity ratio and desiccant temperature were predicted. The deviation between predicted values and experimental data was within 5%, which has been validated in Ref. [17]. This indicated that the model could give reasonable prediction for heat and mass transfer between air and liquid desiccant. Therefore, the model could be used to investigate the effects of inlet parameters.

6.2.2.2 Performance Indexes and Performance Comparison

The regenerator is desired to vaporize water from the desiccant solution as much as possible, so the moisture evaporation rate is taken as a performance index and it is defined as:

$$M_r = M_a(w_{ao} - w_{ai}) \tag{6.38}$$

Since the internally heated regenerator consumes extra energy to provide latent heat, it is necessary to evaluate how much energy actually contributed to the phase transition of water. Thus, regeneration thermal efficiency (η_r) is also taken as performance index and is defined as:

$$\eta_r = \frac{M_a(w_{ao} - w_{ai})r}{Q_h} \tag{6.39}$$

where Q_h is the total heat input to the regeneration.

In addition, lithium chloride aqueous solution is used as desiccant and both air and liquid desiccant enter the regenerator from the top. The inlet conditions are listed in Table 6.7.

Table 6.7 Inlet parameters for internally heated regenerator

Variable	M_a (kg/s)	M_s (kg/s)	M_w (kg/s)	t_a (°C)	t_s (°C)	t_w (°C)	w_a (g/kg)	X_s
M_s	0.015	0.001–0.031	0.02	30.0	65.0	65.0	16.5	0.370
t_s	0.015	0.004	0.02	30.0	50.0–100.0	65.0	16.5	0.370
M_a	0.001–0.021	0.004	0.02	30.0	65.0	65.0	16.5	0.370
t_a	0.015	0.004	0.02	20.0–40.0	65.0	65.0	16.5	0.370
M_w	0.015	0.004	0.003–0.063	30.0	65.0	65.0	16.5	0.370

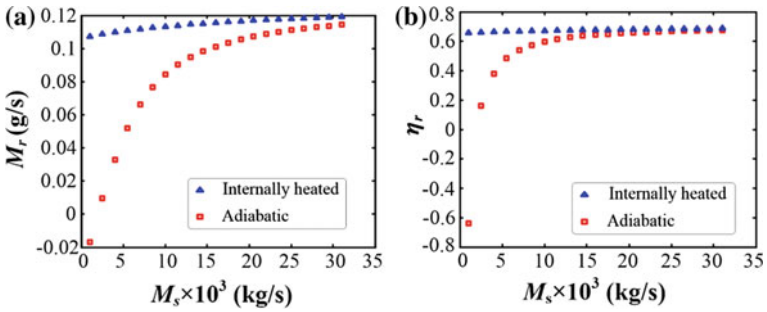

Fig. 6.22 Effects of solution flow rate for internally heated regenerator [11]: **a** moisture evaporation rate M_r; **b** regeneration thermal efficiency η_r

Figure 6.22 presents moisture evaporation rate and regeneration thermal efficiency under different solution mass flow rates. It seems that in the internally heated regenerator, both moisture evaporation rate and regeneration thermal efficiency show weak sensitivity to the solution mass flow rate. However, in the adiabatic regenerator, both moisture evaporation rate and regeneration thermal efficiency firstly increase notably with the solution mass flow rate and afterward keep nearly unchanged. It must be pointed out that when the solution mass flow rate is very low, the moisture evaporation rate is less than zero, which means dehumidification occurs in the adiabatic regenerator. This is because in the adiabatic regenerator, the available heat for regeneration is mainly provided by the liquid desiccant. When the solution mass flow rate is very low, the available heat for regeneration is very little and the solution temperature drops dramatically during regeneration. As a result, the vapor pressure at the solution surface is less than the vapor pressure of the air and dehumidification occurs accordingly. In this case, the heating water helping to maintain the solution temperature can promote the regeneration performance effectively. Thus, the moisture evaporation rate of the internally heated regenerator is much higher than that of the adiabatic regenerator when the solution mass flow rate is low. It can be concluded that the internally heated regenerator shows great superiority in the case of low solution flow rate while the adiabatic regenerator works well only when the solution flow rate is relatively high. Since the low solution flow rate can relieve the problem of carryover, the internally heated regenerator is a potential alternative to the zero-carryover application.

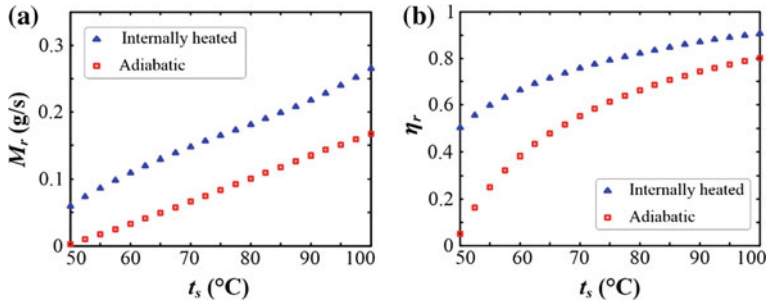

Fig. 6.23 Effects of solution temperature for internally heated regenerator [11]: **a** moisture evaporation rate M_r; **b** regeneration thermal efficiency η_r

Figure 6.23 presents moisture evaporation rate and regeneration thermal efficiency under different solution temperatures. The moisture evaporation rate increases linearly for two types of regenerators due to higher mass transfer potential. The moisture evaporation rate of the internally heated regenerator is higher than that of the adiabatic regenerator on account of the existence of hot water. The regeneration thermal efficiency also increases with an increase in the solution temperature for two types of regenerators. This is because the moisture evaporation rate increases significantly with the temperature.

Figure 6.24 shows the effects of the air mass flow rate. For the internally heated regenerator, the moisture evaporation rate shows an upward trend while for the adiabatic regenerator, the moisture evaporation rate increases when the air flow rate is less than 0.011 kg/s and further increase in the air flow rate will result in reversing this trend. This can be explained as follows. The higher air velocity improves the mass transfer coefficient when the air flow rate is low. Thus, the moisture evaporation rate becomes larger. But further increase in the air velocity causes strong heat transfer between air and liquid desiccant. The solution temperature decreases sharply in the adiabatic regenerator and dehumidification may occur, leading to the reduction of the moisture evaporation rate. In addition, the

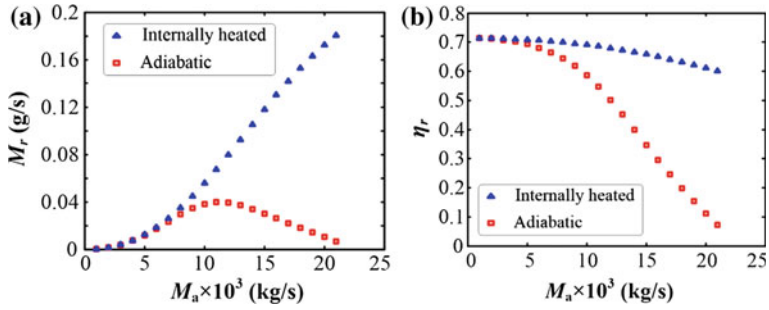

Fig. 6.24 Effects of air flow rate for internally heated regenerator [11]: **a** moisture evaporation rate M_r; **b** regeneration thermal efficiency η_r

mass flow rate has an adverse effect on the regeneration thermal efficiency for both regenerators. In the internally heated regenerator, the regeneration thermal efficiency decreases slightly while in the adiabatic regenerator, the regeneration thermal rate decreases sharply. This is because air with higher velocity carries away considerable heat from the liquid desiccant. So, more heat is wasted without converting into the useful latent heat. Hence, the regeneration thermal efficiency declines. In the adiabatic regenerator, no source is used to compensate the wasted heat, resulting in more rapid decrease of the regeneration thermal efficiency than the internally heated regenerator. This indicates the air flow rate must be selected carefully and has an optimal value in adiabatic regenerator.

In Fig. 6.25, the moisture evaporation rate and the regeneration thermal efficiency are depicted under different air temperatures. As the air temperature rises, almost no change happens to the moisture evaporation rate in the internally heated regenerator. But in the adiabatic regenerator, the moisture evaporation rate increases. For the adiabatic regenerator, the increase in the air temperature can effectively depress the decrease in the solution temperature during regeneration process. However, for the internally heated regenerator, the increase in the air temperature has little effect on the solution temperature due to large heat derived from the heating water. The variations of regeneration thermal efficiency in two types of regenerators are opposite. The decrease of the regeneration thermal efficiency in the internally heated regenerator is because extra heat is used to increase air temperature but little improvement in the evaporation rate is derived. The increase of the regeneration thermal efficiency in the adiabatic regenerator is because more moisture evaporation rate is obtained by increasing the air temperature.

In Fig. 6.26, the effect of the heating water flow rate is illustrated. Since no heating water is used in the adiabatic regenerator, the regeneration performance stays unchanged with the increase in the heating water flow rate. For the internally heated regenerator, the larger heating water flow rate helps to enhance the moisture evaporation rate and the regeneration thermal efficiency. When the heating water flow rate is more than 0.025 kg/s, the moisture evaporation rate as well as the regeneration thermal efficiency almost keeps constant.

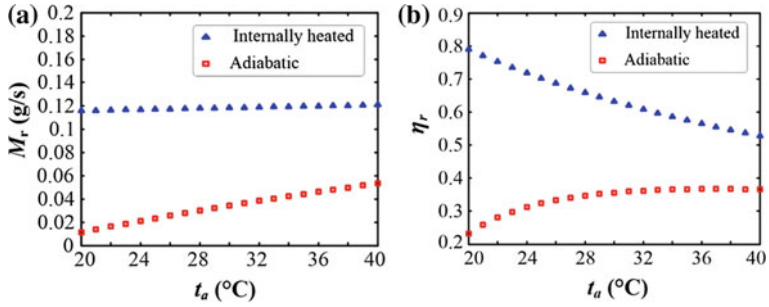

Fig. 6.25 Effects of air temperature for internally heated regenerator [11]: **a** moisture evaporation rate M_r; **b** regeneration thermal efficiency η_r

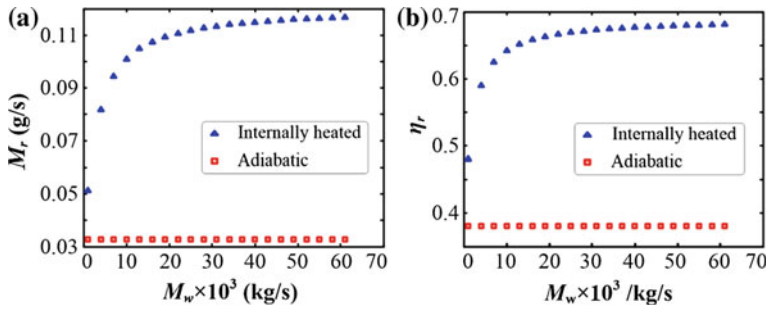

Fig. 6.26 Effects of water flow rate for internally heated regenerator [11]: **a** moisture evaporation rate M_r; **b** regeneration thermal efficiency η_r

From analysis above, the internally heated regenerator has a great advantage over the adiabatic regenerator. Different from the adiabatic regenerator, the internally heated regenerator still shows prominent regeneration performance when the solution flow rate is very low. This helps to develop zero-carryover gas–liquid contactor. In addition, the internally heated regenerator also helps to reduce energy consumption during regeneration because of the high regeneration thermal efficiency. Great importance should be attached to the development of internally heated regenerators.

6.3 Efficient Liquid Desiccant Air-Conditioning Systems

This part aims to provide some efficient air-conditioning systems using liquid desiccant dehumidification technology. As is known, traditional air-conditioning systems suffer from the problem of low efficiency for a long term. This is because the condensation dehumidification is used to remove the latent load. In this method, the water vapor is squeezed out of the humid air until the air temperature is cooled below the dew point. Under this case, usually chilled water of 7 °C is required to meet the demand of indoor humidity, resulting in low coefficient of performance of the chiller. However, the indoor temperature can be controlled at a suitable value using the chilled water of 15 °C, which means the system can be enhanced notably if the condensation method is replaced by other dehumidification methods independent of low-temperature cooling sources. Based on the idea, liquid desiccant dehumidification is expected to be a promising alternative especially when low-grade waste heat or solar energy is available. Since the vapor pressure at the solution surface is lower than that of the humid air, the moisture transfers from the air to the liquid desiccant. As a result, the air becomes dry and the liquid desiccant is diluted. Failing to absorb water vapor effectively, the diluted desiccant has to recover the initial concentration so that dehumidification process can continue. In order to discharge moisture into scavenging air, the vapor pressure at the solution

surface must be increased, which is usually realized by adding heat to increase solution temperature.

Instead of low temperature of air, the vapor pressure difference between the desiccant and air is relied on to remove the moisture for the liquid desiccant dehumidification. However, the absorption of water vapor accompanies the release of the latent heat, which actually converts to sensible heat of the liquid desiccant and air. So the air temperature usually rises to more than the indoor air temperature after desiccant dehumidification. In order to remove the sensible heat, mainly three methods are proposed to combine with the liquid desiccant dehumidification. Most researchers focus on the free cooling and heat pumps [5, 18], while seldom researchers are concerned with the absorption refrigeration [19]. In the next passage, such hybrid air-conditioning systems are provided to set an example for efficient application of liquid desiccant dehumidification.

6.3.1 Liquid Desiccant Systems Combined with Evaporative Cooling

6.3.1.1 Liquid Desiccant Systems Producing Cold and Dry Air

A typical liquid desiccant system contains a dehumidifier, a regenerator, pumps, fans, desiccant tanks, coolers, heaters and heat exchangers. The liquid desiccant system combined with evaporative cooling also contains an evaporative cooler.

Figure 6.27 shows the schematic diagram of a liquid desiccant air-conditioning system integrated with evaporative cooling [20]. Cooling and strong liquid desiccant is delivered to the top of the dehumidifier by pump and distributed evenly over

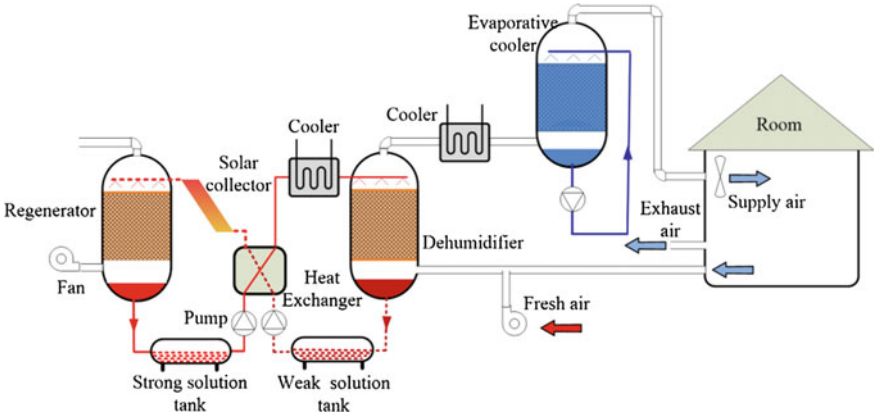

Fig. 6.27 Liquid desiccant system combined with evaporative cooling only producing cold and dry air

the packing to increase heat and mass transfer area. Humid air composed by fresh air and return air enters the dehumidifier from the bottom. The liquid desiccant flowing countercurrently relative to the humid air is brought into contact with the humid air. Then, moisture transfers from the air to the liquid desiccant because the vapor pressure at the solution surface is lower than that of the humid air. As a result, the liquid desiccant becomes warm and weak. The diluted solution flows into and is stored in the weak solution tank. In order to recover the ability of absorbing water vapor, the diluted solution must be concentrated. Hence, the diluted liquid desiccant from the weak solution tank is pumped into the solar collector to obtain high temperature and then enters the regenerator. Due to high temperature, the vapor pressure of the diluted liquid desiccant is much higher than that of the scavenging air. So in the regenerator, moisture transfers from the liquid desiccant to the scavenging air, accompanying the absorption of vaporization heat. Concentrated liquid desiccant from the bottom of the regenerator flows into and is stored in the strong solution tank. Since the concentrated liquid desiccant in the strong solution tank is still hot, its vapor pressure at the surface is relatively high. Under this case, a cooler is required to obtain the cooling and strong solution so that dehumidification cycle can be operated continuously. During dehumidification, the cooling liquid desiccant is expected while during regeneration, the hot solution is expected. So it is economical and beneficial to set a heat exchanger between strong solution and weak solution from tanks. The dry air from the dehumidifier is firstly precooled by a cooler and then enters the evaporative cooler, where water is distributed over the packing. Due to water evaporation, the dry air is humidified and cooled. The cool air is still dry compared with the indoor air and it is transported to the air-conditioning room to control the indoor temperature and humidity. The solar collector in this system can also be replaced by other heat sources. Liquid desiccant systems producing dry air and chilled water.

Figure 6.28 presents another liquid desiccant air-conditioning system integrated with evaporative cooling. The dehumidification cycle of the system is the same with the previous system. It must be noted that in this system, one part of dry air from the dehumidifier is supplied into room to control humidity and the other part of dry air enters evaporative cooler [20]. Due to the water vaporization in the evaporative cooler, water and air are cooled simultaneously. The cold air from the evaporative cooler flows out of the evaporative cooler and further precools the dry air after cooler. In addition, the cold water from the evaporative cooler is used to control the indoor temperature by being transported to the terminal equipment like coils and radiant panels. Hence, independent control of temperature and humidity is realized by dry air from the dehumidifier and cold water from the evaporative cooler, respectively.

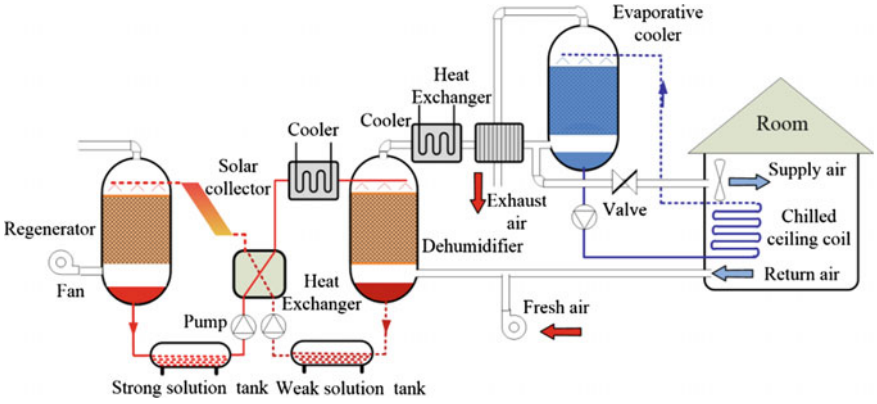

Fig. 6.28 Liquid desiccant system combined with evaporative cooling producing cold water and dry air

6.3.2 *Liquid Desiccant Systems Combined with Heat Pumps*

Figure 6.29 shows a liquid desiccant system combined with a heat pump [5]. In this system, the evaporator is used to cool the strong liquid desiccant during dehumidification and two condensers are used to heat the weak liquid desiccant and scavenging air, respectively, during regeneration. To reduce the cooling load for evaporator as well as heating load for condenser, an interstage cycle is added between the dehumidifier and the regenerator.

Under summer conditions, diluted solution from the weak solution tank is divided into two parts. One part of the diluted solution goes through the first condenser after mixing with a part of the concentrated solution from the strong solution tank. Then, the mixed solution heated by the first condenser enters the regenerator and contacts with the scavenging air heated by the second condenser.

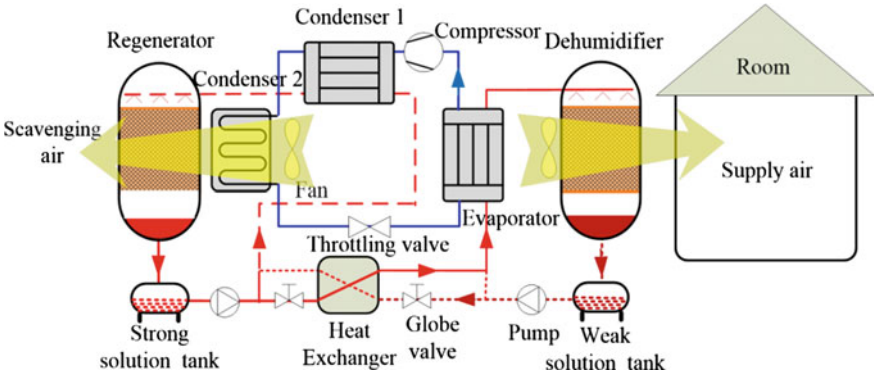

Fig. 6.29 Liquid desiccant system combined with heat pumps having two condensers

After regenerator, the mixed solution is concentrated and flows into the strong solution tank. The other part of the diluted solution from the weak solution tank is mixed with a part of concentrated solution and cooled by the evaporator afterward. The cooled liquid desiccant enters the dehumidifier to produce the cold and dry air, which is supplied to the air-conditioning room to control the indoor temperature and humidity.

References

1. Ali A, Vafai K (2004) An investigation of heat and mass transfer between air and desiccant film in an inclined parallel and counter flow channels. Int J Heat Mass Transf 47:1745–1760
2. Liu XH, Qu KY, Jiang Y (2006) Empirical correlations to predict the performance of the dehumidifier using liquid desiccant in heat and mass transfer. Renew Energy 31:1627–1639
3. Liu XH (2007) Combined heat and mass transfer characteristic in air handling process using liquid desiccant. PhD Thesis, Tsinghua university
4. Yin Y, Zhang X (2008) A new method for determining coupled heat and mass transfer coefficients between air and liquid desiccant. Int J Heat Mass Transf 51:3287–3297
5. Chen Y, Zhang X, Yin Y (2016) Experimental and theoretical analysis of liquid desiccant dehumidification process based on an advanced hybrid air-conditioning system. Appl Therm Eng 98:387–399
6. Zhang L, Hihara E, Matsuoka F, Dang C (2010) Experimental analysis of mass transfer in adiabatic structured packing dehumidifier/regenerator with liquid desiccant. Int J Heat Mass Transf 53:2856–2863
7. Bassuoni MM (2011) An experimental study of structured packing dehumidifier/regenerator operating with liquid desiccant. Energy 36:2628–2638
8. Chen XY, Li Z, Jiang Y, Qu KY (2006) Analytical solution of adiabatic heat and mass transfer process in packed-type liquid desiccant equipment and its application. Sol Energy 80:1509–1516
9. Ren CQ, Tu M, Wang HH (2007) An analytical model for heat and mass transfer processes in internally cooled or heated liquid desiccant-air contact units. Int J Heat Mass Transf 50:3545–3555
10. Liu XH, Chang XM, Xia JJ, Jiang Y (2009) Performance analysis on the internally cooled dehumidifier using liquid desiccant. Build Environ 44:299–308
11. Yin Y, Zhang X (2010) Comparative study on internally heated and adiabatic regenerators in liquid desiccant air conditioning system. Build Environ 45:1799–1807
12. Liu J, Zhang T, Liu X, Jiang J (2015) Experimental analysis of an internally-cooled/heated liquid desiccant dehumidifier/regenerator made of thermally conductive plastic. Energy Build 99:75–86
13. Chung T, Ghosh T, Hines A (1996) Comparison between random and structured packings for dehumidification of air by lithium chloride solutions in a packed column and their heat and mass transfer. Ind Eng Chem Res 35:192–198
14. Al-Farayedhi AA, Gandhidasan P, Al-Mutairi MA (2002) Evaluation of heat and mass transfer coefficients in a gauze-type structured packing air dehumidifier operating with liquid desiccant. Int J Refrig 25:330–339
15. Saman WY, Alizadeh S (2002) An experimental study of a cross-flow type plate heat exchanger for dehumidification/cooling. Sol Energy 73:59–71
16. Yin Y, Zhang X, Wang G, Luo L (2008) Experimental study on a new internally cooled/heated dehumidifier/regenerator of liquid desiccant systems. Int J Refrig 31:857–866

17. Yin Y, Zhang X, Peng D, Li X (2009) Model validation and case study on internally cooled/heated dehumidifier/regenerator of liquid desiccant systems. Int J Therm Sci 48: 1664–1671
18. Yin Y, Qian J, Zhang X (2014) Recent advancements in liquid desiccant dehumidification technology. Renew Sustain Energy Rev 31:38–52
19. Mohammad AT, Bin Mat S, Sulaiman MY et al (2013) Survey of hybrid liquid desiccant air conditioning systems. Renew Sustain Energy Rev 20:186–200
20. Yin YG (2009) Study on the coupled characteristic of heat and mass transfer between air and desiccant in liquid desiccant dehumidification and regeneration. PhD Thesis, Southeast University

Chapter 7
Numerical and Experimental Investigation on Solid Desiccant-Assisted Mobile Air-Conditioning System

Hoseong Lee and Yunho Hwang

Abstract In the conventional mobile air-conditioning system, evaporating temperature should be lower than the dew point temperature of cabin to control the temperature and humidity. Thus, reheating of the air is necessary. These two factors could increase the fuel consumption of the system. To overcome these issues, a solid desiccant-assisted mobile air-conditioning system is proposed and investigated. It is proposed to apply the solid desiccant to the mobile air-conditioning system to handle most of latent load, while the vapor compression cycle (VCC) handles the remaining latent load and sensible load. The model of the proposed concept is developed and validated with experimental data. Then, the possible configurations of the solid desiccant-assisted mobile air-conditioning system are discussed. Lastly, the proposed system is experimentally investigated with various operating conditions.

Keywords Solid desiccant · Desiccant wheel · SSLC · MAC

Nomenclature

Symbols

Eff	Efficiency
h	Enthalpy
P	Pressure

H. Lee
Department of Mechanical Engineering, Korea University, Seoul, Republic of Korea

Y. Hwang (✉)
Center for Environmental Energy Engineering, University of Maryland, 3157 Glenn L. Martin Hall Bldg., College Park, MD 20742, USA
e-mail: yhhwang@umd.edu

N. Enteria et al. (eds.), *Desiccant Heating, Ventilating, and Air-Conditioning Systems*, DOI 10.1007/978-981-10-3047-5_7

Q Heat transfer capacity
T Temperature
W Work input
X Quality
ρ Density

Acronyms

AC Alternating current
COP Coefficient of performance
DC Direct current
DP Pressure drop
DW Desiccant wheel
EES Engineering Equation Solver
FPI Fins per inch
MAC Mobile air-conditioning
MFR Mass flow rate
MRC Moisture removal capacity
PR Pressure ratio
RH Relative humidity
RPM Revolutions per minute
SD Solid desiccant
SSLC Separate sensible and latent cooling
TXV Thermal expansion valve
VCC Vapor compression cycle
VFR Volumetric flow rate

Subscript

amb Ambient
comp Compressor
cond Condenser
DW Desiccant wheel
evap Evaporator
exp Experiment
in Inlet
isen Isentropic
out Outlet
reg Regeneration-side
sim Simulation
vol Volumetric

7.1 Introduction

7.1.1 Background

Improving the energy efficiency of a mobile air-conditioning (MAC) system has been a leading topic in a mobile industry due to fuel saving and climate change. As compared to the residential air-conditioning system, the MAC system has several distinctive features. First, the space and weight are extremely limited, which is directly associated with fuel efficiency. Second, the thermal load of the cabin changes dramatically. This means the MAC must be designed to be capable of operating under a wide range of conditions. Third, not only temperature control but also humidity control is very important because temperature and humidity controls are related to the thermal comfort as well as safety [1].

In the conventional MAC system, the temperature and humidity control is achieved by a vapor compression system that typically consists of a compressor, condenser, drier, evaporator, and expansion valve. The system also has two fans driving the air through the condenser and evaporator. The cooling capacity is obtained from the evaporator, and the heating capacity is obtained by using a heater core heat exchanger. This heat exchanger uses the high-temperature coolant coming from the engine as a heat source to increase the temperature of the air.

The MAC system cools down the air lower than the dew point temperate of the cabin to control the humidity. Thus, reheating of the air is necessary. The performance of the system can be decreased due to the reheating process. The separate sensible and latent cooling (SSLC) system can be a possible solution for this. The SSLC system can be either a hybrid system including liquid or solid desiccant or a modified system with two independent heat exchangers dealing with the sensible and latent load separately [2].

The desiccant-assisted technology can separate the latent heat load from the sensible heat load, which will effectively increase the evaporating temperature and reduce the power consumption of the compressor. Moreover, with the desiccant material, the system can overcome overcooling or reheating which will offset the energy required to regenerate the desiccant, leading to a significant energy saving [3]. The desiccant material is categorized into two kinds: liquid desiccant and solid desiccant. In this study, the solid desiccant material is integrated into the MAC system to see the dehumidification capability enhancement.

The common material of the solid desiccant includes activated carbon, activated alumina, molecular sieve, silica gel, lithium chloride, and calcium chloride. The ideal material for the desiccant shall have a relatively low regeneration temperature as well as a high capability to sorb the water from the humid air. Researchers are still developing novel materials to increase the performance of the solid desiccant. Jia et al. [4] investigated the solid desiccant fabricated with novel composite. They found that the novel material made up by impregnating lithium chloride into open

silica gel pores can remove about 20–40% more water when compared with conventional silica gel solid desiccant. As to the polymer desiccant, White et al. [5] found that a superabsorbent polymer desiccant which was regenerated at 50 °C and working under a high relative humidity (>60%) could achieve a greater dehumidification than the conventional silica gel desiccant wheel (DW). Similarly, Lee and Lee [6] investigated the performance of a polymer desiccant which was named super desiccant polymer and concluded that the material displayed an outstanding durability with a sorption capacity 2–3 times higher than silica gel.

A so-called solid desiccant-assisted air-conditioning system can be either a desiccant air-conditioning system or a hybrid system with desiccant and traditional air-conditioning system. In the hybrid system with desiccant material and vapor compression cycle (VCC), one of the benefits will the downsizing of the VCC system since it handles with the sensible heat only [7]. From the literature review, it was found out that there were extremely limited research on the SSLC including the solid desiccant-assisted MAC system. Therefore, in this paper, the solid desiccant-assisted MAC system design is proposed and its performance is investigated. The all-possible options for solid desiccant-assisted MAC system are discussed.

7.1.2 Solid Desiccant-Assisted MAC System Configuration

Figure 7.1 shows the schematic diagram of the conventional MAC system. As to the refrigerant-side, the VCC consisted of two mini-channel heat exchangers acting as a condenser and evaporator. A thermal expansion valve (TXV) is installed after the condenser, which regulates opening depending upon the degree of superheat. As to the air-side, the condenser and evaporator are located in two separate wind ducts. The fan frequency of the condenser wind duct is controlled by an alternating current (AC) inverter. Air in the evaporator-side is driven by a direct current (DC) blower from the MAC system. A heater core heat exchanger is installed after the evaporator that reheats the air to the target temperature.

Figure 7.2 shows the systematic diagram of the proposed solid desiccant-assisted MAC system. The solid desiccant is designed as a cylindrical shape with honeycomb-shaped cells slowly rotated as it continuously dehumidified the incoming process airflow, which is called a desiccant wheel (DW). The solid desiccant is installed in both process air-side and regeneration air-side. In the process air-side, humid and hot air is cooled down at the evaporator, and then, humid and cold air leaving from the evaporator is dehumidified at the solid desiccant. The moisture in the process air-side is absorbed to the desiccant material, so that dry air can be provided to the space. In the regeneration air-side, the absorbed moisture in the desiccant material is desorbed with hot and dry air, which is heated at the heater core heat exchanger.

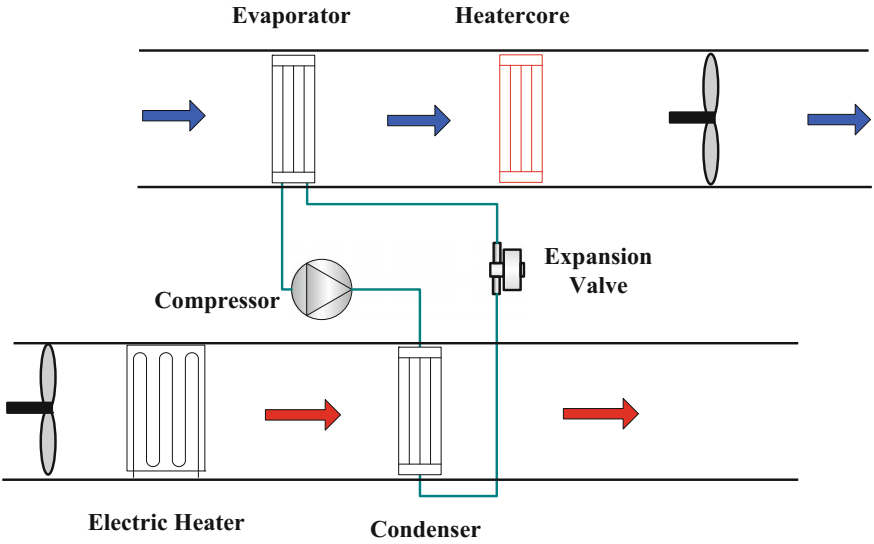

Fig. 7.1 Schematic diagram of baseline MAC

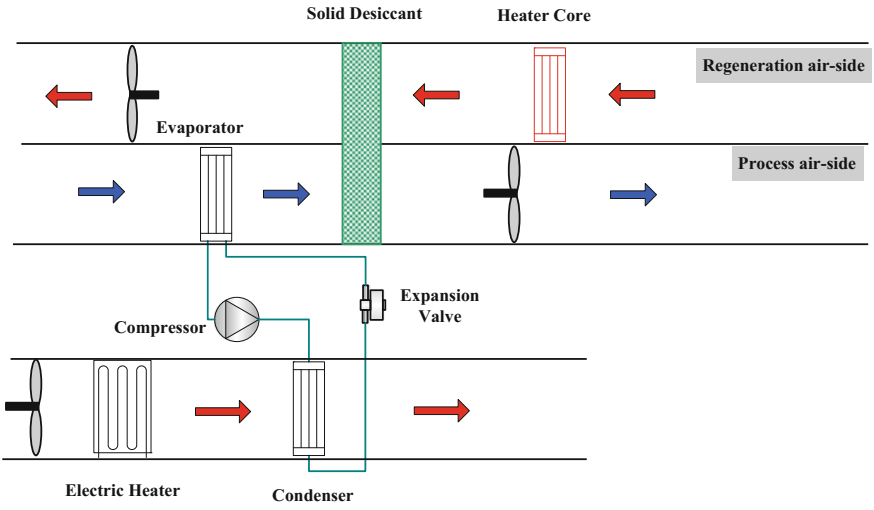

Fig. 7.2 Schematic diagram of solid desiccant-assisted MAC

7.2 Modeling Approach

The models of the baseline MAC system (as shown in Fig. 7.1) and the solid desiccant-assisted MAC system (as shown in Fig. 7.2) are developed using Engineering Equation Solver (EES). The heat exchanger models are developed with CoilDesigner heat exchanger simulation software package and integrated in EES. Figure 7.3 shows a flowchart of the MAC model development. The detailed assumptions adopted for calculating the VCC are following. For each heat exchanger calculation, a database is created by a multiple-variable parametric study in the CoilDesigner. Specifically, for the database of evaporator, evaporating pressure, inlet quality, and mass flow rate were selected as variables, and for the database of condenser, condensing pressure (high-side pressure), inlet temperature, and mass flow rate were selected as variables. Each database had 1000 records. EES imported all the records and saved them as three-dimensional arrays. Linear interpolation method was applied to calculate the results from the database records.

7.2.1 Compressor Modeling

A reciprocating type compressor, which has 33 cc of the displacement volume, is tested, and isentropic efficiency and volumetric efficiency are calculated. Then, the isentropic efficiency and the volumetric efficiency are correlated with a revolution per minute (RPM) and a pressure ratio between suction pressure and discharge pressure. Figure 7.4 shows the performance map of the compressor.

7.2.2 Condenser Modeling

The condenser model is developed with CoilDesigner heat exchanger simulation software package. Table 7.1 shows the specification of the condenser. This heat exchanger is a microchannel heat exchanger. The number of ports is 18, and port height and width are 0.9 mm and 0.6 mm, respectively. Number of banks is one and tubes per bank are 53. The louver fin with 60° is applied. The heat transfer coefficient and pressure drop correlations applied are as follows:

- Air-side heat transfer coefficient: Chang and Wang [8]
- Refrigerant-side liquid-phase heat transfer coefficient: Dittus and Boelter [9]
- Refrigerant-side two-phase heat transfer coefficient: Dobson [10], correction factor: 0.8
- Refrigerant-side vapor-phase heat transfer coefficient: Dittus and Boelter [9]
- Air-side pressure drop: Chang and Wang [8]

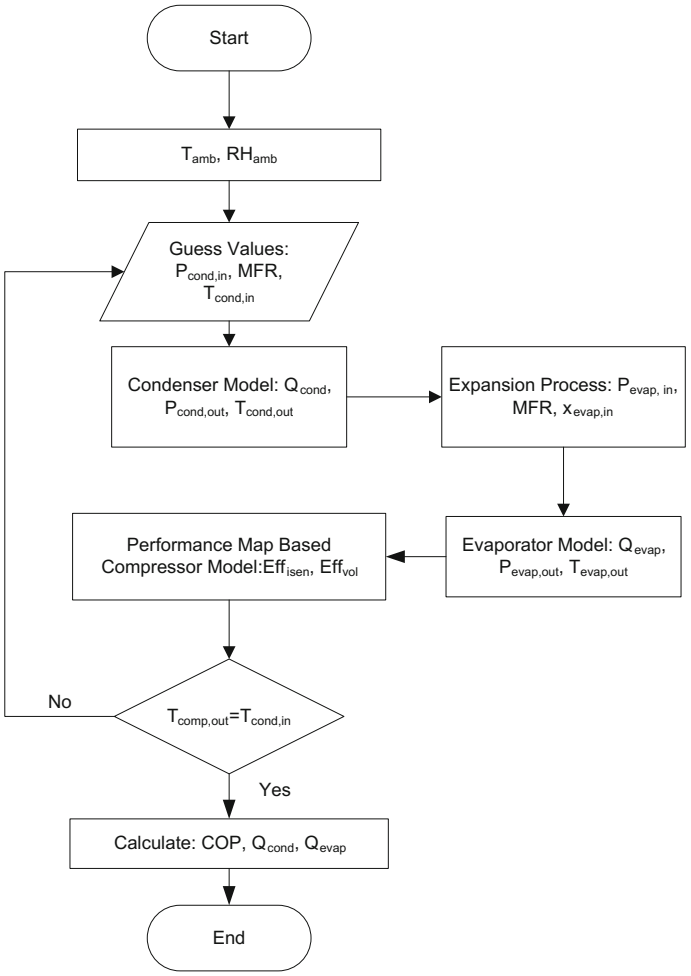

Fig. 7.3 Flowchart of MAC system

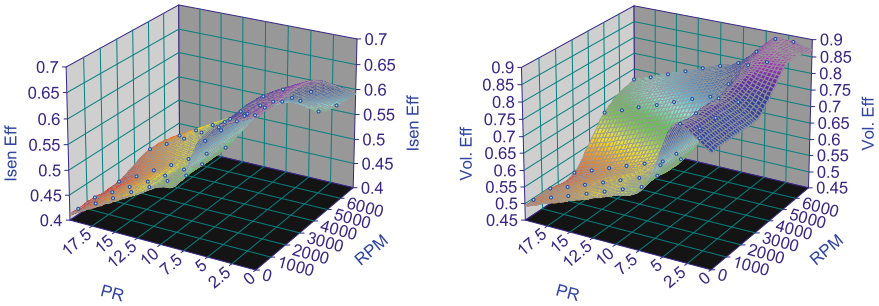

(a) Isentropic efficiency (b) Volumetric efficiency

Fig. 7.4 Performance map of compressor

Table 7.1 Specification of condenser

Geometry	Value	Unit
Number of banks	1	EA
Tubes per bank	53	EA
Tube length	0.677	m
Tube height	0.0014	m
Tube width	0.016	m
Tube vertical spacing	0.007	m
Bank horizontal spacing	0.016	m
Unfinned tube length	0	m
Port per tube	18	EA
Port height	0.0006	m
Port width	0.0009	m
Fin spacing	0.00103	m
Fin thickness	0.00008	m
Fins per inch	22.86	FPI
Louver pitch	0.002	m
Louver length	0.005	m
Louver angle	60	degree
Fin depth	0.016	m

- Refrigerant-side liquid pressure drop: Blasius equation [11]
- Refrigerant-side two-phase pressure drop: Friedel [12], correction factor: 1.4
- Refrigerant-side vapor-phase pressure drop: Blasius equation [11]

7.2.3 Evaporator Modeling

The evaporator model is developed with CoilDesigner. The evaporator is a microchannel heat exchanger. The specification of the evaporator is shown in Table 7.2. Number of banks is two and tubes per bank are 31. The louver fin with 60° is applied. The developed models are validated with in-house data and integrated with EES program. The heat transfer coefficient and pressure drop correlations applied are as follows:

- Air-side heat transfer coefficient: Chang and Wang [8]
- Refrigerant-side liquid-phase heat transfer coefficient: Dittus and Boelter [9]
- Refrigerant-side two-phase heat transfer coefficient: Jung et al. [13], correction factor: 1.3
- Refrigerant-side vapor-phase heat transfer coefficient: Dittus and Boelter [9]
- Air-side pressure drop: Chang and Wang [8]
- Refrigerant-side liquid pressure drop: Blasius equation [11]

Table 7.2 Specification of evaporator

Geometry	Value	Unit
Number of banks	2	EA
Tubes per bank	31	EA
Tube length	0.228	m
Tube height	0.00305	m
Tube width	0.0175	m
Tube vertical spacing	0.00865	m
Bank horizontal spacing	0.035	m
Unfinned tube length	0.004	m
Port per tube	10	EA
Port height	0.00105	m
Port width	0.001	m
Fin spacing	0.00133	m
Fin thickness	0.00008	m
Fins per inch	18.034	FPI
Louver pitch	0.002	m
Louver length	0.005	m
Louver angle	60	degree
Fin depth	0.035	m

- Refrigerant-side two-phase pressure drop: Jung et al. [13], correction factor: 0.95
- Refrigerant-side vapor-phase pressure drop: Blasius equation [11]

7.2.4 Data Reduction

The energy consumption of the whole system consisted of two parts: the compressor power consumption and the blower power. It should be noted that the condenser fan is used for both baseline and SD assisted MAC system, so that the power consumption of the condenser fan is not considered.

$$W_{\text{baseline}} = W_{\text{evap,blower}} + W_{\text{comp}} \tag{7.1}$$

Similarly, in the solid desiccant-assisted MAC system, the energy consumption of the whole system was calculated by taking the power consumptions of the compressor and blowers in both supply air and regeneration sides into consideration.

$$W_{\text{SD,MAC}} = W_{\text{evap,blower}} + W_{\text{reg,blower}} + W_{\text{comp}} + W_{\text{DW}} \tag{7.2}$$

7.3 Modeling Results

7.3.1 Validation of Model

The developed heat exchanger models are validated with in-house experimental data as shown in Tables 7.3 and 7.4. The heat transfer capacity and air-side pressure drop are compared. For the condenser, the mean absolute deviation of the heat transfer capacity is calculated as 1.6% and that of pressure drop is 10.6%. For the evaporator, the mean absolute deviation of the heat transfer capacity is about 2.9%, and that of pressure drop is 6.2%. Based on the validated heat exchanger models, a database was created by a multiple-variable parametric study in CoilDesigner.

The compressor model was validated with in-house data as shown in Table 7.5. The mean absolute deviation of the volumetric efficiency is 2.7%, and that of the isentropic efficiency is 5.9%, which are good enough to use in VCC models.

Table 7.3 Validation results of condenser

Test	Q_{Exp} (W)	Q_{Sim} (W)	Deviation (%)	DP_{Exp} (Pa)	DP_{Sim} (Pa)	Deviation (%)
1	4244	4310	1.6	24	24.7	3
2	6400	6401	0	39	36.5	−6.4
3	7948	8003	0.7	53	45.5	−14.2
4	3723	3791	1.8	18	20.8	15.7
5	5462	5538	1.4	29	30.1	3.7
6	6805	6887	1.2	37	35	−5.5
7	2864	2889	0.9	15	13.4	−10.7
8	4015	3992	−0.6	22	17.3	−21.4
9	5467	5124	−6.3	29	33.4	15

Table 7.4 Validation results of evaporator

Test	Q_{Exp} (W)	Q_{Sim} (W)	Deviation (%)	DP_{Exp} (Pa)	DP_{Sim} (Pa)	Deviation (%)
1	3461	3194	−7.7	15.7	16.1	2.5
2	4565	4447	−2.6	33.3	34.2	2.6
3	5194	5113	−1.6	49	49.2	0.5
4	2830	2728	−3.6	12.7	14.5	13.8
5	3857	3760	−2.5	27.5	29.6	7.7
6	4359	4294	−1.5	41.2	41.1	−0.4
7	1806	1905	5.5	7.9	9.1	15.7
8	2577	2576	0	18.6	17.8	−4.5
9	3328	3391	1.9	29.4	31.9	8.5

Table 7.5 Validation result of compressor

Experiment		Simulation		Deviation vol. eff. (%)	Deviation isen. eff. (%)
Vol. eff.	Isen. eff.	Vol. eff.	Isen. eff.		
0.812	0.646	0.768	0.620	5.5	4.0
0.695	0.608	0.710	0.582	−2.1	4.3
0.615	0.531	0.662	0.546	−7.6	−2.9
0.856	0.603	0.836	0.592	2.3	1.9
0.790	0.591	0.788	0.559	0.2	5.3
0.738	0.557	0.749	0.527	−1.4	5.4
0.879	0.537	0.858	0.519	2.4	3.5
0.834	0.554	0.823	0.492	1.3	11.2
0.782	0.541	0.794	0.464	−1.5	14.2
0.834	0.554	0.823	0.492	1.3	11.2

7.3.2 Simulation Results

7.3.2.1 Comparison Between Baseline and Solid Desiccant-Assisted MAC Systems

Table 7.6 shows the simulation results of the baseline MAC system and the solid desiccant-assisted MAC system. It should be noted that there is no reliable model of the solid desiccant in the open literature, so that an isenthalpic process is applied for the solid desiccant. Later, the efficiency of the solid desiccant is varied and its effect is investigated. For the simulation, air inlet temperature and airflow rate are maintained at constant, and supply air temperature and humidity ratios are fixed at 15 °C and 0.005414 $kg \cdot kg^{-1}$, respectively. The moisture removal for the baseline MAC system is conducted at the evaporator, while that for the solid desiccant-assisted MAC system is conducted at both the solid desiccant and the evaporator. For the solid desiccant-assisted MAC system, the total evaporator capacity is reduced because the solid desiccant handles the part of the latent cooling. In addition, evaporation temperature can be increased so that the total work of the compressor can be reduced significantly. However, the solid desiccant would increase the pressure drop in the air-side, and one more fan needs to be installed in the regeneration air-side. Therefore, the total fan power for the solid desiccant-assisted MAC system is increased. When the solid desiccant is applied to the MAC system, the fan power is increased from 0.22 to 0.61 kW, and the compressor power is reduced from 2.03 to 1.27 kW. Therefore, the total system power consumption is reduced by 26.3%.

Figure 7.5 shows the air cooling and dehumidification process in the baseline MAC system (as shown as dotted blue line) and solid desiccant-assisted MAC system (as shown real red line). For the baseline MAC system, hot and humid air is cooled and dehumidified at the evaporator (1–2), and then the air is heated up at the

Table 7.6 Simulation results

Property		Unit	Baseline	SD-MAC
Air-side	T_{amb}	°C	25	25
	$T_{air,sup}$	°C	15	15
	VRF	$m^3\ s^{-1}$	0.1447	0.1447
Refrigerant-side	$P_{evaporation}$	kPa	320	395
	$P_{condensation}$	kPa	1200	1200
MRC_{DW}		$kg\ s^{-1}$	–	0.340
$MRC_{condensate}$		$kg\ s^{-1}$	0.592	0.252
MRC_{total}		$kg\ s^{-1}$	0.592	0.592
Q_{evap}		kW	3.30	3.16
Q_{latent}		kW	1.40	0.84
$Q_{cooling}$		kW	4.69	4.00
$W_{compressor}$		kW	2.03	1.27
W_{fan}		kW	0.22	0.61
W_{total}		kW	2.25	1.88

heater core heat exchanger to achieve the target temperature (2–3). For the solid desiccant-assisted MAC system, hot and humid air is cooled and dehumidified at the evaporator (1–2′), and then dehumidified again in the solid desiccant (2′–3). This follows the enthalpy line so that the temperature is increased. As shown in Fig. 7.5.

Figure 7.5, the evaporator capacity can be reduced and evaporation temperature can be decreased. This would reduce the compressor power.

7.3.2.2 Effect of Enthalpy Gain in Solid Desiccant

Several researches are conducted for predicting the performance of the solid desiccant. However, it is not easy to have a general correlation. In this section, the enthalpy gain through the solid desiccant is varied and its effect is investigated. Figure 7.6 shows the variation of the moisture removal capacity (MRC) with solid desiccant heat gain. As the heat gain is increased, the MRC from the solid desiccant is decreased and the MRC from the evaporator (condensate water) is increased. When heat gain is increased, air outlet temperature of the solid desiccant is increased. Therefore, air has to be cooled more in the evaporator (2′ point in Fig. 7.5). This will increase the capacity of the evaporator, so that the MRC from the evaporator is increased as shown in Fig. 7.7. To supply same air quality, the MRC from the solid desiccant reduces. The lesson learned from here is that heat gain from the solid desiccant needs to be minimized to save the energy since most of the savings are coming from the low evaporator capacity.

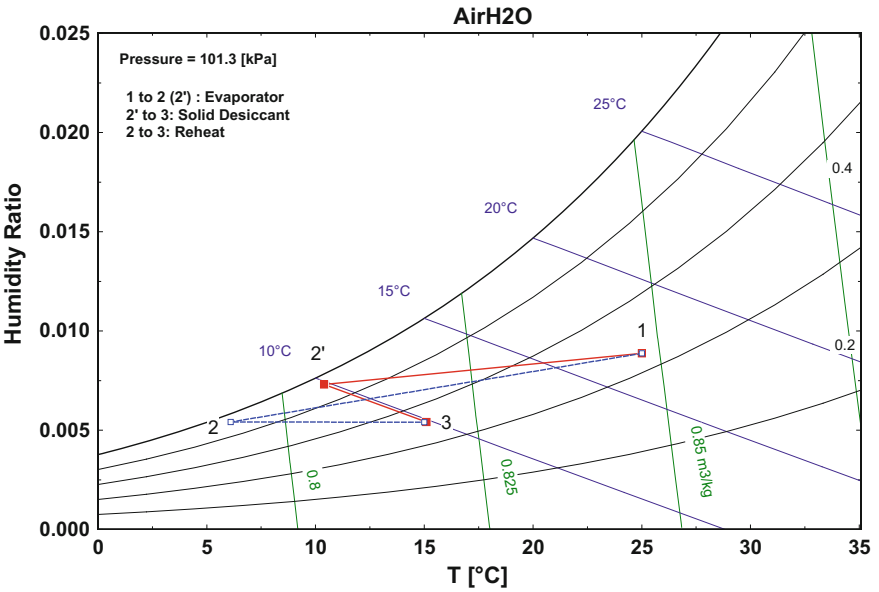

Fig. 7.5 Psychrometric chart of air cooling and dehumidification process

Fig. 7.6 Variation of MRC with SD heat gain

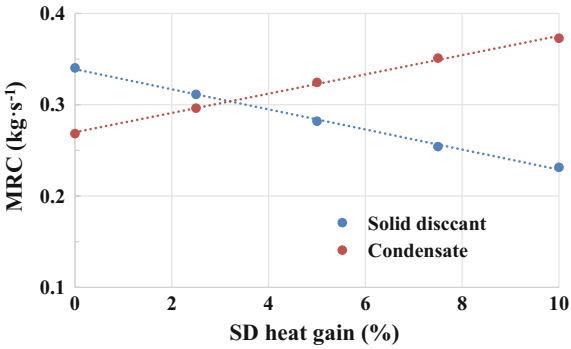

Fig. 7.7 Variation of capacity with SD heat gain (%)

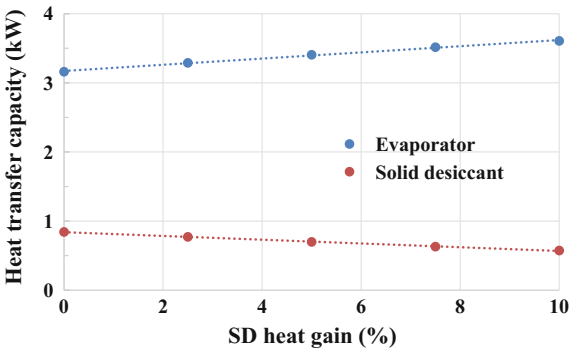

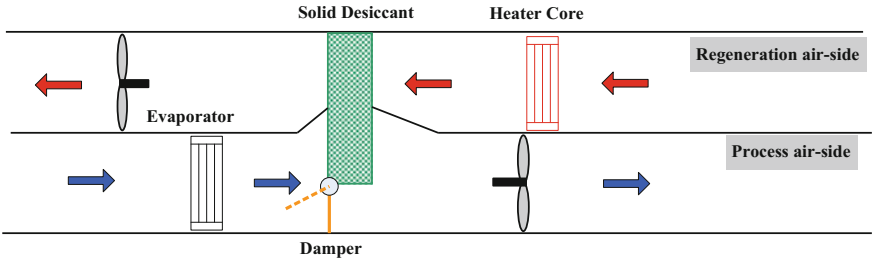

Fig. 7.8 Schematic of air split SD-MAC system

7.3.2.3 Effect of Air Fraction to Solid Desiccant

Figure 7.8 shows the schematic diagram of air split type solid desiccant-assisted MAC system. This concept is initially suggested to utilize the solid desiccant effectively. A damper installed next to the solid desiccant regulates the airflow rate so that the system can operate in either the baseline MAC system or the solid desiccant-assisted MAC system. Figure 7.9 shows the variation of air temperature and humidity ratios with the air fraction to the solid desiccant. As the air fraction to the solid desiccant is reduced, the supply air temperature is increased (point 3 in Fig. 7.5). When air is bypassing the solid desiccant, the solid desiccant should remove more moisture to control the supply humidity. This results in the increase of the air temperature. As air fraction to the solid desiccant is reduced, the capacity of the evaporator needs to be increased to control the supply temperature and the size of the solid desiccant should be increased. Therefore, bypassing the air is not good option.

7.3.2.4 Effect of Solid Desiccant Location

In this section, the effect of solid desiccant location is investigated. As shown in Fig. 7.2, the solid desiccant is located after evaporator. This is designed to

Fig. 7.9 Variation of air temperature and humidity ratios with air fraction to SD

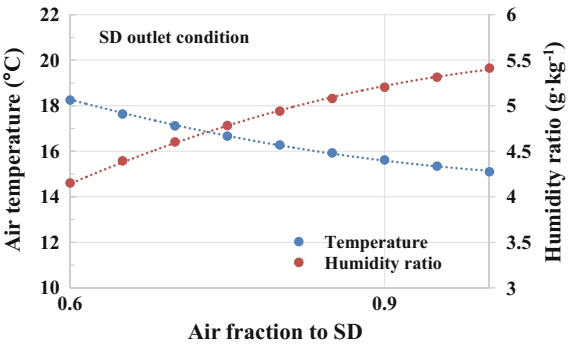

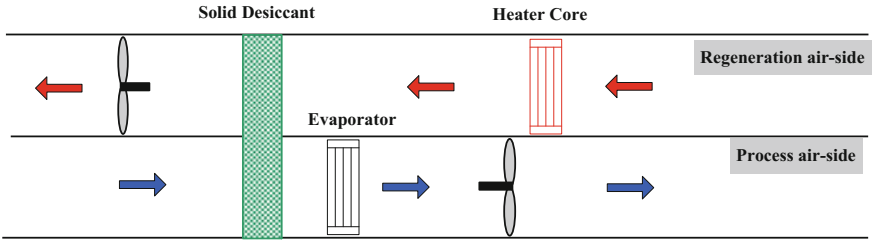

Fig. 7.10 Schematic diagram of solid desiccant–evaporator configuration

maximize the performance of the solid desiccant. High relative humidity exiting from the evaporator and entering to the solid desiccant makes it easier to capture the moisture in the solid desiccant. In another way, the solid desiccant can be located before the evaporator as shown in Fig. 7.10. Hot and humid air is dehumidified at the solid desiccant first. The air exiting from the solid desiccant is cooled down at the evaporator to the target temperature. In this configuration, the solid desiccant only handles the latent cooling and the evaporator handles the sensible cooling. By doing that, there is no condensate water coming out from the evaporator. These two configurations are modeled, and their performance is compared. Evap-SD indicates the model, in which the solid desiccant is located after the evaporator, and SD-Evap indicates the model, in which the solid desiccant is located before the evaporator.

Table 7.7 shows the comparison between Evap-SD and SD-Evap configurations. Evaporation pressure is increased from 395 to 446 kPa so that the pressure ratio between the evaporation-side and the condensation-side is reduced, which results in compressor work reduction. A solid desiccant capacity is increased by 72%, which is shown as latent cooling capacity. As shown in Fig. 7.11, the process conducted

Table 7.7 Simulation results

Property		Unit	Evap-SD	SD-Evap
Air-side	T_{amb}	°C	25	25
	$T_{air,sup}$	°C	15	15
	VFR	$m^3\ s^{-1}$	0.1447	0.1447
Refrigerant-side	$P_{evaporation}$	kPa	395	446
	$P_{condensation}$	kPa	1200	1200
MRC_{DW}		$kg\ s^{-1}$	0.340	0.592
$MRC_{condensate}$		$kg\ s^{-1}$	0.252	–
MRC_{total}		$kg\ s^{-1}$	0.592	0.592
Q_{evap}		kW	3.16	3.12
Q_{latent}		kW	0.84	1.45
$Q_{cooling}$		kW	4.00	4.57
$W_{compressor}$		kW	1.27	1.12
W_{fan}		kW	0.61	0.61
W_{total}		kW	1.88	1.73

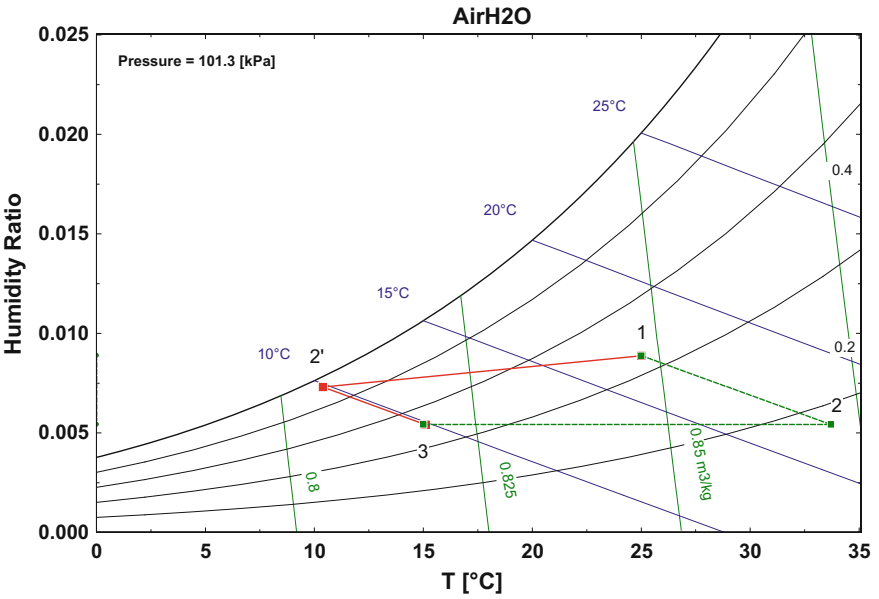

Fig. 7.11 Psychrometric chart of air cooling and dehumidification process

by the solid desiccant (1–2) is much larger compared to the process (2′–3). The compressor work is reduced by 12%. Overall, the energy consumption is reduced by 8%. It is found out that the SD-Evap configuration can reduce the energy consumption, but the solid desiccant size needs to be increased to handle large latent cooling capacity. The configuration can be decided based on the space limitation, system cost, and energy saving target.

7.4 Discussion on System Configurations

In this section, possible system configurations of the solid desiccant-assisted MAC are discussed. For the MAC application, a polymer desiccant can be applied which can be regenerated with low temperature. Depending on the location of the DW and components, five different DW-applied MAC systems are proposed as follows:

- SD-MAC option 1: The evaporator is located before the DW, and two fans are installed in process air-side and regeneration air-side. Airflow for the DW is the counterflow.
- SD-MAC option 2: The DW is located before the evaporator, and two fans are installed in process air-side and regeneration air-side. Airflow for the DW is the counterflow.

- SD-MAC option 3: The evaporator is located before the DW, and only one fan is installed in process air-side and regeneration air-side. Airflow for the DW is the counterflow.
- SD-MAC option 4: The DW is located before the evaporator, and only one fan is installed in process air-side and regeneration air-side. Airflow for the DW is the counterflow.
- SD-MAC option 5: The evaporator is located before the DW, and only one fan is installed in process air-side and regeneration air-side. Airflow for the DW is the parallel flow.

Figure 7.12 shows the schematic diagram of the SD-MAC option 1. Two fans are installed to operate the process air-side (evaporator-side airstream) and regeneration air-side (heater core-side airstream). The cooling capacity of the radiative evaporator is obtained from the VCC. The radiative evaporator is optionally applied. When cooling and dehumidification are required, the damper becomes "a" mode, which directs the air to go to the evaporator. With "a" mode, outside air (or returned air from the cabin) goes to the evaporator and DW (1–2–3–4 as shown in Fig. 7.12). Then, cold and dry air is provided to the cabin. When heating is required, the damper becomes "b" mode. Outside air goes to the heater core and then provided to the cabin (1–5–3–4 as shown in Fig. 7.12). In this case, the evaporator and DW do not work.

Figure 7.13 shows the schematic diagram of the SD-MAC option 2. Working principle is the same as SD-MAC option 1. The difference from the SD-MAC option 1 is the location of the DW. DW is installed before the evaporator. The advantage of SD-MAC option 1 is that hot and humid air is cooled down at the evaporator. Then, the air exiting from the evaporator is very humid, and in other

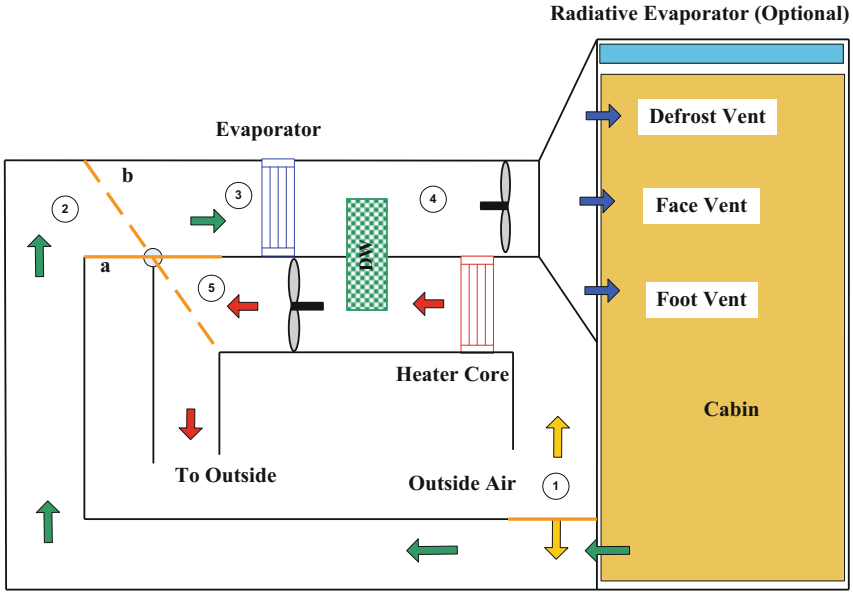

Fig. 7.12 Schematic diagram of SD-MAC option 1

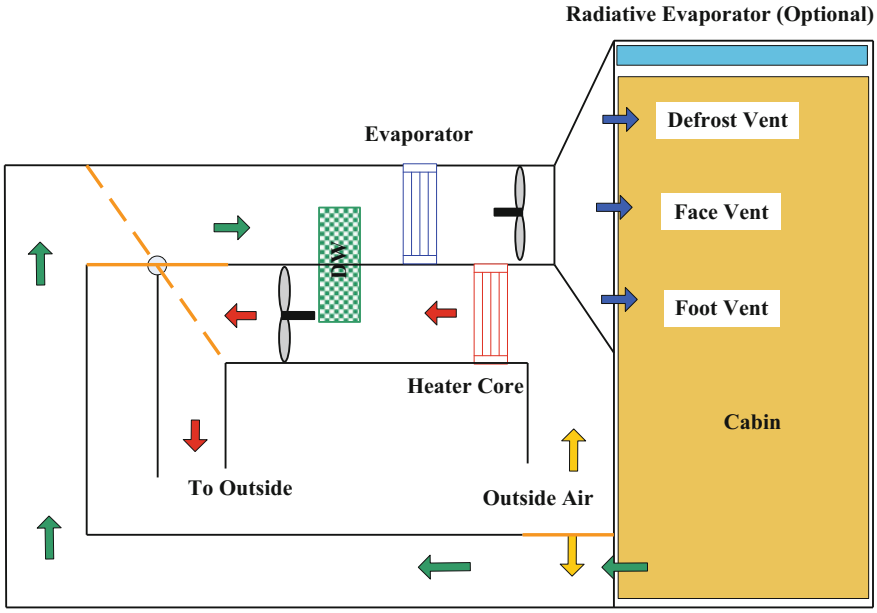

Fig. 7.13 Schematic diagram of SD-MAC option 2

words, the relative humidity is very high. Therefore, the DW performance can be maximized. This means DW size can be compact. However, the air temperature exiting from the DW is increased, since this is an isenthalpic process. In addition, there could be a latent heat transfer in the evaporator. For SD-MAC option 2, hot and humid air goes to the DW first, and then, hot and dry air is cooled down by the evaporator. Since the evaporator only takes care of sensible heat transfer, condensate water from the evaporator can be minimized. In the MAC system, condensate water in the evaporator causes odor problem. Therefore, this option 2 can significantly reduce odor problems caused by condensate water.

Figure 7.14 shows the schematic diagram of the SD-MAC option 3. This option is similar to the SD-MAC option 1, but uses only one fan. The fan is installed to take the outside air (or recirculated air). When cooling is required, the damper mode is "a" mode, and the fan pushes the air to both airstreams, evaporator-side and heater core-side. When heating is required, the damper acts as "b" mode. Then, air exiting from the fan only goes to the heater core. For the heating mode, the fan power can be reduced. As a same manner, the evaporator and DW do not work at the heating mode. Figure 7.15 shows the schematic diagram of SD-MAC option 4. The DW is located before the evaporator and the system are operated with one fan. The working principle is the same as SD-MAC option 3.

Figure 7.16 shows the schematic diagram of the SD-MAC option 5. This option utilizes only one fan. The airstream can be simpler than other options by applying parallel airflow. The performance of the typical DW can be maximized by designing counterairflow as shown in SD-MAC option 1–4. For SD-MAC option 5,

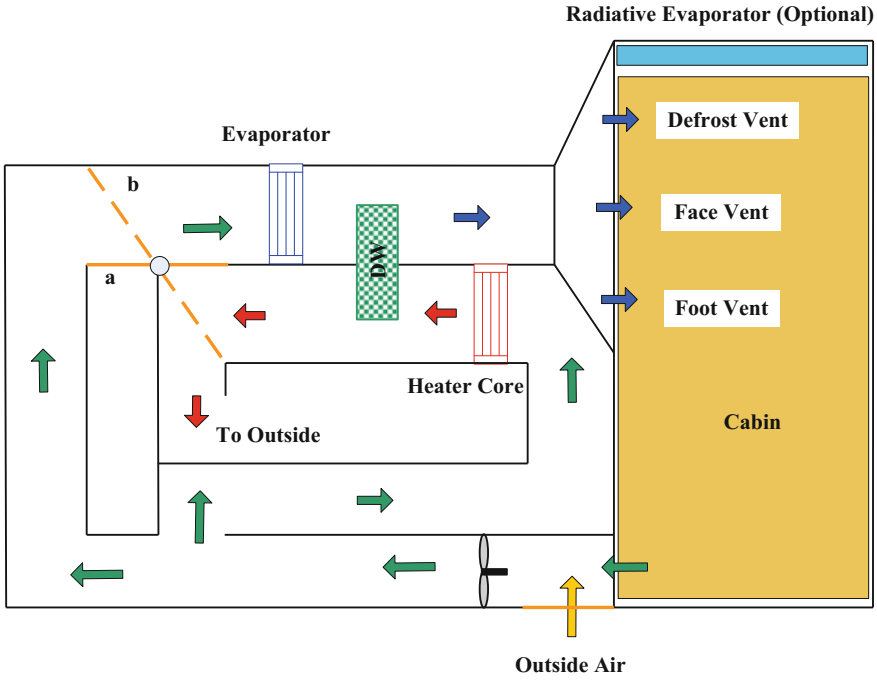

Fig. 7.14 Schematic diagram of SD-MAC option 3

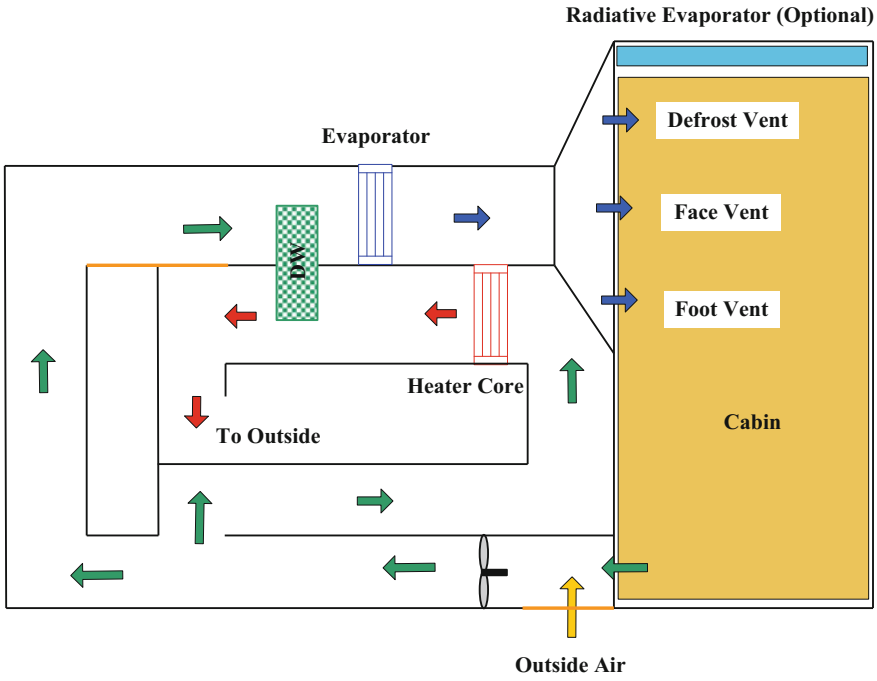

Fig. 7.15 Schematic diagram of SD-MAC option 4

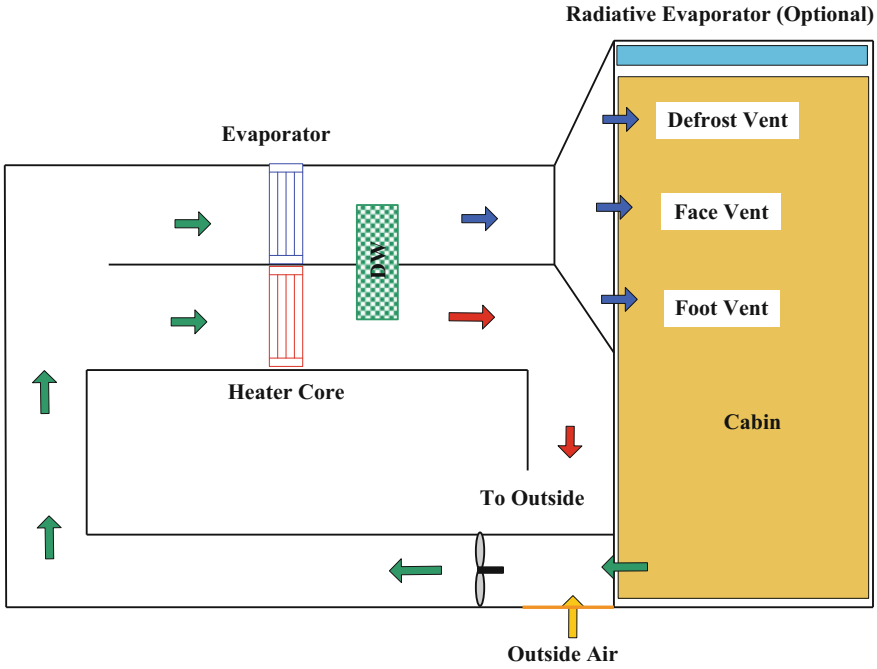

Fig. 7.16 Schematic diagram of SD-MAC option 5

the DW performance can be degraded, which means DW size would be designed larger than other options. However, this option does not require major modification of the current MAC system and easily applicable.

7.5 Experimental Evaluation

In this chapter, experimental evaluation of the solid desiccant-assisted MAC is discussed. The proposed system was built and evaluated with various operating conditions [14].

7.5.1 Test Setup

The testing system was placed in an environmental chamber with a cooling capacity of 35 kW. According to Rugh et al. [15], the representative temperature under which most MAC systems in the USA are working is 25 °C. The chamber temperature was set as 25 °C. Dhar and Singh [16] concluded that the energy saving in hot and humid condition could be achieved only under high latent load conditions.

In summer (especially rainy) times, the MAC would work under an extremely humid condition. A chamber humidifier controlled by a PID module could produce highly humid air near the inlet of the evaporator-side blower. In the baseline tests, the RH sensor of the humidifier was placed before the evaporator. In the SD-MAC system, the PID control module controlled the humidity based on the RH value of the supply air before the solid desiccant. Since it was difficult to maintain relative humidity higher than 90% in either baseline tests or SD-MAC tests, we assumed that the system was working under a rainy condition if the RH in the air ranged from 85 to 90% and kept steady for longer than half an hour.

During the baseline testing, the compressor started at 2000 RPM. The refrigerant charged in the system was R-134a, which is widely used in automotive industry. After the R134a mass flow rate reaches its steady state for longer than half an hour, the rotating speed of the compressor was adjusted to achieve a target air temperature leaving the evaporator to be around 7 °C within a range of 1.5 °C. The baseline tests were conducted under different flow rates, and the performance of the system was evaluated.

With a higher regeneration temperature, the moisture removal capacity of the DW would increase. Moreover, with a higher supply temperature, the evaporating pressure of the refrigerant would be increased, resulting in a reduced pressure ratio across the compressor, which would lead to a lower compressor power consumption when the speed of the compressor is fixed [17]. In the MAC system, the air leaving the condenser could be the heat source of the regeneration air. In this study, during the DW-MAC tests, the air in the regeneration side was heated up to 60 °C.

The rotating speed of the DW would influence the moisture removal capacity of the system. For polymer desiccant, which is regenerated under a lower temperature, the performance testing of a single DW with a thickness of 150 mm and a diameter of 300 mm showed that the best rotating speed is near 35 RPH [18]. In this study, since a DW of 70 mm thickness was used, the rotating speed was varied from 10 RPH to 60 RPH.

Meanwhile, in a DW-assisted MAC system, the supply air leaving the evaporator is supposed to enter the cabin without reheating. Thus, the compressor rotating speed was adjusted until the temperature leaving the evaporator reached 15 or 12 °C.

7.5.2 *Data Reduction*

In the baseline tests, the power consumption of the compressor was read from the CAN module. The air-side capacity was calculated according to the temperature and RH values before and after the evaporator.

$$Q_{\text{eva,air}} = \rho * \text{VFR} * \left(h_{\text{eva,air,in}} - h_{\text{eva,air,out}}\right) \tag{7.3}$$

The R134a-side evaporator capacity is calculated by Eq. 7.4.

$$Q_{\text{eva,R134a}} = \text{MFR} * \left(h_{\text{eva,R134a,out}} - h_{\text{eva,}R134\text{a,in}}\right) \tag{7.4}$$

The energy balance between the air-side and R-134a-side was calculated based on the air-side capacity. During the tests, the energy balance between two sides was kept within 5%.

$$\phi = \frac{Q_{\text{eva,R134a}} - Q_{\text{eva,air}}}{Q_{\text{eva,air}}} * 100\% \tag{7.5}$$

The energy consumption of the whole system consisted of two parts: the compressor power consumption and the blower power. Since the radiator cooling fan is also used for the condenser cooling in the MAC system, the power consumption of the condenser fan is not taken into account in either MAC system or DW-MAC system.

$$W_{\text{baseline}} = W_{\text{eva,blower}} + W_{\text{compressor}} \tag{7.6}$$

Similarly, in the DW-MAC system, the energy consumption of the whole system was calculated by taking the power consumptions of the compressor and blowers in both supply air and regeneration sides into consideration.

$$W_{\text{DW-MAC}} = W_{\text{sup,blower}} + W_{\text{compressor}} + W_{\text{reg,blower}} \tag{7.7}$$

In the DW-MAC system, it is difficult to measure directly the moisture removal capacity of the DW. Therefore, the following approach was used to calculate the moisture removal capacity (MRC) of the DW. As for the supply air, the temperature and humidity ratios at the inlet of the blower and the outlet of the evaporator can be measured. Meanwhile, the amount of condensate leaving the system was collected in every hour. Then, the moisture removed by the DW was calculated by subtracting the condensate from the total moisture removal capacity.

$$\begin{aligned}\text{MRC} = \text{VFR} \cdot \left\{ \rho_{\text{DW,in}} \cdot \left(\frac{\omega_{\text{DW,in}}}{\omega_{\text{DW,in}} + 1} \right) - \rho_{\text{EVA,out}} \cdot \left(\frac{\omega_{\text{EVA,out}}}{\omega_{\text{EVA,out}} + 1} \right) \right\} \\ - M_{\text{condensate}}\end{aligned} \tag{7.8}$$

The humidity ratio of the air was calculated based on the temperature and the RH values. In addition, the condensate leaving the system was collected in every 1 h.

Table 7.8 Baseline results under three airflow rates

Property	Unit	Values		
Airflow rate	$m^3\ h^{-1}$	186	192	236
Evaporator inlet air *T*	°C	24	25	24.1
Evaporator inlet air RH	%	88.7	89.5	89.1
Evaporator outlet air *T*	°C	6.8	6.5	6.2
Evaporator outlet air RH	%	87.8	82.4	92.4
Low-side pressure	kPa	306.5	291	260.7
High-side pressure	kPa	759.9	784.8	791
Condensate	$g\ min^{-1}$	35.8	35.3	44.8
Air-side evaporator capacity	kW	2.77	3.19	3.57
Compressor power	W	598	717	918
Total power	W	706	825	1026
COP	–	3.93	3.86	3.48

7.5.3 Experimental Results

7.5.3.1 Baseline Results

In the baseline tests, the performance of the system was measured under three different airflow rates. The results of the baseline tests are shown in Table 7.8. The total power includes the power of the blower and compressor. It can be found from the table that the evaporator outlet air RH, high-side pressure, condensate, air-side evaporator capacity, and total power increase along with the airflow rate. The low-side pressure and COP decrease with the airflow rate. The baseline result is used later for evaluating the possible energy saving in the DW-MAC tests.

7.5.3.2 Solid Desiccant-Assisted MAC Results

The SD-MAC system was tested under 200 $m^3\ h^{-1}$. The outlet temperature of the evaporator was controlled in 12 and 15 °C by adjusting the rotating speed of the compressor.

The compressor power consumption of the SD-MAC system was investigated under a flow rate of 200 $m^3\ h^{-1}$ as summarized in Table 7.9. The power consumption of the compressor was reduced up to 52% in both 12 and 15 °C cases as compared with the baseline. That is caused by the increased evaporating temperature, which reduces the pressure ratio across the compressor. The power saving of the DW-MAC system is shown in Fig. 7.17. It can be found that the whole system power consumption is reduced by 20% as compared with the baseline.

Table 7.9 Compressor power consumption

DW rotating speed (RPH)	Power at 12 °C (W)	Power at 15 °C (W)	Baseline (W)
10	570	401	717
20	570	401	
30	570	401	
40	570	344	

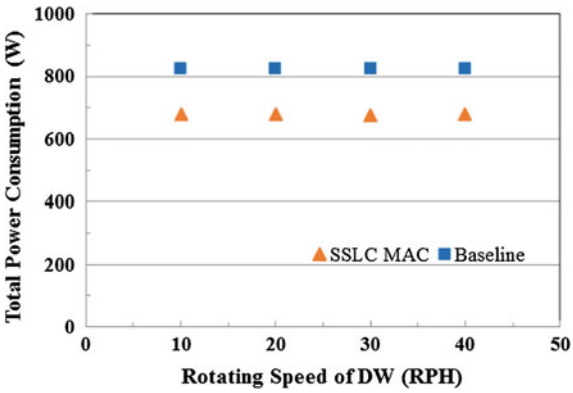

Fig. 7.17 Total power consumption comparison (when the outlet temperature is 15 °C in SD-MAC)

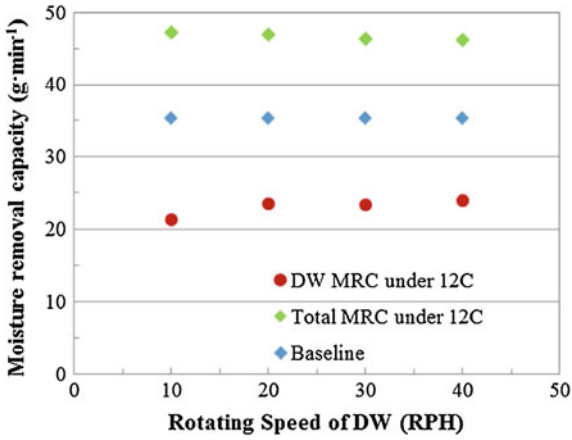

Fig. 7.18 MRC under 200 m^3 h^{-1} tests (air cooled down to 12 °C)

The improvement in the moisture removal capacity of the SD-MAC over the conventional MAC was also investigated. The moisture removal capacity of the SD-MAC system under 200 m^3/h and 12 °C evaporator outlet air temperature is shown in Fig. 7.18. When compared with the baseline results, the total moisture removal capacity increased from 35.30 to 46.7 g min^{-1} among which the DW provides 25 g min^{-1} of dehumidification capacity. In the 12 °C tests, the average condensate water leaving the system is 23.7 g min^{-1}, which is 67.2% of the

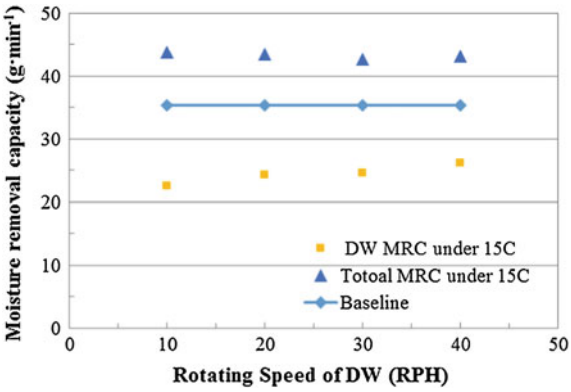

Fig. 7.19 MRC under 200 m^3 h^{-1} tests (air cooled down to 15 °C)

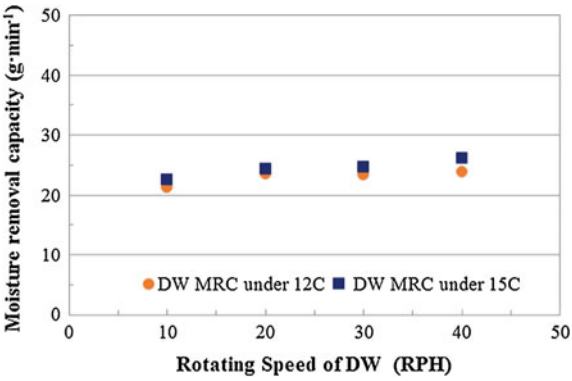

Fig. 7.20 Influence of rotating speed of DW

baseline system. Figure 7.19 shows the moisture removal capacity when the temperature is 15 °C. The water removed by the DW-assisted system is 43.27 g min^{-1} due to a slightly higher evaporator outlet temperature. The moisture removal capacity increases by 22.5%. In the 15 °C tests, the average condensate water leaving the system is 18.9 g min^{-1}, which is 53.4% of the baseline system.

The influence of the rotating speed upon the moisture removal capacity of the solid desiccant was investigated. Figure 7.20 shows the variation of the MRC with the increased rotating speed of the DW when the flow rate is at 200 m^3 h^{-1}. The MRC of the system increases from 21 to 24 g min^{-1}, while the rotating speed of the solid desiccant increases from 10 RPH to 20 RPH. After that, the MRC of the system keeps the same at 30 RPH and 40 RPH. To further investigate the influence of rotating speed over MRC, tests were conducted for a wider range of rotating speed. During all these tests, the air temperature leaving the system was kept at around 15 °C within ±0.5 °C error. The result is shown in Fig. 7.21. The MRC shows a slight decrease when the rotating speed is at 20 RPH. After that, the MRC keeps around 22.5 g min^{-1}, regardless of the rotating speed ranged from 20 RPH to 60 RPH. From the result that the solid desiccant is not sensitive to the rotating

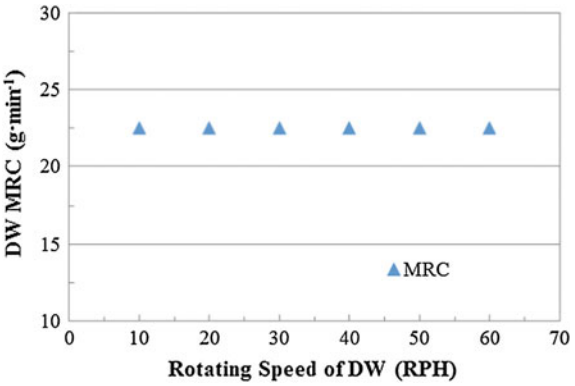

Fig. 7.21 Variation of MRC with the rotating speed of the DW

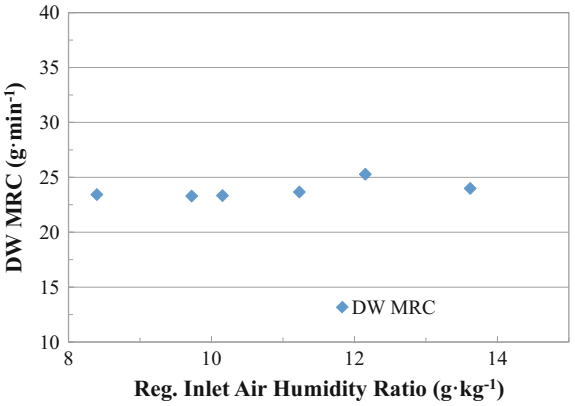

Fig. 7.22 Effect of the regeneration-side inlet humidity ratio on the DW's MRC

speed, the control of the wheel could be more flexible. After considering the factors discussed, the optimal rotational speed of the wheel was determined to be 20 RPH.

In the automotive system, the condenser is installed in front of the radiator. The air leaving the condenser is affected by weather, speed of the vehicle, heat load in the cabin, etc. In this study, the effect of the regeneration-side air inlet humidity ratio was investigated.

In the tests, the airflow rate was maintained at 200 $m^3\ h^{-1}$ and the tests were conducted under a range of humidity ratio from 8 to 14 g kg^{-1} (25 °C with a RH ranging from 40 to 70%). The regeneration temperature was controlled to be 60 °C by PID module. Since the DW dehumidification capacity is not sensitive to the rotating speed, in the tests the DW speed was kept at 20 RPH. Figure 7.22 shows the effect of regeneration temperature on the DW's MRC. It shows that as long as the regeneration temperature is the same, the polymer DW has almost the same dehumidification capacity, regardless of the regeneration inlet humidity ratios. The result that the performance of the polymer solid desiccant is relatively insensitive to

the regeneration-side air humidity ratio would ease the integration of solid desiccant into the MACs.

7.5.4 Discussion

One of the issues of DW operation is the air leakage between the regeneration side and the supply air-side. In order to minimize the cross-contamination through this leakage, the flexible gaskets were used in both sides of the DW. Moreover, the frame of the DW was sealed from both inside and outside. The regeneration energy required for an airflow rate of 200 m^3 h^{-1} is near 2.3 kW. Therefore, the heat from the radiator should be utilized to regenerate the desiccant material. Moreover, the DW needs to be installed either inside of the cabin or engine room. These two factors require the modification of the air duct design in the MAC system.

In this study, the cost of the DW prototype used was $540. The mass production cost of the DW is projected to be $270. The mass of the prototype DW, 2.5 kg, is added in the DW-MAC system. However, in the DW-MAC system, the smaller compressor can be used. Therefore, applying the DW concept to the car would increase its mass by about 2.0 kg. The payback period of the proposed DWMAC system can be estimated to be 5.3 years with following assumptions. (1) A vehicle annually consumes about 247 L of gasoline in the air-conditioning system. (2) The DW-MAC system can reduce 20% of gasoline consumption. (3) 57 L of fuel needed to carry over 100 kg of AC mass per 10,000, 16,300 km annual driving distance. [19] (4) Fuel cost is $1.06 per L. This payback period could be further shortened by mass production and cost down effort.

7.6 Conclusions

In this study, the solid desiccant-assisted MAC system was numerically and experimentally investigated. The desiccant-assisted technology can separate the latent heat load from the sensible heat load, which effectively increases the evaporating temperature and reduce the power consumption of the compressor. The VCC model was developed and validated with experimental data and this model was further investigated for solid desiccant-assisted MAC system. The remarkable conclusions are summarized as follows:

- When the solid desiccant is applied to the MAC system, the total power consumption is reduced by 26.3%.
- As heat gain is increased, the MRC from solid desiccant is decreased and the MRC from the evaporator (condensate water) is increased. When heat gain is increased, air outlet temperature of the solid desiccant is increased.

- As air fraction to the solid desiccant is reduced, the capacity of the evaporator needs to be increased to control the supply temperature and the size of the solid desiccant should be increased. Therefore, bypassing configuration is not good option.
- When SD-Evap configuration is applied, a solid desiccant capacity is increased by 72%, and the energy consumption is reduced by 8%.
- The SD-Evap configuration can reduce the energy consumption, but solid desiccant size needs to be increased to handle large latent cooling capacity. The configuration can be decided based on the space limitation, system cost, and energy saving target.
- Polymer desiccant wheel was integrated into the automotive air-conditioning system equipped with an independent electric compressor. Tests were conducted with both the baseline system and the SD-MAC system.
- The performances of the two systems were compared to evaluate both the power consumption savings and dehumidification capacity improvement of the SD-MAC system.
- The effects of rotating speed and regeneration-side inlet humidity ratio were investigated.
- SD-MAC can reduce the whole system power consumption by 20% when the air is cooled down to 15 °C, while the dehumidification capacity increases by 22.5%.
- As for the compressor, the power consumption is reduced by 46%. The condensate from the evaporator is reduced by 46.6%. The optimal rotating speed for the energy saving is found to be 20 RPH.

Acknowledgments This work was supported by the sponsors of the Center for Environmental Energy Engineering (CEEE), University of Maryland, College Park, MD, USA, and partially supported by a Korea University Grant.

References

1. Lee H, Lin X, Hwang Y, Radermacher R (2016) Performance investigation of solid desiccant assisted MAC system. Appl Therm Eng 103:1370–1380
2. Ling J, Hwang Y, Radermacher R (2010) Theoretical study on separate sensible and latent cooling air-conditioning system. Int J Refrig 33:510–520
3. Daou K, Wang RZ, Xia ZZ (2006) Desiccant cooling air conditioning: a review. Renew Sustain Energy Rev 10:55–77
4. Jia CX, Dai YJ, Wu JY, Wang RZ (2007) Use of compound desiccant to develop high performance desiccant cooling system. Int J Refrig 30:345–353
5. White SD, Goldsworthy M, Reece R, Spillmann T, Gorur A, Lee D-Y (2011) Characterization of desiccant wheels with alternative materials at low regeneration temperatures. Int J Refrig 34:1786–1791
6. Lee J, Lee D-Y (2012) Sorption characteristics of a novel polymeric desiccant. Int J Refrig 35:1940–1949

7. La D, Dai YJ, Li Y, Wang RZ, Ge TS (2010) Technical development of rotary desiccant dehumidification and air conditioning: a review. Renew Sustain Energy Rev 14:130–147
8. Chang Y-J, Wang C-C (1997) A generalized heat transfer correlation for Iouver fin geometry. Int J Heat Mass Transf 40:533–544
9. Dittus FW, Boelter LMK (1985) Heat transfer in automobile radiators of the tubular type. Int Commun Heat Mass Transf 12:3–22
10. Dobson MK, Chato JC (1998) Condensation in smooth horizontal tubes. J Heat Transf 120:193–213
11. Incropera FP, Dewitt DP (1996) Introduction to heat transfer, 3rd edn
12. Friedel L (1979) Improved friction pressure drop correlations for horizontal and vertical two-phase pipe flow. European two-phase flow group meeting, Paper E, vol 2, p 1979
13. Jung DS, McLinden M, Radermacher R, Didion D (1989) A study of flow boiling heat transfer with refrigerant mixtures. Int J Heat Mass Transf 32:1751–1764
14. Lin X, Lee H, Hwang Y, Radermacher R (2014) Experimental investigation on desiccant wheel assisted MAC system. SAE, Detroit
15. Rugh J, Hovland V, Andersen SO (2004) Significant fuel savings and emission reductions by improving vehicle air conditioning. Mobile Air Conditioning Summit
16. Dhar PL, Singh SK (2001) Studies on solid desiccant based hybrid air-conditioning systems. Appl Therm Eng 21(2):119–134. Doi:10.1016/S1359-4311(00)00035-1
17. Ling J, Kuwabara O, Hwang Y, Radermacher R (2011) Experimental evaluation and performance enhancement prediction of desiccant assisted separate sensible and latent cooling air-conditioning system. Int J Refrig 34(4):946–957
18. Lee H, Cao T, Hwang Y, Radermacher R (2013) Experimental investigation of a desiccant wheel cycle. In: Fourth conference on thermophysical properties and transfer processes of refrigerants. Delft
19. Fischer SK, Hughes PJ, Fairchild PD (1991) Energy and global warming impacts of CFC alternative technologies, report to the U.S. DOE

Chapter 8
Desiccant Air Handling Processors Driven by Heat Pump

Tao Zhang, Rang Tu and Xiaohua Liu

Abstract Desiccant air handling processors (DAHP) driven by heat pump have become more and more popular recently due to their compact size and high efficiency. Both the cooling capacity from an evaporator and heat from a condenser are utilized in these systems. How to understand these two kinds of air dehumidification systems comprehensively is an important issue for system design and device selection. In the present chapter, DAHP driven by heat pump (using liquid desiccant or desiccant wheel) will be investigated. Operating principles of DAHP using desiccants will be introduced firstly. System design principles will be proposed with emphasis on the heat and mass transfer characteristics in DAHP. Performances of DAHP will be analyzed and approaches for performance optimization will also be proposed. It is expected that the present study will be useful to cast light on the performances of DAHP using liquid desiccant and desiccant wheel and choose an efficient air dehumidification method in the air-conditioning system.

Keywords Air handling process · Liquid desiccant · Desiccant wheel · Heat pump · Energy performance

8.1 Introduction

Nowadays energy consumed in buildings is an important composition of the total energy consumption in society, as well as the energy consumed by industry or transportation. In China about 20% of the entire energy is consumed by buildings, which is still in rapid progress with the development of economy and society [1]. In commercial buildings, about 30–60% of the total energy is consumed by the

T. Zhang (✉) · X. Liu
Department of Building Science, Tsinghua University, Beijing 100084, China
e-mail: zt2015@tsinghua.edu.cn

R. Tu
School of Mechanical Engineering, University of Science and Technology Beijing, Beijing 100083, China

N. Enteria et al. (eds.), *Desiccant Heating, Ventilating, and Air-Conditioning Systems*, DOI 10.1007/978-981-10-3047-5_8

air-conditioning system [1]. Air dehumidification device is an important component of the air-conditioning system, which is more important in humid regions. It is of great importance to improve the energy performance of air dehumidification devices in reducing building energy consumption. In contrast to the conventional condensing dehumidification method, air dehumidification processes using liquid desiccant (LD) and solid desiccant including desiccant wheel (DW) are becoming more and more popular. It is believed that the air dehumidification systems using desiccant are with superiority in not requiring reheat, utilization of waste heat and etc.

Characteristics of liquid desiccant and desiccant material are treated as the fundamental researches for supporting the development of air handling systems using desiccant [2–4]. Both theoretical models [5] and experimental results [6, 7] have been investigated intensively for the coupled heat and mass transfer processes between air and liquid desiccant or solid desiccant. The basic principle for the air handling processes using LD and DW is to realize humidification or dehumidification with the help of the water vapor pressure difference between air and desiccant. The common aqueous solutions mainly include lithium chloride (LiCl), lithium bromide (LiBr) and calcium chloride ($CaCl_2$) aqueous solutions, while the common solid desiccants include silica gel, zeolite and so on. The solution state could be expressed by the humid air in equilibrium with the desiccant (with the same temperature and vapor pressure). Figure 8.1a illustrates the LiBr aqueous solution in the air psychrometric chart, where X represents the solution concentration and φ denotes the relative humidity. It is indicated that the iso-concentration line of the liquid desiccant coincides with the air iso-relative humidity line. It can reach a larger area compared to water (which is located at the 100% saturated state of air). Similarly state of the solid desiccant could also be presented in an air psychrometric chart, shown in Fig. 8.1b, where W indicates the water content.

The coupled heat and mass transfer processes between air and liquid desiccant in a packed tower is illustrated in Fig. 8.2a, with the air handling process shown in the psychrometric chart in Fig. 8.2b. Variance of the solution concentration is usually

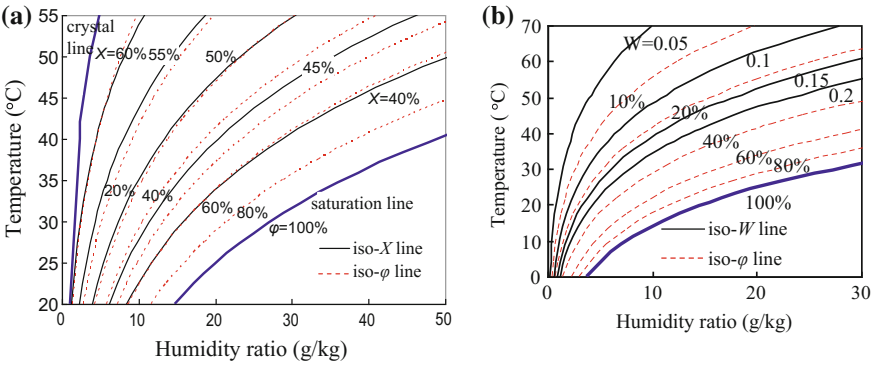

Fig. 8.1 Desiccant states shown in the air psychrometric chart: **a** LiBr solution; and **b** RD silica gel [8]

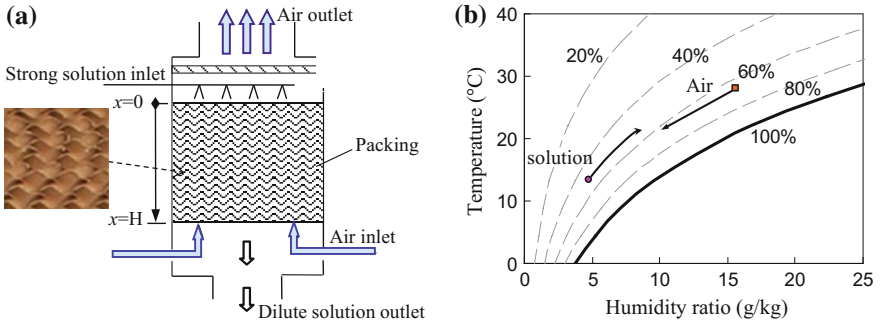

Fig. 8.2 Counter flow process between air and liquid desiccant: **a** operating principle; and **b** air handling process shown in the air psychrometric chart

lower than 1% for the coupled heat and mass transfer processes between air and solution [9]. The solution state could be regarded as almost varying along the iso-concentration line. There could be various inlet air states relative to the solution state, with handling results such as dehumidification or humidification.

Desiccant wheel system is the common method using solid desiccant for air dehumidification and Fig. 8.3a presents its operating principle. Driving force for the mass transfer process is precisely the vapor pressure (or humidity ratio) difference between air and solid desiccant. Porous material is utilized as the substrate with superiority in increasing the specific surface area. There is an obvious gap between the reachable number of transfer unit NTU (equaling to the transfer ability hA divided by the heat capacity $c_p m$) of LD system and DW system. The air side NTU of the DW process is significantly higher than that of the LD process at the same volume. The specific area of DW could be as high as 2000–4000 m^2/m^3. For example, the NTU for the air side is about 5–10 as the thickness of DW is about 10 cm with an air velocity of about 2 m/s. While the specific surface area the

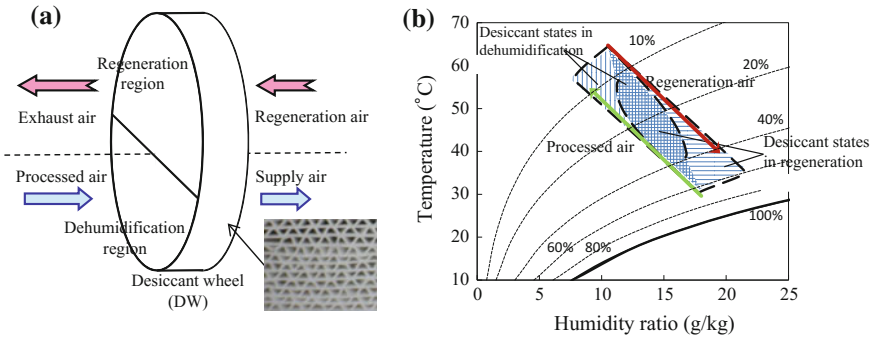

Fig. 8.3 Air handling process using desiccant wheel: **a** operating principle; and **b** air handling process shown in the air psychrometric chart

packing in the LD process is usually lower than 1000 m^2/m^3, the NTU for the air side is only about 1–3. There are dehumidification region and regeneration region along the circumference of the wheel. Moisture is transferred from the air to the desiccant in the dehumidification region with the release of adsorption heat, and from the desiccant to the regeneration air in the regeneration region. The air handling process in the DW process is illustrated in Fig. 8.3b, where the air state varies almost along the isenthalpic line. The air is usually heated to satisfy the heating requirement for desiccant regeneration.

On basis of the performance investigation between air and liquid desiccant or solid desiccant, novel systems and handling devices using LD or DW are also proposed and investigated. Desiccant air handling processors (DAHP) driven by heat pump have become more and more popular recently due to their compact size and high efficiency. Both the cooling capacity from an evaporator and heat from a condenser are utilized in these systems. Taking liquid desiccant as an example, the cooling capacity is used to cool the circulating desiccant to enhance its dehumidification ability and the heat is used to regenerate the desiccant.

Current researches provide sufficient basis to analyze the characteristics of air handling process using either LD or DW. How to understand these two kinds of air dehumidification systems comprehensively is an important issue for system design and device selection. There is seldom study focusing on the comparable performances of these systems, to the disadvantage of a fully understanding on DAHP driven by heat pump. The mathematical models for LD systems and DW systems have been built and validated in the previous studies [10, 11]. In the present chapter, DAHP driven by heat pump (using LD or DW) will be investigated. System design principles will be proposed with emphasis on the heat and mass transfer characteristics in DAHP. It is expected that the present study will be useful to cast light on the performances of DAHP using LD and DW and choose an efficient air dehumidification method in the air-conditioning system.

8.2 Air Handling Process Using Liquid Desiccant

8.2.1 Basic Handling Process and Theoretical Analysis

For air handling processor driven by heat pump using liquid desiccant, there are different ways to utilize the condensing heat for desiccant regeneration. All the condensing heat from the heat pump could put in the solution for regeneration. While all the condensing heat from the heat pump could be removed by the regeneration air rather than by the solution, and the heated air went into the regenerator for desiccant regeneration. The issues of how to evaluate the performances of different HPLD systems and how to pursue a process with better energy efficiency are at the center of current research efforts. There are various kinds of HPLD systems in which condensing heat is usually utilized for desiccant

regeneration, and the cooling capacity of the evaporator is adopted for dehumidification. However, to obtain better mass transfer performance, previous studies have recommended that the cooling capacity should be used to cool the inlet solution rather than the air in the dehumidification process [9]. Accordingly, in the processes analyzed in the present study, the evaporator of the heat pump is utilized to cool the solution for dehumidification.

Figure 8.4a, b shows the operating schematics of two basic HPLD processes. In these processes, an adiabatic dehumidifier/regenerator is adopted. A small part of the diluted solution after dehumidification is sent into the regenerator, and there is also a small amount of concentrated solution after regeneration returning back to the dehumidifier. As the variance of the desiccant concentration is usually lower than 1% [9], the mass flow rates of these two parts of solutions circulating between the dehumidifier and the regenerator are almost the same for these HPLD systems. The solution heat recovery device is used for the heat recovery between the diluted solution sent to the regenerator and the concentrated solution sent to the dehumidifier. The concentrated solution sent to the dehumidifier is then mixed with the rest of the diluted solution after dehumidification and sent to the top of the dehumidifier with the help of a solution pump.

In contrast to the typical adiabatic process where all the solution circulates between the dehumidifier and the regenerator, in the adiabatic dehumidifier/regenerator investigated in the present study, most of the solution circulates only between the packed tower and the evaporator or condenser. The major difference between Basic

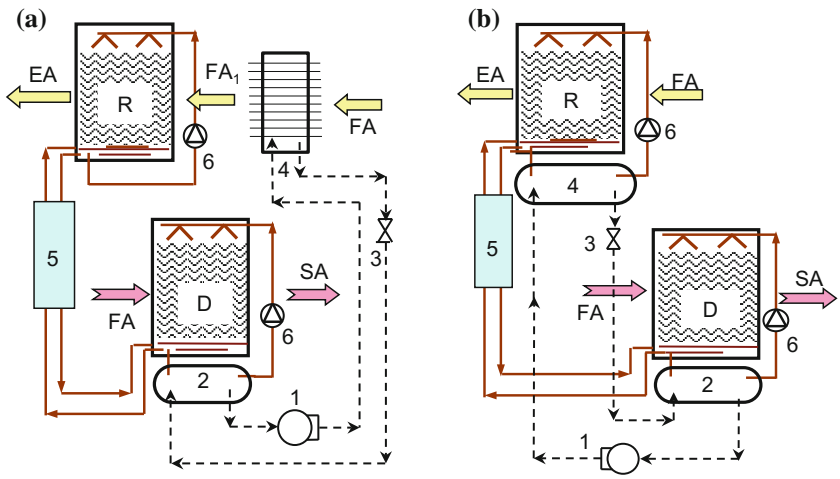

FA-fresh air; SA-supply air; FA_I-fresh air heated by the condenser; EA-exhaustair; D-dehumidifier; R-regenerator; 1-compressor; 2-evaporator; 3-expansion valve; 4-condenser; 5-heat exchanger; 6-pump.

Fig. 8.4 Operating schematic of the HPLD air handling processes with different regeneration modes: **a** Basic Type I (heat inlet air); and **b** Basic Type II (heat inlet solution)

Type I and Basic Type II systems is that the condenser is used for heating different fluids. In Basic Type I, the condenser is an air-cooled type, and the regeneration air is heated by the condensing heat before flowing through the regenerator. A solution-cooled condenser is adopted in Basic Type II, and the solution is heated by the condensing heat instead of the regeneration air.

COP_{hp} and COP_{sys} are chosen as indexes to evaluate the performances of various HPLD systems, calculated by Eqs. (8.1) and (8.2), respectively:

$$COP_{hp} = \frac{Q_{evap}}{P_{com}} \tag{8.1}$$

$$COP_{sys} = \frac{Q_a}{P_{com} + P_{pump}} \tag{8.2}$$

where Q_{evap} and Q_a represent the cooling capacities of evaporator and processed air, respectively; P_{com} and P_{pump} indicate the power consumptions of compressor and solution pumps involved in the handling process, respectively.

There are several key components in the HPLD systems, including the coupled heat and mass transfer components (the dehumidifier and regenerator), the heat pump system, the heat exchanger, etc. On basis of the theoretical models of these key components, a system model for the HPLD process can be established. In previous research [12], a model of this kind of HPLD system was built and the flow chart of the calculating method was also given; to validate the system models, the tested results and simulated results of a three-stage HPLD system were investigated, including the supply air temperature, humidity ratio, compressor power and COP_{hp}. It showed that the mean relative biases between the measured and simulated results of the HPLD device were all lower than 10% and the simulated results showed good agreement with the measured. Thus, the theoretical models of the various components were validated and the system models could be used to analyze the performance of different HPLD systems.

The system simulation method helps to calculate the performance parameters of HPLD systems. However, a simple solution for evaluating performance discrepancies is still lacking. To simplify the comparison of different HPLD systems, the current study investigates the match properties in the key components of the HPLD systems. The unmatched coefficient based on entransy dissipation is adopted, including the sensible heat transfer process and the coupled heat and mass transfer processes. Dissipations occur during the heat and mass transfer processes of the air-desiccant packed tower due to limited transfer capability, flow mismatching, and parameter mismatching, similar to the air-water process [13].

To depict the characteristics of driving forces between air and desiccant, exergy analysis method and unmatched coefficient are adopted as the theoretical indexes. It is indicated that the exergy is provided by the cooling source (ΔE_{wc}), heating source (ΔE_{wh}), and the regeneration air (ΔE_{ea}), and exergy consumption consists of two parts. Part of the exergy is used to increase the exergy of the processed air (ΔE_{sa}). The rest is destroyed during the heat or mass transfer processes in dehumidifier/regenerator

($\Delta E_{de,deh}/\Delta E_{de,reg}$) and heat exchangers ($\Delta E_{de,he}$). Thus, the exergy balance equation of the LD system I can be written as Eq. (8.3):

$$\Delta E_{wc} + \Delta E_{wh} + \Delta E_{ea} = \Delta E_{sa} + \Delta E_{de,deh} + \Delta E_{de,reg} + \Delta E_{de,HE} \tag{8.3}$$

where the subscript wc refers to cooling source (evaporator), wh denotes heating source (condenser), ea refers to regeneration air, sa denotes supply air, de refers to exergy destruction, deh denotes dehumidifier, reg represents regenerator, and HE refers to heat exchangers including solution–solution heat exchanger and air-water heat exchanger.

The exergy of humid air at standard atmospheric pressure is the sum of thermal exergy and humid exergy, expressed as Eq. (8.4) [14].

$$\begin{aligned} \mathrm{ex}_a = {} & (c_{p,a} + \omega c_{p,v}) T_0 \left(\frac{T}{T_0} - 1 - \ln \frac{T}{T_0} \right) \\ & + R_a T_0 \left((1 + 1.608\omega) \ln \frac{1 + 1.608\omega_0}{1 + 1.608\omega} + 1.608\omega \ln \frac{\omega}{\omega_0} \right) \end{aligned} \tag{8.4}$$

where R_a is gas constant for air; subscript R represents reference point of exergy. The reference temperature T_0 is chosen as the outdoor air temperature, and the reference humidity ratio ω_0 is chosen as the saturated humidity ratio of the reference temperature [15].

As for the air handling process between air and solution, its exergy destruction ΔE_{de} is composed of the exergy destruction of sensible heat transfer ($\Delta E_{de,h}$) and that of moisture transfer ($\Delta E_{de,m}$), calculated by Eqs. (8.5)–(8.7) [16].

$$\Delta E_{de} = \Delta E_{de,h} + \Delta E_{de,m} \tag{8.5}$$

$$\Delta E_{de,h} = \int T_0 h \cdot \frac{(\Delta T)^2}{T_a \cdot T_s} \mathrm{d}A \tag{8.6}$$

$$\Delta E_{de,m} = \int T_0 h_v h_m \cdot \frac{\Delta T_{dew} \Delta \omega}{T_{a,dew} \cdot T_{s,dew}} \mathrm{d}A \tag{8.7}$$

where A is the heat or mass transfer area; T_a and T_s are the temperatures of air and solution (in Kelvin); $T_{a,dew}$ and $T_{s,dew}$ are the absolute dew point temperatures of the air and solution, respectively; subscripts h and m of ΔE_{de} represent the exergy destructions of the heat transfer and mass transfer, respectively; ΔT and $\Delta\omega$ are temperature difference and humidity ratio difference between air and solution, respectively; h and h_m represent the convective heat transfer coefficient and mass transfer coefficient, respectively; and h_v denotes the latent heat of vaporization.

The exergy destruction of sensible heat transfer $\Delta E_{de,h}$ and that of moisture transfer $\Delta E_{de,m}$ could be expressed by ξ_h and ξ_m further, shown as Eqs. (8.8)–(8.9), respectively [16].

$$\Delta E_{\mathrm{de,h}} \approx \frac{T_0}{\bar{T}_{\mathrm{a}}\bar{T}_{\mathrm{d}}} \cdot \frac{Q^2}{\mathrm{hA}} \xi_{\mathrm{h}}, \text{where } \xi_{\mathrm{h}} = \frac{\overline{\Delta T^2}}{\overline{\Delta T}^2} = \frac{\frac{1}{A}\iint_A (\Delta T)^2 \mathrm{d}A}{\left(\frac{1}{A}\iint_A \Delta T \mathrm{d}A\right)^2} \tag{8.8}$$

$$\Delta E_{\mathrm{de,m}} \approx \frac{T_0 \lambda h_{\mathrm{v}}}{\bar{T}_{\mathrm{a,dew}}\bar{T}_{\mathrm{s,dew}}} \cdot \frac{m_{\mathrm{w}}^2}{h_{\mathrm{m}} A} \xi_{\mathrm{m}}, \text{ where } \xi_{\mathrm{m}} = \frac{\overline{\Delta \omega^2}}{\overline{\Delta \omega}^2} = \frac{\frac{1}{A}\iint_A (\Delta \omega)^2 \mathrm{d}A}{\left(\frac{1}{A}\iint_A \Delta \omega \mathrm{d}A\right)^2} \tag{8.9}$$

where Q and m_{w} represent the sensible heat exchange and the moisture exchange, respectively; $\overline{\Delta T}$ and $\overline{(\Delta T)^2}$ are the average of ΔT and the average of ΔT^2, respectively; $\overline{\Delta \omega}$ and $\overline{(\Delta \omega)^2}$ are the average of $\Delta \omega$ and the average of $\Delta \omega^2$, respectively; Q and m are the heat exchange amount and water transfer amount, respectively; and λ is the slope of the saturation line in a psychrometric chart, which is simplified to a constant. ξ_{h} or ξ_{m} is an index describing the distribution uniformity of ΔT or $\Delta \omega$, which is always greater than or equal to 1 [13]. Only when the ΔT or $\Delta \omega$ is constant, i.e., the driving force for heat or mass transfer is uniform, will ξ_{h} or ξ_{m} be equal to 1. The greater the value of ξ_{h} or ξ_{m}, the less uniform the heat or mass transfer driving force and the higher exergy destruction with a certain input hA.

Here, we choose a typical condition for these two basic types to investigate system performance. The parameters of the inlet outdoor air are 32 °C, 18 g/kg, and 1.33 kg/s, and the required humidity ratio of the supplied air is 9.5 g/kg. The circulating solute of LiBr in the dehumidifier/regenerator is 1.5 kg/s, while the solute flowing between the dehumidifier and the regenerator is 0.2 kg/s. The input heat transfer capacities of the key components are identical for Basic Types I and II. For example, the UA of the air-cooled condenser in Basic Type I is equal to the UA of the solution-cooled condenser in Basic Type II. $\mathrm{NTU_a}$ of the air-cooled condenser in Basic Type I is 4.8, while $\mathrm{NTU_s}$ of the solution-cooled condenser in Basic Type II is 0.8. Input NTU*s* of regenerator, dehumidifier, evaporator and solution heat exchanger are 2.5, 2.5, 0.8 and 3, respectively.

The typical air handling processes shown are illustrated in Fig. 8.5 in a psychrometric chart, and the typical operating parameters of key components are shown in Fig. 8.6. As indicated by Figs. 8.5a, b, the coupled heat and mass transfer process in the regenerator of Basic Type I proceeds close to the isenthalpic line, while the process of Basic Type II is near the iso-concentration line of the liquid desiccant. As indicated by the simulation results shown in Figs. 8.5 and 8.6, there are significant discrepancies in the operating performances of Basic Types I and II due to the difference between heating the regeneration air and heating the solution.

The unmatched coefficients of key components for Basic Type I and Basic Type II in a typical condition are listed in Table 8.1. As indicated by the match properties of these components, the unmatched coefficients of the evaporator, the dehumidifier, and the heat exchanger are similar for Basic Types I and II. The unmatched coefficient of the dehumidifiers is 1.07 for these two HPLD systems, indicating that the unmatched flow rates and parameters have a relatively limited effect on the dehumidification process. For the condenser and regenerator, there is

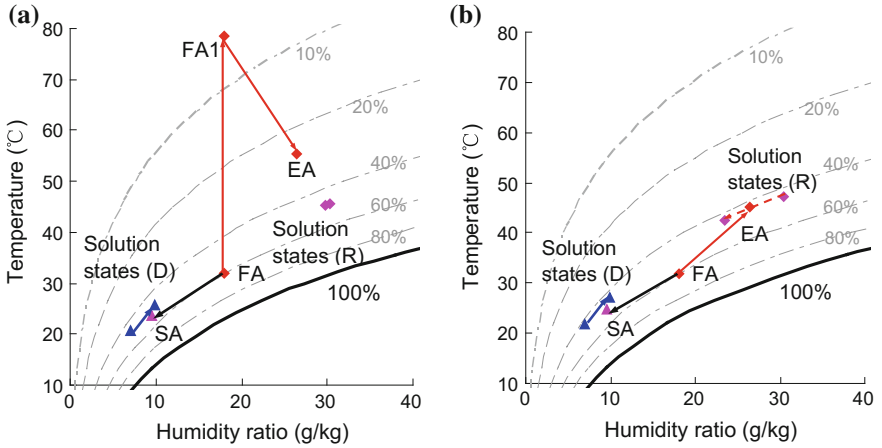

Fig. 8.5 Air and solution states of the heat pump-driven liquid desiccant air handling processes shown in a psychrometric chart: **a** Basic Type I; and **b** Basic Type II

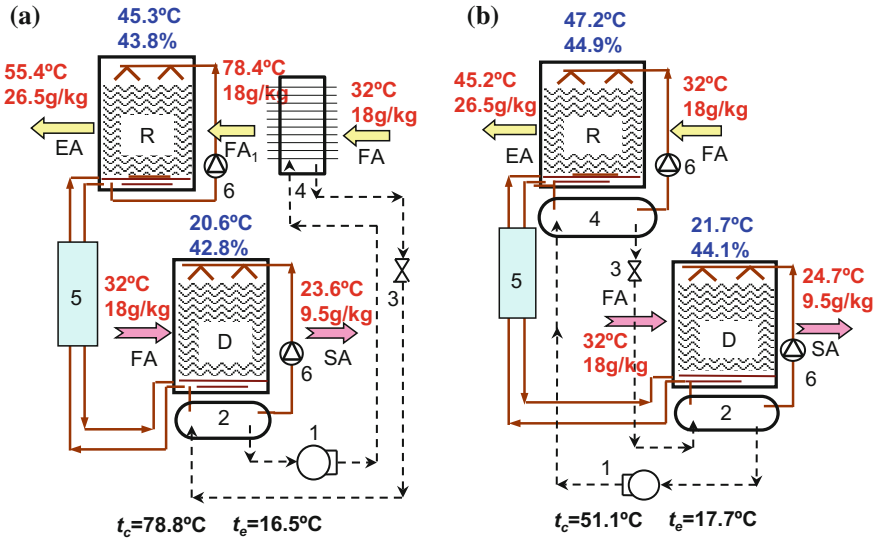

Fig. 8.6 Operating parameters of the HPLD systems in a typical condition: **a** Basic Type I; and **b** Basic Type II

significant variation in the unmatched coefficients of Basic Types I and II. In Basic Type I, ξ of the air-cooled condenser is 2.70 in this typical condition, more than two times higher than that of Basic Type II. This means that, for the air-cooled condenser of Basic Type I, the heat transfer resistance caused by the unmatched flow rates increases 170% on the basis of 1/UA. As indicated by Fig. 8.5a, the regeneration air in Basic Type I has to be heated to a relatively high temperature to satisfy

Table 8.1 System performances of HPLD systems in a typical condition (fresh air: 32 °C, 18 g/kg)

Type	Unmatched coefficients ξ				Supply air	Performance of the heat pump cycle			
	Cond	Reg	Evap	Deh		t_c	t_e	COP_{hp}	COP_{sys}
Basic Type I	2.70	1.34	1.07	1.07	23.6 °C, 9.5 g/kg	78.8 °C	16.5 °C	1.89	1.83
Basic Type II	1.07	1.05	1.05	1.07	24.7 °C, 9.5 g/kg	51.1 °C	17.7 °C	4.53	4.17
Improved Type II	1.07 (1.07)	1.03 (1.07)	1.05 (1.05)	1.06 (1.08)	25.2 °C, 9.5 g/kg	49.6 °C (52.0 °C)	18.6 °C (18.7 °C)	4.70	4.32

Cond condenser; *Deh* dehumidifier; *Evap* evaporator; *Reg* regenerator

the requirement for desiccant regeneration before flowing through the regenerator, which leads to a high ξ of the air-to-solution condenser. As a result, the unmatched coefficient of the regenerator is 1.34, still significantly higher than that of Basic Type II. This implies that, in order to overcome the mass transfer resistance caused by unmatched flow rates and parameters, more heat and mass transfer capacity or a higher heat source temperature is required in Basic Type I compared to Basic Type II. In summary, the match properties of Basic Type II are much better than those of Basic Type I.

The significant difference in unmatched coefficients of Basic Types I and II is similar to the performance discrepancy between the simulated HPLD systems. The operating parameters of the HPLD systems in this typical condition are also listed in Table 8.1, including the evaporating and condensing temperatures of the heat pump, COP_{hp}, and COP_{sys}. The evaporating temperatures (t_e) and the supply air temperatures are similar for Basic Types I and II. However, the condensing temperature (t_c) of Basic Type I (78.8 °C) is much higher than that of Basic Type II (51.1 °C), indicating that the condensing temperature increases due to the unmatched flow rates of the air-cooled condenser. The increase of the condensing temperature results in a COP_{hp} of 1.89 in Basic Type I, lower than half of the COP_{hp} of Basic Type II (4.53).

As indicated by the analysis on match properties and simulated performances of HPLD systems, the handling process along the iso-concentration line is better than that along the isenthalpic line. And the process of heating the solution for regeneration is recommended over heating the regeneration air. The unmatched coefficients of key components in the HPLD systems help to evaluate the performance of the process, providing a relatively simple and effective method to guide the construction of an HPLD system. Thus, a principle for system construction is indicated based on the match property analysis: lower unmatched coefficients (ξ close to 1) mean the heat or mass transfer resistance caused by the unmatched flow rates or parameters is lower, and the system will demonstrate better energy performance. The unmatched coefficient based on exergy analysis can help to determine the key issues restricting the operating performance, providing the direction for constructing a better HPLD system. Compared with the system simulation method, the match property method is more simple and feasible.

To improve the performance of the HPLD system further, grading is proposed as an approach. Figure 8.7a gives the operating schematic of a two-stage HPLD system (Improved Type II), and the typical air handling process is shown in Fig. 8.7b. In contrast to Basic Type II, there are two-stage dehumidifier/regenerator and heat pump cycles in Improved Type II. The humid fresh air flows through

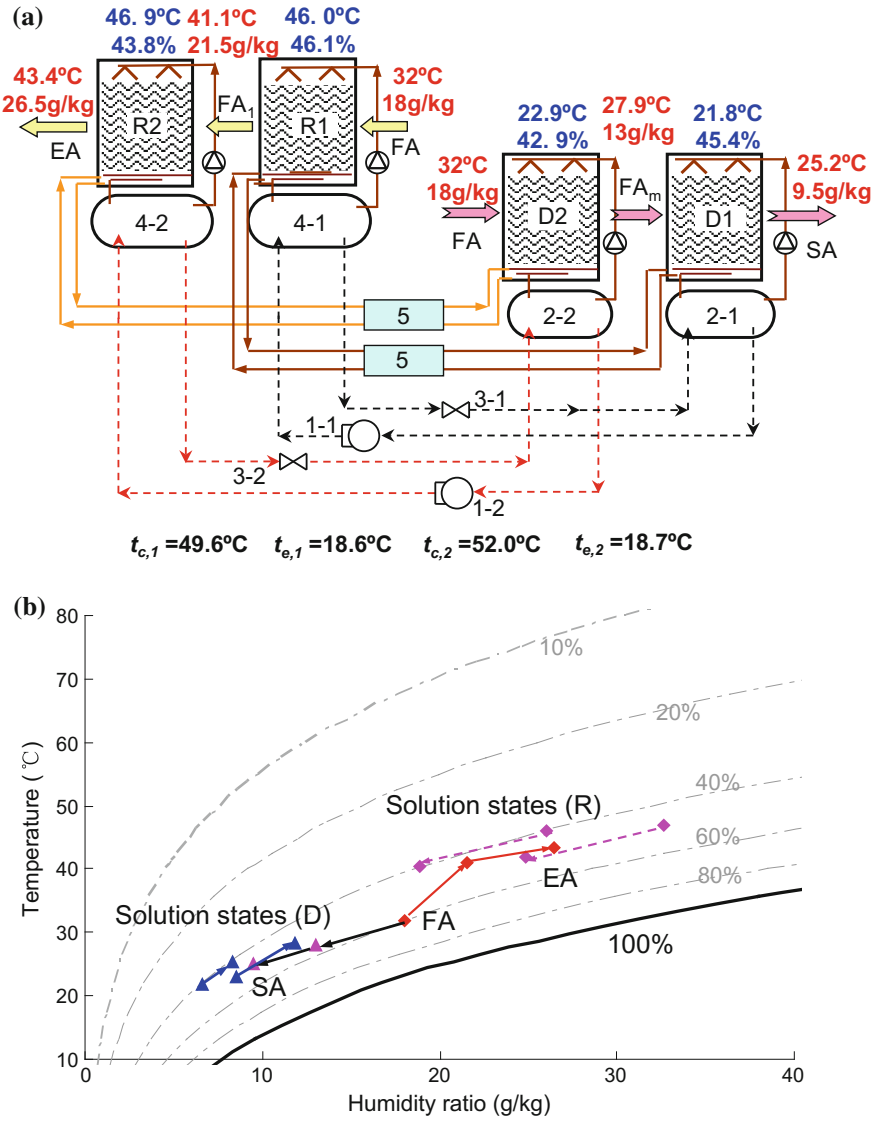

Fig. 8.7 Operating principle of Improved Type II: **a** system schematic; and **b** air handling process shown in a psychrometric chart

dehumidifiers D2 and D1 successively and is then dehumidified to the required state, while the regeneration air flows through regenerators R1 and R2 step-by-step for desiccant regeneration. The operating parameters of this two-stage HPLD system are also given in Fig. 8.7a, with the same fresh air parameters and required humidity ratio of the supply air analyzed previously. The unmatched coefficients of the key components and system operating performance of this improved system are listed in Table 8.1. The parameters in the brackets of Table 8.1 are the unmatched coefficients and performance parameters of the second stage.

As indicated by the match properties of this two-stage HPLD system, ξ_M of the regenerator or the dehumidifier for the first stage is a bit lower than in Basic Type II, but for the second stage, it is a bit higher. There is no significant difference between the unmatched coefficients of Basic Type II and Improved Type II. The simulated operating performances of this system confirm the results from the analysis of match properties. The condensing temperature of the first stage in Improved Type II is a bit lower than in Basic Type II, but that of the second stage is a bit higher. COP_{hp} of Improved Type II in this typical condition is 4.70, a bit higher than that of Basic Type II. Thus, compared with Basic Type II, the grading method (Improved Type II) leads to an improvement in the operating performance of the HPLD system. Thus utilizing the condensing heat to heat solution for regeneration is recommended rather than heating the regeneration air. And a multi-stage scenario is also recommended in the HPLD system to improve the system performance.

8.2.2 Tested Performance of Liquid Desiccant Outdoor Air Handling Processors

For liquid desiccant outdoor air handling processors operating in summer, the outdoor air is dehumidified in the dehumidifier and then the diluted solution is regenerated in the regenerator. According to whether there is indoor exhaust air that can be adopted as regeneration air, a distinction can be made between two different kinds of outdoor air handling processors that use liquid desiccant. If there is sufficient indoor exhaust air, the processor with enthalpy recovery from the indoor exhaust air and the process of utilizing the indoor exhaust air for desiccant regeneration could be adopted for outdoor air dehumidification. Alternatively, if there is not sufficient indoor exhaust air to be utilized directly, outdoor air could be adopted as the regeneration air, and a process using high-temperature chilled water to precool the outdoor air could be constructed to improve the performance of the outdoor air handling process. The following subsection examines the performance of the liquid desiccant outdoor air handling processors with indoor exhaust air as regeneration air. In such processors, the exhaust heat from the condenser is utilized to heat the desiccant coming into the regenerator, so the air handling processes are close to the iso-relative humidity line (rather than the isenthalpic line).

Figure 8.8 demonstrates the operating principle of a two-stage heat pump-driven liquid desiccant outdoor air processor operating in summer, which is composed of a two-stage enthalpy recovery device (spray modules numbered I and II), a two-stage dehumidifier/regenerator, and a vapor compression refrigeration cycle. In this figure, the straight lines and dashed lines stand for liquid desiccant and refrigerant, respectively. The top channel is for the indoor exhaust air, and the bottom channel is for the outdoor air. The outdoor air first enters the two-stage enthalpy recovery

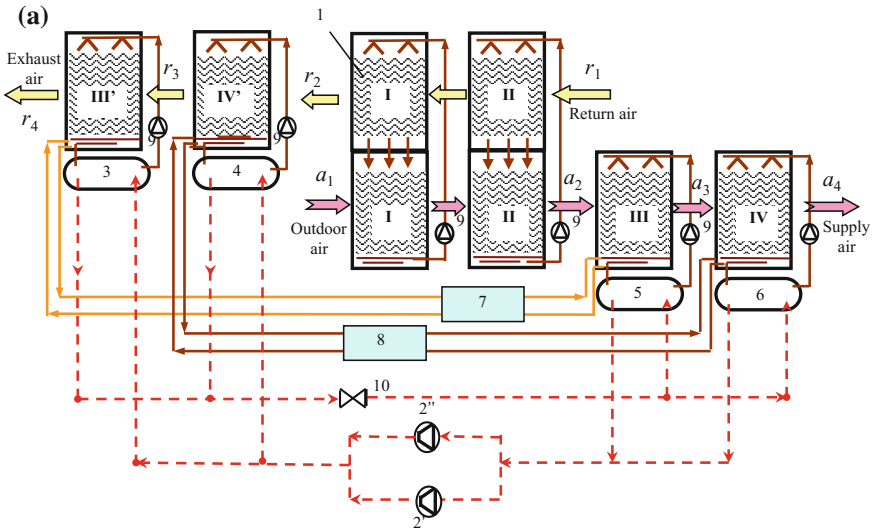

1-heat recovery module; 2-compressor; 3-condenser I; 4-condenser II; 5-evaporator I; 6-evaporator II; 7-plate heat exchanger I; 8-plate heat exchanger II; 9-solution pump; 10-expansion valve

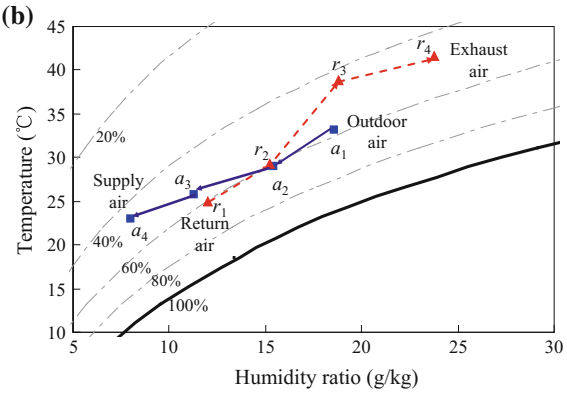

Fig. 8.8 Summer operation principle of the two-stage liquid desiccant outdoor air processor with enthalpy recovery: **a** operating schematic; and **b** air handling process

device and then flows into the evaporator-cooled two-stage dehumidification modules (numbered III and IV) before being supplied into occupied spaces. In the same way, the indoor exhaust air first enters the enthalpy recovery device and then flows into the condenser-heated modules (numbered IV′ and III′) before being exhausted to the outdoor environment. The evaporator of the heat pump is adopted to further cool and dehumidify the outdoor air coming out of the enthalpy recovery device to the desired supplied temperature and humidity ratio.

The liquid desiccant in this outdoor air processor is divided into two parts. One part is stored in spray modules I and II (in Fig. 8.8) for the purpose of enthalpy recovery, the equivalent state of which is decided by the outdoor air and the indoor exhaust air simultaneously. The other part is stored in spray modules III, III′, IV and IV′ to exchange heat with the evaporator and condenser, respectively. Taking the solution circulating between spray modules III and III′ as an example to illustrate the operating principle in summer, the solution is first cooled by the evaporator (labeled 5 in Fig. 8.8a), and then exchanges heat and mass with the outdoor air in spray module III, where the solution is diluted and heated. The solution heated by the condenser (labeled 3 in Fig. 8.8a) enters spray module III′ to be regenerated. The diluted solution and the regenerated solution are connected by solution pipes, and a plate heat exchanger (labeled 7 in Fig. 8.8a) is adopted for the internal heat recovery of the solution. The principle of spray modules IV and IV′ is similar to that of modules III and III′. It is obvious that the enthalpy recovery device can efficiently reduce the energy consumption of the outdoor air handling processor. The cooling capacity and condensation heat of the heat pump are both effectively utilized in this outdoor air processor. Two parallel compressors are utilized in the heat pump cycle to operate efficiently under the partial load condition, so that the processor can have higher energy efficiency and control accuracy at partial load.

1. **Tested performance at full load (typical hot and humid condition)**

Because the heat pump system in the outdoor air processor utilizes two compressors working in parallel, and the solution in each stage exchanges heat with an individual evaporator (condenser), the dehumidification requirement at partial load can be achieved by adjusting the on–off time of these two compressors. As the required cooling temperature of the solution is about 15–20 °C, the evaporating temperature can be increased to about 7 °C. Meanwhile, the condensing temperature is only around 45 °C since the required heating temperature of the solution is about 40 °C. The test results of the outdoor air processor shown in Fig. 8.8 under the summer design condition are listed in Table 8.2. The coefficient of performance COP_{air} is defined as

$$COP_{air} = \frac{\text{Cooling capacity of the outdoor air}}{\text{Power consumption of compressor and solution pumps}} \tag{8.10}$$

The COP of the heat pump (COP_{hp}) in the outdoor air processor is 4.0, while COP of the processor (COP_{air}) is as high as 5.0.

Table 8.2 Test results of the outdoor air processor under the summer design condition

Parameter	Unit	Value	Parameter	Unit	Value
Outdoor air flow rate	m^3/h	4058	Exhaust air flow rate	m^3/h	4021
Outdoor air dry-bulb temperature	°C	36.0	Return air dry-bulb temperature	°C	26.0
Outdoor air humidity ratio	g/kg	25.8	Return air humidity ratio	g/kg	12.6
Supply air dry-bulb temperature	°C	17.3	Exhaust air dry-bulb temperature	°C	39.1
Supply air humidity ratio	g/kg	9.1	Exhaust air humidity ratio	g/kg	38.6
Evaporating temperature	°C	7.0	Condensing temperature	°C	45.0
Power consumption of the compressors	kW	14.6	Power consumption of the solution pump	kW	1.92
Outdoor air cooling capacity	kW	82.7	Exhaust air heating capacity	kW	101.9
Outdoor air dehumidification rate	kg/h	80.1	Cooling capacity of the heat pump	kW	59.0
COP_{air}	W/W	5.0	COP_{hp} of the heat pump	W/W	4.0

2. **Tested performance and analysis at partial load (summer)**

Based on the test results under the design condition, performance of the processor at partial load was then tested, and the main results are listed in Table 8.3. Since only one compressor is in operation at partial load, while the heat transfer area of the evaporator and that of the condenser are identical, the heat transfer between the refrigerant and the solution became more sufficient and the heat transfer temperature differences decrease accordingly. As a result, the evaporating temperature rises and the condensing temperature drops. As indicated by the test results listed in Table 8.3, the evaporating temperature increases to 11 °C, while the

Table 8.3 Test results of the outdoor air processor at partial load under the summer condition

Parameter	Unit	Value	Parameter	Unit	Value
Outdoor air flow rate	m^3/h	4058	Exhaust air flow rate	m^3/h	4021
Outdoor air dry-bulb temperature	°C	30.0	Return air dry-bulb temperature	°C	26.0
Outdoor air humidity ratio	g/kg	17.4	Return air humidity ratio	g/kg	12.7
Supply air dry-bulb temperature	°C	17.3	Exhaust air dry-bulb temperature	°C	39.1
Supply air humidity ratio	g/kg	9.6	Exhaust air humidity ratio	g/kg	26.6
Evaporating temperature	°C	11.0	Condensing temperature	°C	37.6
Power consumption of the compressors	kW	5.8	Power consumption of the solution pump	kW	1.43
Outdoor air cooling capacity	kW	42.7	Cooling capacity of the heat pump	kW	33.2
COP_{air}	W/W	5.9	COP_{hp} of the heat pump	W/W	5.7

condensing temperature decreases by 7.4 °C compared to the full-load condition to 37.6 °C. Thus, COP_{hp} and COP_{air} increase to 5.7 and 5.9, respectively. As the outdoor air handling processor was running at partial load for more than 70% of the time, the comprehensive energy efficiency of this liquid desiccant processor could be as high as 5.5.

Based on these test results, it can be seen that the heat pump-driven liquid desiccant outdoor air processor can effectively meet the dehumidification requirement in summer with high comprehensive energy efficiency. The humidity ratio of the dehumidified outdoor air can meet the demand for humidity control with the supply air temperature around 17 °C, which could be supplied directly into the conditioned room without further reheating or cooling. Moreover, the enthalpy recovery modules are adopted in this process to recover energy from the indoor exhaust air. In summary, the outdoor air processor can meet the needs of running at full load and partial load with comprehensive energy efficiency up to 5.5.

8.2.3 *Applications of Liquid Desiccant System in Buildings*

Temperature and humidity independent control (THIC) air-conditioning system is proposed as an efficient air-conditioning system [8]. Figure 8.9 illustrates the operating principle of the THIC air-conditioning system, with an outdoor air handling subsystem and a relatively high-temperature cooling source subsystem that can separately regulate the indoor temperature and humidity, respectively. As indoor temperature and humidity are regulated by independent subsystems, the THIC system can satisfy the variance of the indoor heat moisture ratio. Therefore, the THIC system can avoid the imbalance of indoor parameters, and it addresses the conventional system's inability to meet temperature and humidity requirements simultaneously.

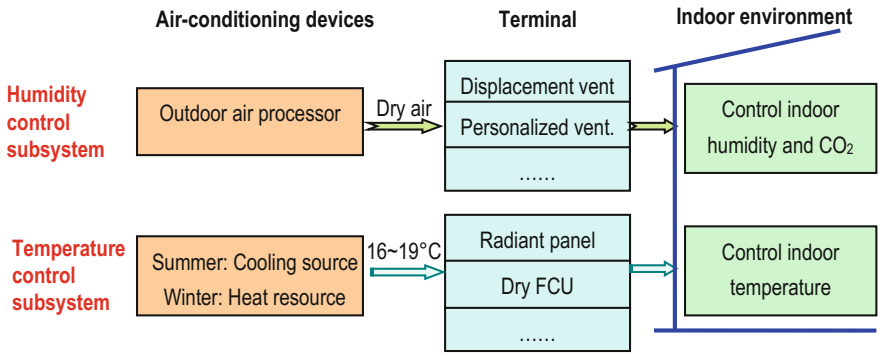

Fig. 8.9 Operating principle of the THIC air-conditioning system

HPLD systems could be applied as the humidity control device in the THIC system. It is responsible for dehumidifying humid air and supplying dry air to the indoor space. There have been numerous applications using HPLD systems in China. An office building will be taken as an example in this section.

8.2.3.1 Basic Information

A 5-story office building, as shown in Fig. 8.10, is located in Shenzhen, China, with total building area of 21,960 m^2 and the areas of 5940, 5045, 3876, 3908, 3191 m^2 for the 1st to 5th floor, respectively. The main functions of the 1st floor are mess hall, archive and carport, while the 2nd to 4th floors are the office rooms, with the 5th floor as the meeting room. And there is a vestibule vertically through up the 2nd to 4th floors in the north of this building.

The outdoor condition in Shenzhen is rather hot and humid all through the year. The annual outdoor air relative humidity is about 80% and humidity ratio in summer is as high as 20 g/(kg dry air). The building requires both cooling and dehumidification in a long period of time, and no heating and humidification requirement in winter. Therefore, how to handle the moisture efficiently is the key issue in such a subtropical area.

The THIC system serves from 1st to 4th floor with the net air-conditioning area of 13,180 m^2 (the total area of 18,769 m^2), and the 5th floor is served by several stand-alone air-conditioners and is not within the scope of our discussion. The schematic of the THIC system is represented in Fig. 8.11 with the parameters of main devices in the humidity control subsystem listed in Table 8.4.

The right side of Fig. 8.11 is the humidity control subsystem, including 9 liquid desiccant outdoor air handling units that supply adequate dry outdoor air into the occupied spaces. As the flow rate of the supplied outdoor air is proportional to the

Fig. 8.10 The tested office building in Shenzhen

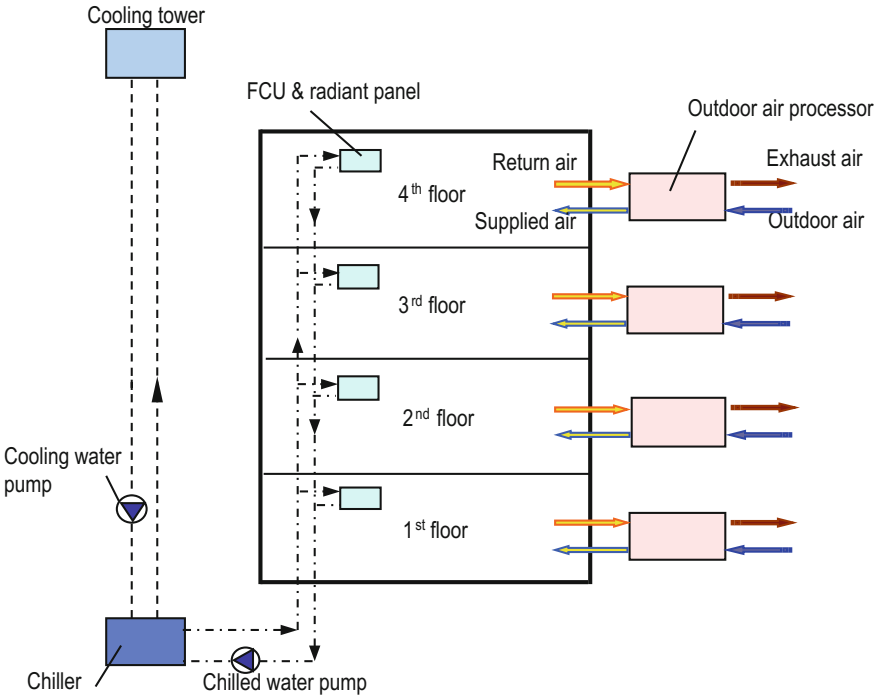

Fig. 8.11 Schematic of the THIC air-conditioning system

Table 8.4 Main devices of the humidity control system in the office building

Subsystem	Device	Rated parameters
Humidity control subsystem	Outdoor air handling units	Fresh air flow rate 2000 m^3/h, cooling capacity 39 kW, power consumption[a] 10 kW; for offices in the 4th floor
		Fresh air flow rate 4000 m^3/h, cooling capacity 83 kW, power consumption[a] 25 kW; for offices in the 4th floor
		Fresh air flow rate 5000 m^3/h, cooling capacity 103 kW, power consumption[a] 28 kW; 2 units for the 2nd floor, and 2 units for the 3rd floor
		Fresh air flow rate 8000 m^3/h, cooling capacity 166 kW, power consumption[a] 45 kW, for vestibule in the 2nd floor
		Fresh air flow rate 10000 m^3/h, cooling capacity 196 kW, power consumption[a] 45 kW, for restaurant in the 1st floor

[a]Including power consumption of compressors, solution pumps, and fans inside the outdoor air units

number of people, the pollutants, CO_2 and latent heat produced by human bodies can be removed by outdoor air. The schematic of the heat pump-driven outdoor air processors using liquid desiccant is illustrated in Fig. 8.8, which is composed of a two-stage enthalpy recovery device and a two-stage air handling device coupled with refrigeration cycles. LiBr aqueous solution is employed as liquid desiccant in these air processors. The enthalpy recovery device is used to recover the energy from indoor exhaust air to decrease the energy consumption of the outdoor air handling process. And in the heat pump-driven air handling device, the diluted solution from the dehumidification modules is heated by the exhaust heat from the condenser and concentrated in the regeneration modules. Then, the hot concentrated solution is cooled by passing through the heat exchanger and evaporator before it enters the dehumidification modules, and lastly used to remove moisture from the outdoor air.

8.2.3.2 Energy Efficiency of Humidity Control Subsystem

The performances of the liquid desiccant outdoor air units were tested one by one on May 27, 2009, according to the measured flow rates, air inlet and outlet parameters through the processor and input power of compressors, solution pumps and fans. The tested results of seven outdoor air units are summarized in Table 8.5; the other two processors are neglected due to the difficulty of installing the sensors.

The east side processor of the 2nd floor is a typical example for the outdoor air unit, and its specific operation information is shown in Table 8.6. The outdoor air flow rate was 5059 m^3/h, the outdoor air parameters were 29.3 °C and 20.3 g/kg, and the supply air parameters were 17.1 °C and 6.2 g/kg. So the cooling capacity (Q_{air}), calculated by energy balance equation, was 82.6 kW. The power consumption of compressors together with solution pumps (P_{air}) inside the processor was 17.8 kW, and the power consumption of the supply air and exhaust air fans (P_{fan}) was 2.2 kW. Therefore, the performance of the outdoor air unit (COP_{air}), the transport coefficient of fans (TC_{fan}) and the performance of the entire humidity handling process (COP_{hum}), as shown in Eqs. (8.11)–(8.13), are 4.7, 37.5 and 4.2, respectively.

$$COP_{air} = \frac{Q_{air}}{P_{air}} \tag{8.11}$$

$$TC_{fan} = \frac{Q_{air}}{P_{fan}} \tag{8.12}$$

$$COP_{hum} = \frac{Q_{air}}{P_{air} + P_{fan}} \tag{8.13}$$

Table 8.5 Performance of the outdoor air handling units (outdoor condition: 29.3 °C and 20.3 g/kg)

Location	Supply outdoor air			Cooling capacity/kW	Power consumption/kW		COP_{air}	TC_{fan}	COP_{hum}
	Flow rate/(m^3/h)	Temperature/°C	Humidity ratio/(g/kg)		Compressors and solution pumps	Fans			
East side of 2nd floor	5059	17.1	6.2	82.6	17.8	2.2	4.7	37.5	4.2
West side of 2nd floor	5195	16.7	6.1	86.0	17.6	2.3	4.9	37.4	4.3
East side of 3rd floor	4972	16.8	6.5	80.4	18.2	2.2	4.4	36.5	4.0
West side of 3rd floor	5215	16.6	6.2	86.4	17.6	2.2	4.9	39.3	4.4
East side of 4th floor	4261	16.7	6.4	69.5	15.0	1.7	4.6	40.9	4.2
Middle side of 4th floor	1940	16.5	6.2	32.1	7.1	0.9	4.5	35.7	4.0
West side of 4th floor	4307	16.3	6.1	72.0	15.3	1.8	4.7	40.0	4.2

Table 8.6 Operation condition of a typical outdoor air handling unit (east side of 2nd floor)

Outdoor condition	Supplied outdoor air	Stage	Evaporating temperature/°C	Condensing temperature/°C	Solution parameter (temperature and concentration)	
Temperature: 29.3 °C Humidity ratio: 20.3 g/kg	Temperature: 17.1 °C Humidity ratio: 6.2 g/kg Flow rate: 5059 m^3/h	I	11.0	50.8	Dehumidification module	Inlet: 15.8 °C, 34.6% Outlet: 20.5 °C, 34.4%
					Regeneration module	Inlet: 44.2 °C, 34.9% Outlet: 38.3 °C, 35.2%
		II	4.4	51.3	Dehumidification module	Inlet: 9.0 °C, 44.1% Outlet: 14.0 °C, 43.9%
					Regeneration module	Inlet: 44.3 °C, 44.8% Outlet: 37.9 °C, 45.1%

As shown in Table 8.5, the COP_{air} of the tested seven outdoor air units were in the range of 4.4–4.9, the TC_{fan} of the fans were 35–40, and the COP_{hum} of the entire humidity handling processes were 4.0–4.4.

According to the tested data and rated parameters of the outdoor air units and fans, the calculated cooling capacity of the entire humidity control subsystem was 773.0 kW with total inside compressors and solution pumps input power of 166.9 kW and total fans input power of 20.0 kW, so the coefficient of performance of the humidity control subsystem (COP_{HUM}), shown in Eq. (8.14), is 4.1.

$$COP_{HUM} = \frac{\Sigma Q_{air}}{\Sigma (P_{air} + P_{fan})} \tag{8.14}$$

Similarly, on the basis of the tested data of another day, the COP_{HUM} under the design condition was 4.1, with the calculated cooling capacity of 915.0 kW, total inside compressors and solution pumps input power of 194.4 kW and total fans input power of 25.1 kW.

8.2.3.3 Energy Performance of the Entire THIC System

Calculated from the above tested data, the overall COP of the THIC system (COP_{SYS}) under partial load condition and design condition were 4.0 and 4.1, respectively, as shown in Eq. (8.15).

$$COP_{SYS} = \frac{Q_{CH} + \Sigma Q_{air}}{(P_{CH} + P_{CT} + P_{CTP} + P_{CWP} + P_{FCU}) + \Sigma (P_{air} + P_{fan})} \tag{8.15}$$

where Q_{CH} refers to the cooling capacity of water chiller; $\sum Q_{air}$ indicates the sum of cooling capacities of outdoor air handling processors using liquid desiccant; P_{CH}, P_{CT}, P_{CTP}, P_{CWP} and P_{FCU} represent the power consumptions of water chiller, cooling tower, cooling water pump, chilled water pump and FCU, respectively. P_{air} and P_{fan} represent the power consumptions of outdoor air handling processors and fans for air supply, respectively.

Based on the tested results of these two typical operating conditions, it is convinced that the THIC system in this office building has achieved a high efficiency with its total COP over 4.0. By comparison, the measured average coefficient of performance of whole system in traditional fan-coil systems is usually around 3.0. Therefore, there is a remarkable energy efficiency improvement of the THIC system comparing with the conventional system.

Energy consumption of the THIC system was measured by the power metering monitoring system. Figure 8.12 shows the monthly power consumption of the system from 15 April to 15 October (apart from weekends and statutory holidays). The total energy consumption was 425,000 kWh during the cooling season, and the humidity control subsystem occupied 61% of the total power consumption which

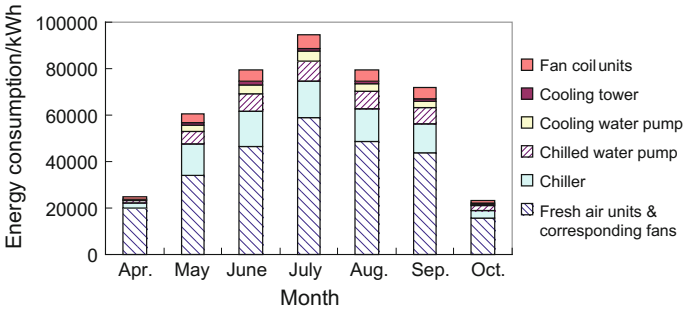

Fig. 8.12 Monthly power consumption of the THIC system

was proportional to the ratio of cooling load that the humidity control subsystem undertook.

The annual energy consumption in unit building area and unit net air-conditioning area of the tested THIC system were 22.6 kWh/(m^2 year) and 32.2 kWh/(m^2 year), respectively. However, the average energy consumption levels of office building of the similar building envelope and occupant density during the same time in Shenzhen were around 42–49 kWh/(m^2 year) according to the investigated results. Therefore, the THIC system in this office building achieved noticeable energy saving in operation compared with the conventional air-conditioning system, and the added cost can be recalled within two years.

8.3 Air Handling Process Using Desiccant Wheel

The DW, the subsidiary cooling systems and the heating devices are three main parts of a typical DW-based air handling system. Heating devices can be electrical heating, gas burner, solar energy, heat pump systems, etc., depending on regeneration temperature T_r. T_r is influenced not only by the DW, but also by the cooling method. As for the DW, its performances are influenced by a variety of parameters, such as the wheel's dimensions and the structure of air channels, rotation speed, inlet states of the air, regeneration air mass flow rate, area ratio of regeneration section, purge section, etc. Tu et al. [17] found that, when the wheel's structure and working conditions are fixed, the lowest T_r can be achieved for DWs with the facial area ratio and the air flow rate ratio of the two streams of air being both equal to 1. In this section, performances of a one-stage system and a two-stage system with identical heat transfer areas are compared, with particular emphasis on the required heating source temperature. Heat pump cycle is utilized for desiccant regeneration, and the condensing temperature is regarded as the heating source temperature.

8.3.1 *Operating Principle of the Heat Pump-Driven Multi-stage DW System*

The operating principle of the heat pump-driven multi-stage DW system is depicted in Fig. 8.13 (taking 2-stage as an example). For the *N*-stage system, there are N DWs and one heat pump system, with $N + 1$ condensers being used as heaters and *N* evaporators being used as coolers. Taken the two-stage system in Fig. 8.13 as an example, the operating principle are as follows. The processed air is dehumidified by DW 1 (A_{Pin}-A_{P1}) before flowing into evaporator 1 to be cooled (A_{P1}-A_{P2}). After being dehumidified by DW 2 (A_{P2}-A_{P3}), it is cooled by evaporator 2 (A_{P3}-A_{Pout}) before being introduced into occupied spaces. The regeneration air is heated by condenser 2 (A_{Rin}-A_{R1}), humidified by DW 2 (A_{R1}-A_{R2}), heated by condenser 1 (A_{R2}-A_{R3}), humidified by DW 1 (A_{R3}-A_{R4}), and finally used to dissipate the extra heat from condenser 0 (A_{R4}-A_{Rout}) before being exhausted to the outdoor environment. The air handling processes of the heat pump-driven one-stage and two-stage desiccant dehumidification system are shown in psychrometric chart in Fig. 8.14. Compared with one-stage system, during this stage-by-stage dehumidification process of the multi-stage system, the processed air is cooled down before the temperature rises too high in the wheel. Thus, the processed air can remain in a low temperature range, which ensures that the desiccant can stay in a low temperature range. Furthermore, the desiccant water content can be relatively higher while still reaching the same supplied air humidity ratio, and the corresponding regeneration temperature can be reduced as well.

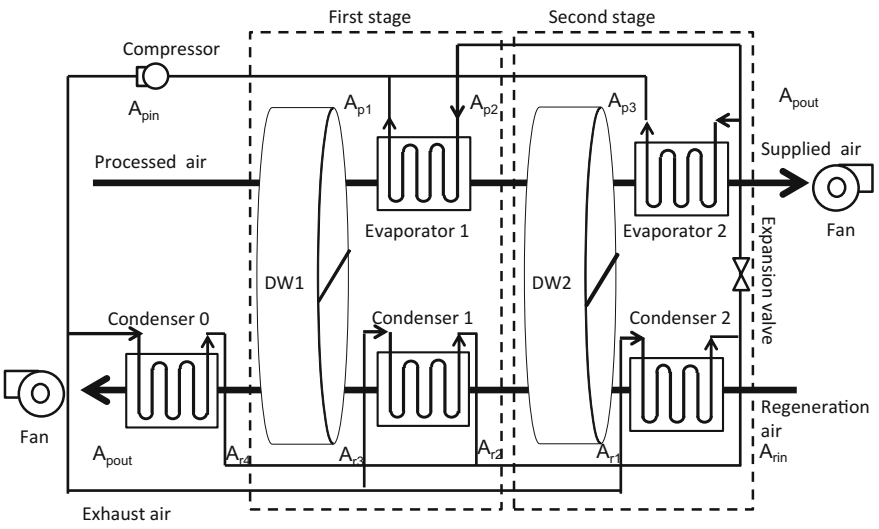

Fig. 8.13 Schematic of a heat pump-driven two-stage DW cooling system

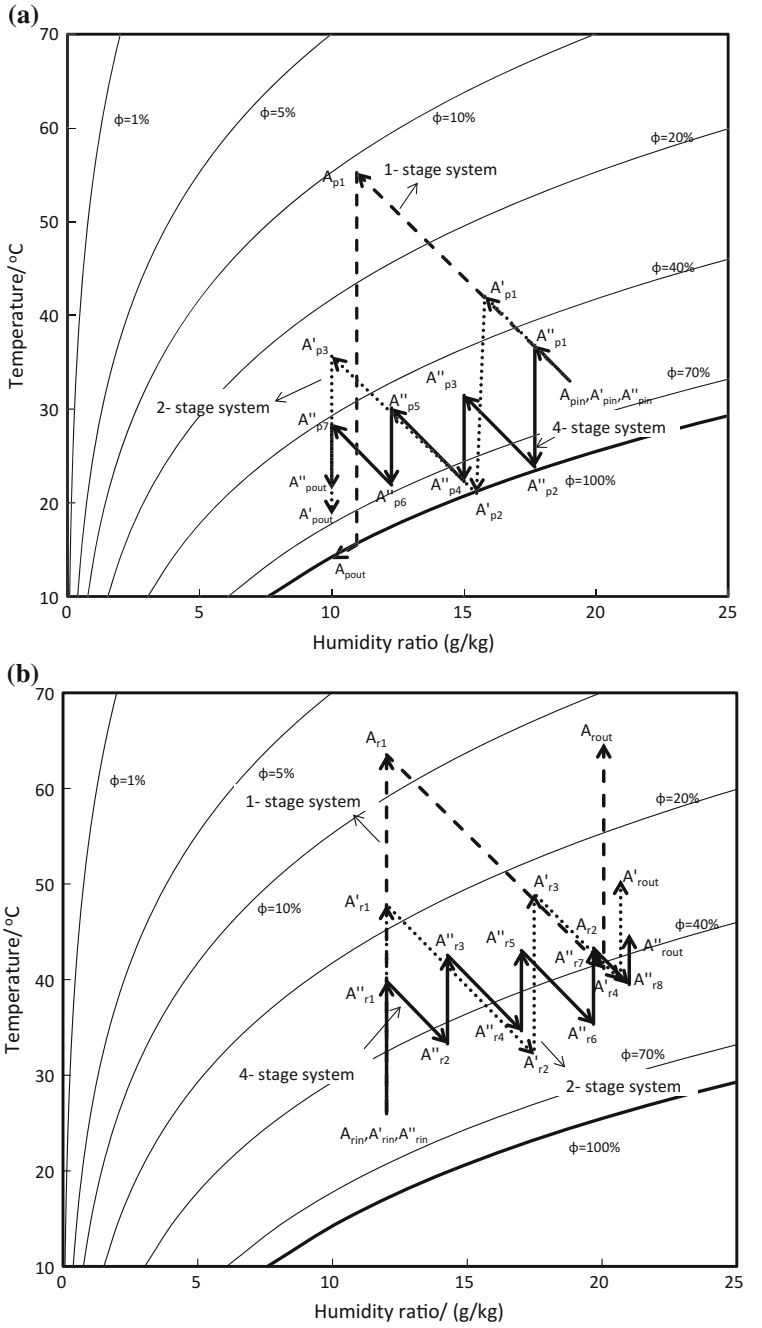

Fig. 8.14 Air handling process with different numbers of stages: **a** processed air; and **b** regeneration air

For heat pump-driven systems, power input from the compressor is required to transfer heat from evaporators to condensers. The coefficient of performance of this system (COP_R) is calculated by dividing the cooling capacity of the processed air (Q_c) by the power input of the compressor (E_c), as shown as:

$$COP_R = \frac{m_p\left(i_{pin} - i_{pout}\right)}{P} = \frac{m_p\left(i_{pin} - i_{pout}\right)}{Q_c}\frac{T_{evap}}{T_{cond} - T_{evap}}\varepsilon \tag{8.16}$$

Q_c is calculated by the enthalpy variance of the processed air and the mass flow rate of the processed air (m_P).

8.3.2 Performances of the Heat Pump-Driven Multi-stage DW System

In this section, the influences of the number of stages on COP_R of the heat pump-driven DW system are investigated, with the same entire heat and mass transfer areas for different systems. The thickness of the DW and the heat transfer area of all the heat exchangers, i.e., evaporators and condensers are evenly divided in the multi-stage system. The wheel's facial area is evenly divided for dehumidification and regeneration. The operating conditions and component information are shown in Table 8.7. For all systems and cases, the DWs are operated at the optimum rotation speeds. In this way, the required heat source temperatures can be evaluated and compared.

The influences of stage number on the performances of the system are shown in Fig. 8.15. It can be seen that, when the supplied humidity ratio is fixed at 10 g/kg, as the increase of stage number, the change of supplied air temperature is not obvious. However, the evaporating temperature is increasing and the condensing temperature, which is also the heat source temperature, is decreasing. This is beneficial for the increase of COP_R, since the work of the compressor (P) is reducing when the total heat change of the processed air (Q_c) is almost constant, according to Eq. (8.16). For one-stage, two-stage and four-stage systems, COP_R are 2.41, 3.74 and 4.50, respectively.

In the next part, the reasons behind the fact that heat pump-driven multi-stage DW system has higher performances than single-stage system will be explained

Table 8.7 Information related to working conditions, desiccant wheels, and the heat pump system

Operating conditions	DW	Heat pump system
Processed air: 33 °C, 19 g/kg, 0.8 kg/s Regeneration air: 26 °C, 12 g/kg, 0.8 kg/s Supplied air: 10 g/kg	Radius: 0.5 m Total thickness: 0.2 m Material: silica gel *Nu* of air channels: 2.463	Total air side NTU for evaporators (NTU_c): 5 Total air side NTU for condensers (NTU_h): 5 Thermodynamic perfectness of the compressor: 0.5

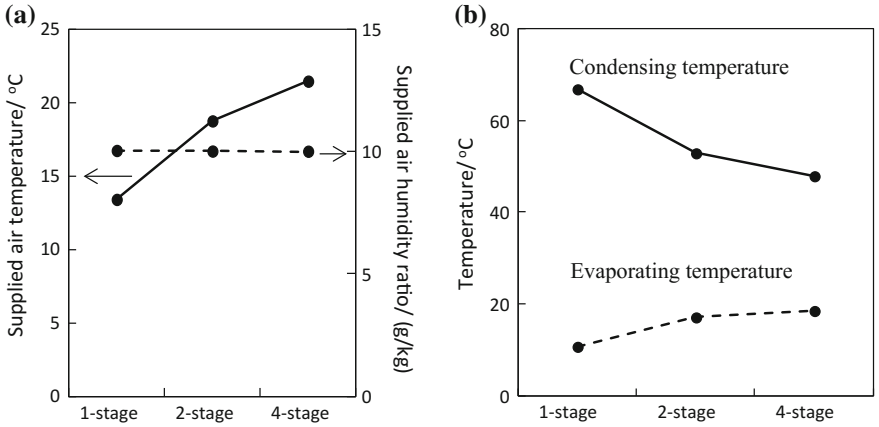

Fig. 8.15 Effect of the number of stages on: **a** supplied air temperature and humidity ratio; **b** evaporating temperature and condensing temperature

from the perspective of unmatched coefficients. And expressions of unmatched coefficients in heat and mass transfer processes between air and solid desiccant are the same as those between air and liquid desiccant expressed in Eqs. (8.8) and (8.9).

8.3.3 *Theoretical Analysis Using Unmatched Coefficients*

When the air is handled in the desiccant wheels and heat exchangers (i.e., evaporators and condensers), there exists heat and mass transfer exergy destruction because of the temperature and humidity ratio differences. Input power consumption P can be written as Eq. (8.17) [17].

$$P = m_{\mathrm{p}}\left(e_{\mathrm{pout}} - e_{\mathrm{pin}}\right) + m_{\mathrm{r}}\left(e_{\mathrm{rout}} - e_{\mathrm{rin}}\right) + \Delta E_{\mathrm{DW}} + \Delta E_{\mathrm{HE}} + \Delta E_{\varepsilon} \tag{8.17}$$

where ΔE_{DW} and ΔE_{HE} are the exergy destruction of all the desiccant wheels and all the heat exchangers, respectively; and ΔE_{ε} is the exergy destruction of the compressor, which is equal to $T_0\left(Q_{\mathrm{cond}}/T_{\mathrm{cond}} - Q_{\mathrm{evap}}/T_{\mathrm{evap}}\right)$, resulting from thermodynamic perfectness (ε) of the compressor being lower than 1.

For the heap pump-driven multi-stage DW system, according to Eq. (8.17), under the fixed inlet and outlet states of the processed air, when exergy destruction decreases, P can also decrease. And it can be obtained from Eq. (8.16) that the condensing temperature (T_{cond}) is reduced and the evaporating temperature (T_{evap}) increases accordingly. In summary, the heat source temperature (T_{cond}) is determined by the required P. In order to reduce T_{cond}, the systems' exergy destruction should be reduced.

It is indicated the factors that influence the heat and mass transfer exergy destruction are heat and mass transfer capacities, heat and mass transfer area and unmatched coefficient. For the cases talked about in this part, the total heat and mass transfer area for each kind of component are identical and the total heat and mass transfer capacities are almost the same. Therefore, unmatched coefficients are the main performance influencing factor under different number of stages.

Figure 8.16 shows the exergy destructions under different number of stages. Table 8.8 listed the detailed information about unmatched coefficients and heat transfer capacities. As for the desiccant wheels, the unmatched coefficients for all

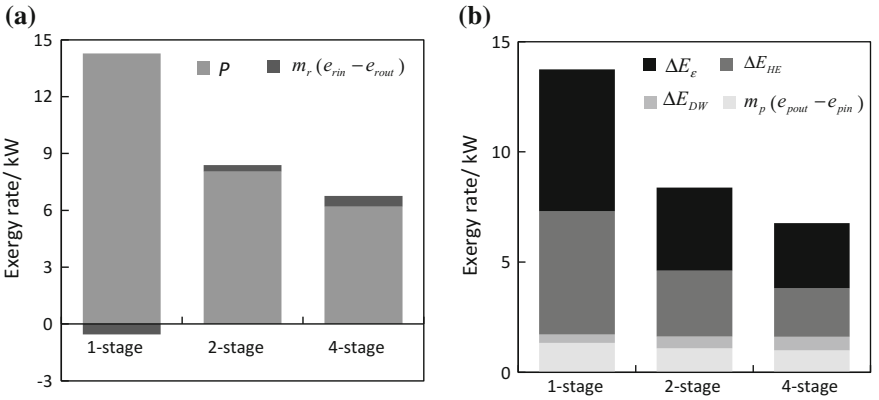

Fig. 8.16 Effect of the number of stages on: **a** exergy provided by the compressor and the regeneration air; **b** exergy destruction and exergy obtained by the processed air

Table 8.8 Heat and mass transfer capacities and unmatched coefficients in multi-stage desiccant wheel systems

	1-stage system	2-stage system	4-stage system
Unmatched coefficient of desiccant wheel	1.12 (Average)	1.10 (Average)	1.15 (Average)
Q_c/kW	36.1	18.8 (Evap. 1), 13.8 (Evap. 2)	10.8 (Evap. 1), 7.6 (Evap. 2), 6.7 (Evap. 3), 5.7 (Evap. 4)
Unmatched coefficient of evaporators	2.53 (Average)	1.47 (Average)	1.13 (Average)
Q_h/kW	19.6 (Cond. 0), 30.8 (Cond. 1)	8.8 (Cond. 0), 14.0 (Cond. 1), 17.9 (Cond. 2)	4.5 (Cond. 0), 6.6 (Cond. 1), 6.9 (Cond. 2), 7.6 (Cond. 3), 11.4 (Cond. 4)
Unmatched coefficient of condensers	1.47 (Average)	1.22 (Average)	1.08 (Average)
COP_R	2.41	3.74	4.50

the DWs in one system are almost the same. Therefore, only the average values are provided.

It can be seen from Fig. 8.16 that, as the number of stages increases, P decreases. The reduction of P mainly results from the reduction of both the exergy destruction of the evaporators and condensers (ΔE_{HE}) and the exergy destruction of the compressor (ΔE_{ε}). The exergy destructions of desiccant wheels are almost constant. It can be seen from Table 8.8 that, as the number of stages increases from 1 to 4, the unmatched coefficients of the DW vary little. However, those for evaporators and condensers decrease from 2.53 to 1.13 and from 1.47 to 1.08. The exergy destruction of all the evaporators (or condensers) decreases from 2.80 kW (or 3.06 kW) in the single-stage system to 1.36 kW (or 1.62 kW) in the two-stage system, and then to 0.97 kW (or 1.23 kW) in the four-stage system.

In conclusion, for the heat pump-driven multi-stage DW systems, as the number of stages increases, the condensing temperature, which represents the heat source temperature, decreases; the unmatched coefficient and the exergy destruction decrease, too. Higher $\mathrm{COP_R}$ values can be obtained. When the number of stages is larger than 4, the rate of improvement slows down due to the insignificant change of the unmatched coefficient. A 4-stage system with $\mathrm{COP_R}$ around 4.5 is preferable.

8.4 Discussion

There are similarities for air dehumidification systems using LD and desiccant wheel (DW). The liquid desiccant and solid desiccant could both be presented in an air psychrometric chart. They are both coupled heat and mass transfer processes between air and desiccant. Temperature difference ΔT and humidity ratio difference $\Delta\omega$ between air and desiccant are the driving forces of heat and mass transfer processes, respectively. States of solution and solid desiccant are influenced with the adsorption or desorption of latent heat of vaporization. A dehumidification and regeneration process is of the essence to complete the handling cycle using LD or DW. Heating source is also required to provide a sufficient driving force to realize the regeneration.

However, there are obvious distinctions between the air handling processes using LD and DW from the perspective of driving forces and system scenarios, which could be summarized as following.

1. Characteristics of the driving forces are different for the processes using LD and DW. ξ_{h} and ξ_{m} are approaching to 1, i.e., both ΔT and $\Delta\omega$ are relatively uniform in the DW process when the facial area ratio and the air flow rate of the two streams of air being both equal to 1. As for the LD process, the distribution of ΔT or $\Delta\omega$ is influenced by the inlet states of air and solution; ξ_{h} and ξ_{m} could be approaching to 1 only when the inlet air is near the desiccant iso-concentration line.

2. The regeneration process in LD system is similar to that in the DW system if heating source is adopted to heat the regeneration air. However, solution could be heated for regeneration in the LD process attributing to the liquidity of fluid. Unmatched coefficient is reduced to a great extent and a regeneration process approaching to the iso-concentration line is realized, which is beneficial to lower the regeneration temperature of liquid desiccant systems.
3. Air handling process in the DW system is always approaching to the isoenthalpic line. Although the driving forces between air and solid desiccant are relatively uniform, the regeneration temperature of the DW process is fairly high due to the isoenthalpic process. A multi-stage process using DW is helpful to lower the required heating source temperature.
4. Besides, there are also distinctions in configurations of the air handling processes using LD and DW. For example, a solution–solution heat exchanger could be set in the LD process, which is responsible to recover heat between the solutions circulating between the regenerator and the dehumidifier. Air–air heat exchanger is recommended between the processed air out of the DW and the inlet regeneration air, which could be used for preheating the regeneration air. However, in DW system, desiccant material directly enters the regeneration region or the dehumidification region after dehumidification or regeneration, which leads to unavoidable heat and cold offset due to the rotation of DW [11].

References

1. THUBERC (2015) Status quo of building energy consumption in China. In: 2015 annual report on China building energy efficiency. China Architecture & Building Press, Beijing, pp 1–39
2. Al-Alili A, Hwang Y, Radermacher R (2015) Performance of a desiccant wheel cycle utilizing new zeolite material: experimental investigation. Energy 81:137–145
3. Enteria N, Yoshino H, Mochida A et al (2015) Exergoeconomic performances of the desiccant-evaporative air-conditioning system at different regeneration and reference temperatures. Int J Refrig 56:81–98
4. Nawaz K, Schmidt SJ, Jacobi AM (2015) A parametric study on mass diffusion coefficient of desiccants for dehumidification applications: silica aerogels and silica aerogel coatings on metal foams. Sci Technol Built Environ 21:637–647
5. Bellemo L, Elmegaard B, Kærn MR et al (2015) Formulation and validation of a two-dimensional steady-state model of desiccant wheels. Sci Technol Built Environ 21:300–311
6. Chua KJ (2015) Heat and mass transfer of composite desiccants for energy efficient air dehumidification: modelling and experiment. Appl Therm Eng 89:703–716
7. De Antonellis S, Intini M, Joppolo CM (2015) Desiccant wheels effectiveness parameters: correlations based on experimental data. Energ Build 103:296–306
8. Liu XH, Jiang Y, Zhang T (2013) Key components of the THIC system: outdoor air handling methods. Temperature and humidity independent control (THIC) of air-conditioning system. Springer Press, Berlin, pp 119–153
9. Liu XH, Li Z, Jiang Y (2009) Similarity of coupled heat and mass transfer between air–water and air–liquid desiccant direct-contact systems. Build Environ 44:2501–2509

10. Liu XH, Jiang Y, Xia JJ et al (2007) Analytical solutions of coupled heat and mass transfer processes in liquid desiccant air dehumidifier/regenerator. Energ Convers Manage 48:2221–2232
11. Tu R, Liu XH, Jiang Y (2013) Performance comparison between enthalpy recovery wheels and dehumidification wheels. Int J Refrig 36:2308–2322
12. Zhang T, Liu XH, Jiang Y (2012) Performance optimization of heat pump driven liquid desiccant dehumidification systems. Energ Build 52:132–144
13. Zhang T, Liu XH, Jiang Y (2013) Performance comparison of liquid desiccant air handling processes from the perspective of matched properties. Energ Convers Manage 75:51–60
14. Bejan A (1997) Advanced engineering thermodynamics, 2nd edn. Wiley, New York
15. Zhang L, Liu XH, Jiang Y (2014) Exergy calculation and analysis of a dehumidification system using liquid desiccant. Energ Build 69:318–328
16. Liu XH, Zhang T, Zheng YW et al (2016) Performance investigation and exergy analysis of two-stage desiccant wheel systems. Renew Energ 86:877–888
17. Tu R, Liu XH, Jiang Y (2015) Lowering the regeneration temperature of a rotary wheel dehumidification system using exergy analysis. Energ Convers Manage 89:162–174

Chapter 9
Emerging Energy Efficient Thermally Driven HVAC Technology: Liquid Desiccant Enhanced Evaporative Air Conditioning

Muhammad Mujahid Rafique, Palanichamy Gandhidasan and Haitham Muhammad Bahaidarah

Abstract Thermal cooling using low-grade energy resources such as solar energy, waste heat, biomass is one of the key solutions to the environmental degradation and fast depletion of primary energy resources. Liquid desiccant-based evaporative cooling is an environment-friendly and cost-effective alternative to the conventional air-conditioning systems due to its energy-saving potential. The idea of a liquid desiccant evaporative cooling system is to combine liquid desiccant dehumidification with an evaporative cooling system in order to advance the overall system performance and to utilize clean and renewable energy resources. In this chapter, desiccant-enhanced evaporative cooling systems have been discussed from variety of aspects including background and need of alternative cooling systems, concept of desiccant-based evaporative coolers, system configurations, as well as developments of technology. The research indicates that the technology of liquid desiccant-based evaporative cooler has a great potential of providing human thermal comfort conditions in hot and humid climatic conditions at the expense of less primary resources of energy as compared to conventional cooling systems. Furthermore, recent developments for liquid desiccant dehumidifiers and evaporative cooling technology along with future view of research in the field of desiccant cooling technology have been presented.

Keywords Thermal cooling · Liquid desiccant cooling · Clean and green technology · Energy and environment · Solar energy · Evaporative cooler

M.M. Rafique · P. Gandhidasan (✉) · H.M. Bahaidarah
Department of Mechanical Engineering, King Fahd University of Petroleum and Minerals, Dhahran 31261, Saudi Arabia
e-mail: pgandhi@kfupm.edu.sa

N. Enteria et al. (eds.), *Desiccant Heating, Ventilating, and Air-Conditioning Systems*, DOI 10.1007/978-981-10-3047-5_9

Nomenclature

E Electric power (kW)
H Specific enthalpy (kJ kg^{-1})
h_{fg} Latent heat of vaporization (kJ kg^{-1})
$\dot{m}$ Mass flow rate (kg s^{-1})
M Moisture removal rate (kg s^{-1})
T Temperature (°C)

Greek Symbols

ε Effectiveness (–)
ω Humidity ratio ($kg_v\ kg_a^{-1}$)
β Equivalent conversion coefficient (–)

Subscripts

a Air
amb Ambient
p Process
r Regeneration
s Supply

9.1 Introduction

During the operation of an air-conditioning system, latent and sensible loads need to be controlled simultaneously to provide thermal comfort conditions. The two components of the load are described by the sensible heat ratio which is the ratio between sensible load to the total load. Smaller the value of sensible heat ratio, larger the value of latent cooling load. The value of sensible heat ratio is about 0.75 for the commonly used conventional vapor compression air-conditioning systems which means that 75% capacity of the system is used to control the sensible load and the remaining 25% for the latent load. Hence, the conventional cooling systems can provide the comfort conditions only when sensible heat ratio is greater than 0.75 [1]. The value of designed sensible heat ratio can be significantly less than 0.75 for hot and humid climates and which cannot be achieved using a conventional air-conditioning system, and hence, thermal comfort conditions cannot be achieved. Further, the condensate can evaporate back to the conditioned space which may result in increased humidity level in the comfort zone [2].

Some alternative low energy consuming cooling systems which directly utilize the thermal energy and also reduce the emission of greenhouse gases are desiccant and absorption cooling. Among these systems, desiccant cooling is the main focus

of many researchers for the past few years. The desiccant-based evaporative cooling is a combination of a desiccant dehumidifier and evaporative cooler. The energy used in this system is only to drive the fans and water pump and to regenerate the desiccant during the regeneration process. This energy can be provided from any low-grade thermal energy source such as solar energy, waste heat, biomass. This system can operate on wide range of sensible heat ratios because of the individual control of sensible and latent cooling loads.

9.2 Liquid Desiccant-Based Evaporative Cooling

In general, evaporative cooling systems are applied when the wet bulb temperature does not exceed 25 °C frequently. The evaporative cooling units can operate with a high coefficient of performance (COP) in dry climatic conditions. But because of the air saturation of the surrounding air in humid climates, the effectiveness of these cooling systems drops remarkably. That is why the individual use of evaporative cooling is best suited for sensible cooling, while for both sensible and latent cooling, it is used in conjunction with some other dehumidification system. The application of desiccant-based dehumidification will allow the effective use of direct as well as indirect evaporative coolers in hot and humid climates [3].

The liquid desiccant dehumidifier comprises of some desiccant material (salts of halides, zeolites, etc.). A desiccant material is one which absorbs and holds water vapor from the humid air by the process of absorption. The evaporative desiccant cooling system comprises of a desiccant dehumidifier, a regenerator and an evaporative cooler. The air is dehumidified using desiccant dehumidifier, and its temperature is lowered using evaporative cooler or some other sensible cooling device. For continuous operation of the system, the desiccant dehumidifier is regenerated by using heat energy provided by solar collectors or some other low-grade source of energy. Some heat recovery units are also utilized to make the system more efficient.

In desiccant-based evaporative cooling technique, latent and sensible loads are separately removed using desiccant dehumidification system and cooling unit, respectively. The type of cooling units used to reduce the temperature of dehumidified air mainly defines the type of hybrid desiccant cooling system. The selection of the cooling unit depends on operating conditions, that is, humidity and temperature of the air.

The liquid desiccant-based evaporative cooling systems lead to a remarkable reduction in electrical energy consumption as compared to conventional units, and it also reduces the number of discomfort hours inside the conditioned space. A liquid desiccant dehumidifier using lithium bromide as liquid desiccant in conjunction with direct evaporative cooler without the circulation of air was proposed by Oliveira et al. [4]. The simulation results showed that this alternative novel air-conditioning system has a great potential to replace conventional air-conditioning systems with initial cost lower than the conventional system.

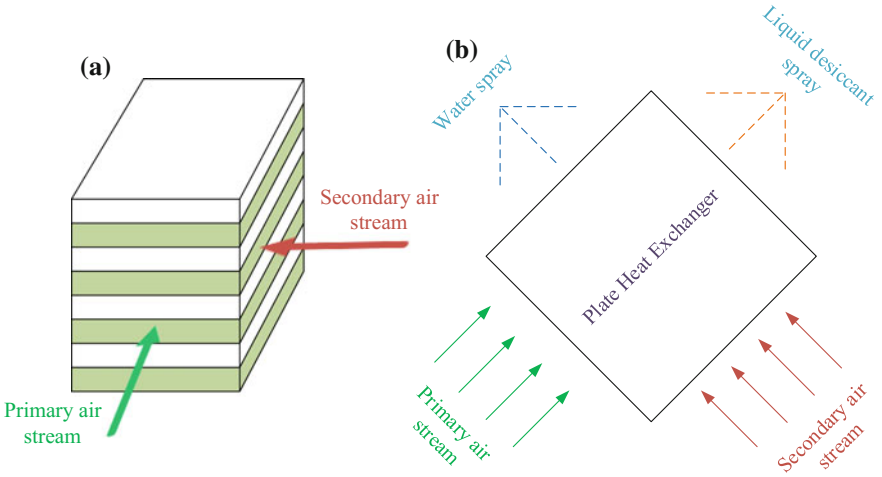

Fig. 9.1 Schematic of compact cross-flow-type plate heat exchanger [5]

Saman and Alizadeh [5] proposed a liquid desiccant cooling system in conjunction with an indirect evaporative cooling system as shown in Fig. 9.1. It is a plate-type heat exchanger (PHE) of counter-flow configuration having a number of air–water and desiccant solution passages separated from each other using plastic thin plates. The thin plates also provide contact surface for heat and mass transfer between air–water and desiccant solution. Secondary air which is cooled by direct evaporative cooler is brought in contact with the water on one side of the separating plate. The cooled secondary air removes heat from the primary air on the other side of the plate, thus making use of indirect evaporative cooling. This primary air is dehumidified concurrently using desiccant solution sprayed on cross-flow contact area. The performance of the proposed model was observed theoretically and then experimentally under climatic conditions of Brisbane, Australia. It was found that the effectiveness of the evaporative cooler could reach 75% for the exchanger angle (angle made by the direction of desiccant spray with the horizontal) of 45°.

Many researchers have studied the heat and mass transfer of liquid desiccant-enhanced evaporative cooling systems applying energy and mass balance equations for individual components without analyzing the performance of overall system. Radhwan et al. [6] mathematically modeled a solar-assisted liquid desiccant (calcium chloride)-based evaporative cooling system and observed the system performance for long-term operation under conditions of Jeddah, Saudi Arabia. System thermal ratio (STR), desiccant replacement factor (DRF) and solar utilization factor (SUF) were defined to observe the system performance for different conditions of weather. The results showed that system has a good performance for hot and humid climates. Bellemo et al. [7] numerically studied dew point evaporative cooler, also called as regenerative indirect evaporative cooler, which is a part of desiccant cooling system and analyzed its performance for different flow rates of air, inlet air conditions and

recirculation fractions. The results showed that cooling capacity of dew point evaporative cooler was maximized for recirculation fraction of about 0.3 and supply conditions were mostly affected by the inlet air humidity ratio. Because of the regenerative arrangement, dew point evaporative cooler did not require secondary air stream as required in indirect evaporative cooler.

9.3 Advantages of Liquid Desiccant-Aided Evaporative Cooling

The liquid desiccant cooling systems are energy-efficient, ecofriendly and cost-effective alternative to conventional air-conditioning. The independent control of latent and sensible loads and use of alternative energy sources for the operation of these devices is very important factor. The major advantages of liquid desiccant-enhanced evaporative cooling technology in comparison with the conventional cooling systems are:

- It can be used for hot and humid climates because evaporative cooling alone is not feasible for such conditions.
- A lot of energy can be saved as compared to vapor compression cycle because no reheating is required.
- Environment-friendly system because of no use of refrigerant which affects the ozone layer.
- Separate and better control of sensible and latent loads. The liquid desiccant dehumidifier controls the latent part and the evaporative cooler controls the sensible load.
- The overall system has low maintenance cost because it operates at almost atmospheric conditions.
- Low-grade energy such as solar, waste heat, and biomass can be effectively used to drive the system.
- The concentrated liquid desiccant can be stored in an uninsulated tank.
- Heat exchanger can be used for precooling and preheating the desiccant solution.
- Small pump is required for circulation of fluid.

The above-mentioned advantages of desiccant technology over conventional units are causing a fast development in this technology and its applications are spreading in both residential and industrial sectors. Jiang et al. [8] also compared liquid desiccant cooling system and conventional air-conditioning systems which are listed in Table 9.1.

Table 9.1 Comparison between different cooling techniques [8]

Parameter	Mechanical vapor compression	Evaporative cooling	Desiccant-based evaporative cooling
Cost of operation	High	Low	Low
Input energy resource	Electricity, natural gas	Low-grade thermal energy	Low-grade energy, e.g., solar energy, waste heat
Latent load control	Average	Low	Accurate
Sensible load control	Accurate	Accurate	Accurate
Quality of indoor air	Average	Good	Very good
System installment	Average	Average	Slightly complicate
Emission of greenhouse gases	High	Low	Low
Market potential	Dominate the air-conditioning market	Limited application	Immature technology with limited application

9.4 Basic Principle and Types of Evaporative Cooler

Evaporative cooling is an energy-saving, cost-effective, simple and environment-friendly air-conditioning technique. These systems are suitable for dry and high-temperature climatic conditions [9] and can be used as direct contact evaporative cooling unit, indirect contact evaporative cooling or as combination of both. Technologies which make use of evaporative cooler to cool down the air without adding moisture content to it are commonly known as indirect evaporative cooling. In the indirect evaporative system, the process air stream does not interact directly with the cooling fluid stream rather it is cooled sensibly. The cooling process inside an indirect evaporative cooler is represented on psychrometric chart shown in Fig. 9.2. The temperature of air is lowered using some type of heat exchange arrangement in which primary air is cooled sensibly using a secondary air stream. The secondary air is cooled using water. In the indirect evaporative cooling system, both dry and wet bulb temperatures of the air are lowered. The indirect evaporative cooling has an efficiency of 60–70%. The schematic and flow arrangements inside the indirect evaporative cooler are shown in Figs. 9.3 [10] and 9.4, respectively.

In direct evaporative cooling system, moisture is added to the cooled air stream because process air comes in direct contact with the cooling water. In direct evaporative cooling system, the temperature of the process air is lowered because of the high moisture content in the air. That is why direct evaporative cooler is only suitable for hot and dry climates, and for hot and humid climates, indirect evaporative cooler is preferred. The wet bulb temperature is an important parameter for the performance of direct evaporative cooler. The effectiveness of a well-made

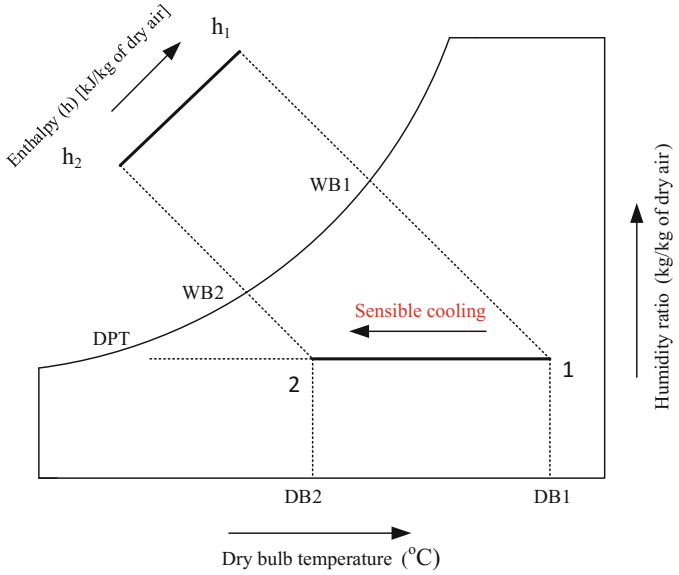

DPT-Dew point temperature , WB-Wet bulb temperature , DB-Dry bulb temperature

Fig. 9.2 Cooling process representation of indirect evaporative cooler on psychrometric chart

direct evaporative cooler reaches an effectiveness of approximately 85% [11]. Both the schematic and psychrometric processes of the direct evaporative cooler are shown in Fig. 9.5. The ambient air comes in direct contact with the sprayed water which decreases the temperature of the supply air and adds moisture content to it as shown in the psychrometric chart.

9.5 Liquid Desiccant Materials

A desiccant material attracts the water vapor toward itself, and these materials are used where air of low dew point is needed. The strength of a liquid desiccant can be measured by its equilibrium vapor pressure, which is water vapor pressure that is in equilibrium with liquid desiccant material. The vapor pressure exponentially increases with the temperature of the desiccant and also increases as the water is absorbed by the desiccant, that is, equilibrium vapor pressure will be higher for a dilute liquid desiccant than for a concentrated one [12]. A good desiccant should have the following properties:

- Large saturation absorption capacity
- Low regeneration temperature
- Low viscosity

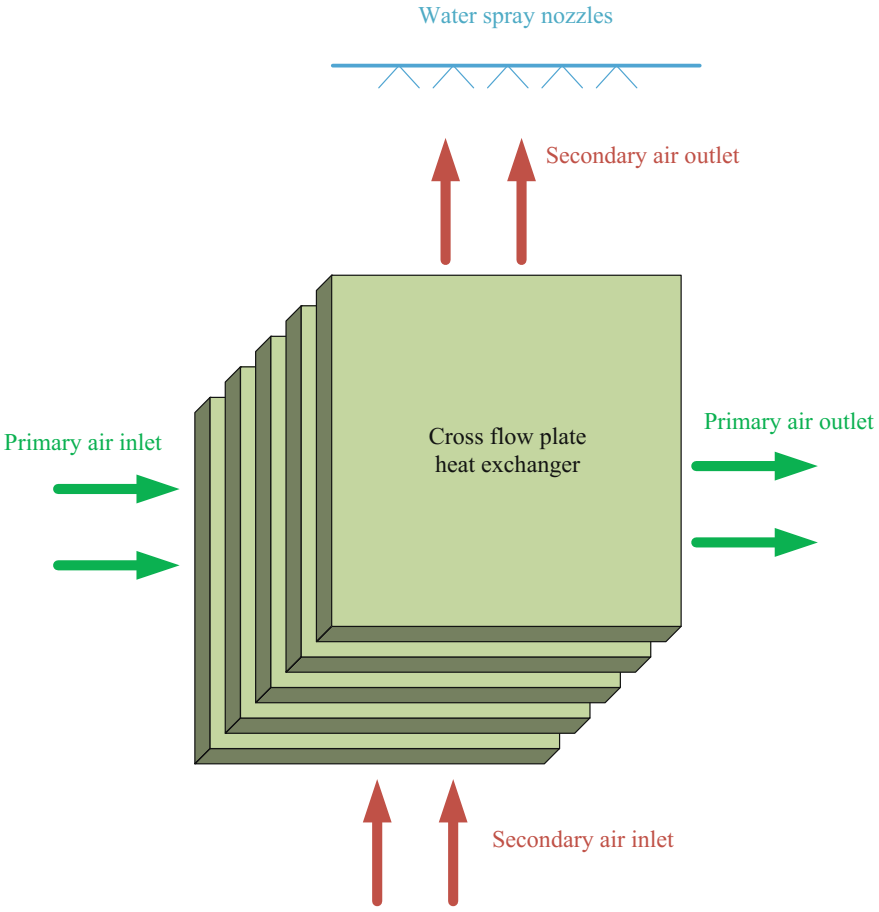

Fig. 9.3 The schematic of the indirect evaporative cooler [10]

- High heat transfer
- Nonvolatile
- Non-corrosive
- Odorless
- Non-toxic
- Nonflammable
- Stable
- Inexpensive

Surface tension plays important role in static holdup and surface wetting of heat and mass exchanger of liquid desiccant system.

The earliest used liquid desiccant is triethylene glycol, but its use is limited because it has high viscosity which causes system operation unstable because of

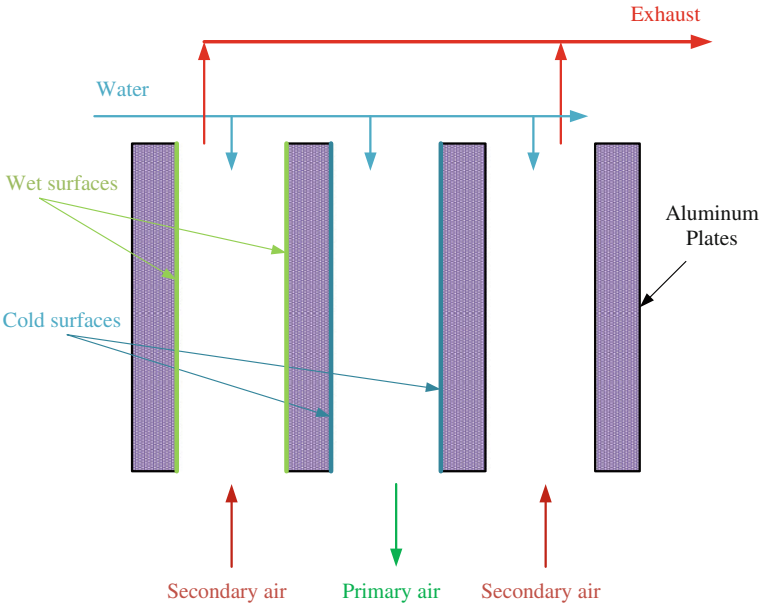

Fig. 9.4 Flow arrangement inside indirect cooler

liquid residence. They are low toxic and compatible with most of the metals, but all glycols are volatile because of very low surface vapor pressure, and some of it evaporates with air into the conditioned space which sometimes makes them unacceptable for air-conditioning applications [13]. The dew point temperature of air by using a solution of triethylene glycol (96%) and water (4%) can be achieved with lithium chloride (LiCl) solution concentration of 42% by weight. But at equilibrium point, the molar concentration of the glycol in the air will be in the order of 1% that of the water vapor which means annual loss of triethylene glycol in air-conditioning applications will be very high.

Salts of halides such as LiCl and LiBr can dry air to 15 and 6% relative humidity, respectively, but these salts are naturally corrosive. LiCl is a very good desiccant because at ambient conditions, it will not vaporize and it has low viscosity which reduces the required pumping power, but its mixing with the process air must be avoided. Halide salts are relatively expensive in nature [13].

Another alternate of low-corrosive and nonvolatile desiccants is salts of weak organic acids such as potassium or sodium formate and acetate. Potassium acetate is less expensive, and it can dry air up to 25% relative humidity, but its viscosity becomes very high. At a temperature of 27 °C and concentration of 70% by weight, potassium acetate has a viscosity of about 28 cp (0.028 Pa/s), but LiCl solution of concentration of 43.l% by weight at the same temperature has almost half of that viscosity [14]. Although potassium formate is a relatively weaker desiccant as

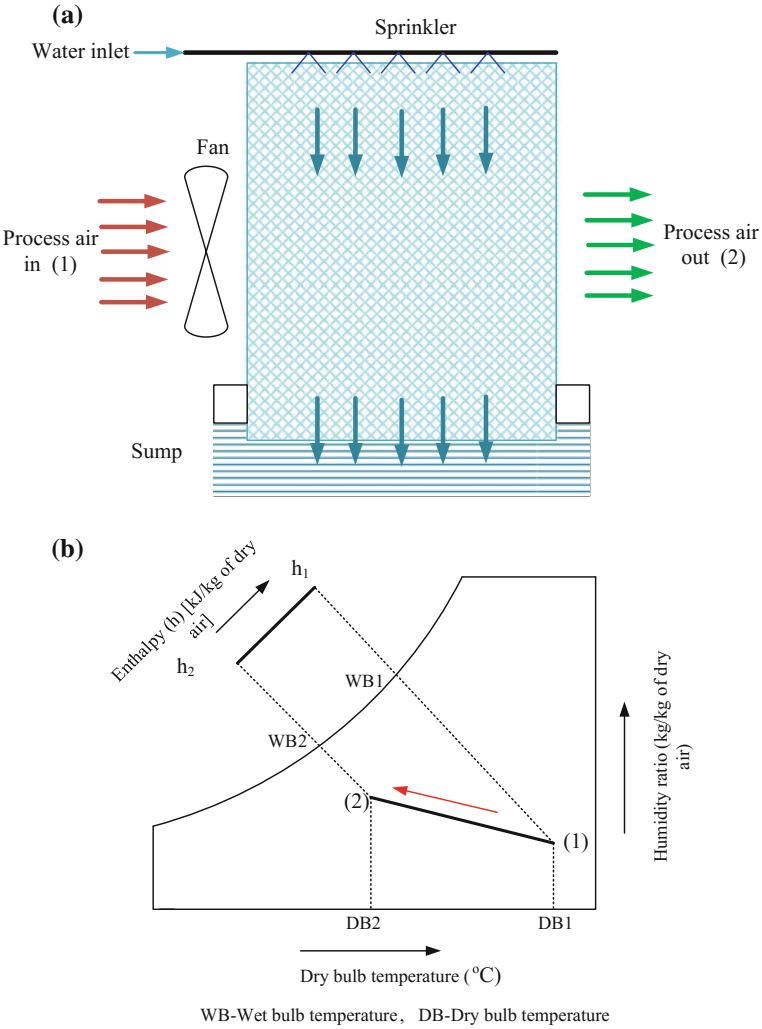

Fig. 9.5 Direct evaporative cooler **a** schematic diagram, **b** psychrometric representation

compared to LiBr or LiCl, it has the ability to dry the air below 30% relative humidity and it can be a good alternative desiccant for many applications [15].

From the various liquid desiccants, some figures of merit can be developed for the selection of suitable desiccant. These figures of merits are listed in Table 9.2 [16]. The term heat of mixing or differential heat of solution represents the amount of heat liberated by absorption of water into a solution of desiccant at a fixed composition. A relatively low heat of mixing is desirable. Parasitic power losses represent the pumping power required for the circulation of desiccant solution.

Table 9.2 Weighing factors and figures of merit for desiccant selection [16]

Characteristics	Weighting factor	Figure of merit
Safety	1.0	Lethal dose (LD50)
Corrosion	0.8	Corrosion rate
Mass transfer potential	0.8	Equilibrium vapor pressure
Heat of mixing	0.6	Energy/kg of absorbed water
Cost of desiccant	0.5	Cost/100 kg of solution
Heat transfer potential	0.5	Thermal conductivity
Parasitic power losses	0.3	Viscosity

9.6 Liquid Desiccant Dehumidifier

The liquid desiccant dehumidifier comprised of a desiccant material which removes moisture from the air by the process of dehumidification. Different desiccant materials attract the moisture from the air at different capacities. The commonly used desiccant materials are calcium chloride, lithium bromide and lithium chloride. The desiccant dehumidifier is regenerated using the heat. Several researchers used solar energy as the input source for regeneration of desiccant dehumidifier. The process of dehumidification and regeneration of a desiccant is illustrated in Fig. 9.6 [17]. The desiccant removes moisture from the air (1–2), and desiccant is regenerated by removing moisture from it using hot air (2–3). During process (3–1), desiccant is cooled down again. Solar energy can be used effectively to provide heat for regeneration.

The application of a desiccant dehumidification unit is for transfer of mass and heat between process air and the desiccant solution. For a high performance, liquid desiccant dehumidifiers should have the following characteristics:

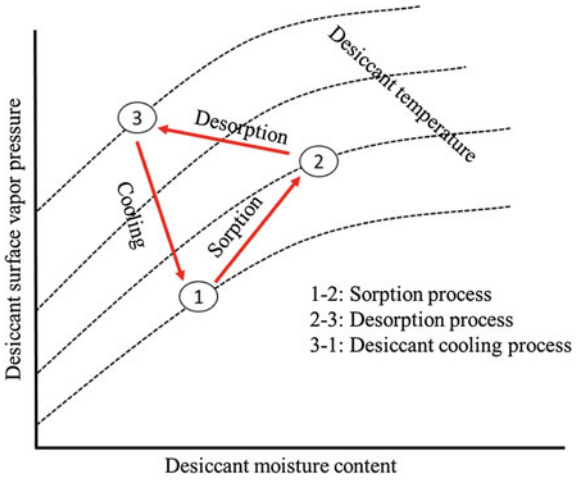

Fig. 9.6 Dehumidification and regeneration process of a desiccant [17]

- High rates of mass and heat transfer.
- Low pressure drop of the process air stream while passing through the dehumidifier.
- Small liquid side resistance to moisture diffusion.
- Large surface contact area per unit volume.
- In order to avoid corrosion, the dehumidifier should be made of a material compatible with the liquid desiccant. The material should be inexpensive too.
- There should be no liquid desiccant carryover with the process air.

Liquid desiccant dehumidifiers are classified as adiabatic and internally cooled. The air directly contacts with the desiccant solution in the adiabatic dehumidifiers, while in internally cooled dehumidifiers apart from the contact between two streams, desiccant solution is cooled down using some cooling medium to increase the system performance.

9.6.1 Adiabatic Dehumidifiers

One of the adiabatic dehumidifiers, namely packed bed dehumidifier, is the main focus of most of the researchers. Fumo and Goswami [18] modeled a packed bed dehumidifier for heat and mass transfer using packing of polypropylene having a volumetric surface area of 210 m^2/m^3 and experimentally measured its performance with LiCl solution. They concluded that because of the high surface tension, solution of LiCl did not wet the packing uniformly. An empirical formula for estimation of fraction of bed wetted surface area was developed, and the performance results of the theoretical model were found in good agreement with the measured results.

Liu et al. [19] used structured packing with a solution of LiCl for estimation of a cross-flow desiccant dehumidifier performance. They presented the experimental results in terms of rate of moisture removal and the dehumidifier performance for various values of desiccant flow rates, air flow rates, desiccant and air inlet temperature, desiccant inlet concentration, and specific humidity of inlet air.

Liu and Jiang [20] presented an analytical solution for the coupled heat and mass transfer for a packed bed system by using the assumptions of minimal change in desiccant concentration and Lewis number of one. The results of analytical solutions are closely in agreement with exact numerical solutions and with experimental data.

Jain and Bansal [21] used empirical relations to predict the performance of packed bed dehumidifiers comprising of three different liquid desiccant materials ($CaCl_2$, LiCl and triethylene glycol). It was found that the value of dehumidifier effectiveness varies from 10 to 50% or more. The results also showed that more comprehensive empirical models are required for better estimation of liquid desiccant dehumidifier performance.

Katejaneken et al. [22] experimentally studied a liquid desiccant (LiCl) ventilation preconditioning system. The results showed that the system can reduce the relative humidity by about 11%, while the temperature remains almost equal to the ambient air temperature. It has also been found that evaporation rate remains always greater than the absorbed moisture by the liquid dehumidifier which makes the system well feasible for continuous operation.

Seenivasan et al. [23] investigated the effect of different parameters such as desiccant concentration, desiccant solution temperature, desiccant and air flow rates, and relative humidity on the effectiveness of liquid desiccant dehumidifier using $CaCl_2$ as the desiccant material. The optimum values of these parameters were found for high effectiveness of dehumidifier under the following operating conditions: desiccant temperature 25 °C, concentration 40%, desiccant flow rate 2.25 kg/m^2 s, air flow rate 1 kg/m^2 s and relative humidity (RH) 85%.

Gommed et al. [24] experimentally measured the performance of packed bed heat and mass exchangers using LiCl solution. The copper and polypropylene tubes were used as contact surfaces in the dehumidifier. The results showed that the copper tubes are more active to corrosion while in contact with the desiccant solution, and on the other hand, wetting is much difficult while using polypropylene tubes. Then, the researchers employed adiabatic packed beds of 285 m^2/m^3. The results showed that dripping of LiCl solution over the packing with suitable drop size to avoid carryover of the desiccant is better than spraying.

Chen et al. [25] used four cross-flow packed bed dehumidifiers with 42–48% (by weight) LiBr solution to conduct a field test for liquid desiccant cooling system. The air flows in series through all the four beds. The flow of air and the desiccant was in counter flow so that the air can flow in direction of increasing desiccant concentration through the bed. Hot water at about 69 and 73 °C was used as regeneration sources for the desiccant. The obtained results showed that the unit had an average COP of 1.5.

So'Brien and Satcunanathan [26] proposed a liquid desiccant cooling system with simultaneous dehumidification of air and regeneration of desiccant solution without using any mechanical circulation. The proposed system consists of two chambers made of stainless steel. One chamber is dehumidifying chamber, and the other one is regenerating chamber. The chambers are interconnected by two passages. The upper passage is filled with porous material, and lower one is unfilled. In order to avoid the mixing between the air flowing over the surface of the solution in the dehumidifying chamber and that in the regenerating chamber, the both chambers are filled with liquid desiccant to the level where the porous material is completely submerged. The COP of the system was found in the order of 0.3 even at lower regeneration temperature of 50 °C which makes the use of solar energy feasible for the continuous operation of the system.

The adiabatic dehumidifiers are widely used for commercial as well as residential cooling applications because it allows large contacting area between air and desiccant with simple configuration. The heat and mass transfer efficiency of these dehumidifiers is very high, but it causes a large pressure drop on process air side while flowing through the packing material. Another drawback of these dehumidifiers is the

desiccant temperature increase during removal of moisture from the process air which decreases the dehumidifier performance and in turn air temperature and humidity cannot be controlled efficiently. Also, for complete wetting of packing material and to avoid desiccant solution temperature to rise, the flow rates should be high in packed bed dehumidifiers. The condition of complete wetting can be fulfilled at low desiccant flow rates by the addition of surfactants to the desiccant or by increasing surface energy of the packing by different treatments. However, again in order to keep the desiccant at low temperature, a high flow rate will always be required.

9.6.2 Dehumidifier with Inner Cooling

In order to avoid the above problems associated with the adiabatic dehumidifiers and to remove heat generated inside the dehumidifier, dehumidifier with inner cooling is gaining attention, as shown in Fig. 9.7. These are good alternative in which high wetting of surface as well as lower temperature of desiccant solution can be achieved without high flow rates and desiccant droplets carryover as well as the higher pressure drop can be avoided. During the dehumidification, the embedded cooling coils in the packing material removes heat from the dehumidifier and the outer insulation layer serves to prevent transfer of heat from outside air to the dehumidification unit. Scalabrin and Scaltriti [27] simulated a dehumidifier with internal cooling and heated regenerator of an open processed summer air-conditioning system. At a low temperature of liquid desiccant, more moisture can be absorbed because of low vapor pressure.

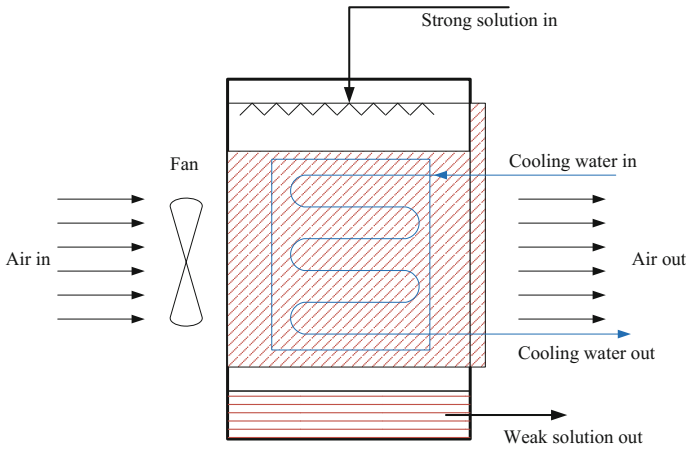

Fig. 9.7 Schematic diagram of dehumidifier with inner cooling

The embedded cooling coils in the consecutive plates of the packing layers are another possible configuration for inner cooled dehumidifier to remove the heat during moisture removal process. In order to increase the desiccant and air contacting area, corrugated plates can be used instead of consecutive plates [28]. Yoon et al. [29] proposed dehumidifier with different channels with one for the flow of air and desiccant solution and the other for the flow of cooling water or cooling air.

The droplet carryover from liquid desiccant dehumidifiers in which halide salts are used is a dangerous and discouraging issue for air-conditioning applications. This problem can be eliminated by using internally cooled dehumidifiers which can work at relatively very low flow rates.

An internally cooled conditioner does not require high thermal capacitance of the desiccant to lower the desiccant temperature during absorption, but for complete wetting of the packing, still high flow rate is required. Coil- or tube-type dehumidifiers are rarely used with halide salts desiccants because of corrosion and high cost. Figure 9.8 shows an internally cooled/heated liquid desiccant dehumidification system [30]. The system uses LiCl as desiccant material and water as cooling fluid. It was concluded that temperature of the desiccant solution plays a major role in the system performance. Humidity of air, flow rate of air, solution concentration and flow rate of solution also significantly influence the performance of the system.

Khan and Sulsona [31] presented an internally cooled desiccant dehumidifier in which solution of LiCl is uniformly sprayed over evaporator coil bundle as shown in Fig. 9.9. The desiccant and air flow in counter-flow arrangement. The cooling and dehumidification of outside air are achieved by direct contact of air with the

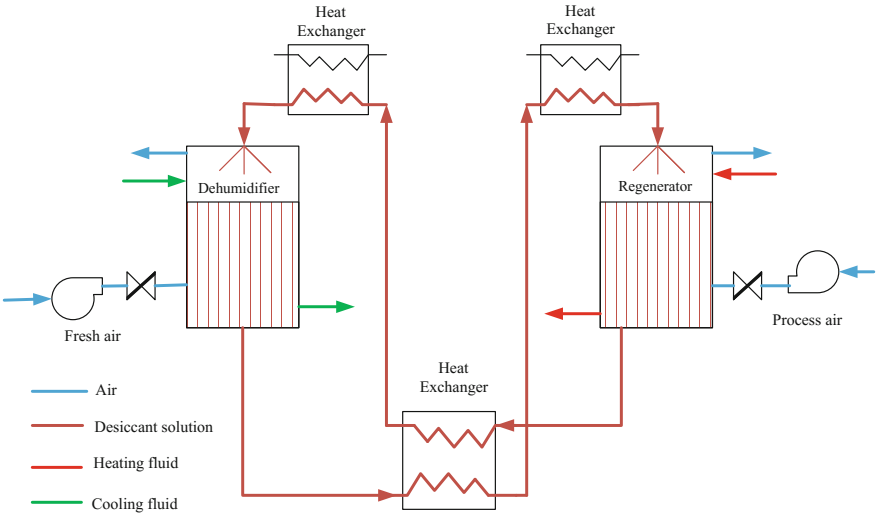

Fig. 9.8 Schematic of internally cooled/heated liquid desiccant dehumidification [30]

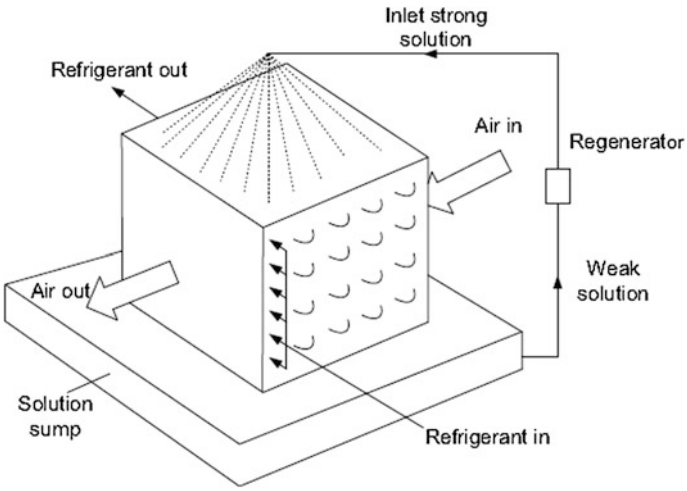

Fig. 9.9 Schematic of spray-type internally cooled dehumidifier [31]

desiccant solution on the coil surface. The weak desiccant solution is collected in a sump underneath the tube bundle. The effect of desiccant temperature and process air temperature on the system performance was analyzed in this study.

9.7 Performance Parameters

The primary purpose of the desiccant dehumidifier is to dehumidify the air. The dehumidification capacity is represented by moisture removal which is the amount of water desorbed from the process air by the desiccant. Moisture removal capacity of the desiccant dehumidifier can be written as:

$$M = \dot{m}_{\mathrm{p}} \times (\omega_{\mathrm{a,in}} - \omega_{\mathrm{a,out}}) \tag{9.1}$$

Latent effectiveness of the dehumidifier is given as:

$$\varepsilon = \frac{(\omega_{\mathrm{a,in}} - \omega_{\mathrm{a,out}})}{(\omega_{\mathrm{a,in}} - \omega_{\mathrm{a,outideal}})} \tag{9.2}$$

where $\omega_{\mathrm{a,out\,ideal}}$ represents the ideal specific humidity ratio. Assuming that at this point, air is completely dehumidified, $\omega_{\mathrm{a,outideal}} = 0$.

Dehumidification coefficient of performance (DCOP) is another parameter used to represent the desiccant dehumidifier capacity to dehumidify the air. For the different mass flow rates of process and regeneration air, DCOP is given as:

$$\mathrm{DCOP} = \frac{\dot{m}_{\mathrm{p}} \times h_{\mathrm{fg}} \times (\omega_{\mathrm{a,in}} - \omega_{\mathrm{a,out}})}{\dot{m}_{\mathrm{r}} \times (h_{\mathrm{r}} - h_{\mathrm{amb}})} \tag{9.3}$$

A higher DCOP indicates a better system performance because the energy input to the regeneration air is utilized in a better way or less heat is being used to heat up the desiccant.

The sensible energy ratio (SER) is also used when evaluating the desiccant dehumidifier. The SER can quantify additional sensible load to be handled by some additional cooling mechanism at the downstream such as an evaporative cooling or a vapor compression cycle. The SER is given by:

$$\mathrm{SER} = \frac{\dot{m}_{\mathrm{p}} \times (T_{\mathrm{a,out}} - T_{\mathrm{a,in}})}{\dot{m}_{\mathrm{r}} \times (T_{\mathrm{r}} - T_{\mathrm{amb}})} \tag{9.4}$$

For better dehumidification performance of the desiccant system, the value of SER should be lower. The higher value of SER means more cooling load on the cooling device because of higher temperature of process air at exit of desiccant dehumidifier. Lower values of SER mean that the desiccant dehumidifier is creating a lower sensible cooling load, which indicates better performance of the system.

The cooling provided by the desiccant system is defined as cooling capacity. The difference in enthalpy between outdoor and supply air is used to represent overall cooling capacity because it includes both sensible and latent loads.

$$\text{Cooling capacity}(\mathrm{CC}) = \dot{m}_{\mathrm{p}}(h_{\mathrm{amb}} - h_{\mathrm{s}}) \tag{9.5}$$

The overall performance of the system is represented by COP.

$$\mathrm{COP} = \frac{\mathrm{CC}}{E_{\mathrm{thermal}} + \frac{(E_{\mathrm{cool}} + E_{\mathrm{pumping}})}{\beta}} \tag{9.6}$$

where β is equivalent conversion coefficient of electric power and thermal energy and its value is taken as 0.3 [32].

The ratio between the CC and electrical energy consumption is given by electrical coefficient of performance (ECOP), while ratio between CC to consumption of thermal energy is represented by thermal coefficient of performance (TCOP).

$$\mathrm{ECOP} = \frac{\mathrm{CC}}{E_{\mathrm{cool}} + E_{\mathrm{pumping}}} \tag{9.7}$$

$$\mathrm{TCOP} = \frac{\mathrm{CC}}{E_{\mathrm{thermal}}} \tag{9.8}$$

9.8 Developments of Liquid Desiccant-Enhanced Evaporative Air-Conditioning

9.8.1 Developments of Liquid Desiccant Dehumidifier

The desiccant solution must be cooled before it is pumped to the desiccant dehumidifier, but temperature increase in liquid desiccant solution as it absorbs moisture will reduce the heat and mass transfer potential between air and desiccant solution. This problem may lead to the lower overall performance of the single-stage dehumidification system. To overcome this adverse temperature increase, the idea of multistage liquid desiccant dehumidifier was presented by Jiang et al. [8]. In this system, several desiccant dehumidifiers are connected in series as shown in Fig. 9.10. The desiccant solution is cooled in every stage of the dehumidifier separately, to increase the overall system performance. On the other hand, instead of cooling/heating the solution internally in each stage of dehumidifier, the system performance can be improved by cooling/heating the desiccant solution using some external auxiliary cooling/heating medium [33]. Li [34] studied and compared irreversible losses for multistage dehumidifier and conventional single-stage dehumidifier.

Xiong et al. [35, 36] observed an increase in the system COP from 0.23 to 0.72 by using a two-stage novel liquid desiccant cooling system. On the process side, the air is first dehumidified in the first dehumidifier using solution of $CaCl_2$, and then, in the second dehumidifier air is further dehumidified by solution of LiCl up to the desired humidity of air. Kumar et al. [37] carried out the performance analysis of

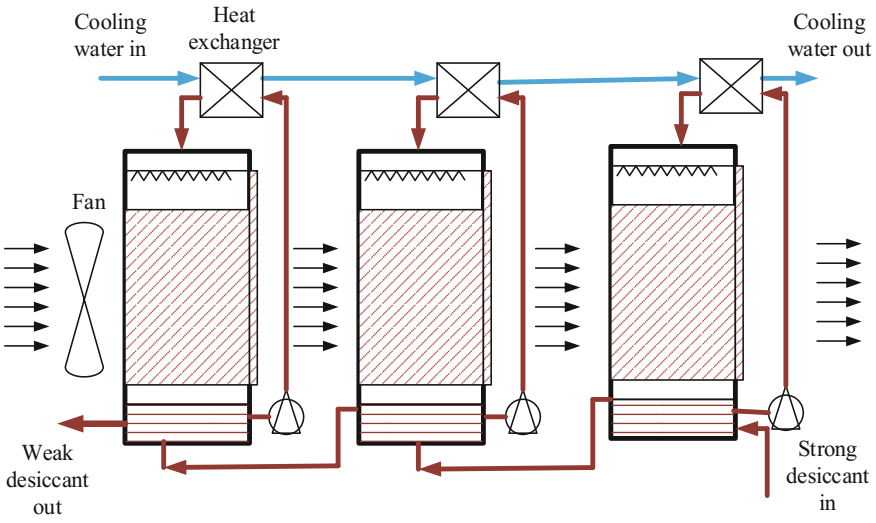

Fig. 9.10 Multistage liquid desiccant dehumidifier [8]

falling film liquid desiccant dehumidifier operating on two new liquid desiccant cycles (multi-absorber cycles) and found that performance of the system is improved significantly by using these cycles.

The parallel-plate membrane modules can be used as air-to-air heat and mass exchanger. Figure 9.11 [38] shows parallel-plate membrane module used as liquid desiccant dehumidifier. The flow channels were created by keeping the equal spacing between the membrane modules. The desiccant solution and air flow through the flow channels in counter-flow arrangement. The desiccant solution absorbs the moisture from the air through the membrane, eliminating the problem of desiccant carry over.

A flat-plate internally cooled dehumidifier using water as the cooling fluid is shown in Fig. 9.12 [39]. Cooling water is circulated through the polypropylene double plates. The air flows upward, and desiccant solution flows downward across

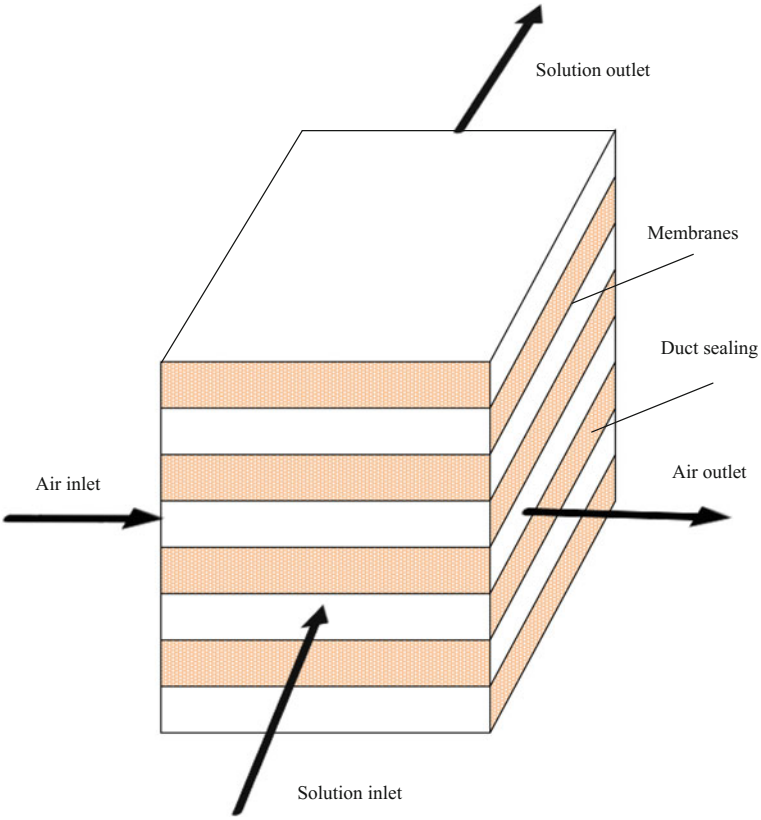

Fig. 9.11 Structure of a parallel-plate membrane module [38]

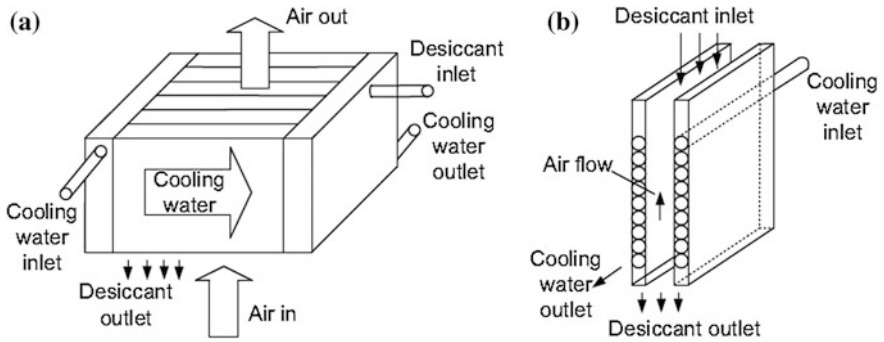

Fig. 9.12 Internally cooled vertical flat-plate dehumidifier [39]. **a** Side view; **b** inner view

the polypropylene plates. For uniform flow of the desiccant solution, a desiccant distributer is provided on top of each plate.

Cheng [40] developed a liquid desiccant dehumidifier using fin-plastic tube heat exchanger. The developed system has great potential for corrosion prevention and can be used as internally cooled/heated dehumidifier/regenerator. Kim et al. [41] investigated the annual operating energy performance of a desiccant-based evaporative cooling-assisted 100% outdoor air system. The proposed system shows operating energy savings of 82% over the conventional cooling system during the summer, and 54 and 37% in the winter and the intermediate season operations, respectively. A new energy-efficient refrigeration system subcooled by liquid desiccant dehumidification and evaporation was proposed by She et al. [42]. Results show that the proposed refrigeration system achieves significantly higher COP than conventional vapor compression refrigeration system. The maximum COPs of the hybrid systems using hot air and ambient air are 18.8 and 16.3%, respectively, higher than that of the conventional vapor compression refrigeration system under varied conditions.

Rotary liquid desiccant dehumidifier is another possible configuration which provides the research community with practical and reliable liquid desiccant rotary dehumidification system [43]. As desiccant dehumidifier is the most crucial component of the desiccant cooling system, it has a significant effect on overall system performance. The rotary liquid desiccant dehumidifier is a rotary wheel of radius R and width L. The rotor consists of number of identical narrow slots uniformly distributed over its cross section as shown in Fig. 9.13. The slots are covered with porous media impregnated with solution of liquid desiccant. The wheel has separate sections for the flow of process air and regeneration air. One-fourth portion of the wheel is regenerating the desiccant, and three-fourths are for process air. These two streams of air flow in counter arrangement.

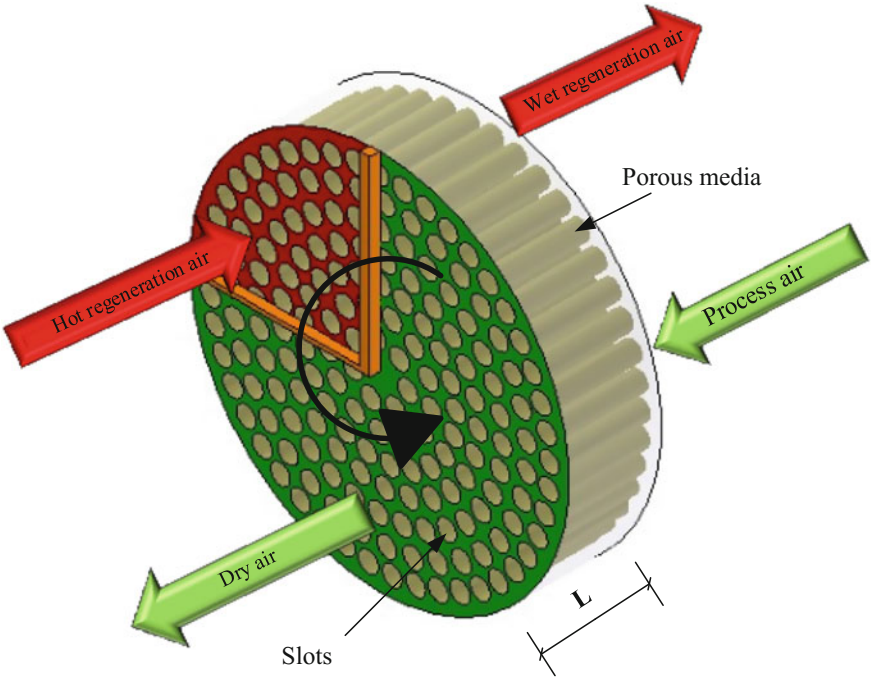

Fig. 9.13 Schematic of rotary liquid desiccant dehumidifier [43]

9.8.2 Developments in Evaporative Cooling Research

Because of the increasing interest and significant potential of the technology, various methods of evaporative cooling have been investigated by many researchers. Recently, evaporative-based air-conditioning units are not commonly used as small household units. Alonso et al. [44] developed a universal heat and mass transfer model for design and optimization of indirect evaporative coolers. The results of detailed numerical study showed that transfer of heat from gas–liquid interface is determined by the latent heat transfer.

Jain and Hindoliya [45] tested a regenerative evaporative cooler. It was developed by adding water-to-air heat exchanger in the path of outgoing air stream from the direct evaporative cooler. It was found that the COP and efficiency of the unit increase 20–25% because of the higher cooling capacity of regenerative evaporative cooler. Kulkarni and Rajput [46] theoretically analyzed the performance of two-stage evaporative cooler for the climatic conditions of Bhopal, India. The results showed that for the air flow rate of primary air 0.3–1.25 kg s^{-1}, the effectiveness of indirect evaporative cooler varied from 0.95 to 0.82. For the two-stage

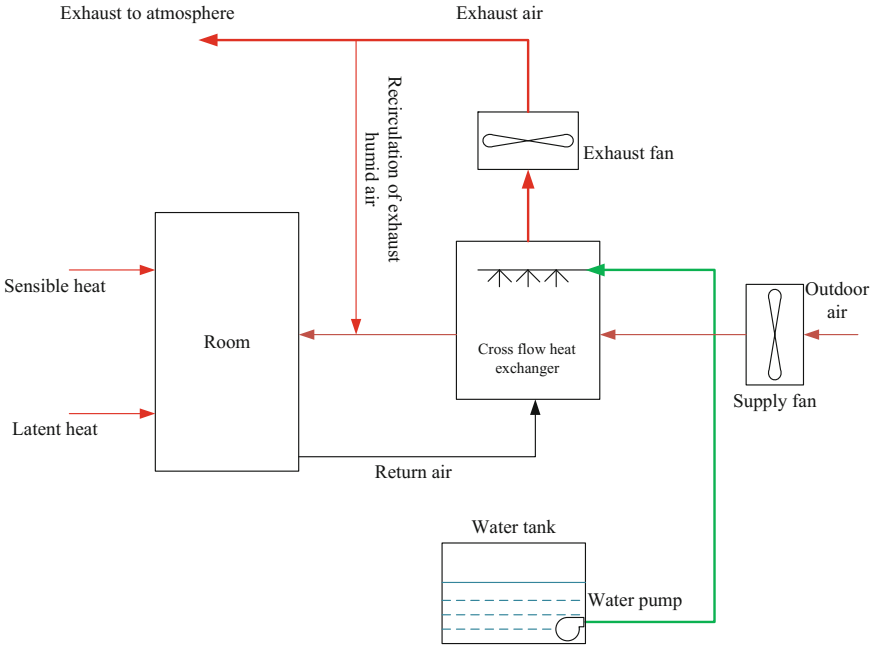

Fig. 9.14 Schematic diagram of modified indirect evaporative cooler [48]

combined operation, saturation efficiency varied between 121 and 107% and cooling load capacity from 5.06 to 20.50 kW as compared to saturation efficiency of 89–64% and cooling capacity of 3.18–16.6 kW for single-stage direct evaporative cooling. The temperature obtained at the outlet of the cooler lies between 22.5 and 24.6 °C for ambient dry bulb temperature and relative humidity of 39.9 °C and 32.8%, respectively. Maclaine-Cross and Banks [47] developed a model for wet surface heat exchangers which can be used to predict the performance of different types of evaporative coolers. The results showed that by using such a heat exchanger, the proposed regenerative evaporative cooling unit has excellent overall performance.

Bisoniya et al. [48] presented a model for modified indirect evaporative cooler and compared results of theoretical and experimental thermal analysis. The presented model is shown in Fig. 9.14 which is a cross-flow heat exchanger with one fluid mixed and other unmixed. The results showed that theoretical model presented can be used to predict the performance of the modified indirect evaporative cooler. The results also showed that the evaporative cooler had best performance in hot and dry climatic conditions. The evaporative cooling technology is under process of development. Some important steps need to be taken for development of this technology are summarized in Table 9.3.

Table 9.3 Needed R&D for desiccant-based evaporative cooling technology

Topic	Actions to be taken
Technology development	• Development of different tools and software for modeling • Collaborative partnership between desiccant-based evaporative cooling manufacturers, the HVAC industry and researchers need to be established
Field testing and performance mapping	• Additional field trials to be conducted • Performance maps development for different climatic conditions and operating parameters
Tools and software	• Simulation software tools should incorporate evaporative cooling technologies

9.9 Best Use of Desiccant-Based Cooling Technology

The liquid desiccant-based evaporative cooling technology can first be targeted for commercial buildings rather than residential buildings because of high energy and financial payback in hot and humid climatic areas. The combination of recent advances in desiccant materials and the evaporative cooling technology must be used to design cheaper, reliable and compact cooling systems. The conditions for the best use of desiccant-based evaporative cooling are illustrated in Fig. 9.15,

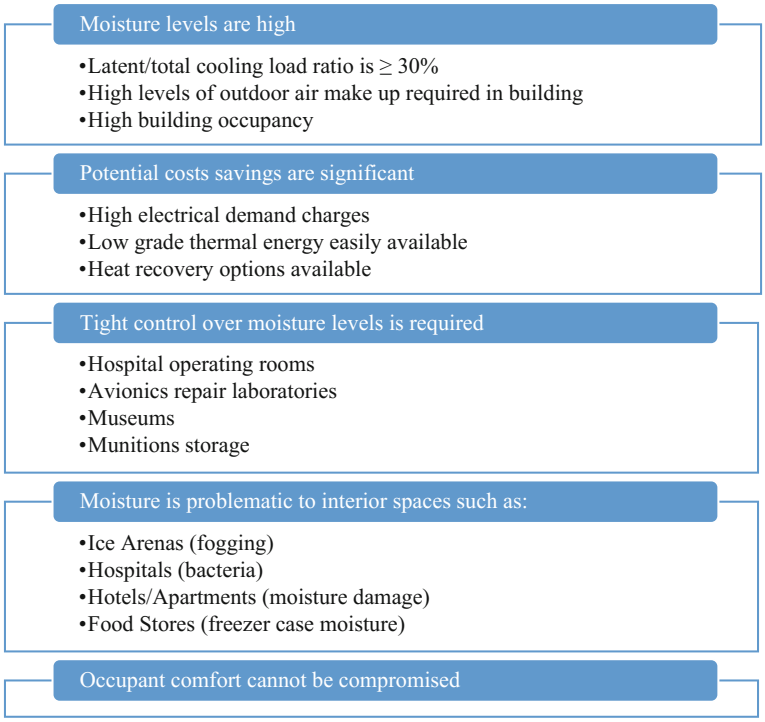

Fig. 9.15 Conditions for the best use of desiccant-based evaporative cooling

Table 9.4 Typical applications and benefits for desiccant dehumidification

Application	Benefits of desiccant dehumidification
Supermarket	• Energy savings through reduced refrigeration display compressor loads • Fewer defrost cycles in refrigerated display systems • Eliminates condensation on display cases • Customer comfort in frozen food aisles
Ice rinks	• Energy savings through reduced latent loads • Less ice resurfacing • Eliminates fogging • Reduced building maintenance
Refrigerated warehouse	• Energy savings through reduced latent loads • Eliminates temperature fluctuations • Reduces workplace hazards (slick and icy floors)
Hospital operating room	• Eliminates perspiration of surgeons • Eliminates fungal amplification in ductwork • Eliminates condensation in operating room
Movie theater	• Increased customer comfort • Allows increased ventilation in response to ASHRAE Standard 62 • Increases useful life of seats and carpets that are damaged by the presence of high moisture levels
School	• Reduced health risks associated with airborne infectious agents • Decreased levels of indoor CO_2 • Lower energy costs
Fast food restaurant	• Allows increased ventilation in response to ASHRAE Standard 62 • Increased customer comfort • Lower energy costs
Hotel	• Increased customer comfort • Allows increased ventilation in response to • Increases useful life of wallpaper, tapestries and carpets that are damaged by the presence of high moisture levels

whereas typical applications and benefits for desiccant dehumidification are listed in Table 9.4 [49].

9.10 Future View of Research in the Field of Desiccant Cooling Technology

The major drawbacks of desiccant cooling technology are the lack of knowledge about system performance, low familiarity, high investment cost and cost/benefit ratio. This technology is relatively immature in terms of production scale as compared to the conventional cooling systems. Furthermore, the environmental, economic and social impacts which are related to this technology need to be investigated, and a clear understanding and knowledge of these issues should be addressed.

The desiccant cooling technology should be converted into products which are market attractive. In the last ten years, significant progress has been made in the basic components of desiccant technology. In the future, desiccant systems are likely to expand their range of applications. Trends which suggest this conclusion include:

- Increased competition among desiccant manufacturers.
- Basic advances in desiccant materials, with resulting improvements in system COP.
- The current trend to increase the amount of fresh air used in buildings.
- Recognition of the harmful effects of excess humidity on indoor air quality, building furnishings, and structural elements.

9.11 Conclusions

The liquid desiccant-enhanced evaporative cooling system is relatively a new technology and is a good alternative for conventional mechanical vapor compression air-conditioning system especially in hot and humid climatic conditions but less familiar as compared to conventional cooling system. In this chapter, the recent works on liquid desiccant-based evaporative cooling and its various applications are presented. Also, a basic working principle of desiccant-enhanced evaporative cooling cycle is provided. Standardizations, legislations, public awareness and regulations are the main issues need to be focused for such cooling systems. The main concluding remarks are outlined as follows:

- The evaporative cooling system becomes less efficient in hot and humid climatic conditions. Under these conditions, evaporative cooling system can be operated in conjunction with desiccant dehumidifier with high efficiency.
- The main advantage of a liquid desiccant-based evaporative cooling technology is its ability to control latent and sensible load separately.
- As a working principle, a direct evaporative cooling system adds moisture to the process air, while an indirect evaporative cooling system provides only sensible cooling to the supply air without adding any moisture. This feature makes indirect systems more attractive than direct evaporative cooling systems.
- In modified evaporative cooler, the air can be cooled to the temperature lower than the temperature achieved by indirect or direct evaporative cooler without disturbing the humidity of the air.
- Low-grade thermal energy such as solar, biomass can be effectively used for the continuous operation of the desiccant-based evaporative cooling system.
- To improve the characteristics of a single desiccant material such as to improve its absorption capability and to lower its regeneration temperature, a number of composite desiccant materials have been developed.

- Desiccant dehumidifier is the heart of a liquid desiccant cooling system which is mostly of adiabatic type or inner cooled. The adiabatic-type dehumidifier requires high flow rates for complete wetting of the surface which causes desiccant carry over. This problem of required high flow rates and carry over can be avoided by using inner cooled dehumidifier.
- Internally cooled dehumidifiers can substantially advance the performance in comparison with adiabatic dehumidifiers.
- The corrosive nature of a desiccant can be dealt with very low flow rate of the desiccant both in the dehumidifier and the regenerator. To operate the system at these low flow rates, continuous cooling of the desiccant in the dehumidifier is required which has been carried out by many researchers by proposing different configurations of inner cooled dehumidifiers.
- More field work is required to design and specify liquid desiccant cooling systems which can comfortably replace the conventional air conditioners.

Acknowledgments The authors would like to acknowledge the support provided by the Deanship of Scientific Research (DSR) at King Fahd University of Petroleum and Minerals (KFUPM) for funding this work through project no. RG1321-1.

References

1. Rafique MM, Gandhidasan P, Rehman S, Al-Hadhrami LM (2015) A review on desiccant based evaporative cooling systems. Renew Sustain Energy Rev 45:145–159
2. Henderson HI, Rengarajan K (1996) Model to predict the latent capacity of air-conditioners and heat pumps at part-load conditions with constant fan operation. ASHRAE Trans 102 (1):266–274
3. Jain S, Dhar PL, Kaushik SC (1994) Evaluation of liquid desiccant based evaporative cooling cycles for typical hot and humid climates. Heat Recovery Syst 14(6):621–632
4. Oliveira AC, Afonso CF, Riffat SB, Doherty PS (2010) Thermal performance of a novel air conditioning system using a liquid desiccant. Appl Therm Eng 20(13):1213–1223
5. Saman WY, Alizadeh S (2001) Modelling and performance analysis of a cross-flow type plate heat exchanger for dehumidification/cooling. Sol Energy 70(4):361–372
6. Radhwan AM, Elsayed MM, Gari HN (1999) Mathematical modeling of solar operated liquid desiccant-evaporative air conditioning system. Eng Sci 11(1):119–141
7. Bellemo L, Elmegaard B, Reinholdt LO, Kern MR (2013) Modeling of a regenerative indirect evaporative cooler for a desiccant cooling system. In: 4th IIR conference on thermo physical properties and transfer processes of refrigerants, Delft, The Netherlands, 2013
8. Jiang Y, Li Z, Chen XL, Liu XH (2004) Liquid desiccant air conditioning system and its applications. Heat Vent Air Conditioning 34:88–98
9. Rafique MM, Gandhidasan P, Rehman S, Al-Hadhrami LM (2016) Energy, exergy and anergy analysis of a solar desiccant cooling system. J Clean Energy Technol 4(1):78–83
10. Shariaty-Niassar M, Gilani N (2009) An investigation of indirect evaporative coolers, IEC with respect to thermal comfort criteria. Iran J Chem Eng 6(2):14–28
11. Bruno F (2010) An indirect evaporative cooler for supplying air near the dew point. In: 48th AuSES annual conference, Canberra, ACT, Australia 2010
12. Gandhidasan P, Mohandes MA (2008) Predictions of vapor pressures of aqueous desiccants for cooling applications by using artificial neural networks. Appl Therm Eng 28(2):126–135

13. Elsarrag E (2006) Dehumidification of air by chemical liquid desiccant in a packed column and its heat and mass transfer effectiveness. HVAC&R Res 12(1):3–16
14. Rafique MM, Gandhidasan P, Bahaidarah HM (2016) Liquid desiccant materials and dehumidifiers—a review. Renew Sustain Energy Rev 56:179–195
15. Ertas A, Anderson EE, Kiris I (1992) Properties of a new liquid desiccant solution—lithium chloride and calcium chloride mixture. Sol Energy 49(3):205–212
16. Studak JW, Peterson JL (1992) A preliminary evaluation of alternative liquid desiccants for a hybrid desiccant air conditioner. Desiccant cooling and dehumidification, ASHARE, Atlanta, GA 1992
17. Nayak SM (2005) Experimental and theoretical investigation of integrated engine generator—liquid desiccant system. Ph.D. thesis, College Park, University of Maryland, United States
18. Fumo N, Goswami DY (2002) Study of an aqueous lithium chloride desiccant system: air dehumidification and desiccant regeneration. Sol Energy 72(4):351–361
19. Liu XH, Zhang Y, Qu KY, Jiang Y (2006) Experimental study on mass transfer performances of cross flow dehumidifier using liquid desiccant. Energy Convers Manag 47(15–16):2682–2692
20. Liu XH, Jiang Y (2008) Coupled heat and mass transfer characteristic in packed bed dehumidifier/regenerator using liquid desiccant. Energy Convers Manag 49(6):1357–1366
21. Jain S, Bansal PK (2007) Performance analysis of liquid desiccant dehumidification systems. Int J Refrig 30(5):861–872
22. Katejanekarn T, Chirarattananon S, Kumar S (2009) An experimental study of a solar-regenerated liquid desiccant ventilation pre-conditioning system. Sol Energy 83 (6):920–933
23. Seenivasan D, Selladurai V, Senthil P (2014) Optimization of liquid desiccant dehumidifier performance using Taguchi method. Adv Mech Eng, Article ID 506487:1–6
24. Gommed K, Ziegler F, Grossman G (2004) Experimental investigation of a LiCl-water open absorption system for cooling and dehumidification. J Sol Energy Eng 126(2):710–715
25. Chen XY, Jiang Y, Li Z, Qu KY (2005) Field study on independent dehumidification air-conditioning system-I: Performance of liquid desiccant dehumidification system. ASHRAE Trans 111(2):271–276
26. So'Brien GC, Satcunanathan S (1989) performance of a novel liquid desiccant dehumidifier/regenerator system. J Sol Energy Eng 111(4):345–352
27. Scalabrin G, Scaltriti GA (1990) Liquid sorption-desorption system for air conditioning with heat at lower temperature. J Sol Energy Eng 112(2):70–75
28. Brundrett GW (2013) Handbook of dehumidification technology. Butterworth-Heinemann
29. Yoon JI, Phan TT, Moon CG, Bansal P (2005) Numerical study on heat and mass transfer characteristic of plate absorber. Appl Therm Eng 25(14):2219–2235
30. Qi R, Lu L, Yang H (2012) Quick performance prediction for internally cooled/heated liquid desiccant dehumidification system. Build Serv Eng Res Technol 1–15. doi:10.1177/0143624412468890
31. Khan AY, Sulsona FJ (1998) Modeling and parametric analysis of heat and mass transfer performance of refrigerant and cooled liquid desiccant absorbers. Int J Energy Res 22(9):813–832
32. Abdel-Salam AH, Ge G, Simonson GJ (2013) Performance analysis of a membrane liquid desiccant air-conditioning system. Energy Build 62:559–569
33. Liu XH, Geng KC, Lin BR, Jiang Y (2004) Combined cogeneration and liquid desiccant system applied in a demonstration building. Energy Build 36(9):945–953
34. Li Z (2003) Liquid desiccant air conditioning and independent humidity control air conditioning systems. Heat Vent Air Condition 33:26–31
35. Xiong ZQ, Dai YJ, Wang RZ (2010) Development of a novel two-stage liquid desiccant dehumidification system assisted by $CaCl_2$ solution using exergy analysis method. Appl Energy 87(5):1495–1504

36. Xiong ZQ, Dai YJ, Wang RZ (2009) Investigation on a two-stage solar liquid-desiccant (LiBr) dehumidification system assisted by $CaCl_2$ solution. Appl Therm Eng 29(5–6): 1209–1215
37. Kumar R, Dhar PL, Jain S, Asati AK (2009) Multi absorber stand-alone liquid desiccant air-conditioning systems for higher performance. Sol Energy 83(5):761–772
38. Huang SM, Zhang LZ, Tang K, Peil X (2012) Fluid flow and heat mass transfer in membrane parallel-plates channels used for liquid desiccant air dehumidification. Int J Heat Mass Transf 55(9–10):2571–2580
39. Liu XH, Chang XM, Xia JJ, Jiang Y (2009) Performance analysis on the internally cooled dehumidifier using liquid desiccant. Build Environ 44(2):299–308
40. Cheng L (2009) The performance and the applied research of liquid desiccant fresh air conditioning system. Ph.D. thesis, Tsinghua University, Beijing, China
41. Kim MH, Park JY, Sung MK, Choi AS, Jeong JW (2014) Annual operating energy savings of liquid desiccant and evaporative-cooling-assisted 100% outdoor air system. Energy Build 76:538–550
42. She X, Yin Y, Zhang X (2014) Thermodynamic analysis of a novel energy efficient refrigeration system sub cooled by liquid desiccant dehumidification and evaporation. Energy Convers Manag 78:286–296
43. Rafique MM (2015) Investigation of a solar assisted thermally activated air conditioning system. MS Thesis in Mechanical Engineering, King Fahd University of Petroleum and Minerals Dhahran, Saudi Arabia
44. Alonso JFS, Martínez FJR, Gómez EV, Plasencia MA (1998) Simulation model of an indirect evaporative cooler. Energy Build 29(1):23–27
45. Jain JK, Hindoliya DA (2012) Development and testing of regenerative evaporative cooler. Int J Eng Trends Technol 3(6):694–697
46. Kulkarni RK, Rajput SPS (2011) Performance evaluation of two stage indirect/direct evaporative cooler with alternative shapes and cooling media in direct stage. Int J Appl Eng Res 1(4):800–812
47. Maclaine-Cross IL, Banks PJ (1981) A general theory of wet surface heat exchangers and its application to regenerative evaporative cooling. J Heat Transf 103(3):579–585
48. Bisoniya TS, Rajput SPS, Kumar A (2011) Comparative thermal analysis of theoretical and experimental studies of modified indirect evaporative cooler having cross flow heat exchanger with one fluid mixed and the other unmixed. Int J Energy Environ 2(5):921–932
49. Rutherford TR (2000) Desiccant cooling technology resource guide. US Army Construction Engineering Research Laboratory

Chapter 10
Application of Desiccant Cooling to Trigeneration Systems

Kwong-Fai Fong and Chun-Kwong Lee

Abstract The application of trigeneration systems as distributed power sources to reduce carbon dioxide emission and energy consumption is getting increased consideration in recent years. Desiccant cooling is deemed to be effective in handling the latent load in hot and humid weather. Hence, in this study, performance evaluation is made for gas-engine-primed trigeneration systems with desiccant cooling when applied to a reference office building, hotel building and sports center under the sub-tropical climate. In all cases, both the primary energy consumption (*PEC*) and carbon dioxide emission (*CDE*) can be reduced. The maximum saving in *PEC* occurs when applied to the sports center which exceeds 17%, while the saving in *CDE* is the highest for use in the hotel building which reaches nearly 33%. The results highlight the application potential of desiccant cooling in trigeneration systems.

Keywords Desiccant cooling · Trigeneration · Gas engine · Primary energy consumption · Carbon dioxide emission

10.1 Introduction

To relieve global warming, the reduction in energy consumption is one of the key issues. While the energy demand may not be able to be decreased in view of the consideration of economic and/or population growth, the more efficient utilization of energy becomes a very important direction of research and development. The enhancement of the power generation efficiency of course is direct and effective mean, but this can be a very time-consuming process in large power plants. In this

K.-F. Fong (✉) · C.-K. Lee
Division of Building Science and Technology, City University of Hong Kong, Tat Chee Avenue, Kowloon Tong, Hong Kong
e-mail: bssquare@cityu.edu.hk

C.-K. Lee
e-mail: chunklee@cityu.edu.hk

N. Enteria et al. (eds.), *Desiccant Heating, Ventilating, and Air-Conditioning Systems*, DOI 10.1007/978-981-10-3047-5_10

regard, distributed power generation in district or even building level is a suitable alternative. In particular, trigeneration systems, which recover the waste heat from the prime movers for providing cooling and/or heating in buildings, offer extra energy saving potential due to the better utilization of the fuel energy. In fact, the combined efficiency of trigeneration systems can exceed 80% as compared to less than 50% for common power plants.

There are currently different kinds of thermal cooling technologies available. These include the absorption chiller, the adsorption chiller, the ejector cooling cycle and the solid/liquid desiccant cooling system. Desiccant cooling is beneficial for treating fresh air which yields a higher coefficient of performance as compared to the other thermal cooling technologies with similar driving temperature level, in particular applied to tropical/sub-tropical regions. Various published researches can be found in the literature. Intini et al. [1] investigated the performance of a solid desiccant cooling cycle coupled with auxiliary cooling and heating coils for sensible cooling and heating. The driving heat and the electricity required by the auxiliary vapor-compression chiller and pumps are provided by a polymer electrolyte fuel cell. The weather profiles of three European cities were considered, but it was found the resulting primary energy savings were limited. Angrisani et al. [2] also adopted a similar desiccant cooling system but without evaporative coolers which was primed by a gas engine. The resulting fuel energy saving ratio was 7.7% with 15.3% reduction in carbon dioxide emission when applied to a lecture room in Italy. The corresponding payback period was nearly 17 years. Badami et al. [3] as well as Badami and Portoraro [4] investigated the performance of a gas-engine-primed trigeneration system which utilized a liquid desiccant cooling cycle. The best primary energy saving was around 12% with a payback period of around 7 years based on presumed operating profiles of the trigeneration system. Angrisani et al. [5, 6] studied experimentally the performance of a solid desiccant cooling system primed by a gas engine. They found that both primary energy saving and carbon dioxide emission reduction could be achieved at higher outdoor temperature and humidity ratio, affirming that desiccant cooling is suitable in hot and humid climates. Nayak et al. [7] tested a liquid desiccant cooling system primed by a gas engine for use in a four-storey office building in the USA. They remarked that the primary energy saving was around 4% at rated conditions. Gao [8] analyzed a diesel-engine-primed trigeneration system for use in an industrial park in China. Both the liquid desiccant dehumidification system and absorption chiller were employed as thermal cooling equipment. Through performance evaluation at design conditions, the introduction of the liquid desiccant dehumidification system improved the energy utilization coefficient, energy saving ratio as well as the energy saving ratio by 20, 14 and 5%, respectively, while the payback period was shortened by more than 2 years. Zaltash et al. [9] considered a micro-turbine-primed trigeneration system with combined use of solid desiccant cooling cycle and absorption chiller. They concluded that the use of the solid desiccant system increased the overall efficiency of the integrated system by 5–7%. Casas and Schmitz [10] investigated a gas-engine-primed solid-desiccant-cooled trigeneration system coupled with ground heat exchangers for convective and radiative cooling of a three-storey office building in Germany.

Auxiliary boiler was adopted for the convective and radiative heating of the building. They commented that 70% reduction in primary energy consumption could be achieved in case electric chiller was used in place of the ground heat exchangers. Liu et al. [11] studied the performance of a gas-engine-primed trigeneration system which employed a liquid desiccant dehumidification cycle and absorption chiller as well as auxiliary vapor-compression chiller for use in an office building in China. Thermal and desiccant storage were also provided. It was found that the adoption of storage reduced the capacity of auxiliary chiller and desiccant dehumidifier by more than 40% with a year-round reduction of carbon dioxide emission by 40%. Meanwhile, the payback period was around 2 years.

So far in the above research works, the integrated system performances of trigeneration systems with desiccant cooling were disseminated; however, the independent performance of desiccant cooling was not addressed. About the scope of study, only one type of building was considered each time. Hence, in this study, the merits of employing desiccant cooling in trigeneration systems are analyzed and compared when applied to various building types based on the weather conditions of sub-tropical Hong Kong. Gas engines are adopted as the prime movers of the trigeneration systems. Three types of buildings, namely office, hotel and sports center are considered with different loading characteristics. The solid desiccant cooling cycle is used to pre-treat the fresh air, while the conventional vapor-compression chiller handles the system sensible load.

10.2 System Description

Figure 10.1 shows the schematic diagram of the trigeneration system considered. Here, two sources of waste heat are collected from the gas engine, namely the engine jacket and the exhaust flue gas. A single regenerative water circuit is adopted which connects the two waste heat sources in series through two heat exchangers. The recovered waste heat is then used to provide desiccant cooling, space heating and water heating where applicable. Respective heat exchangers are added to separate the regenerative water from the space heating water and the potable water. Individual auxiliary heaters are included for space heating and water heating which ensure that the water temperature for space heating and water heating can reach the design level. An auxiliary water cooler is required to provide the necessary cooling in the engine jacket in case the demand of waste heat from desiccant cooling/space heating/water heating is low. To minimize the duty of the auxiliary water cooler, the regenerative water will bypass the exhaust heat exchanger when the auxiliary water cooler is in operation.

The solid desiccant cooling unit, which comprises a desiccant wheel, a regenerative coil and a rotary heat exchanger, is used to dehumidify the fresh air. The treated fresh air is then mixed with the return air and fed into the supply air cooling coil which provides the necessary sensible and latent cooling from the auxiliary

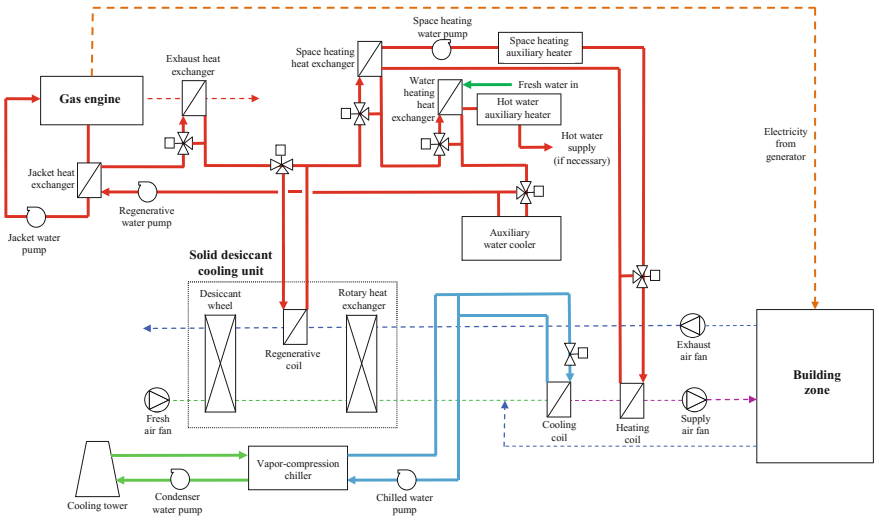

Fig. 10.1 Schematic diagram of a gas-engine-primed trigeneration system incorporating a solid desiccant cooling cycle

vapor-compression chiller. Additional fresh and exhaust air fans are needed to cater for the pressure drop of the fresh and exhaust air across the desiccant wheel, the regenerative coil and the rotary heat exchanger.

Figures 10.2, 10.3 and 10.4 show the floor layouts of a reference office building, hotel building and sports center for use in the present study. The office building consists of 30 storeys and the hotel building is 20-storey high. Meanwhile, the sports center has only single storey. Each floor of the office building is divided into three zones, namely the exterior zone, the interior zone and the lift lobby. For the hotel building, five zones are adopted, namely the east guestroom zone, the west guestroom zone, the south guestroom zone, the lift lobby and the housekeeping zone. Only two zones are used for the sports center, namely the indoor games hall and the back of house. Fan coil units are used to provide air-conditioning for the office and hotel buildings, while air handling units are employed for the sports center. Space heating is required for the external zone of the office and the guestrooms of the hotel only. Meanwhile, hot water for bathing and washing is to be supplied for the hotel building and the sports center.

10.3 System Specification

To size the gas engine and other equipment of the trigeneration system, the design electricity, cooling and heating demands of the various building types considered have to be determined first. The local design guidelines [12], which specify the

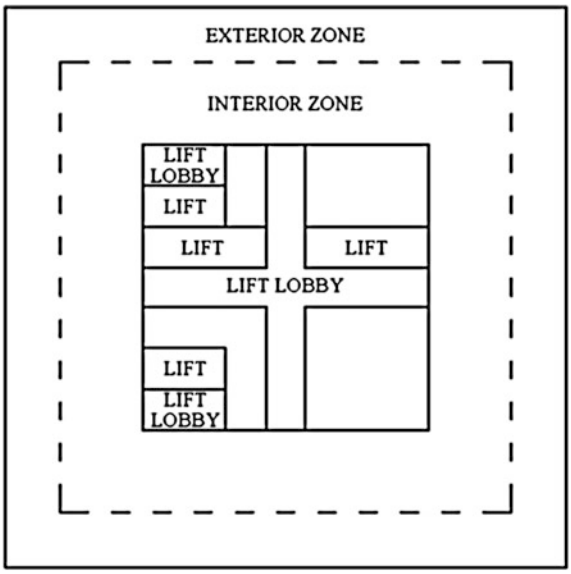

Fig. 10.2 Typical floor layout of the office building

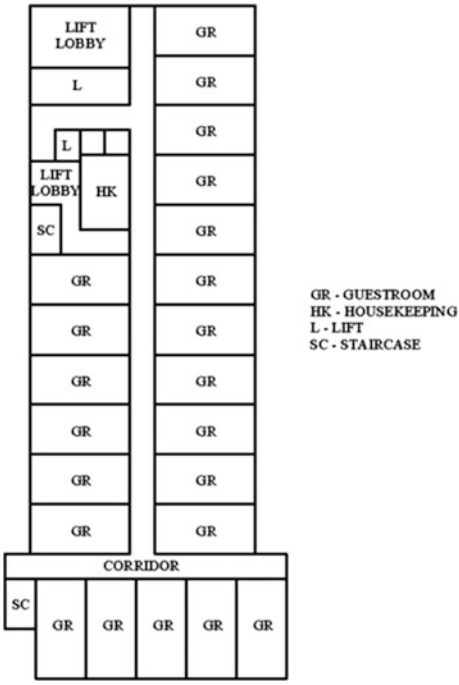

Fig. 10.3 Typical floor layout plan of hotel building

intensity and profiles of the different building loads, are followed where applicable. For the air-conditioning systems of the office and hotel buildings, the design indoor conditions for cooling are 24 °C and 54% RH, while that for heating is 20 °C.

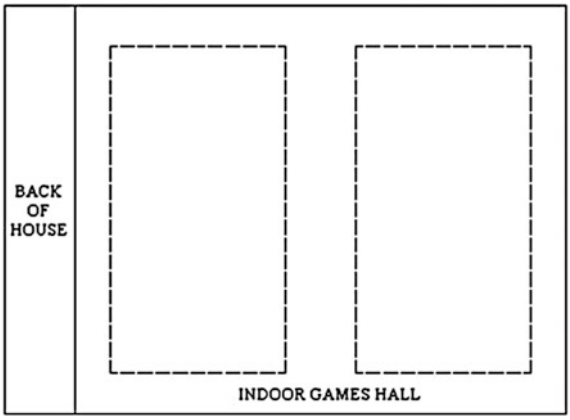

Fig. 10.4 Floor layout plan of sports center

Regarding the sports center, the design cooling condition is 22 °C and 60% RH. Table 10.1 summarizes the internal loadings of the various building types adopted in the study.

The TRNSYS [13] simulation software together with its TESS library [14] is employed to determine the air-conditioning profiles and hence the design cooling and heating loads based on the weather data of typical meteorological year of sub-tropical Hong Kong [15]. The design regenerative water supply temperature is 90 °C in view of the normal temperature level of the engine jacket water and the fact that a single regenerative water circuit is adopted. The capacity of the desiccant cooling unit is then determined based on a regenerative air temperature of 85 °C leaving the regenerative coil. The flow rates of the exhaust air fans are taken as 90% of those for the fresh air fans. A constant temperature effectiveness of 0.8 is adopted for the rotary heat exchanger. The 1-D model proposed by Zhang et al. [16] is employed for the desiccant wheel. Here, it is assumed that individual desiccant cooling unit is provided for each floor of the office and hotel buildings. Table 10.2 shows the respective design parameters of the trigeneration systems for the various

Table 10.1 Summarized building loads of the various building types

Loading type	Office	Hotel	Sports center
Maximum occupancy	8 m^2/person	2 persons/room	3 m^2/person at games hall and 4 m^2/person at back of house
Maximum lighting load	20 W/m^2	18 W/m^2	17 W/m^2 at games hall and 13 W/m^2 at back of house
Maximum equipment load	10 W/m^2	900 W/room	N.A.
Fresh air flow	8 L/s/person	30 L/s/room	13 L/s/person at games hall and 8 L/s/person at back of house
Maximum occupancy	8 m^2/person	2 persons/room	3 m^2/person at games hall and 4 m^2/person at back of house

Table 10.2 Summarized design parameters of the trigeneration systems for the various building types

Design parameter	Office	Hotel	Sports center
Design system sensible load per floor (kW)	108	54.0	179
Design system latent load per floor (kW)	78.8	35.5	327
Design desiccant cooling load per floor (kW)	58.6	29.0	230
Total design supply air flow rate of building (m^3/s)	204	68.8	14.7
Total design fresh air flow rate of building (m^3/s)	52.1	17.0	6.37
Design chiller total capacity (kW)	3846	1210	393
Design total regenerative heat demand (kW)	1196	392	151
Design total space heating demand (kW)	1230	491	0
Design total water heating demand (kW)	0	404	231
Design building total electrical demand (kW)	2518	1033	159

building types. It can be found that the desiccant cooling cannot handle all the system latent load. Hence, part of the system latent load and the whole system sensible load are to be fulfilled by the vapor-compression chiller through the supply air cooling coil.

The sizing of the gas engine is based on the design electrical demand of the building. Otto cycle is adopted for modeling the gas engine as detailed by Fong and Lee [17]. The gas engine is to be fueled by natural gas (assumed to be pure methane). Part-load control is provided for the gas engine which modulates the fuel injection rate according to the electricity demand of the building. As the performance of the gas engine deteriorates substantially at a low part-load ratio, a minimum part-load ratio is adopted when the gas engine is in operation. In view of this and to allow more flexible operation for the vapor-compression chiller system, multiple units for the gas engine and the vapor-compression chiller are employed where applicable as shown in Table 10.3. Since the required chiller capacity of the sports center is small, only one unit is offered. The use of three gas engines for the hotel building is based on the consideration that at least one gas engine is in operation under the minimum part-load ratio throughout the year. As the electricity demand of the office building and the sports center at midnight is very low, the gas engines are switched off during that period of time and the electricity demand is then fulfilled by the power grid. This also applies to the office building during the holidays. The respective control logic and sizing of the auxiliary equipment can be found in Fong and Lee [17].

Table 10.3 Summarized configurations of the trigeneration systems for the various building types

	Office	Hotel	Sports center
No. of gas engines	2	3	2
No. of vapor-compression chillers	2	2	1
No. of desiccant cooling units	30	20	2

10.4 Methodology of Analysis

To investigate the benefit of applying desiccant cooling in trigeneration systems, year-round dynamic simulations are performed using TRNSYS based on a simulation time step of 6 min. TRNSYS adopts a component-based platform for building a system. It offers many standard components such as the multi-zone building, the vapor-compression chiller, the fan and pump, the cooling tower, the heat exchanger, the cooling and heating coil, the auxiliary heater and the auxiliary water cooler which are required for the trigeneration system. For the desiccant wheel and the gas engine, new components are developed which determine the equipment performance by interpolating through external performance data files generated by using the models from Zhang et al. [16] and Fong and Lee [17], respectively. For the office and hotel buildings, it is assumed that the system performance on each floor is the same and that the behaviors of the guestrooms on the same direction of the hotel building are also identical.

The total primary energy consumption (*PEC*) and the carbon dioxide emission (*CDE*) are taken as the parameters to assess the energy and environmental merits of the respective trigeneration systems in comparison with the corresponding conventional systems in which all space cooling is provided by vapor-compression chillers. Here, the thermal efficiency and carbon dioxide emission index of the grid electricity is taken as 36% and 0.7 kg/kWh of generated electricity according to the major local power company [18] and guidelines [19]. Besides, the overall performance of the trigeneration system can also be represented by energy utilization factor (*EUF*) as defined by

$$EUF = \frac{\dot{W}_{\text{out}} + \dot{Q}_{\text{dc}} + \dot{Q}_{\text{sh}} + \dot{Q}_{\text{wh}}}{m_{\text{f}}\text{LHV}_{\text{f}}} \times 100\ \% \tag{10.1}$$

Here, $\dot{W}_{\text{out}}$ is the power output of the gas engine, $\dot{Q}_{\text{dc}}$, $\dot{Q}_{\text{sh}}$ and $\dot{Q}_{\text{wh}}$ is the waste heat recovered for desiccant cooling, space heating and water heating, respectively. Meanwhile, m_{f} is the fuel injection rate and LHV_{f} is the lower heat value of the fuel.

10.5 Results and Discussions

Table 10.4 summarizes the year-round performances of the conventional and trigeneration systems for the various building types investigated. Here, the gas engine generator electrical efficiency (*GEE*) is also included for reference. A higher *GEE* is noted for use in the office building due to the much higher design capacity of the gas engines with reference to reviewing Tables 10.2 and 10.3. It can be found that the percentage reduction in *PEC* and *CDE* are the lowest which measures 3.8 and 21.3% when the trigeneration system with desiccant cooling is used in the office

Table 10.4 Summarized year-round performances of the various systems considered

Case	Averaged *GEE* (%)	Averaged *EUF* (%)	Total *PEC* (MWh)	Total *CDE* (Ton)
Office, conventional	N.A.	N.A.	23362	5887
Office, trigeneration	39.8	49.1	22480 (↓3.8%)	4634 (↓21.3%)
Hotel, conventional	N.A.	N.A.	13733	3357
Hotel, trigeneration	36.7	66.2	11404 (↓17.0%)	2252 (↓32.9%)
Sports center, conventional	N.A.	N.A.	2197	517
Sports center, trigeneration	35.3	81.6	1814 (↓17.4%)	367 (↓29.0%)

building. This can be explained by the fact only part of the available waste heat is utilized by the desiccant cooling as reflected by the lowest *EUF* (less than 50%) of the trigeneration system, bearing in mind that the demand for space heating is very limited for the office building. The use of the trigeneration system in the sports center yields the highest *EUF* which exceeds 80%. The main reason is that the fresh air ratio of the air-conditioning system in the sports center is the largest which is over 43% according to Table 10.2. Hence, the offered ratio of the desiccant cooling capacity to the total system cooling load (sensible plus latent) is also the highest as found in Table 10.2. In this regard, the required capacity of the auxiliary vapor-compression chiller can be smaller. Another reason is the high water-heating-to-power ratio. However, the lower *GEE* of the gas engine (due to the much smaller design capacity) impairs the energy and economic merits of the trigeneration system used in the sports center. In fact, the percentage reduction in *PEC* is only 17.4% which is slightly higher than that achieved for use in the hotel building. Meanwhile, the percentage saving in *CDE* is the highest for the trigeneration system applied to the hotel building which reaches nearly 33%.

Figures 10.5, 10.6 and 10.7 compare the change in the monthly total *PEC* and *CDE* between the conventional and trigeneration systems for the various building types considered. The profiles for the *PEC* generally resemble those of the *CDE* in all the cases investigated. For the trigeneration system used in the office building, the reduction in *PEC* is minimal between November and April inclusive, while the maximum saving occurs during the peak-load season in summer. On the other hand, the saving in *CDE* is comparatively stable throughout the year. Both the *PEC* and *CDE* reach the peak values in August. For the trigeneration systems used in the hotel building and the sports center, substantial reductions in both the *PEC* and *CDE* can be found in the whole year. However, unlike the case for the office building, both the *PEC* and *CDE* are the highest in July for use in the hotel building, while it is still August in the sports center.

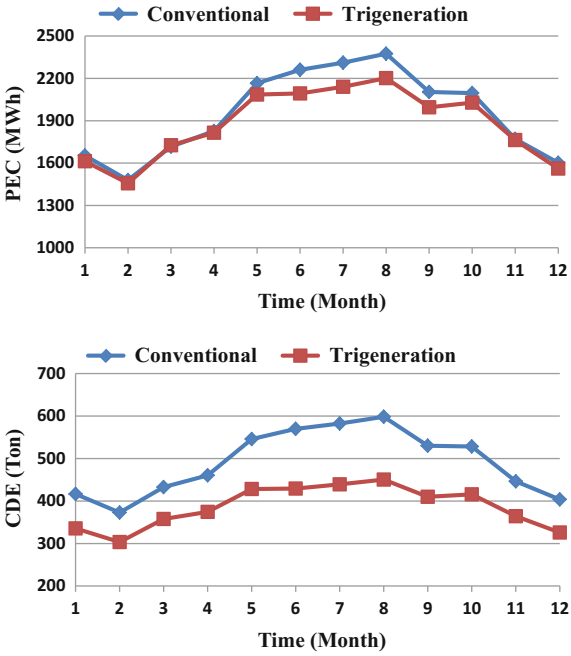

Fig. 10.5 Comparison of the monthly total *PEC* (*above*) and *CDE* (*below*) between the conventional and trigeneration system for use in the office building

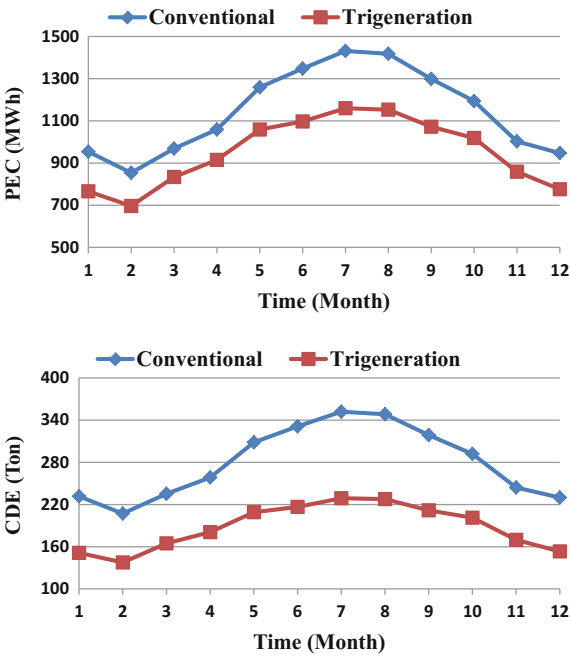

Fig. 10.6 Comparison of the monthly total *PEC* (*above*) and *CDE* (*below*) between the conventional and trigeneration system for use in the hotel building

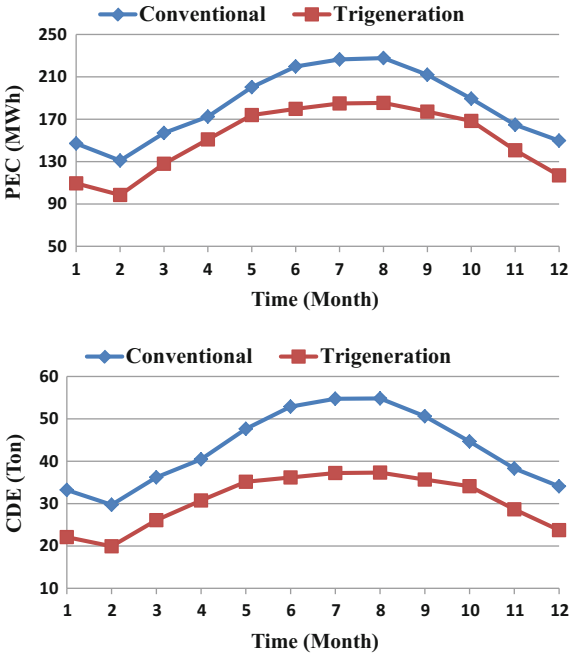

Fig. 10.7 Comparison of the monthly total *PEC* (*above*) and *CDE* (*below*) between the conventional and trigeneration system for use in the sports center

So far in Table 10.4, the *EUF* refers to the entire trigeneration system according to Eq. (10.1). Hence, the role or significance of the desiccant cooling may not be easily compared among the various building types. As such, an energy utilization factor for desiccant cooling (EUF_{dc}) is specifically employed as defined by

$$EUF_{dc} = \frac{\dot{Q}_{dc}}{m_f \mathrm{LHV}_f} \times 100\ \% \tag{10.2}$$

EUF_{dc} represents the proportion of fuel input energy that is utilized by the desiccant cooling. Figure 10.8 shows the variation of the monthly-averaged EUF_{dc} for the three types of buildings considered. It is evident that for the trigeneration system used in the sports center, the desiccant cooling offers the highest utilization of the fuel energy. The situation is the worst when applied to the office building although the averaged EUF_{dc} is only mildly lower than that of the trigeneration system used in the hotel building. Indeed, the fresh air ratios of the air-conditioning systems in the office and hotel buildings are very close to each other. The substantially higher averaged *EUF*, *PEC* and *CDE* reductions for the hotel building are mainly attributed to the much higher heating demand. Nevertheless, the above analyses demonstrate the energy and environmental merits of applying trigeneration system with desiccant cooling to various types of buildings in the sub-tropical Hong Kong.

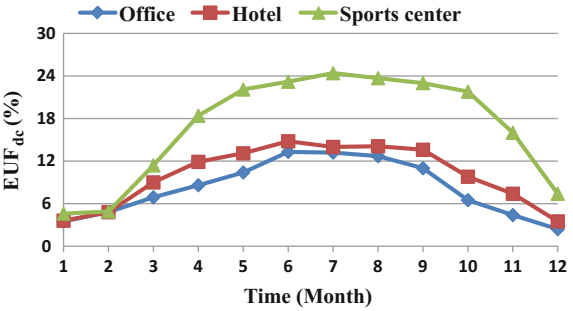

Fig. 10.8 Variation of the monthly-averaged EUF_{dc} for the building types investigated

10.6 Conclusions

The benefits of applying desiccant cooling to trigeneration systems were investigated in which a solid desiccant cooling unit was employed to treat the fresh air and handle part of the latent cooling load, while the conventional vapor-compression chiller was used to meet the remaining cooling demand. A gas engine, fueled by natural gas, was adopted to provide the electricity required by the building with the recovered waste heat from the engine jacket and exhaust flue gas used to regenerate the desiccant wheel. Three types of buildings, namely office, hotel and sports center, were considered for use in the sub-tropical Hong Kong. The energy and environmental merits of the trigeneration systems involved were assessed when compared with the conventional ones.

Through year-round dynamic system simulations using TRNSYS, it was found that both the reductions in primary energy consumption and carbon dioxide emission could be achieved for all the building types considered, which ranged from 3.8 to 17.4% and 21.3 to 32.9%, respectively. The saving in primary energy consumption was the highest for use in the sports center in which the fresh air ratio as well as the waste heat utilization were also the largest among the three building types investigated. Meanwhile, the reduction in carbon dioxide emission was the highest for use in the hotel building. The results demonstrated the application potential of desiccant cooling in trigeneration systems for various building types, in particular those with substantial latent cooling load and heating demand. Desiccant cooling can perform better than the other type of heat-driven cooling equipment, such as absorption or adsorption chiller, in trigeneration system if room humidity control is essential to the building operation.

Acknowledgments The work described in this paper is fully supported by a grant from the Research Grants Council of the Hong Kong Special Administrative Region, China (Project No. CityU 11200315).

References

1. Intini M, De Antonellis S, Joppolo CM et al (2015) A trigeneration system based on polymer electrolyte fuel cell and desiccant wheel—part B: overall system design and energy performance analysis. Energy Convers Manag 106:1460–1470
2. Angrisani G, Roselli C, Sasso M et al (2014) Dynamic performance assessment of a micro-trigeneration system with a desiccant-based air handling unit in Southern Italy climatic conditions. Energy Convers Manag 80:188–201
3. Badami M, Ferrero M, Portoraro A (2013) Experimental tests of a small-scale microturbine with a liquid desiccant cooling system. Int J Energy Res 37(9):1069–1078
4. Badami M, Portoraro A (2009) Performance analysis of an innovative small-scale trigeneration plant with liquid desiccant cooling system. Energy Build 41(11):1195–1204
5. Angrisani G, Minichiello F, Roselli C et al (2011) Experimental investigation to optimise a desiccant HVAC system coupled to a small size cogenerator. Appl Therm Eng 41(4):506–512
6. Angrisania G, Minichiellob F, Roselli C et al (2010) Desiccant HVAC system driven by a micro-CHP: experimental analysis. Energy Build 42(11):2028–2035
7. Nayak SM, Hwang Y, Radermacher R (2009) Performance characterization of gas engine generator integrated with a liquid desiccant dehumidification system. Appl Therm Eng 29 (2–3):479–490
8. Gao L, Wu H, Jin H et al (2008) System study of combined cooling, heating and power system for eco-industrial parks. Int J Energy Res 32(12):1107–1118
9. Zaltash A, Petrov AY, Rizy DT et al (2006) Laboratory R&D on integrated energy systems (IES). Appl Therm Eng 26(1):28–35
10. Casas W, Schmitz G (2005) Experiences with a gas driven, desiccant assisted air conditioning system with geothermal energy for an office building. Energy Build 37(5):493–501
11. Liu XH, Geng KC, Lin BR et al (2004) Combined cogeneration and liquid-desiccant system applied in a demonstration building. Energy Build 36(9):945–953
12. EMSD (2007) Performance-based building energy code. Electrical and Mechanical Services Department, The Hong Kong Special Authority Region
13. TRNSYS (2010) TRNSYS 17, a TRaNsient SYstem Simulation program. The Solar Energy Laboratory, University of Wisconsin-Madison
14. TESS (2010) TESS library documentation. Thermal Energy System Specialists
15. Chan ALS, Chow TT, Fong SKF et al (2006) Generation of a typical meteorological year for Hong Kong. Energy Convers Manag 47:87–96
16. Zhang XJ, Dai YJ, Wang RZ (2003) A simulation study of heat and mass transfer in a honeycombed rotary desiccant dehumidifier. Appl Therm Eng 23(8):989–1003
17. Fong KF, Lee CK (2015) Performance analysis of internal-combustion-engine primed trigeneration systems for use in high-rise office buildings in Hong Kong. Appl Energy 160:793–801
18. CLP (2015) CLP holdings 2015 annual report. CLP Holdings Limited
19. BEAM (2012) BEAM plus for new buildings Version 1.2. BEAM Society Limited

Chapter 11
Application of Desiccant Heating, Ventilating, and Air-Conditioning System in Different Climatic Conditions of East Asia Using Silica Gel (SiO_2) and Titanium Dioxide (TiO_2) Materials

Napoleon Enteria, Hiroshi Yoshino, Akashi Mochida, Akira Satake, Ryuichiro Yoshie, Rie Takaki and Hiroshi Yonekura

Abstract This chapter shows the numerical investigation of the developed solar–DHVAC system applied in the East Asian climatic conditions with two different desiccant wheel coating materials—the Silica Gel (SiO_2) and the Titanium Dioxide (TiO_2). The system was applied in temperate climate (Beijing and Tokyo), subtropical climate (Taipei and Hong Kong) and tropical climate (Manila and Singapore). The study showed that the specification of the solar–DHVAC system varies depending on the climatic conditions. In the comparison of the two materials, it was found that the TiO_2 can support lower indoor temperature and humidity ratio than the SiO_2 with the same specification of the solar thermal system and DHVAC system. In general, the solar–DHVAC system can provide the required indoor temperature and humidity ratio. However, for the hot and humid climate such as in tropical, large size of the solar thermal system is needed. In addition, higher volumetric flow of air to support the high cooling load is required.

This chapter is a modified version of our paper [1].

N. Enteria (✉)
Building Research Institute, Tsukuba, Japan
e-mail: napoleon@kenken.go.jp; enteria@enteria-ge.com

H. Yoshino · A. Mochida · H. Yonekura
Tohoku University, Sendai, Japan

A. Satake
Maeda Corporation, Tokyo, Japan

R. Yoshie
Tokyo Polytechnic University, Atsugi, Japan

R. Takaki
Akita Prefectural University, Akita, Japan

N. Enteria et al. (eds.), *Desiccant Heating, Ventilating, and Air-Conditioning Systems*, DOI 10.1007/978-981-10-3047-5_11

Keywords Solar energy · Desiccant dehumidification · Evaporative cooling · Silica Gel · Titanium dioxide · East asia

Nomenclature

C_P	Specific heat (kJ/kg-K)
DHVAC	Desiccant heating, ventilating and air-conditioning
DCOP	Desiccant coefficient of performance (-)
E	End
EA	Exit air
$E_{F,1}$	Electric energy consumption of fan 1 (kJ)
$E_{F,2}$	Electric energy consumption of fan 2 (kJ)
$E_{H,1}$	Electric energy consumption of heater 1 (kJ)
$E_{H,2}$	Electric energy consumption of heater 2 (kJ)
E_{OP}	Off-peak electric energy consumption (kJ)
E_P	Peak electric energy consumption (kJ)
$E_{P,1}$	Electric energy consumption of pump 1 (kJ)
$E_{P,2}$	Electric energy consumption of pump 2 (kJ)
h	Moist air enthalpy (kJ/kg)
H_{Con}	Latent heat of condensation (kJ/kg)
I_{Cur}	Electric current (A)
m	Mass flow (kg/s)
OA	Outdoor air
OPEC	Off-peak electric energy consumption (-)
PA	Processed air
Q_{CL}	Cooling load (kJ)
$Q_{H,1}$	Thermal energy supplied by electric heater number 1 (kJ)
$Q_{H,2}$	Thermal energy supplied by electric heater number 2 (kJ)
Q_{LE}	Latent energy (kJ)
$Q_{L,1}$	Thermal energy load number 1 (kJ)
$Q_{L,2}$	Thermal energy load number 2 (kJ)
Q_{SC}	Solar energy collected (kJ)
Q_{SE}	Sensible energy (kJ)
RA	Return/room air
S	Start
SF	Solar fraction (-)
SCOP	System coefficient of performance (-)
SHR	Sensible heat ratio (-)
t	Time (s)
T	Temperature (°C)
TCOP	Thermal coefficient of performance (-)
U	Over-all heat transfer coefficient (W/m^2K)
V_{ol}	Electrical voltage (V)
X	Humidity ratio (kg_{H20}/kg_{Air})

Subscripts

A	Air
CE	Cooling effect
CL	Cooling load
Col	Collector
I	Inlet
O	Outlet
OA	Outdoor air
SA	Supply air
1..12	State points

11.1 Introduction

With respect to the building energy consumption, in Japan, building energy consumption is increasing even with the decreasing population [2]. In China, the rapid economic development resulted in urbanization and human demand for better thermal comfort [3]. In Taiwan, energy consumption is high with problem of energy resources [4]. In Hong Kong, several studies had been conducted to lessen the energy consumption particularly in the building sector [5]. In the Philippines, rapid increase in energy consumption is abreast with improving economy [6]. In Singapore, some measures to address building energy consumption become avenues for investigation [7]. Therefore, energy conservation through utilization of alternative energy resources and development of new technologies is imperative to lessen the problems of energy and environment [8]. Solar–DHVAC system is a potential alternative cooling system due to its capability in the utilization of free solar energy [9] and application of natural sorption dehumidification process [10]. Several studies have been conducted on the potentials of the solar–DHVAC system in many regions of the world. In East Asia, solar–DHVAC system is a potential alternative system [11].

Solar–DHVAC system investigation is being conducted in some of the East Asian countries notably China [12–16], Korea [17], Malaysia [18], Thailand [19] and Japan [20–22]. However, majority of the East Asian countries have little research, development and application of the solar–DHVAC system [10]. Several studies show that the solar–DHVAC system is potential for building applications [10, 23–27]. Enteria et al. [28] show that the DHVAC system is potential in Japan climatic condition which is a temperate climate. Some innovation of the solar–DHVAC system had been done in Asia-Pacific region such as using 4-rotor or by

staging to reduce the required regeneration temperature [20, 29]. Fong et al. [30] show that the solar–DHVAC is potential for application in subtropical climate of Hong Kong. Sekhar [31] shows that the DHVAC system is one of the alternative HVAC systems for tropical climate. In fact, in tropical climate, some initial researches are being done for the application of the DHVAC system [18, 19]. Furthermore, Enteria et al. [11, 32] show that the solar–DHVAC system is a potential cooling system in different climates of Asia-Pacific region as long as proper dimensioning and specifications will be determined. Hence, ongoing research efforts are being conducted in the region for the application of the DHVAC system at different designs and methods.

To further increase the performance of the solar–DHVAC system, development of sorbent material is one of the major factors since the dehumidifier is the major performance indicator of the solar–DHVAC system [33]. In this present study, the developed TiO_2 desiccant material is applied as the desiccant dehumidifier. The TiO_2 desiccant material performance is compared to the Silica Gel desiccant material. The sorption isotherm of the TiO_2 and the Silica Gel desiccant wheel is presented in Fig. 11.1. It shows that the Titanium Dioxide desiccant wheel has higher sorption capacity particularly from 60% and above relative humidity. Figure 11.2 shows the performance of the two materials based on the numerical investigation [34]. Figure 11.2a shows the setup for the study of the simple DHVAC system with air heater and cross-flow heat exchanger. The air heater provided the required regeneration temperature, while the heat exchanger is used to investigate the cooling of the processed air (state 2 to state 3) and at the same time preheat the return air (state 4) to state 5. Figure 11.2b shows the increase in processed air temperature upon dehumidification process (state 1 to state 2). The results show the increase in processed air temperature as regeneration temperature

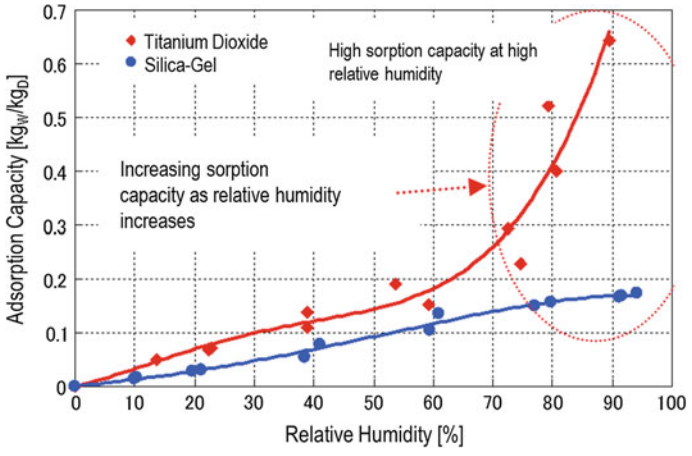

Fig. 11.1 Sorption isotherm of the Silica Gel and the Titanium Dioxide desiccant wheel. The isotherm was measured for the desiccant wheel coated with Silica Gel and Titanium Dioxide

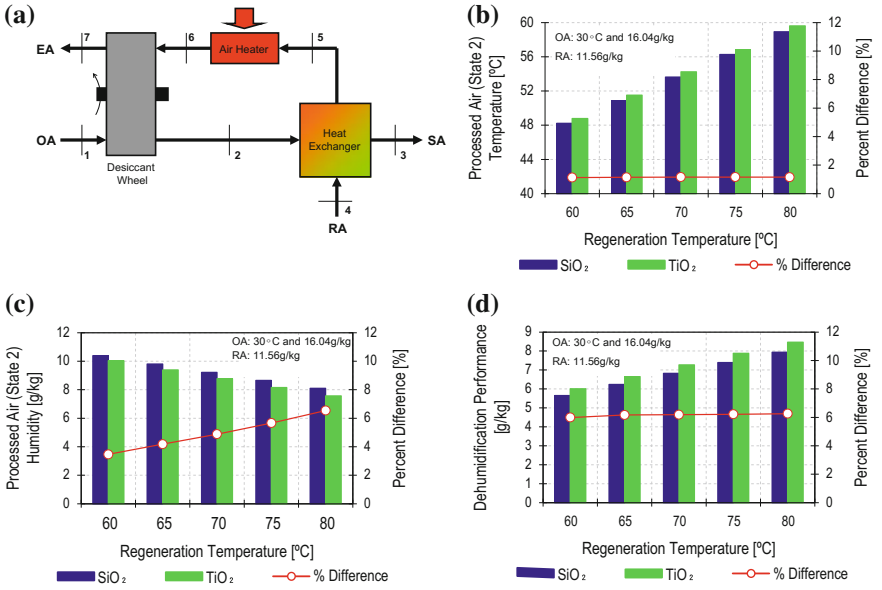

Fig. 11.2 Comparison of the dehumidification and cooling performance of the Silica Gel and Titanium Dioxide desiccant wheel applied in the simple model of the DHVAC system: **a** simple DHVAC system; **b** effect of the regeneration temperature to the processed air temperature (state 2); **c** effect of the regeneration temperature to the processed air humidity ratio (state 2); and **d** dehumidification performance (difference between the humidity ratio of outdoor air (OA)/state 1 and processed air (PA)/state 2

increases due to the release of heat of sorption and heat transfer between the two streams of air. Figure 11.2c shows the humidity ratio of the processed air (state 2) upon dehumidification process. The humidity ratio of the supply air decreases as the regeneration temperature increases due to the complete drying of the desiccant material upon higher regeneration temperature. Figure 11.2d shows the dehumidification performance of the two desiccant materials. It shows that the TiO_2-coated wheel has higher dehumidification performance from 5.99 to 6.26% compared to SiO_2.

In our previous studies [11, 32], the potential of solar–DHVAC system in Asia-Pacific region was presented. This paper presents the additional numerical study of the solar–DHVAC system with the developed Titanium Dioxide desiccant wheel and compared to the performance of the system with Silica Gel wheel. The main objective of the study is to evaluate the solar–DHVAC system performance with the new desiccant material at different climates of East Asia.

11.2 System Description

11.2.1 Solar–DHVAC System

The solar–DHVAC system is generally designed to collect solar thermal energy during daytime and convert off-peak electric energy to thermal energy during nighttime for thermal storage. The concept is explained in details by our previous paper [21]. The design of the DHVAC system utilizes the constant humidity air cooling process as discussed by Enteria et al. [21]. Figure 11.3 shows the schematic diagram of the solar–DHVAC system under investigation. This system is investigated to operate in the Asia-Pacific climates based on the numerical investigation conducted [11].

11.2.2 Solar Thermal Operation

The main operational concept of the solar thermal system is the operation of the nighttime electric heating for thermal storage for the operation of DHVAC when solar radiation is not enough, on the following day to support the high-temperature regeneration air. Based on the numerical study [35], two-hour electric heating is enough to support for following day early operation of the desiccant cooling. During the daytime, when solar radiation is high enough, the solar thermal collection started to support the operation of the DHVAC system and the excess collected solar energy is stored in the thermal storage tank for late day operation of the DHVAC system. However, during daytime, when solar radiation suddenly drops, due to sudden rain or cloudy sky, a backup daytime heating is operated which can be sourced from either the electric heater or any kind of air-heating devices.

11.2.3 DHVAC Operation

The DHVAC system processing of air is shown in Fig. 11.4. Figure 11.4a shows the air processes for the previous system [21], and Fig. 11.4b shows the air processes for the present system. The comparison shows the reduction in the supply air (SA) due to the application of the second evaporative cooler. As presented, the outdoor air (state 1/2) is dehumidified upon passing the rotating desiccant wheel, but its temperature increases due to the conversion of air latent energy to sensible energy, heat of sorption and heat carryover (state 3). The air in state 3 is pre-cooled by the big sensible heat exchanger and split for states 4 and 4′. The air at state 4′ is cooled and humidified using the evaporative cooler (state 5′). The cooled air of state 5′ is used to cool the state 4 air as the supply air (state 5). The air after the smaller

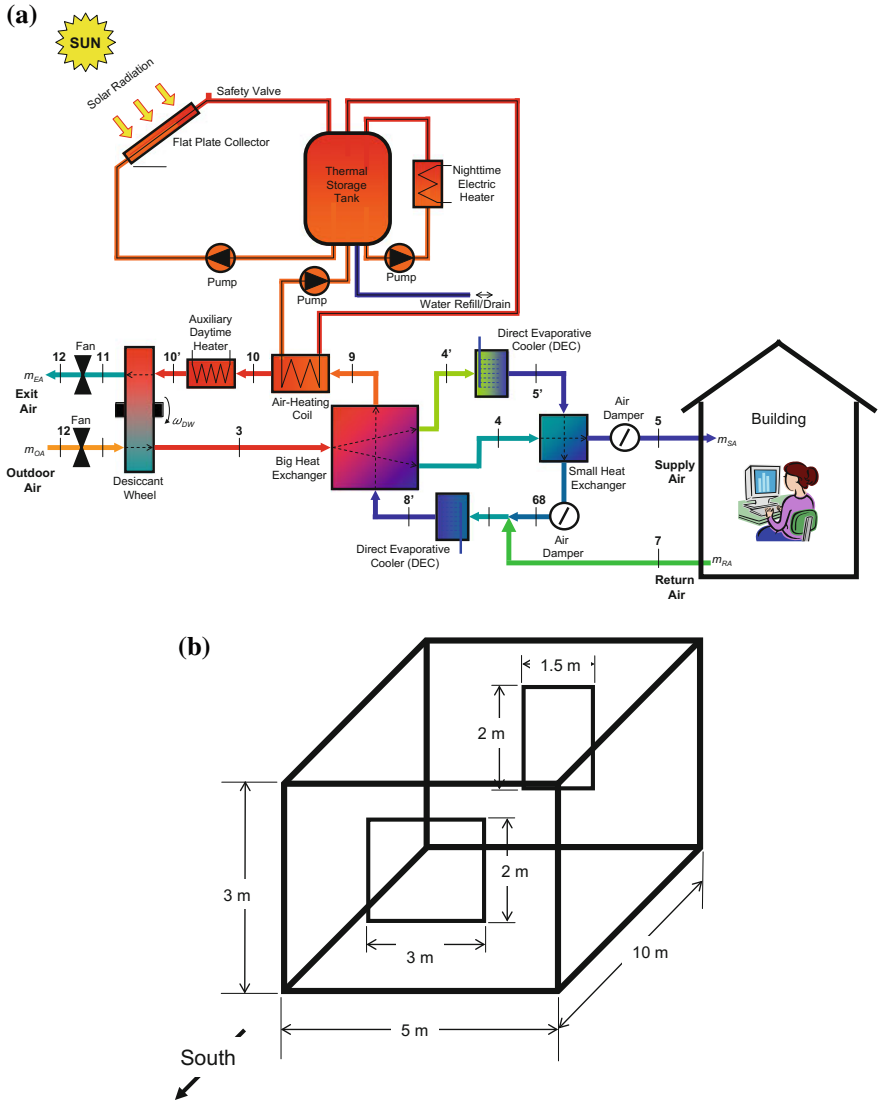

Fig. 11.3 Schematic diagram of the solar-DHVAC system coupled to the hypothetical building: **a** solar-DHVAC system schematic design and **b** hypothetical building dimensions and specifications

heat exchanger (state 6) is combined with the return air (state 7) for further cooling by the evaporative cooler (state 8). This air (state 8) is used to pre-cool the air of state 3 mentioned above. Upon passing the big heat exchanger, the state 8 air is preheated (state 9). The preheated air (state 9) passes the air-heating coil as the regeneration air (state 10). In case of cloudy/rain day, the auxiliary daytime heater

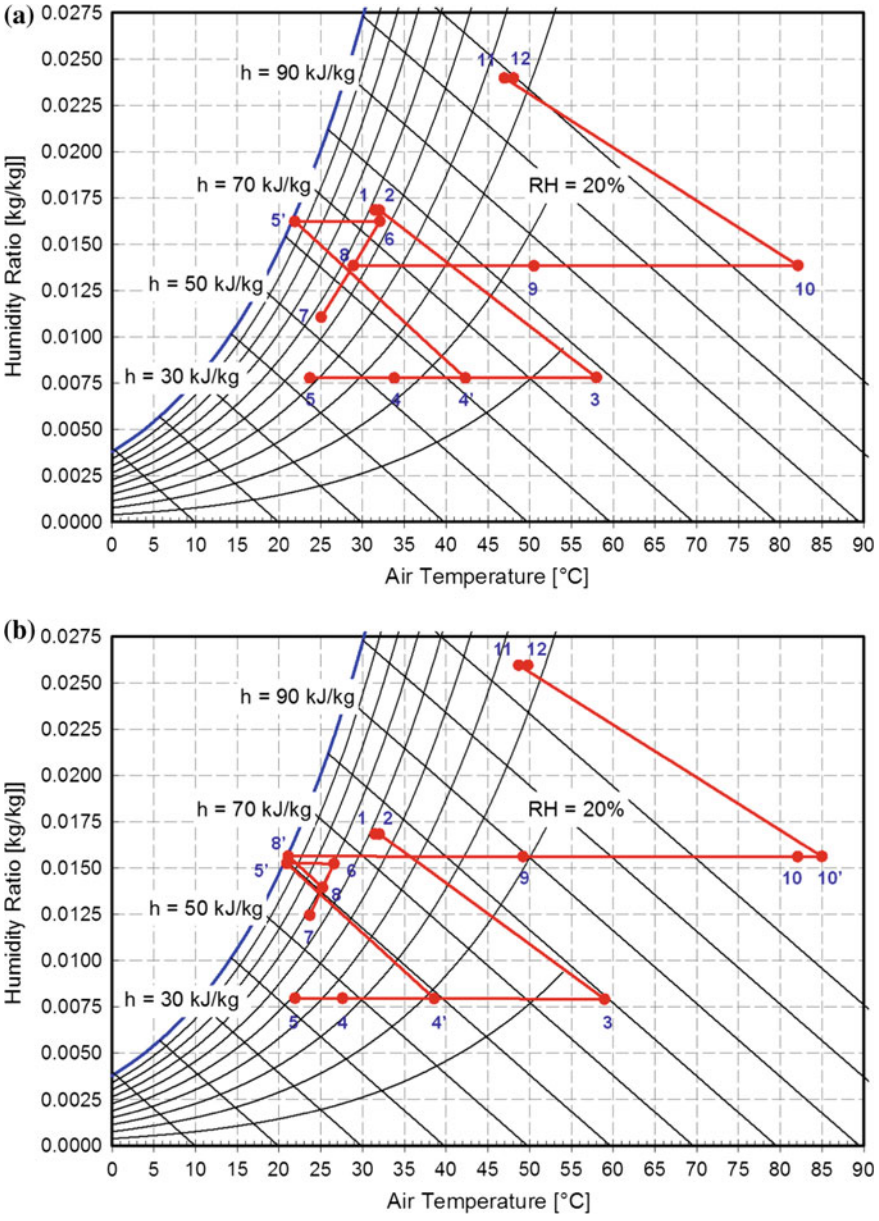

Fig. 11.4 Psychrometric chart showing the states of air of the DHVAC system: **a** original DHVAC system developed by the authors and **b** upgraded design of the DHVAC system presented in Fig. 11.3a. State (1) is the outdoor air (OA), and the state (5) is the supply air (SA). These charts show the comparison of air processes for the desiccant cooling system for understanding of the system air processes and states

operates to augment the regeneration thermal energy requirement (state 10′). The regeneration air (states 10/10′) is used to regenerate the rotating desiccant wheel. The air (states 11/12) becomes moist due to the removal of moisture from the desiccant wheel and is exhausted to the outdoor environment (state 12).

11.3 System Modeling

11.3.1 System Model

The solar–DHVAC system is modeled in the transient system simulation (TRNSYS) program [28]. The model considered the heat losses in the piping network as observed in the actual operation of the system [21]. The model used the flat plate collector, stratified thermal storage tank, electric heater, air-heating coil, water pump, water pipe, desiccant wheel, cross-flow heat exchangers, evaporative cooler and air fans. This system model follows the system design of the solar–DHVAC system of Enteria et al. [28, 35].

11.3.2 Model Validation

The developed model was validated by experimental results [35]. Comprehensive validation of model was done by Enteria [36]. The optimization procedure for system sizing is schematically shown in Fig. 11.5. The selection of the indoor thermal comfort conditions is based on the indoor temperature and humidity ratio not more than 26 °C and 13.5 g/kg. This is based on the evaluation of the East Asian region indoor conditions [14, 37–45].

11.3.3 Model Application

The developed model is used to investigate the performance of the solar–DHVAC system with Silica Gel and Titanium Dioxide desiccant wheels. The solar–DHVAC system is applied in a hypothetical building shown in Fig. 11.3 [11]. The specifications are shown in Table 11.1. The selection of the building envelope U values was based on the gathered information from the East Asian region [13, 30, 39, 46–51]. The building is rectangular in shape with all four walls as external. The building is cool and ventilated using the solar–DHVAC system from 8 A.M. to 6 P.M. during weekdays (Monday to Friday). There are five people inside the office buildings doing light work each with computer and printer. Each worker is assumed to have sensible gain of 75 W and latent gain of 75 W. They worked from 8 A.M.

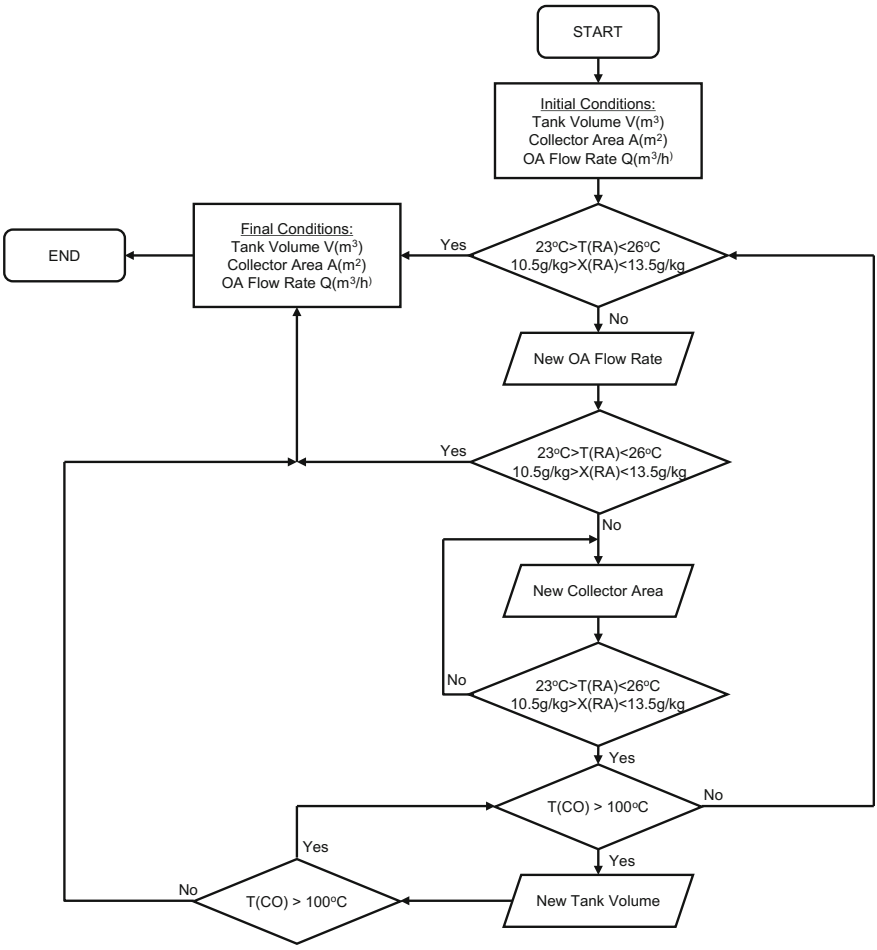

Fig. 11.5 Optimization procedure of the solar–DHVAC system for application in different climatic conditions. (*OA*) is outdoor air; (*RA*) is return air; (*T*) is temperature; (*X*) is humidity ratio; and (*CO*) is solar collector outlet

to 6 P.M. The computer has thermal gain of 230 W. The office lighting has 17 W/m^2. The building air infiltration is assumed to be 0.5 ACH (air change per hour). All the thermal gains from computers, lighting and occupants started from 8 A.M. and ended at 6 P.M. The system is applied in temperate climate (Tokyo, Beijing), subtropical climate (Hong Kong, Taipei) and tropical climate (Philippines, Singapore). Table 11.2 shows the geographical locations of the different cities for the system application. Figure 11.6 shows the outdoor air conditions for the countries and cities where the solar–DHVAC system is investigated. The system is applied during the hottest week of the year based on the typical metrological year (TMY). Figure 11.6 shows the climatic conditions of the different places for the

Table 11.1 Hypothetical building construction material specifications and description

Building part	Part materials	Material thickness [m]	Total thickness [m]	U value [W/m^{2}K]
Roof	Plaster board	0.010	0.140	0.316
	Fiberglass quilt	0.112		
	Roof deck	0.019		
External walls	Concrete block	0.100	0.170	0.511
	Foam insulation	0.061		
	Wood sliding	0.009		
Glass windows	Insulating glass	–	–	2.800
Floor	Concrete slab	0.080	0.080	0.040
	Insulation back			

Table 11.2 Different climates of the East Asia with the specified countries and its cities showing the coordinates for the application of the solar–DHVAC system

Climate	Country	City	Latitude	Longitude
Temperate	China	Beijing	39°54′50″N	116°23′30″E
	Japan	Tokyo	35°42′2″N	139°42′54″E
Subtropical	Taiwan/China	Taipei	25°2′0″N	121°38′0″E
	China SAR	Hong Kong	22°15′0″N	114°10′0″E
Tropical	Philippines	Manila	14°35′0″N	120°58′0″E
	Singapore	Singapore	1°17′0″N	103°50′0″E

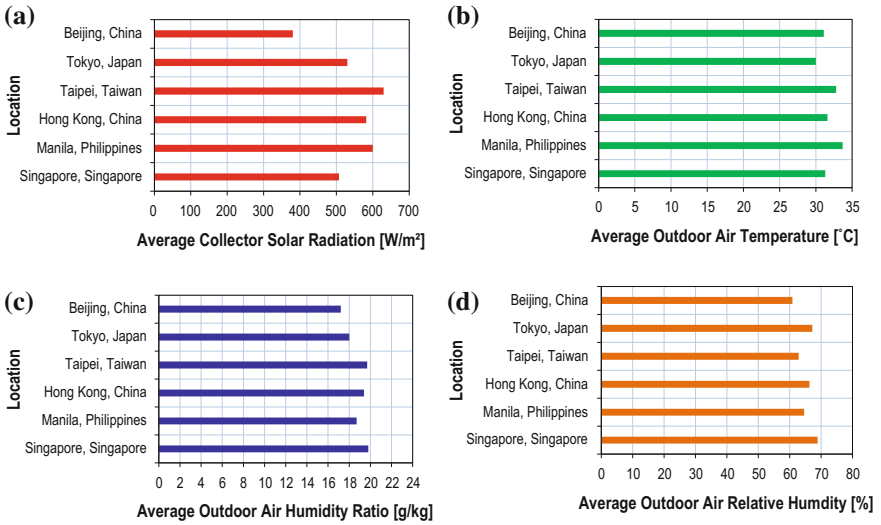

Fig. 11.6 Average climatic condition in the East Asia during the hottest summer day of the year based on the typical metrological year (TYM) in the Meteonorm weather data in TRNSYS: **a** solar radiation in the collector surface; **b** outdoor air temperature; **c** outdoor air humidity ratio; and **d** outdoor air relative humidity. Data for Beijing, China (July 10); Tokyo, Japan (August 1); Hongkong, China (August 20); Taipei, Taiwan (July 19); Manila, Philippines (May 21); and Singapore, Singapore (May 21)

application of the solar–DHVAC system. Figure 11.6a shows the available average solar energy in the surface of the solar collector during the hottest day based on the typical meteorological year (TMY). The solar collector inclination angle is optimized to its latitude [35]. It shows that higher solar radiation is available in Taipei and Hong Kong compared to Beijing, Tokyo, Manila and Singapore. It also shows that solar radiation in Manila and Singapore is higher compared to Beijing and Tokyo during this day. Figure 11.6b shows the average outdoor air temperature. It shows that Manila has the higher outdoor air temperature. However, all the outdoor air temperatures are above 30 °C. Figure 11.6c shows the average outdoor air humidity ratio. The trend shows that the humidity increases from Beijing to Singapore. The humidity ratio in Singapore is almost 20 g/kg and the same in Taipei. Beijing has the lowest outdoor air humidity ratio around 17 g/kg. Figure 11.6d shows the equivalent relative humidity. It also shows that the relative humidity trend increasing from Beijing to Singapore. It means that the nearer the location to the equator (tropical climate) in the selected region, the higher the humidity ratio compared to the northern location (temperate climate). As seen in Fig. 11.6a, the available solar energy in the collector is not as high compared to the solar collector in the location of Taipei and Hong Kong.

11.4 Performance Indices

11.4.1 Solar Thermal System

The performance of the solar thermal system is presented as the thermal coefficient of performance (TCOP)

$$\mathrm{TCOP} = \frac{\int_S^E \left(\dot{Q}_{L,1}\right)\mathrm{d}t + \int_S^E \left(\dot{Q}_{L,2}\right)\mathrm{d}t}{\int_S^E \left(\dot{E}_{H,1}\right)\mathrm{d}t + \int_S^E \left(\dot{E}_{H,2}\right)\mathrm{d}t} \tag{11.1}$$

where;

$$\dot{Q}_{L,1} = \dot{m}_{10}(h_{11} - h_{10});\ \dot{Q}_{L,2} = \dot{m}_{10}(h_{12} - h_{11})$$

$$\dot{E}_{H,1} = (V_{\mathrm{ol}} I_{\mathrm{Cur}} \varphi_{\mathrm{PF}})_{H,1};\ \dot{E}_{H,2} = (V_{\mathrm{ol}} I_{\mathrm{Cur}} \varphi_{\mathrm{PF}})_{H,2}$$

The amount of solar energy contribution in the requirement of the thermal energy for the operation of the DHVAC system is expressed as the solar fraction (SF)

$$\mathrm{SF} = \frac{\int_S^E (\dot{Q}_{\mathrm{SC}})\mathrm{d}t}{\int_S^E (\dot{Q}_{H,1})\mathrm{d}t + \int_S^E (\dot{Q}_{H,2})\mathrm{d}t + \int_S^E (\dot{Q}_{\mathrm{SC}})\mathrm{d}t} \tag{11.2}$$

where;

$$\dot{Q}_{\mathrm{SC}} = \dot{m}_{\mathrm{Col}} C_{P,\mathrm{Col}} (T_o - T_i)$$

11.4.2 DHVAC System

The DHVAC system performance is expressed as the desiccant coefficient of performance (DCOP)

$$\mathrm{DCOP} = \frac{\int_S^E (\dot{Q}_{\mathrm{CL}})\mathrm{d}t}{\int_S^E (\dot{Q}_{H,1})\mathrm{d}t + \int_S^E (\dot{Q}_{H,2})\mathrm{d}t} \tag{11.3}$$

where

$$\dot{Q}_{\mathrm{CL}} = \dot{m}_{\mathrm{SA}}(h_{\mathrm{OA}} - h_{\mathrm{SA}});\ \dot{Q}_{H,1} = \dot{m}_{10}(h_{11} - h_{10});\ \dot{Q}_{H,2} = \dot{m}_{10}(h_{12} - h_{11})$$

The calculations of the sensible heat ratio (SHR) are based on the cooling load (CL) and the cooling effect (CE). The calculation of the sensible heat ratio based on cooling load is expressed as the

$$\mathrm{SHR}_{\mathrm{CL}} = \frac{\int_S^E (\dot{Q}_{\mathrm{SE}})_{\mathrm{CL}}\mathrm{d}t}{\int_S^E (\dot{Q}_{\mathrm{SE}})_{\mathrm{CL}}\mathrm{d}t + \int_S^E (\dot{Q}_{\mathrm{LE}})_{\mathrm{CL}}\mathrm{d}t} \tag{11.4}$$

where

$$\dot{Q}_{\mathrm{SE}} = \dot{m}_{\mathrm{SA}} C_{P,A}(T_{\mathrm{OA}} - T_{\mathrm{SA}});\ \dot{Q}_{\mathrm{LE}} = \dot{m}_{\mathrm{SA}} H_{\mathrm{Con}}(X_{\mathrm{OA}} - X_{\mathrm{SA}})$$

while the calculation of the sensible heat ratio based on cooling effect (CE) is based on the

$$\mathrm{SHR}_{\mathrm{CE}} = \frac{\int_S^E (\dot{Q}_{\mathrm{SE}})_{\mathrm{CE}}\mathrm{d}t}{\int_S^E (\dot{Q}_{\mathrm{SE}})_{\mathrm{CE}}\mathrm{d}t + \int_S^E (\dot{Q}_{\mathrm{LE}})_{\mathrm{CE}}\mathrm{d}t} \tag{11.5}$$

where

$$\dot{Q}_{\mathrm{SE}} = \dot{m}_{\mathrm{SA}} C_{P,A}(T_{\mathrm{RA}} - T_{\mathrm{SA}});\ \dot{Q}_{\mathrm{LE}} = \dot{m}_{\mathrm{SA}} H_{\mathrm{Con}}(X_{\mathrm{RA}} - X_{\mathrm{SA}})$$

11.4.3 Total System

The performance of the total system based on the electric energy consumption is based on the off-peak electric energy consumption (OPEC) [11]. The OPEC is calculated on the total system electric energy consumption during off-peak and peak time. The off-peak electric energy consumption is based on the electric energy consumed from 12 midnight to 6 A.M. for the nighttime thermal energy storage and pump power consumption.

$$\mathrm{OPEC} = \frac{\int_S^E \left(\dot{E}_{\mathrm{OP}}\right)\mathrm{d}t}{\int_S^E \left(\dot{E}_{OP}\right)\mathrm{d}t + \int_S^E \left(\dot{E}_P\right)\mathrm{d}t} \tag{11.6}$$

where;

$$\dot{E}_{OP} = \dot{E}_{H,1} + \dot{E}_{P,1};\ \dot{E}_P = \dot{E}_{H,2} + \dot{E}_{P,1} + \dot{E}_{P,2} + \dot{E}_{F,1} + \dot{E}_{F,2}$$

It is assumed that air fans consumed 100 W per 200 m^3/h of air flow rate. This assumption is based on the experimental setup installation. The water pump has a power consumption of 20 W for the water pump going to the solar collector and electric heater (experimental setup installation). A 10 W is for the pump going to the air-heating coil (experimental setup installation). The electric heater has a power consumption of 3 kW each (experimental setup installation). The total system performance is based on the system coefficient of performance (SCOP) expressed as

$$\mathrm{SCOP} = \frac{\int_S^E \left(\dot{Q}_{\mathrm{CL}}\right)\mathrm{d}t}{\int_S^E \left(\dot{E}_{\mathrm{OP}}\right)\mathrm{d}t + \int_S^E \left(\dot{E}_P\right)\mathrm{d}t} \tag{11.7}$$

11.5 Results and Discussion

11.5.1 Solar Thermal Performance

Figure 11.7 shows the average outlet temperature of the solar collector and the collector efficiency. It shows that the collector outlet temperature is maintained above 90 °C for all the location. It shows that it has higher temperature for the cases of Taipei and Manila compared to the other locations. This is due to the higher average solar radiation as presented in Fig. 11.6. In addition, the collector efficiency is maintained between 50 and 70%. However, as presented in the results, the efficiency increases from Beijing to Singapore. This is mainly due to the lower inlet temperature of water circulating in the collector resulting from bigger thermal storage tank as presented in Table 11.3.

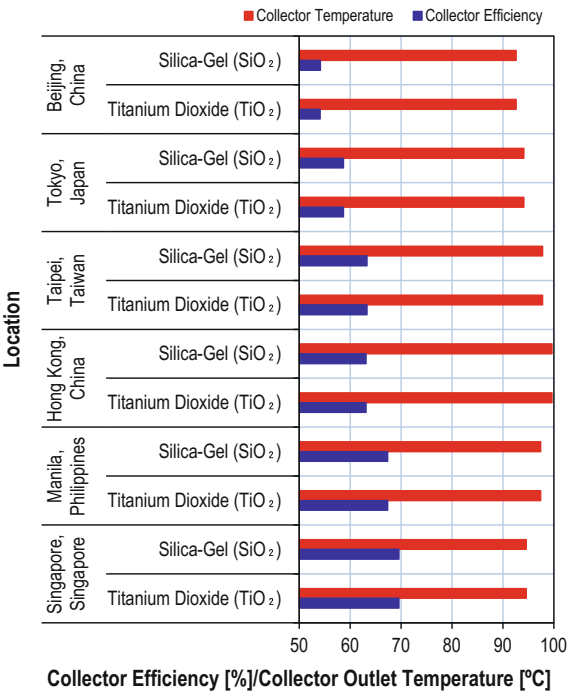

Fig. 11.7 Solar thermal collector performance at different climatic conditions with respect to the different cities

Figure 11.8 shows the solar energy fraction called solar fraction (SF) in its contribution to the thermal energy requirement of the solar–DHVAC system and the electric energy consumption during off-peak load from 3 A.M. to 5 A.M. Based on the optimized and specified solar–DHVAC system, the solar energy contributed between 65 and 90% of the system thermal energy requirement. This is the same for both the Titanium Dioxide and Silica Gel desiccant wheel since the specification is

Table 11.3 Specifications of the solar–DHVAC system under investigation when applied in the different climatic conditions in East Asian countries representing the temperate, subtropical and tropical climates

Country	City	Flat plate collector		Thermal storage tank		Air flow rate	
		Inclination angle (°)	Surface area (m^2)	Volume (m^3)	Height (m)	Outdoor air (m^3/h)	Supply air (m^3/h)
China	Beijing	39	12	0.644	1.7	700	350
Japan	Tokyo	35	10	0.644	1.7	800	400
Taiwan/China	Taipei	25	14	0.966	1.7	1200	600
China SAR	Hong Kong	22	12	0.966	1.7	1200	600
Philippines	Manila	14	14	1.288	1.7	1000	500
Singapore	Singapore	1	14	1.288	1.7	1500	750

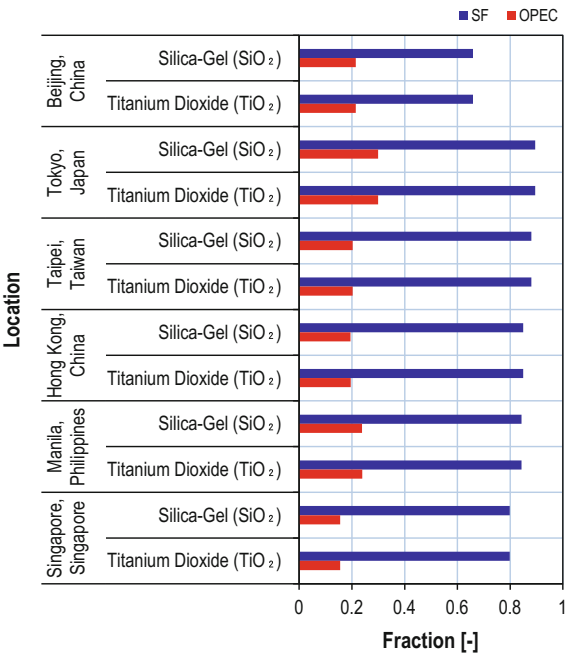

Fig. 11.8 Solar fraction (*SF*) and off-peak electric energy consumption (*OPEC*) during the solar-DHVAC system operation at different cities for two kinds of desiccant wheel

the same for the same place. Also, it shows that the OPEC is between 15 and 30%. The SF is higher in almost all places except China. The lower SF in China is due to the lower solar energy as shown in Fig. 11.6a. It also shows that the higher OPEC is in Tokyo due to the higher SF. But it does not mean that when SF is higher, the OPEC is also higher as in the case of Hong Kong. Factors such as outdoor air conditions affected the auxiliary electric heating operation.

11.5.1.1 DHVAC Performance

Figure 11.9 shows the regeneration temperature "RegT(Solar Thermal)" provided by the solar collection through the heat exchanger shown in state 10 (Fig. 11.3). This is the maximum possible temperature which can be provided by the solar thermal system since increasing this regeneration temperature makes the outlet temperature of solar collector to increase up to 100 °C and results in the opening of the collector safety valve. Thereof, the auxiliary heater provided after the heat exchanger supported the increase in the required regeneration temperature "RegT (Daytime Heater)." As shown in the results, in Beijing, higher support of the auxiliary daytime heater is needed as the available solar radiation is lower shown in Fig. 11.6 compared to other location. However, in most cases, the augmentation of the daytime heater to support the required regeneration temperature is lower or less

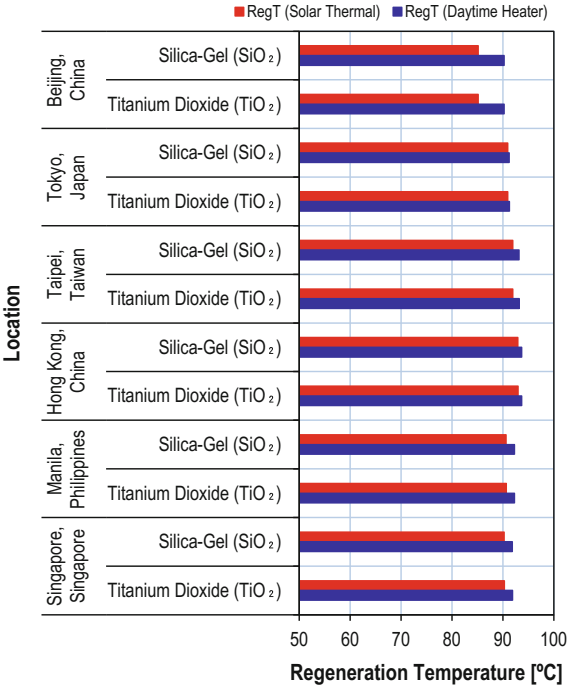

Fig. 11.9 Regeneration temperature supported by the solar thermal (*RegT-Solar Thermal*) and the regeneration temperature after the auxiliary heater (*RegT-Daytime Heater*) during the solar-DHVAC system operation at different cities for two kinds of desiccant wheel

than 2% percent difference between "RegT(Solar Thermal)" and "RegT(Daytime Heater)."

Figure 11.10 shows the effectiveness of the evaporative coolers (DEC1 and DEC2). The locations of the two coolers are shown in Fig. 11.3. As shown in the results, the effectiveness of the two evaporative coolers is more than 90% for all locations. In addition, the application of the Titanium Dioxide desiccant wheel makes the effectiveness higher. The situation is due to the lower moisture content of the intake air to the evaporative cooler when using the Titanium Dioxide desiccant wheel. However, the increase in temperature of the intake air using the Titanium Dioxide wheel contributed to lower percent difference between the effectiveness using the Silica Gel and Titanium Dioxide wheel of less than 2%.

Figure 11.11 shows the cooling load (CL) and the cooling effect (CE). It shows that the cooling load increases from Beijing to Singapore. This means that large amount of thermal energy (sensible and latent) is required to maintain the indoor thermal comfort condition in the Southeast Asia compared to Northeast Asia. This situation resulted in higher volumetric air flow needed for indoor thermal load and to maintain the comfortable indoor environment (indoor temperature and humidity ratio).

Figure 11.12 shows the content of latent energy and the sensible energy in the air based on the CL and the CE presented in Fig. 11.11. The latent and sensible energy contents are based on the sensible heat ratio (SHR). It shows that the SHR

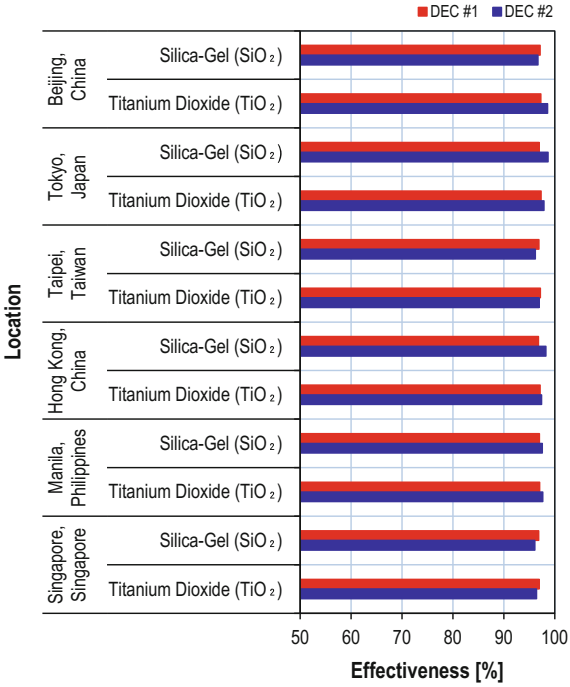

Fig. 11.10 Effectiveness for the direct evaporative cooler 1 (*DEC #1*) and direct evaporative cooler 2 (*DEC #2*) during the solar-DHVAC system operation at different cities for two kinds of desiccant wheel

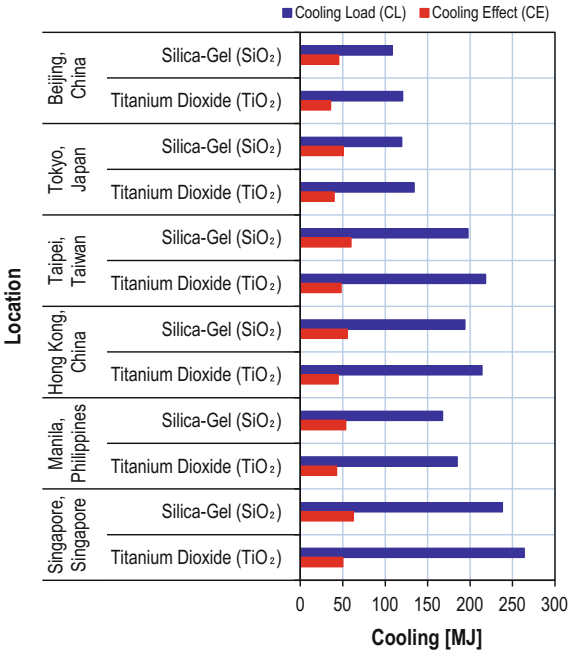

Fig. 11.11 Cooling effect (*CE*) and cooling load (*CL*) during the solar-DHVAC system operation at different cities for two kinds of desiccant wheel

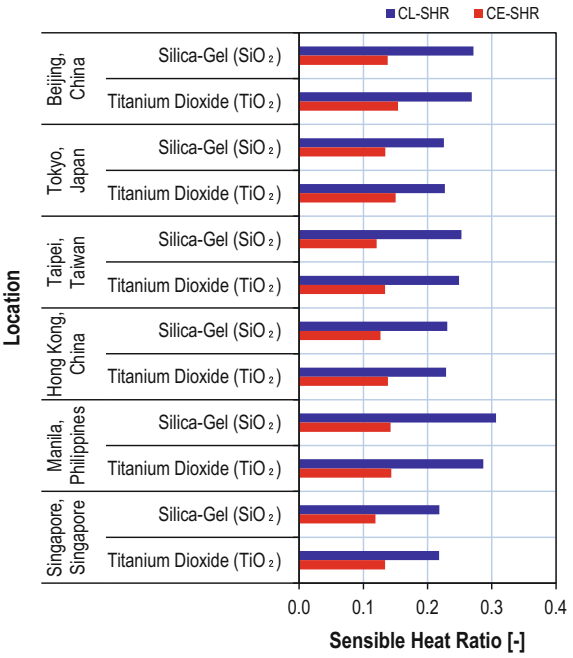

Fig. 11.12 Cooling effect–sensible heat ratio (*CE-SHR*) and cooling load–sensible heat ratio (*CL-SHR*) during the solar-DHVAC system operation at different cities for two kinds of desiccant wheel

for the cooling load (CL-SHR) is lower than the cooling effect (CE-SHR). It means that the CE has lower sensible energy content compared to the CL. It also shows that the SHR for both CL and CE for different climates is almost the same. It means that even in the Southeast Asian with higher latent energy content due to the higher moisture in the air, the air temperature is also high resulting in higher sensible energy content.

11.5.2 Building Performance

Figure 11.13 shows the outdoor air temperature (OA), supply air (SA) temperature and the room air (RA) temperature. The room temperature can be maintained between 26.5 and 23.5 °C using the system specification mentioned in Table 11.3. The supply air temperature is 2–3 °C lower than that of the room temperature. It also shows that the solar–DHVAC system with Titanium Dioxide desiccant wheel can provide lower supply air temperature resulting in the maintenance of room temperature below 25 °C compared to the system with Silica Gel desiccant wheel.

Figure 11.14 shows the OA humidity ratio, SA humidity ratio and the RA humidity ratio. It shows that the specified solar–DHVAC system shown in Table 11.3 provided the required indoor humidity ratio between 11 and 12.5 g/kg. In addition, it shows that the Titanium Dioxide desiccant wheel can provide much

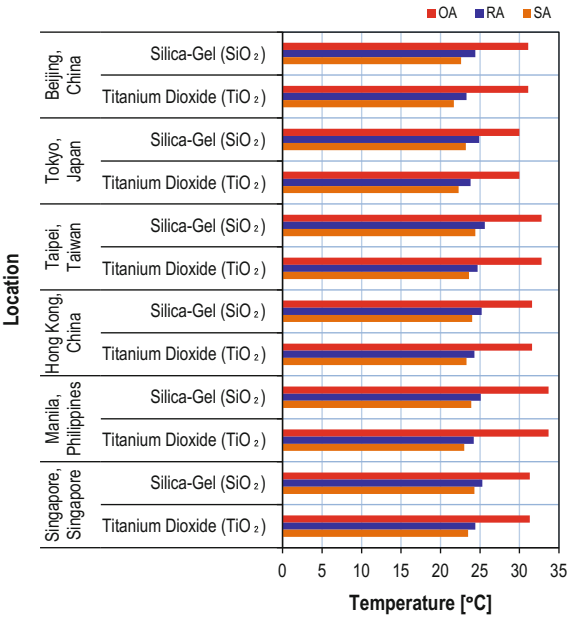

Fig. 11.13 Temperature of outdoor air (*OA*), supply air (*SA*) and return air (*RA*) during the solar-DHVAC system operation at different cities for two kinds of desiccant wheel

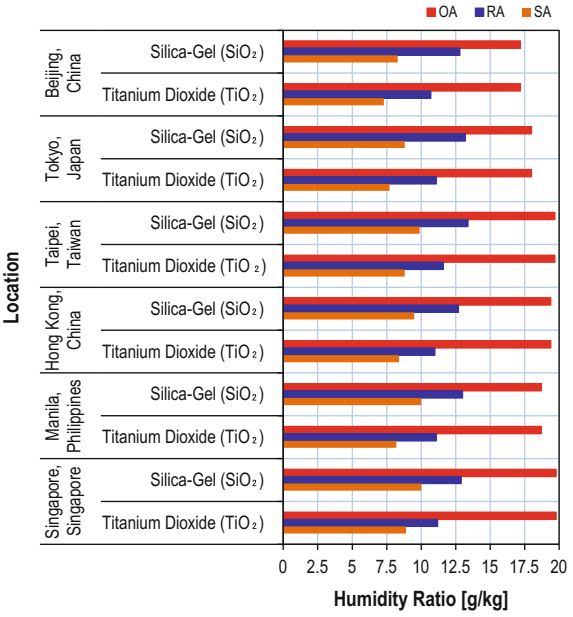

Fig. 11.14 Humidity ratio of outdoor air (*OA*), supply air (*SA*) and return air (*RA*) during the solar-DHVAC system operation at different cities for two kinds of desiccant wheel

lower humidity ratio compared to the Silica Gel desiccant wheel of the same system size. It shows that the Titanium Dioxide material can provide supply air (SA) humidity ratio as low as 7.5 g/kg compared to the Silica Gel of around 8.5 g/kg in the case of Beijing.

Figure 11.15 shows the equivalent relative humidity for the temperature and humidity ratio given in Figs. 11.13 and 11.14 for the outdoor air OA, SA and RA. It shows that the supply air relative humidity is between 45 and 55% for both the Silica Gel and Titanium Dioxide desiccant wheels. However, the Titanium Dioxide desiccant wheel produces lower relative humidity which is between 45 and 50%. This result is due to the lower humidity ratio produced by the Titanium Dioxide desiccant wheel presented in Fig. 11.14 compared to Silica Gel.

11.5.3 Total System Performance

Figure 11.16 shows the performance of the specified solar–DHVAC system. The figure shows the (SCOP, TCOP) and the DCOP. It shows that the DHVAC system has a COP between 1.5 and almost 3. The highest performance is in the Southeast Asia due to the higher dehumidification performance as outdoor air has higher humidity content. The TCOP is between 1 and 5.5 and higher in Tokyo due to the higher solar energy collection as presented in Fig. 11.8. The SCOP shows that it is between 1.5 and almost 3. It shows that the system has higher SCOP in the

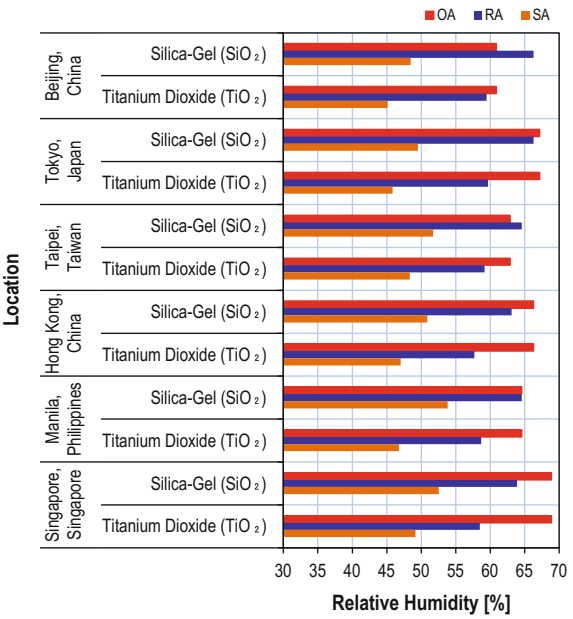

Fig. 11.15 Relative humidity of outdoor air (*OA*), supply air (*SA*) and return air (*RA*) during the solar-DHVAC system operation at different cities for two kinds of desiccant wheel

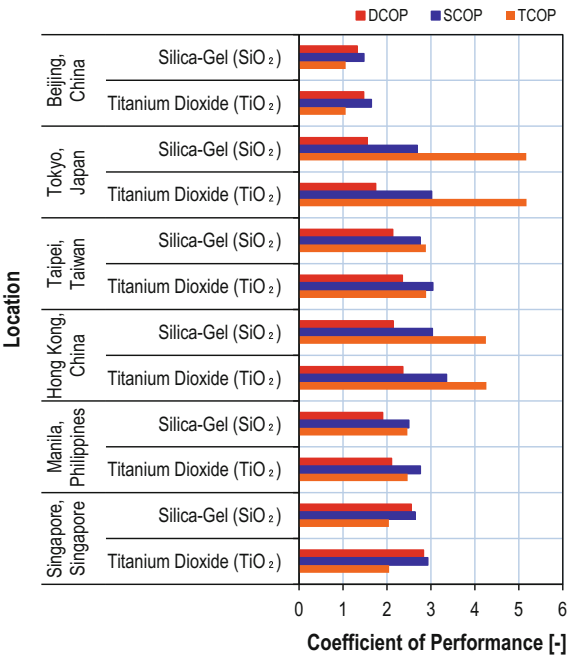

Fig. 11.16 System coefficient of performance (*SCOP*), thermal coefficient of performance (*TCOP*) and desiccant coefficient of performance (*DCOP*) during the solar-DHVAC system operation at different cities for two kinds of desiccant wheel

Southeast Asia due to the high solar energy collection (Fig. 11.8) and higher cooling load (Fig. 11.11).

Figure 11.17 shows the correlation between the outdoor air conditions (air temperature and humidity ratio) to the required ventilation flow rates. Figure 11.17a shows for the outdoor air temperature to the ventilation flow rates, and it shows that Beijing has lower required ventilation flow rate compared to Singapore. Beijing is in the northernmost of all cities investigated, while Singapore is the nearest to the equator. Based on Fig. 11.17b, for the correlation between the outdoor air humidity ratio to the required ventilation flow rate, it shows that Singapore with highest outdoor air humidity ratio to the required higher ventilation flow rate compared to other cities such as Beijing and Tokyo which are temperate. However, the required ventilation for Manila, Taipei and Hong Kong is 500–600 m^3/h since these cities are near to each other.

Figure 11.18 shows the correlation between the available solar energy in the surface of the solar collector and the required size of the solar collector and the thermal tank volume. As presented in Fig. 11.18a, for higher available solar energy in the collector, obviously the required size of the solar energy collector will be smaller; however, as the required regeneration energy will be higher, the required solar collector area will be large also. In addition, as shown in Fig. 11.18b, the required size of the thermal storage tank increases as the available solar radiation is getting larger due to the increase in the surface area of the solar collector presented

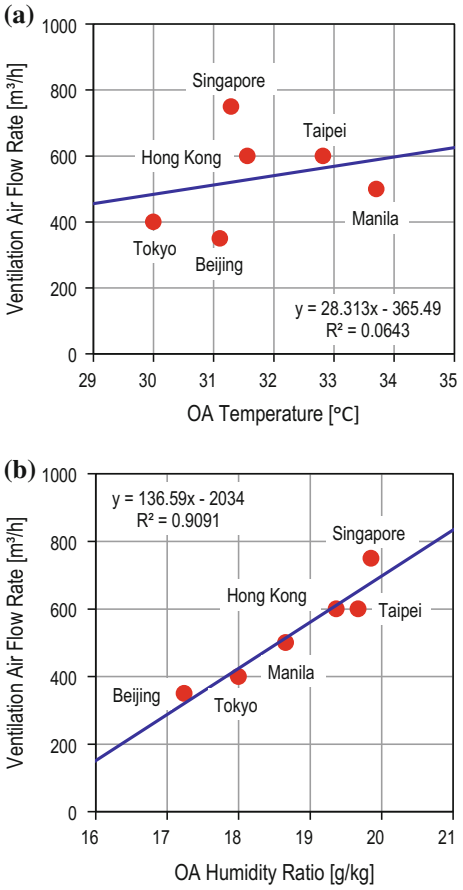

Fig. 11.17 Correlation between the outdoor air conditions and the required ventilation air flow rates: **a** correlation between the outdoor air temperature and the ventilation air flow rate, and **b** correlation between the outdoor air humidity ratio and the ventilation air flow rate

in Fig. 11.18a. This is due to the requirement of higher thermal buffer storage when the amount of collected solar energy is getting higher as presented in Fig. 11.19.

Figure 11.19 shows the correlation for the thermal storage tank size to the required solar collector area. As shown in the result, temperate climate required lesser size of thermal storage tank and solar thermal collector area. The next with lesser size of the required thermal storage tank and solar collector area is in the case of subtropical climate, while for the case of tropical climate, it required larger size of the thermal storage tank and larger surface area of solar thermal collector. This result is due to the higher volumetric air flow requirement from temperate climate to tropical climate.

The solar–DHVAC system is optimized to provide the needed indoor thermal comfort conditions through the determination of the solar collector area, thermal storage tank and air flow rate. Based on the optimization conducted for the application of the system in the different climates in the East Asia, Table 11.3 shows the required solar–DHVAC system specification.

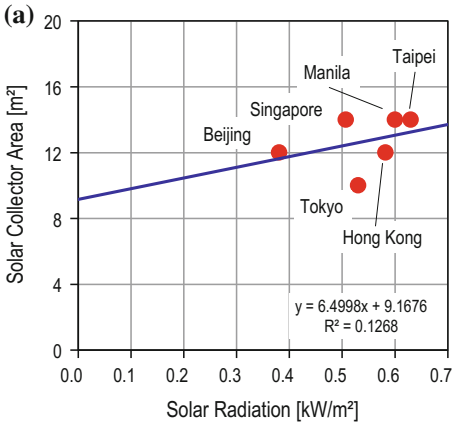

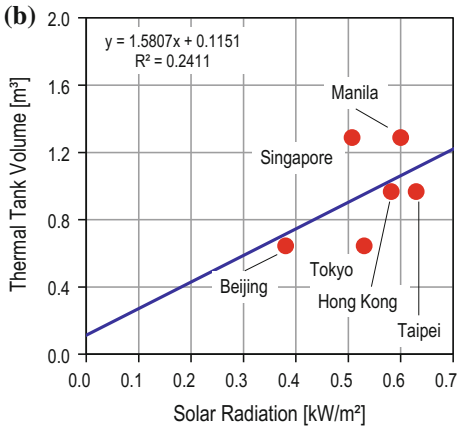

Fig. 11.18 Correlation between the solar radiation available in the inclined solar thermal collector to the size of the solar thermal collector and the thermal storage tank:
a correlation between the solar radiation available in the surface of the inclined solar collector to the area of the solar collector, and
b correlation between the solar radiation available in the surface of the inclined solar collector to the volume of the thermal storage tank

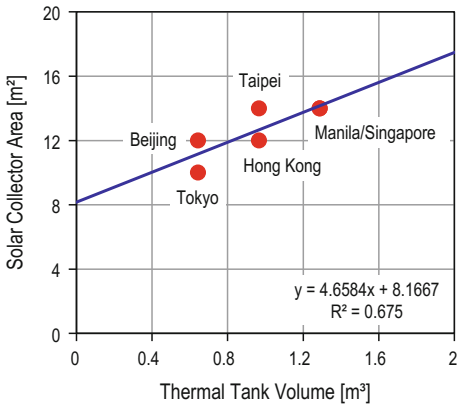

Fig. 11.19 Correlation between the thermal storage tank volume and the solar collector area for the different cities in East Asian climates

It shows that the needed collector surface area in the Southeast Asia is bigger than of the Northeast Asia. In addition, the required thermal storage tank is bigger in the Southeast Asia than that of the Northeast Asia. Also, the required air flow rate is higher in the Southeast Asia than in the Northeast Asia. White et al. [52] show also that in warm climate, higher ventilation rate is needed. The larger required size of the solar collector is due to the higher air flow rate requirement to maintain the indoor comfortable temperature and humidity ratio conditions. In addition, due to the higher thermal energy collection in the Southeast Asia, the thermal storage tank requirement is also bigger. This situation resulted in bigger system size in the Southeast Asia compared to the Northeast Asia.

11.6 Conclusions

The solar–DHVAC system using Silica Gel and Titanium Dioxide materials in the desiccant wheel was numerically investigated in different climates in East Asia—temperate, subtropical and tropical using the transient system simulation (TRNSYS) program. The investigation centered on the optimal design of the system which can deliver the required indoor thermal comfortable conditions—temperature and humidity ratio.

The specific conclusions show that:

- The performance of the Titanium Dioxide desiccant wheel is higher than the Silica Gel desiccant wheel in reducing air moisture content.
- The solar–DHVAC system with Titanium Dioxide desiccant wheel can produce lower supply air humidity ratio and temperature resulting in the maintenance of the indoor humidity ratio and temperature at lower value than with the Silica Gel desiccant wheel.
- Large surface area of solar collector is needed in the tropical climate compared to the temperate climate to support the higher air flow rate requirement of the building to maintain the required indoor thermal comfortable conditions. This resulted in large volume of thermal storage tank to accommodate the collected solar thermal energy
- The SCOP is within 1.5–3 in which the OPEC contributed from 15 to 30% of the system total electric energy consumption.
- As high air volumetric flow rates are required in the more humid tropical climate, large amount of electric energy is used to support the air fans power requirements.
- The contribution of solar energy for the required thermal energy of the DHVAC system operation is between 65 and 90% (SF).
- Even with the SCOP between 1.5 and 3 when compared to the conventional vapor compression system, the solar–DHVAC system consumed OPEC from 15 to 30%.

- The solar–DHVAC system is applicable under East Asian climatic conditions as long as the proper specifications are applied such as the size of the flat plate collector, inclination of the collector plate, thermal storage tank volume and the required air flow rates going to the building.

The TiO_2 material used in the desiccant wheel can have higher dehumidification and cooling performance when applied as a replacement of the common Silica Gel desiccant wheel due to the higher dehumidification capability. Using TiO_2 desiccant wheel, the cooling load(Q_{CL}) can be increased by 10.05% in Beijing, 10.88% in Tokyo, 9.50% in Taipei, 9.43% in Hong Kong, 9.34% in Manila and 9.75% in Singapore. The cooling effect (Q_{CE}) can also be increased by 21.36% in Beijing, 21.28% in Tokyo, 19.65% in Taipei, 19.49% in Hong Kong, 20.32% in Manila and 19.88% in Singapore.

When using the solar–DHVAC system with high volumetric flow of air, fan power consumption should be considered when implementing. As daytime electric heating is required in case of rainy or cloudy day, auxiliary heating powered by other sources of thermal energy such as waste heat or gas can reduce daytime electric energy consumption. As presented in the results, the application of DHVAC system increases the volumetric requirement of the supply air particularly for tropical climate. Thereof, alternative system which air cooling can be done independently from the DHVAC system can reduce the air flow rate requirement as DHVAC system cannot support lower supply air temperature.

References

1. Enteria N, Yoshino H, Mochida A et al (2012) Performance of solar-desiccant cooling system with silica-gel (SiO_2) and titanium dioxide (TiO_2) desiccant wheel applied in East Asian climates. Sol Energy 86:1261–1279
2. Murakami S, Levine MD, Yoshino H et al (2009) Overview of energy consumption and GHG mitigation technologies in the building sector of Japan. Energ Effi 2:179–194
3. Liu W, Lung H, Mathiesen BV et al (2011) Potential of renewable energy systems in China. Appl Energ 88:518–525
4. Chen F, Lu SM, Tseng KT et al (2010) Assessment of renewable energy reserves in Taiwan. Renew Sust Energ Rev 14:2511–2528
5. Lam JC, Wan KKW, Lam TNT et al (2010) An analysis of future building energy use in subtropical Hong Kong. Energy 35:1482–1490
6. Sahakian MD (2011) Understanding household energy consumption patterns: when "West Is Best" in Metro Manila. Energ Policy 39:596–602
7. Wong NH, Jusuf SK, Syafii NI (2011) Evaluation of the impact of the surrounding urban morphology on building energy consumption. Sol Energy 85:57–71
8. Enteria N, Yoshino H, Mochida A (2008) Synergization of clean energy utilization, clean technology development and controlled clean environment through thermally activated desiccant cooling system. Paper presented at the 2nd ASME Energy Sustainability International Conference, Jacksonville, FL, USA, 10–14 Aug 2008. Paper No. ES2008-54103

9. Enteria N (2013) Solar-desiccant air-conditioning systems. In: Enteria N, Akbarzadeh A (eds) Solar energy sciences and engineering applications. CRC Press, Boca Raton
10. Enteria N, Mizutani K (2011) The role of the thermally activated desiccant cooling technologies in the issue of energy and environment. Renew Sust Energ Rev 15:2095–2122
11. Enteria N, Mizutani K, Yoshino H et al (2010) Potential of the solar-desiccant dehumidification and cooling in Asia-Pacific region. Paper presented at the 2010 AIVC International Conference, Paper No. 8A-1
12. Ge T, Ziegler F, Wang R et al (2010) Performance comparison between a solar driven rotary desiccant cooling system and conventional vapour compression system (performance study of desiccant cooling). Appl Therm Eng 30:724–731
13. Lam JC, Wan KKW, Tsang CL et al (2008) Building energy efficiency in different climates. Energ Convers Manage 49:2354–2366
14. Fong KF, Chow TT, Li C et al (2010) Effect of neutral temperature on energy saving of centralized air-conditioning systems in subtropical Hong Kong. Appl Therm Eng 30:1659–1665
15. Liu X, Jiang Y, Liu S et al (2010) Research progress in liquid desiccant air-conditioning devices and systems. Front Energy Power Eng China 4:55–65
16. Ge FH, Guo XL, Hu ZC et al (2011) Energy savings potential of a desiccant assisted hybrid air source heat pump system for residential building in hot summer and cold winter zone in China. Energ Buildings 43:3521–3527
17. Chung JD, Lee DY (2011) Contributions of system components and operating conditions to the performance of desiccant cooling systems. Int J Energ Res 34:922–927
18. Rachman A, Sopian K, Mat S (2011) Feasibility study and performance analysis of solar assisted desiccant cooling technologies in hot and humid climate. Am J Environ Stud 7:207–211
19. Hirunbalabh J, Charoenwat R, Khedari J et al (2007) Feasibility study of desiccant air-conditioning system in Thailand. Build Environ 42:572–577
20. Ando K, Kodama A, Hirose T et al (2005) Experimental study on a process design for adsorption desiccant cooling driven with a low-temperature heat. Adsorption 11:631–636
21. Enteria N, Yoshino H, Mochida et al (2011) Initial operation and performance evaluation of the solar thermal desiccant cooling system. Exp Heat Transfer 24:59–87
22. Jeong JS, Yamaguchi S, Saito K et al (2011) Performance analysis of desiccant dehumidification systems driven by low-grade heat source. Int J Energ Res 34:928–945
23. Davanagere BB, Sherif SA, Goswami DY (1999) A feasibility study of solar desiccant air-conditioning systems—part 1: psychrometrics and analysis of the conditioned zone. Int J Energ Res 23:7–21
24. Henning HM, Erpenbeck T, Hindenburg C et al (2001) The potential of solar energy use in desiccant cooling cycles. Int J Energ Res 24:220–229
25. Balaras CA, Grossman G, Henning HM et al (2007) Solar air-conditioning in Europe—an overview. Renew Sust Energ Rev 11:299–314
26. Wang RZ, Ge TS, Chen CJ et al (2009) Solar sorption cooling systems for residential applications: options and guidelines. Int J Energ Res 32:638–660
27. Desideri U, Proietti S, Sdringola P (2009) Solar-powered cooling systems: technical and economic analysis on industrial refrigeration and air-conditioning applications. Appl Energ 86:1376–1386
28. Enteria N, Yoshino H, Mochida A et al (2008) Modeling and simulation of the combined solar thermal and electric desiccant cooling system. Paper presented at the 2008 annual meeting of the society of heating, air-conditioning and sanitary engineers of Japan, Kusatsu, Shiga, Japan, 27–29 Aug 2008. Paper No. C-10

29. Ge T, Li Y, Wang R et al (2009) Experimental study on a two-stage rotary desiccant cooling system. Int J Energ Res 32:498–508
30. Fong KF, Chow TT, Lee CK et al (2010) Comparative study of different solar cooling systems for buildings in subtropical city. Sol Energy 84:227–244
31. Sekhar SC (2007) A review of ventilation and air-conditioning technologies for energy-efficient healthy buildings in the tropics. Ashrae Tran 113:426–434
32. Enteria N, Mizutani K, Yoshie R et al (2011) Solar-desiccant cooling in Asia-Pacific Region. In: Harris AM (ed) Clean energy: resources, production and development. Nova Science Publishers Inc, New York
33. Enteria N, Yoshino H, Mochida A et al (2010) Experimental heat and mass transfer of the separated and coupled rotating desiccant wheel and sensible wheel. Exp Therm Fluid Sci 34:603–615
34. Enteria N (2011) Performance of desiccant cooling system with silica-gel and new titanate wheel. Internal Report. Tohoku University
35. Enteria N, Yoshino H, Satake A et al (2009) Numerical evaluation and optimization of the combined solar thermal and electric desiccant cooling system. Paper presented at the 2009 ASME International Mechanical Engineering Congress and Exposition, Lake Buena Vista, FL, USA, 13–19 Nov 2009, Paper No. IMECE2009-12800
36. Enteria N (2009) Development and evaluation of the combined solar thermal and electric desiccant cooling system, Ph.D. Thesis, Tohoku University
37. Singapore Local Energy Code. www.bdg.nus.sg/BuildingsEnergy/regulations/index. Accessed 8 Mar 2013
38. Federspiel CC (1998) Statistical analysis of unsolicited thermal sensation complaints in commercial buildings. Ashrae Tran 104:912–923
39. Lin HT, Wang JC (2003) The design index of building energy conservation and CAD program beep in Taiwan. Paper presented at the Eight International IBPSA Conference. Eindhoven, Netherlands. 11–14 Aug, 2003
40. Andamon MM (2006) Thermal comfort and building energy consumption in the Philippine context. Paper presented at the 23rd conference on passive and low energy architecture, 6–8 Sept 2006. Geneva, Switzerland
41. Li YA, Liu XL, Chen HL et al (2006) Study on condensation phenomenon in floor radiant cooling systems. Int J Architectural Sci 7:61–66
42. Goto T, Mitamura T, Yoshino H et al (2007) Long-term survey of thermal adaptation in office buildings in Japan. Build Environ 42:3944–3954
43. Zhou YP, Wu JY, Wang RZ (2007) Effects of weathers and indoor temperatures on performance of energy recovery ventilator. Paper presented at the Building Simulation, Beijing, China. 3–6 Sept, 2007
44. Eang LS, Priyadarsini R (2008) Building energy efficiency labeling programme in Singapore. Energ Policy 36:3982–3992
45. Zhao K, Liu XH, Zhang T et al (2011) Performance of temperature and humidity independent control air-conditioning system in an office buildings. Energ Buildings 43:1895–1903
46. Philippine Department of Energy (http://www.doe.gov.ph/Downloads/GuidelinesCDBUS.pdf). Accessed 26 July 2014
47. Turiel I, Curtis R, Levine MD (1985) Analysis of energy conservation standards for Singapore office buildings. Energy 10:95–107
48. Levine M, Urge-Vorsatz D, Blok K et al (2007) Residential and commercial buildings. In: Metz B, Davidson OR, Bosch PR et al (eds) Climate change 2007: mitigation. Contribution of working group III to the fourth assessment report of the intergovernmental panel on climate. Cambridge University Press, Cambridge, UK and New York, USA. (http://www.ipcc.ch/pdf/assessment-report/ar4/wg3/ar4-wg3-chapter6.pdf. Accessed 24 Nov 2013

49. Yang L, Lam JC, Tsang CL (2008) Energy performance of building envelopes in different climate zones in China. Appl Energ 85:800–817
50. Laustsen J (2008) Energy efficiency requirements in building codes, energy efficiency policies for new buildings. International Energy Agency, Paris, France
51. Evans M, Shui B, Takagi T (2009) Country report on building energy codes in Japan. US Department of Energy (http://www.energycodes.gov/publications/research/documents/countryReports/CountryReport_Japan.pdf). Accessed 5 Mar 2013
52. White SD, Kohlenbach P, Bongs C (2009) Indoor temperature variations resulting from solar desiccant cooling in a building without thermal backup. Int J Energ Res 32:695–704

Chapter 12
In-Situ Performance Evaluation of the Desiccant Heating, Ventilating, and Air-Conditioning System Using Multiple Tracer Gas Dilution Method

Napoleon Enteria, Hiroshi Yoshino, Akashi Mochida, Rie Takaki, Akira Satake, Seizo Baba and Yasumitsu Tanaka

Abstract The desiccant heating, ventilating and air-conditioning system (DHVAC) consists of many heat and mass transfer components operating together with air fans. The performance test using the multiple tracer gas dilution method is important for knowing the internal and external flow rates, including the air leakages. The results of the test show the actual internal air flow rates and the sources of air leakage, and also show the interaction of air in the air-conditioned lecture room and in the mechanical room. The performance test using the multiple tracer gas dilution method in air flow and air leakages is important for a detailed evaluation of DHVAC.

Keywords Tracer gas · Air flow diagnostics · HVAC system · Desiccant materials · Evaporative cooling

This chapter is an expanded version of our paper [1].

N. Enteria (✉)
Building Research Institute, Tsukuba, Japan
e-mail: napoleon@kenken.go.jp; enteria@enteria-ge.com

H. Yoshino · A. Mochida · Y. Tanaka
Tohoku University, Sendai, Japan

R. Takaki
Akita Prefectural University, Akita, Japan

A. Satake
Maeda Corporation, Tokyo, Japan

S. Baba
Earth Clean Tohoku Co., Ltd., Sendai, Japan

N. Enteria et al. (eds.), *Desiccant Heating, Ventilating, and Air-Conditioning Systems*, DOI 10.1007/978-981-10-3047-5_12

Nomenclatures

A	Air
C_i	Tracer gas inlet concentration (m^3/m^3)
C_e	Tracer gas outlet concentration (m^3/m^3)
C_o	Initial tracer gas concentration (m^3/m^3)
DHVAC	Desiccant heating, ventilating and air-conditioning
F_t, Q_i	Inlet air flow rate (m^3/s)
HVAC	Heating, ventilating and air-conditioning system
I, Q_t	Tracer gas flow rate (m^3/s)
Q_e	Outlet air flow rate (m^3/s)
Q_o	Initial air flow rate (m^3/s)
ppm	Part per million
SF_6	Sulfur hexafluoride
TG	Tracer gas
T	Time (s)
V	Control volume (m^3)

Subscript

a	Air
i	Node i
j	Node j
k	Tracer gas type k
t	Tracer gas

12.1 Introduction

Maintenance of the indoor thermal comfort level is one of the major energy consumers in houses and buildings, especially in hot and humid climates, where the air-conditioning system consumes a sizable percentage of energy [2, 3]. The desiccant heating, ventilating and air-conditioning system is one of the alternative HVAC systems as it can utilize alternative energy sources available on-site [3–6]. Another advantage of the desiccant HVAC system is its capability to control air humidity, air chemical content and air biological content at the same time.

In most cases, the performance of the laboratory measured HVAC system is far higher than in the field system due to environmental conditions during testing such as space requirements, and also the fabrication and assembly method. However, on-site assembled and installed HVAC system suffered higher pressure losses, air leakage and lower performance due to the different existing conditions compared with the laboratory. Such situations resulted in lower cooling or heating capacity due to higher internal air flow resistance, air leakage and air recirculation [7].

To immediately resolve the problem, the building occupants sometimes increase the air flow rates, lower the temperature setting for summer, or they raise the temperature setting for winter. These immediate solutions performed by the occupants increase the energy consumption of the HVAC system and can also increase cross-contamination in the air streams. As the desiccant HVAC system consists of many components for heat and mass transfer to condition the supply air for the buildings, the complexity of the components results in the many possible sources of air leakages, increase or loss of internal pressure, and possible causes for air cross-contamination. As a simple visual inspection and typical air flow evaluation is difficult, the above problems may cause the system to perform poorly [8].

The tracer gas dilution method is one of the most reliable methods in on-site air flow measurement due to its simplicity in implementation and availability of the portable equipment. Cheong [9] showed that measurements of airflow obtained by using tracer gas and the pitot-static traverse method were in close agreement; thus the tracer gas method was found to be a relatively simple and useful method for measuring airflow in HVAC systems. Riffat et al. [10] showed the use of the portable SF_6 system as an inexpensive and simple way of estimating the two-zone air flows in houses. Sherman [11] showed that multi-gas is capable of uniquely determining the entire matrix of air flows for multi-zone air flow rate determination. Sandberg and Stymne [12] show that when the air supply and extract points are well known, the effect of incomplete mixing can be minimized by locating the tracer gas source in the room with the largest inflow of air and the measuring point in the room with the largest extraction of air. For multi-zone air flow measurement, the application of multiple tracer gas is important; hence, Laurence Berkeley National Laboratory (LBNL) developed the multi-tracer measurement system (MTMS) to provide full multi-zone air flow information in an accurate and real-time manner [13].

Manz et al. [7] used tracer gas techniques to measure air leakage rates from ventilation units. Riffat [14] compared the measurements of airflow rate through a heat exchanger coil made with a rotating vane anemometer using a tracer gas technique. The two sets of data were generally found to be in close agreement. The tracer gas technique is found to be simple to use in practice and also has additional advantages. Roulet et al. [15] used the tracer gas dilution technique for measuring the leakage from exhaust to supply in several units. It was suggested that leakage can be strongly reduced through a proper installation of the wheel, good maintenance of the gasket, proper installation of a purging sector and by maintaining a positive pressure differential from supply to exhaust duct at wheel level. Results from Cheong [16] tests indicate that measurements obtained by using the constant injection technique are in close agreement with the measurements obtained by the pitot-static traverse method. It shows that turbulence, air flow, filters, heat exchanger coils and bends in the air handling unit and exhaust duct systems have brought about a good tracer to air mixture in a short mixing length of duct. The constant-injection tracer gas technique is a simple and convenient way of measuring and balancing air flow in an HVAC system. The HVAC system can be balanced in

a short period of time with a high degree of accuracy as compared to using the traditional pitot-static traverse method.

This paper presents the application of the tracer gas dilution method through multiple injection and sampling of the tracer gas in the installed desiccant HVAC system. It investigates air flow rates, air leakages and the exchanges of the air between the surroundings (mechanical room and lecture room) and the desiccant HVAC system. The desiccant HVAC system is installed in a new building at the university, and is the primary air-conditioning system of the building's largest lecture room [17]. The objective of the study is to determine the possible sources of air leakages both internal and external, and to determine the actual flow rate of air flowing through the internal components of the system, and to know the air flow rates in the HVAC system.

12.2 Methodology

12.2.1 Field Measurement

The tracer gas dilution method is applied through the multiple injection and sampling in the installed desiccant HVAC system of the ECOLLAB building at Tohoku University [17]. Figure 12.1 shows the schematic diagram of the desiccant HVAC

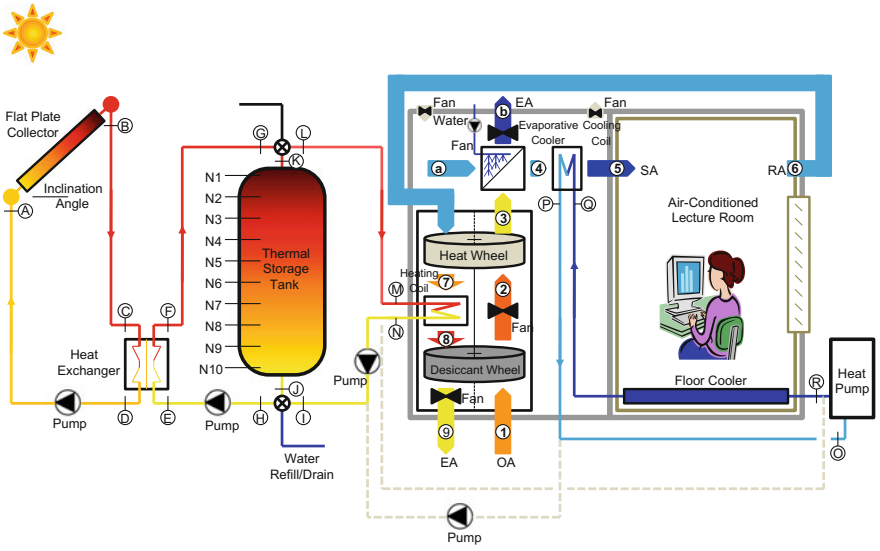

Fig. 12.1 Schematic diagram of installed desiccant heating, ventilating and air-conditioning system in one of the university buildings to support the air-conditioning requirement of the one of the main lecture rooms

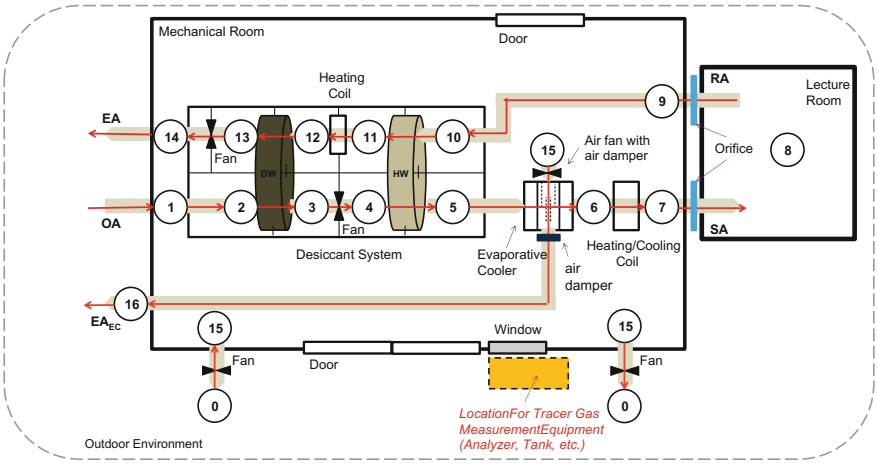

Fig. 12.2 Schematic diagram of the installed desiccant heating, ventilating and air-conditioning system in the building mechanical room showing the different components and the air flow direction

system in the building. The system is supported by solar thermal energy for the regeneration of the desiccant wheel used in the dehumidification of air. An indirect evaporative cooler is utilized to cool the air after the dehumidification by desiccant wheel and pre-cooling by heat wheel. A refrigerant heat pump is used to further cool the supply air after the evaporative cooler using the cooling coil in case the air from the system is not enough to support the cooling requirement of the lecture room. As shown in Fig. 12.2, the desiccant HVAC system internal devices are presented as well as the supposed air flow directions.

12.2.2 Node by Node Method

For a single node, the generalized air flow conservation for air and tracer gas is shown as

$$C_i Q_i + C_o Q_o + I - C_e Q_e = V \frac{\mathrm{d}C}{\mathrm{d}t} \tag{12.1}$$

The first expression is the inlet condition of the air and tracer gas, the second expression is the initial air and tracer gas condition in the single zone, the third expression is the tracer gas injection into the inlet of the zone; and the fourth expression is the outlet condition of the tracer gas and air. The right-side expression is the change in tracer gas concentration in the zone.

For multiple nodes, Eq. (12.1) is expanded to cover the number of nodes and the inter-nodal air flow rate as [18]

$$\sum_{j=0}^{N} C_{i/k} Q_{i/j}\left(1 - d_{i/j}\right) + C_{0/k} Q_{i/0} + I_{i/k} - \sum_{j=0}^{N} C_{i/k} Q_{j/i}\left(1 - d_{i/j}\right) = V_i \frac{\mathrm{d}C_{i/k}}{\mathrm{d}t} \quad (12.2)$$

Based on the air flow and tracer gas conservation equation, the airflow rate entering the node is determined as [18]

$$-I_{i/k} = \sum_{j=0}^{N} \left[C_{j/k} - C_{i/k}\right] Q_{j/i} \quad (12.3)$$

The air flow leaving the nodes is determined as [18]

$$Q_{i/0} = \sum_{j=0}^{N} \left[1 - d_{i/j}\right] Q_{j/i} - \sum_{j=0}^{N} \left[1 - d_{i/j}\right] Q_{i/j} \quad (12.4)$$

12.2.3 Mathematical Modeling

Figure 12.3 shows the expected air flow direction in the installed desiccant HVAC system together with the mechanical room and the lecture room. Hence, air leakage is expected to occur. Based on Fig. 12.3, the possible air flow in the system network of nodes is determined as presented in Table 12.1. Using the seven cases for injection of tracer gas shown in Fig. 12.3, the system of air flow conservation equations for the nodes is developed.

- Node 1:

$$0 = \left(C_{0/1} - C_{1/1}\right) Q_{0/1} + \left(C_{7/1} - C_{1/1}\right) Q_{11/1} + \left(C_{10/1} - C_{1/1}\right) Q_{15/1} \quad (12.5a)$$

$$0 = \left(C_{0/2} - C_{1/2}\right) Q_{0/1} + \left(C_{7/2} - C_{1/2}\right) Q_{11/1} + \left(C_{10/2} - C_{1/2}\right) Q_{15/1} \quad (12.5b)$$

$$0 = \left(C_{0/3} - C_{1/3}\right) Q_{0/1} + \left(C_{7/3} - C_{1/3}\right) Q_{11/1} + \left(C_{10/3} - C_{1/3}\right) Q_{15/1} \quad (12.5c)$$

$$0 = \left(C_{0/4} - C_{1/4}\right) Q_{0/1} + \left(C_{7/4} - C_{1/4}\right) Q_{11/1} + \left(C_{10/4} - C_{1/4}\right) Q_{15/1} \quad (12.5d)$$

$$0 = \left(C_{0/5} - C_{1/5}\right) Q_{0/1} + \left(C_{7/5} - C_{1/5}\right) Q_{11/1} + \left(C_{10/5} - C_{1/5}\right) Q_{15/1} \quad (12.5e)$$

$$0 = \left(C_{0/6} - C_{1/6}\right) Q_{0/1} + \left(C_{7/6} - C_{1/6}\right) Q_{11/1} + \left(C_{10/6} - C_{1/6}\right) Q_{15/1} \quad (12.5f)$$

$$0 = \left(C_{0/7} - C_{1/7}\right) Q_{0/1} + \left(C_{7/7} - C_{1/7}\right) Q_{11/1} + \left(C_{10/7} - C_{1/7}\right) Q_{15/1} \quad (12.5g)$$

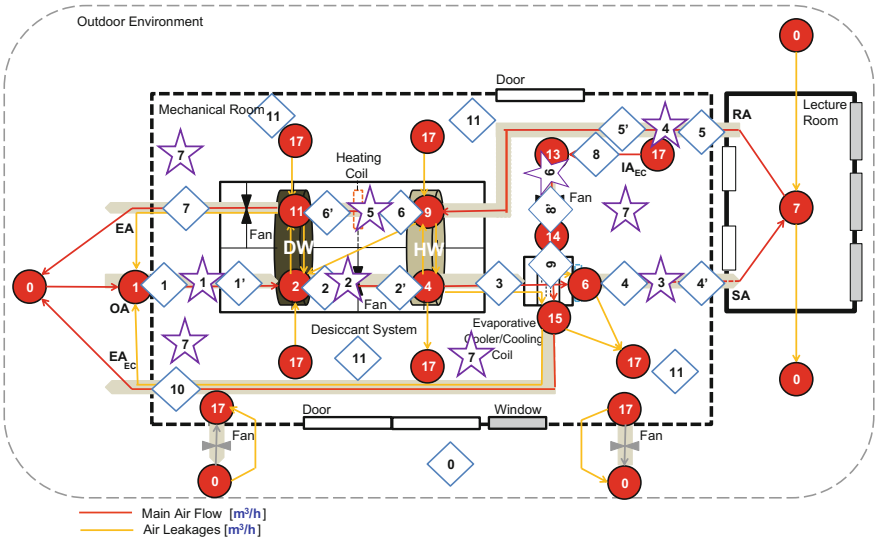

Fig. 12.3 Schematic diagram of the installed desiccant heating, ventilating and air-conditioning system showing the tracer gas injection points (*star*) and sampling points (*diamond*) for seven cases for the multiple injections and sampling of tracer gas

Table 12.1 Possible air flow in desiccant heating, ventilating and air-conditioning system network of nodes presented in Fig. 12.2

From Node \ Into Node	0	1	2	4	6	7	9	11	13	14	15	17
0		**$Q_{0/1}$**				$Q_{0/7}$						**$Q_{0/17}$**
1			**$Q_{1/2}$**									
2				**$Q_{2/4}$**				$Q_{2/11}$				
4					**$Q_{4/6}$**		$Q_{4/9}$				$Q_{4/15}$	$Q_{4/17}$
6						**$Q_{6/7}$**						$Q_{6/17}$
7	$Q_{7/0}$						**$Q_{7/9}$**					
9			$Q_{9/2}$	$Q_{9/4}$				**$Q_{9/11}$**				
11	**$Q_{11/0}$**	$Q_{11/1}$	$Q_{11/2}$									
13										**$Q_{13/14}$**		
14					$Q_{14/6}$						**$Q_{14/15}$**	
15	**$Q_{15/0}$**	$Q_{15/1}$										$Q_{15/17}$
17	**$Q_{17/0}$**		$Q_{17/2}$				$Q_{17/9}$	$Q_{17/11}$	**$Q_{17/13}$**			

The bold letter is the supposed air flow, and the normal letter is the assumed air flow leakages

- Node 2:

$$-I_{2/1} = (C_{1/1} - C_{2/1})Q_{1/2} + (C_{7/1} - C_{2/1})Q_{11/2} + (C_{11/1} - C_{2/1})Q_{17/2} + (C_{6/1} - C_{2/1})Q_{9/2} \tag{12.6a}$$

$$0 = (C_{1/2} - C_{2/2})Q_{1/2} + (C_{7/2} - C_{2/2})Q_{11/2} + (C_{11/2} - C_{2/2})Q_{17/2} + (C_{6/2} - C_{2/2})Q_{9/2} \tag{12.6b}$$

$$0 = (C_{1/3} - C_{2/3})Q_{1/2} + (C_{7/3} - C_{2/3})Q_{11/2} + (C_{11/3} - C_{2/3})Q_{17/2} + (C_{6/3} - C_{2/3})Q_{9/2} \tag{12.6c}$$

$$0 = (C_{1/4} - C_{2/4})Q_{1/2} + (C_{7/4} - C_{2/4})Q_{11/2} + (C_{11/4} - C_{2/4})Q_{17/2} + (C_{6/4} - C_{2/4})Q_{9/2} \tag{12.6d}$$

$$0 = (C_{1/5} - C_{2/5})Q_{1/2} + (C_{7/5} - C_{2/5})Q_{11/2} + (C_{11/5} - C_{2/5})Q_{17/2} + (C_{6/5} - C_{2/5})Q_{9/2} \tag{12.6e}$$

$$0 = (C_{1/6} - C_{2/6})Q_{1/2} + (C_{7/6} - C_{2/6})Q_{11/2} + (C_{11/6} - C_{2/6})Q_{17/2} + (C_{6/6} - C_{2/6})Q_{9/2} \tag{12.6f}$$

$$0 = (C_{1/7} - C_{2/7})Q_{1/2} + (C_{7/7} - C_{2/7})Q_{11/2} + (C_{11/7} - C_{2/7})Q_{17/2} + (C_{6/7} - C_{2/7})Q_{9/2} \tag{12.6g}$$

- Node 4:

$$0 = (C_{2/1} - C_{3/1})Q_{2/4} + (C_{6/1} - C_{3/1})Q_{9/4} \tag{12.7a}$$

$$-I_{4/2} = (C_{2/2} - C_{3/2})Q_{2/4} + (C_{6/2} - C_{3/2})Q_{9/4} \tag{12.7b}$$

$$0 = (C_{2/3} - C_{3/3})Q_{2/4} + (C_{6/3} - C_{3/3})Q_{9/4} \tag{12.7c}$$

$$0 = (C_{2/4} - C_{3/4})Q_{2/4} + (C_{6/4} - C_{3/4})Q_{9/4} \tag{12.7d}$$

$$0 = (C_{2/5} - C_{3/5})Q_{2/4} + (C_{6/5} - C_{3/5})Q_{9/4} \tag{12.7e}$$

$$0 = (C_{2/6} - C_{3/6})Q_{2/4} + (C_{6/6} - C_{3/6})Q_{9/4} \tag{12.7f}$$

$$0 = (C_{2/7} - C_{3/7})Q_{2/4} + (C_{6/7} - C_{3/7})Q_{9/4} \tag{12.7g}$$

- Node 6:

$$0 = \left(C_{3/1} - C_{4/1}\right)Q_{4/6} + \left(C_{9/1} - C_{4/1}\right)Q_{14/6} \tag{12.8a}$$

$$0 = \left(C_{3/2} - C_{4/2}\right)Q_{4/6} + \left(C_{9/2} - C_{4/2}\right)Q_{14/6} \tag{12.8b}$$

$$0 = \left(C_{3/3} - C_{4/3}\right)Q_{4/6} + \left(C_{9/3} - C_{4/3}\right)Q_{14/6} \tag{12.8c}$$

$$0 = \left(C_{3/4} - C_{4/4}\right)Q_{4/6} + \left(C_{9/4} - C_{4/4}\right)Q_{14/6} \tag{12.8d}$$

$$0 = \left(C_{3/5} - C_{4/5}\right)Q_{4/6} + \left(C_{9/5} - C_{4/5}\right)Q_{14/6} \tag{12.8e}$$

$$0 = \left(C_{3/6} - C_{4/6}\right)Q_{4/6} + \left(C_{9/6} - C_{4/6}\right)Q_{14/6} \tag{12.8f}$$

$$0 = \left(C_{3/7} - C_{4/7}\right)Q_{4/6} + \left(C_{9/7} - C_{4/7}\right)Q_{14/6} \tag{12.8g}$$

- Node 7:

$$0 = \left(C_{0/1} - C_{5/1}\right)Q_{0/7} + \left(C_{4/1} - C_{5/1}\right)Q_{6/7} \tag{12.9a}$$

$$0 = \left(C_{0/2} - C_{5/2}\right)Q_{0/7} + \left(C_{4/2} - C_{5/2}\right)Q_{6/7} \tag{12.9b}$$

$$-I_{7/3} = \left(C_{0/3} - C_{5/3}\right)Q_{0/7} + \left(C_{4/3} - C_{5/3}\right)Q_{6/7} \tag{12.9c}$$

$$0 = \left(C_{0/4} - C_{5/4}\right)Q_{0/7} + \left(C_{4/4} - C_{5/4}\right)Q_{6/7} \tag{12.9d}$$

$$0 = \left(C_{0/5} - C_{5/5}\right)Q_{0/7} + \left(C_{4/5} - C_{5/5}\right)Q_{6/7} \tag{12.9e}$$

$$0 = \left(C_{0/6} - C_{5/6}\right)Q_{0/7} + \left(C_{4/6} - C_{5/6}\right)Q_{6/7} \tag{12.9f}$$

$$0 = \left(C_{0/7} - C_{5/7}\right)Q_{0/7} + \left(C_{4/7} - C_{5/7}\right)Q_{6/7} \tag{12.9g}$$

- Node 9:

$$0 = \left(C_{3/1} - C_{6/1}\right)Q_{4/9} + \left(C_{5/1} - C_{6/1}\right)Q_{7/9} + \left(C_{11/1} - C_{6/1}\right)Q_{17/9} \tag{12.10a}$$

$$0 = \left(C_{3/2} - C_{6/2}\right)Q_{4/9} + \left(C_{5/2} - C_{6/2}\right)Q_{7/9} + \left(C_{11/2} - C_{6/2}\right)Q_{17/9} \tag{12.10b}$$

$$0 = \left(C_{3/3} - C_{6/3}\right)Q_{4/9} + \left(C_{5/3} - C_{6/3}\right)Q_{7/9} + \left(C_{11/3} - C_{6/3}\right)Q_{17/9} \tag{12.10c}$$

$$-I_{9/4} = \left(C_{3/4} - C_{6/4}\right)Q_{4/9} + \left(C_{5/4} - C_{6/4}\right)Q_{7/9} + \left(C_{11/4} - C_{6/4}\right)Q_{17/9} \tag{12.10d}$$

$$0 = \left(C_{3/5} - C_{6/5}\right)Q_{4/9} + \left(C_{5/5} - C_{6/5}\right)Q_{7/9} + \left(C_{11/5} - C_{6/5}\right)Q_{17/9} \quad (12.10e)$$

$$0 = \left(C_{3/6} - C_{6/6}\right)Q_{4/9} + \left(C_{5/6} - C_{6/6}\right)Q_{7/9} + \left(C_{11/6} - C_{6/6}\right)Q_{17/9} \quad (12.10f)$$

$$0 = \left(C_{3/7} - C_{6/7}\right)Q_{4/9} + \left(C_{5/7} - C_{6/7}\right)Q_{7/9} + \left(C_{11/7} - C_{6/7}\right)Q_{17/9} \quad (12.10g)$$

- Node 11:

$$0 = \left(C_{2/1} - C_{7/1}\right)Q_{2/11} + \left(C_{6/1} - C_{7/1}\right)Q_{9/11} + \left(C_{11/1} - C_{7/1}\right)Q_{17/11} \quad (12.11a)$$

$$0 = \left(C_{2/2} - C_{7/2}\right)Q_{2/11} + \left(C_{6/2} - C_{7/2}\right)Q_{9/11} + \left(C_{11/2} - C_{7/2}\right)Q_{17/11} \quad (12.11b)$$

$$0 = \left(C_{2/3} - C_{7/3}\right)Q_{2/11} + \left(C_{6/3} - C_{7/3}\right)Q_{9/11} + \left(C_{11/3} - C_{7/3}\right)Q_{17/11} \quad (12.11c)$$

$$0 = \left(C_{2/4} - C_{7/4}\right)Q_{2/11} + \left(C_{6/4} - C_{7/4}\right)Q_{9/11} + \left(C_{11/4} - C_{7/4}\right)Q_{17/11} \quad (12.11d)$$

$$-I_{11/5} = \left(C_{2/5} - C_{7/5}\right)Q_{2/11} + \left(C_{6/5} - C_{7/5}\right)Q_{9/11} + \left(C_{11/5} - C_{7/5}\right)Q_{17/11} \quad (12.11e)$$

$$0 = \left(C_{2/6} - C_{7/6}\right)Q_{2/11} + \left(C_{6/6} - C_{7/6}\right)Q_{9/11} + \left(C_{11/6} - C_{7/6}\right)Q_{17/11} \quad (12.11f)$$

$$0 = \left(C_{2/7} - C_{7/7}\right)Q_{2/11} + \left(C_{6/7} - C_{7/7}\right)Q_{9/11} + \left(C_{11/7} - C_{7/7}\right)Q_{17/11} \quad (12.11g)$$

- Node 15:

$$0 = \left(C_{3/1} - C_{10/1}\right)Q_{4/15} + \left(C_{9/1} - C_{10/1}\right)Q_{14/15} \quad (12.12a)$$

$$0 = \left(C_{3/2} - C_{10/2}\right)Q_{4/15} + \left(C_{9/2} - C_{10/2}\right)Q_{14/15} \quad (12.12b)$$

$$0 = \left(C_{3/3} - C_{10/3}\right)Q_{4/15} + \left(C_{9/3} - C_{10/3}\right)Q_{14/15} \quad (12.12c)$$

$$0 = \left(C_{3/4} - C_{10/4}\right)Q_{4/15} + \left(C_{9/4} - C_{10/4}\right)Q_{14/15} \quad (12.12d)$$

$$0 = \left(C_{3/5} - C_{10/5}\right)Q_{4/15} + \left(C_{9/5} - C_{10/5}\right)Q_{14/15} \quad (12.12e)$$

$$0 = (C_{3/6} - C_{10/6})Q_{4/15} + (C_{9/6} - C_{10/6})Q_{14/15} \tag{12.12f}$$

$$0 = (C_{3/7} - C_{10/7})Q_{4/15} + (C_{9/7} - C_{10/7})Q_{14/15} \tag{12.12g}$$

- Node 17:

$$0 = (C_{0/1} - C_{11/1})Q_{0/17} + (C_{3/1} - C_{11/1})Q_{4/17} + (C_{4/1} - C_{11/1})Q_{6/17} + (C_{10/1} - C_{11/1})Q_{15/17} \tag{12.13a}$$

$$0 = (C_{0/2} - C_{11/2})Q_{0/17} + (C_{3/2} - C_{11/2})Q_{4/17} + (C_{4/2} - C_{11/2})Q_{6/17} + (C_{10/2} - C_{11/2})Q_{15/17} \tag{12.13b}$$

$$0 = (C_{0/3} - C_{11/3})Q_{0/17} + (C_{3/3} - C_{11/3})Q_{4/17} + (C_{4/3} - C_{11/3})Q_{6/17} + (C_{10/3} - C_{11/3})Q_{15/17} \tag{12.13c}$$

$$0 = (C_{0/4} - C_{11/4})Q_{0/17} + (C_{3/4} - C_{11/4})Q_{4/17} + (C_{4/4} - C_{11/4})Q_{6/17} + (C_{10/4} - C_{11/4})Q_{15/17} \tag{12.13d}$$

$$0 = (C_{0/5} - C_{11/5})Q_{0/17} + (C_{3/5} - C_{11/5})Q_{4/17} + (C_{4/5} - C_{11/5})Q_{6/17} + (C_{10/5} - C_{11/5})Q_{15/17} \tag{12.13e}$$

$$0 = (C_{0/6} - C_{11/6})Q_{0/17} + (C_{3/6} - C_{11/6})Q_{4/17} + (C_{4/6} - C_{11/6})Q_{6/17} + (C_{10/6} - C_{11/6})Q_{15/17} \tag{12.13f}$$

$$-I_{17/7} = (C_{0/7} - C_{11/7})Q_{0/17} + (C_{3/7} - C_{11/7})Q_{4/17} + (C_{4/7} - C_{11/7})Q_{6/17} + (C_{10/7} - C_{11/7})Q_{15/17} \tag{12.13g}$$

Using seven cases of tracer gas injections shown in Fig. 12.3, the systems of equations for the nodes are presented as follows based on Table 12.1.

- Node 0:

$$Q_{7/0} + Q_{11/0} + Q_{15/0} + Q_{17/0} = Q_{0/1} + Q_{0/7} + Q_{0/17} \tag{12.14}$$

- Node 1:

$$Q_{0/1} + Q_{11/1} + Q_{15/1} = Q_{1/2} \tag{12.15}$$

- Node 2:

$$Q_{1/2} + Q_{11/2} + Q_{17/2} + Q_{9/2} = Q_{2/4} + Q_{2/11} \tag{12.16}$$

- Node 4:

$$Q_{4/6} + Q_{4/9} + Q_{4/15} + Q_{4/17} = Q_{2/4} + Q_{9/4} \tag{12.17}$$

- Node 6:

$$Q_{4/6} + Q_{14/6} = Q_{6/7} + Q_{6/17} \tag{12.18}$$

- Node 7:

$$Q_{0/7} + Q_{6/7} = Q_{7/0} + Q_{7/9} \tag{12.19}$$

- Node 9:

$$Q_{4/9} + Q_{7/9} + Q_{17/9} = Q_{9/4} + Q_{9/11} + Q_{9/2} \tag{12.20}$$

- Node 11:

$$Q_{2/11} + Q_{9/11} + Q_{17/11} = Q_{11/0} + Q_{11/1} + Q_{11/2} \tag{12.21}$$

- Node 13:

$$Q_{17/13} = Q_{13/14} \tag{12.22}$$

- Node 14:

$$Q_{13/14} = Q_{14/15} + Q_{14/6} \tag{12.23}$$

- Node 15:

$$Q_{4/15} + Q_{14/15} = Q_{15/0} + Q_{15/1} + Q_{15/17} \tag{12.24}$$

- Node 17:

$$Q_{0/17} + Q_{4/17} + Q_{6/17} + Q_{15/17} = Q_{17/0} + Q_{17/2} + Q_{17/9} + Q_{17/11} + Q_{17/13} \tag{12.25}$$

The various air flow rates in the air handling system presented in Fig. 12.3 are determined as;

- Outdoor air flow rate

$$Q_{1/2} = \frac{I_{2/1}}{\left(C_{1'/1} - C_{1/1}\right)} \tag{12.26}$$

- Supply air flow rate

$$Q_{6/7} = \frac{I_{7/3}}{\left(C_{4'/3} - C_{4/3}\right)} \tag{12.27}$$

- Return air flow rate

$$Q_{7/9} = \frac{I_{9/4}}{\left(C_{5'/4} - C_{5/4}\right)} \tag{12.28}$$

- Evaporative cooler air flow rate

$$Q_{13/14} = \frac{I_{13/6}}{\left(C_{8'/6} - C_{8/6}\right)} \tag{12.29}$$

- From Eqs. (12.22) and (12.29)

$$Q_{17/13} = Q_{13/14} \tag{12.30}$$

- From Eq. (12.9c)

$$Q_{0/7} = \frac{I_{7/3} + \left(C_{4/3} - C_{5/3}\right)Q_{6/7}}{\left(C_{5/3} - C_{0/3}\right)} \tag{12.31}$$

- From Eq. (12.21)

$$Q_{7/0} = \left(Q_{0/7} + Q_{6/7}\right) - Q_{7/9} \tag{12.32}$$

- From Eq. (12.8f)

$$Q_{14/6} = Q_{6/7}\left(\frac{C_{3/6} - C_{4/6}}{C_{3/6} - C_{9/6}}\right) \tag{12.33}$$

- From Eq. (12.25)

$$Q_{14/15} = Q_{13/14} - Q_{14/6} \tag{12.34}$$

- From Eq. (12.13f)

$$Q_{4/15} = Q_{14/15}\left(\frac{C_{9/6} - C_{10/6}}{C_{10/6} - C_{3/6}}\right) \tag{12.35}$$

- The air flow from node 2–4 is,

$$Q_{2/4} = \frac{I_{4/2}}{\left(C_{2'/2} - C_{2/2}\right)} \tag{12.36}$$

- The air flow from node 9–11 is,

$$Q_{9/11} = \frac{I_{11/5}}{\left(C_{6'/5} - C_{6/5}\right)} \tag{12.37}$$

- From Eq. (12.7a)

$$Q_{9/4} = Q_{2/4}\left(\frac{C_{2/1} - C_{3/1}}{C_{3/1} - C_{6/1}}\right) \tag{12.38}$$

- From Eqs. (12.10a) and (12.10d)

$$Q_{4/9} = -\frac{\left[I_{9/4}\left(C_{6/1} - C_{11/1}\right)\right] + Q_{7/9}\left[\left(C_{6/1} - C_{11/1}\right)\left(C_{5/4} - C_{6/4}\right) + \left(C_{11/4} - C_{6/4}\right)\left(C_{5/1} - C_{6/1}\right)\right]}{\left[\left(C_{6/1} - C_{11/1}\right)\left(C_{3/4} - C_{6/4}\right) + \left(C_{11/4} - C_{6/4}\right)\left(C_{3/1} - C_{6/1}\right)\right]} \tag{12.39}$$

- From Eqs. (12.25), (12.26), (12.13a), (12.13b), (12.13f) and (12.13g)

$$Q_{4/17} = \frac{\left\{\langle (x-y)[(ag-ec)(pi-ml) + (oi-mk)(ed-ah)]\rangle - \left[I_{17/7}(edi-ahi)\right]\right\}}{\langle [(ag-ec)(pi-ml) + (oi-mk)(ed-ah)] - [(af-eb)(pi-ml) + (ni-mj)(ed-ah)]\rangle} \tag{12.40}$$

where; $a = \left(C_{0/1} - C_{11/1}\right)$; $b = \left(C_{3/1} - C_{11/1}\right)$; $c = \left(C_{4/1} - C_{11/1}\right)$;
$d = \left(C_{10/1} - C_{11/1}\right)$; $e = \left(C_{0/2} - C_{11/2}\right)$; $f = \left(C_{3/2} - C_{11/2}\right)$;
$g = \left(C_{4/2} - C_{11/2}\right)$; $h = \left(C_{10/2} - C_{11/2}\right)$; $i = \left(C_{0/6} - C_{11/6}\right)$;
$j = \left(C_{3/6} - C_{11/6}\right)$; $k = \left(C_{4/6} - C_{11/6}\right)$; $l = \left(C_{10/6} - C_{11/6}\right)$;
$m = \left(C_{0/7} - C_{11/7}\right)$; $n = \left(C_{3/7} - C_{11/7}\right)$; $o = \left(C_{4/7} - C_{11/7}\right)$;
$p = \left(C_{10/7} - C_{11/7}\right)$; $x = Q_{2/4} + Q_{9/4} + Q_{14/6}$; $y = Q_{4/9} + Q_{4/15} + Q_{6/7}$

- From Eqs. (12.17) and (12.18)

$$Q_{6/17} = \left(Q_{2/4} + Q_{9/4} + Q_{14/6}\right) - \left(Q_{4/9} + Q_{4/15} + Q_{6/7} + Q_{4/17}\right) \tag{12.41}$$

- From Eqs. (12.13f) and (12.13g)

$$Q_{15/17} = \frac{\left[i\left(I_{17/7}\right) + Q_{4/17}(ni - mj) + Q_{6/17}(oi - mk)\right]}{(ml - pi)} \tag{12.42}$$

where;

$i = (C_{0/6} - C_{11/6})$; $k = (C_{4/6} - C_{11/6})$; $l = (C_{10/6} - C_{11/6})$;
$m = (C_{0/7} - C_{11/7})$; $n = (C_{3/7} - C_{11/7})$; $o = (C_{10/7} - C_{11/7})$;
$p = (C_{10/7} - C_{11/7})$

- From Eq. (12.13g)

$$Q_{0/17} = \frac{[I_{17/7} + Q_{4/17}(C_{3/7} - C_{11/7}) + Q_{6/17}(C_{4/7} - C_{11/7}) + Q_{15/17}(C_{10/7} - C_{11/7})]}{(C_{11/7} - C_{0/7})} \tag{12.43}$$

- From Eq. (12.17)

$$Q_{4/6} = (Q_{2/4} + Q_{9/4}) - (Q_{4/9} + Q_{4/15} + Q_{4/17}) \tag{12.44}$$

- From Eqs. (12.6a), (12.6b), (12.6c), (12.6d) and (12.6e)

$$Q_{17/2} = -Q_{1/2}\left[\frac{(fa + bd)}{(fc + be)}\right] \tag{12.45}$$

where;

$a = [(C_{1/4} - C_{2/4})(C_{6/5} - C_{2/5})] - [(C_{1/5} - C_{2/5})(C_{6/4} - C_{2/4})]$;
$b = [(C_{7/4} - C_{2/4})(C_{6/5} - C_{2/5})] - [(C_{7/5} - C_{2/5})(C_{6/4} - C_{2/4})]$;
$c = [(C_{11/4} - C_{2/4})(C_{6/5} - C_{2/5})] - [(C_{11/5} - C_{2/5})(C_{6/4} - C_{2/4})]$;
$d = [(C_{6/3} - C_{2/3})(C_{1/2} - C_{2/2})] - [(C_{6/2} - C_{2/2})(C_{1/3} - C_{2/3})]$;
$e = [(C_{11/2} - C_{2/2})(C_{6/3} - C_{2/3})] - [(C_{11/3} - C_{2/3})(C_{6/2} - C_{2/2})]$;
$f = [(C_{7/3} - C_{2/3})(C_{6/2} - C_{2/3})] - [(C_{7/2} - C_{2/3})(C_{6/3} - C_{2/3})]$

- From Eqs. (12.6a) and (12.6c)

$$Q_{11/2} = \frac{Q_{1/2}d + Q_{17/2}e}{f} \tag{12.46}$$

where;

$d = [(C_{6/3} - C_{2/3})(C_{1/2} - C_{2/2})] - [(C_{6/2} - C_{2/2})(C_{1/3} - C_{2/3})]$;
$e = [(C_{11/2} - C_{2/2})(C_{6/3} - C_{2/3})] - [(C_{11/3} - C_{2/3})(C_{6/2} - C_{2/2})]$;
$f = [(C_{7/3} - C_{2/3})(C_{6/2} - C_{2/3})] - [(C_{7/2} - C_{2/3})(C_{6/3} - C_{2/3})]$

- From Eq. (12.10d)

$$Q_{17/9} = \frac{[(C_{3/4} - C_{6/4})Q_{4/9} + (C_{5/4} - C_{6/4})Q_{7/9} + I_{9/4}]}{(C_{6/4} - C_{11/4})} \tag{12.47}$$

- From Eqs. (12.11e) and (12.11f)

$$Q_{17/11} = -\frac{I_{11/5}(C_{2/6} - C_{7/6}) + Q_{9/11}[(C_{6/6} - C_{7/6})(C_{7/5} - C_{2/5}) + (C_{2/6} - C_{7/6})(C_{6/5} - C_{7/5})]}{[(C_{11/6} - C_{7/6})(C_{7/5} - C_{2/5}) + (C_{2/6} - C_{7/6})(C_{11/5} - C_{7/5})]} \tag{12.48}$$

- From Eq. (12.11d)

$$Q_{2/11} = \frac{\left[Q_{9/11}\left(C_{6/4} - C_{7/4}\right) + Q_{17/11}\left(C_{11/4} - C_{7/4}\right)\right]}{\left(C_{7/4} - C_{2/4}\right)} \tag{12.49}$$

- From Eq. (12.25)

$$Q_{17/0} = \left(Q_{0/17} + Q_{4/17} + Q_{6/17} + Q_{15/17}\right) - \left(Q_{17/2} + Q_{17/9} + Q_{17/11} + Q_{17/13}\right) \tag{12.50}$$

- From Eqs. (12.15), (12.5e) and (12.5f)

$$Q_{15/1} = Q_{1/2}\frac{(a+b)}{(c+d)} \tag{12.51}$$

where;
$a = \left(C_{0/5} - C_{1/5}\right)\left[\left(C_{0/6} - C_{1/6}\right) - \left(C_{7/6} - C_{1/6}\right)\right]$;
$b = \left(C_{0/6} - C_{1/6}\right)\left[\left(C_{7/5} - C_{1/5}\right) - \left(C_{0/5} - C_{1/5}\right)\right]$;
$c = \left[\left(C_{10/6} - C_{1/6}\right) - \left(C_{0/6} - C_{1/6}\right)\right]\left[\left(C_{7/5} - C_{1/5}\right) - \left(C_{0/5} - C_{1/5}\right)\right]$;
$d = \left[\left(C_{10/5} - C_{1/5}\right) - \left(C_{0/5} - C_{1/5}\right)\right]\left[\left(C_{0/6} - C_{1/6}\right) - \left(C_{7/6} - C_{1/6}\right)\right]$

- From Eq. (12.5e)

$$Q_{11/1} = \frac{\left\langle Q_{1/2}\left(C_{0/5} - C_{1/5}\right) + Q_{15/1}\left[\left(C_{10/5} - C_{1/5}\right) - \left(C_{0/5} - C_{1/5}\right)\right]\right\rangle}{\left[\left(C_{0/5} - C_{1/5}\right) - \left(C_{7/5} - C_{1/5}\right)\right]} \tag{12.52}$$

- From Eq. (12.15)

$$Q_{0/1} = Q_{1/2} - \left(Q_{11/1} + Q_{15/1}\right) \tag{12.53}$$

- From Eq. (12.24)

$$Q_{15/0} = \left(Q_{4/15} + Q_{14/15}\right) - \left(Q_{15/1} + Q_{15/17}\right) \tag{12.54}$$

- From Eq. (12.21)

$$Q_{11/0} = \left(Q_{2/11} + Q_{9/11} + Q_{17/11}\right) - \left(Q_{11/1} + Q_{11/2}\right) \tag{12.55}$$

- From Eq. (12.16)

$$Q_{9/2} = \left(Q_{2/4} + Q_{2/11}\right) - \left(Q_{1/2} + Q_{11/2} + Q_{17/2}\right) \tag{12.56}$$

12.2.4 Field Application

The tracer gas injection and sampling points are presented in Fig. 12.3. Based on the number of these sampling points, the inter-nodal air flow rates can be determined. As the installation is a compact system having possible obstacles for mixing tracer gas and reversed flow, the tracer gas injection point and sampling points' installation are done properly to minimize the possible misdistribution of tracer gas in the stream of air. ASTM E 2029-99 shows the suggestions in multiple tracer gas injection and sampling for different sizes of air ducting [19]. Also, application of the multiple micro-jets for both the injection and sampling probes installed in the air stream was implemented in this study [20]. Silva and Afonso [20] shows also that it is difficult to accurately measure the air flow rate when the distance between the tracer gas injector and downstream sampler is less than four times the duct diameter. Hence, in this study, proper installation and preparation was done to account for the distances between the injector and sampler.

In this study, the SF_6 tracer gas is used in the multiple tracer gas points' evaluation through a constant flow rate. The purpose of SF_6 as a tracer gas is due to its absence in the environment which, otherwise, might cause an error in reading the tracer gas sampling. Based on the Occupational Safety and Health Administration (OSHA) regulation [21], the SF_6 concentration in air should not be above 100 ppm. Since the purpose of this evaluation method is for field or on-site evaluation with uncontrolled movement of people in the vicinity, 75 ppm as a maximum limit was selected to provide an additional safety margin.

The measurements are performed after the steady-state conditions. At first, the system is operated until the steady-state conditions are attained. Afterward, the tracer gas is injected from Point 1 (Case 1) to Point 7 (Case 7). The subsequent injections of tracer gas (Case 1 to Case 7) are performed only after the removal of all tracer gases from the previous injections.

The multi-point dozer and sampler with a photoacoustic gas monitor are used in the tracer gas injection, sampling and measurement as shown in Fig. 12.4. The fabricated multiple tracer gas injector and sampling with multiple micro-jets are used for the measurement as suggested [20].

12.3 Results and Discussion

12.3.1 Tracer Gas Concentration

Figure 12.5 shows the gathered raw data for two hours after the stabilization of the tracer gas concentration and constant injection of the tracer gas. Based on the observation during the dry run and testing, the stabilization time between cases was at least two hours. The data were gathered for two hours so as to have an ample amount of data. Based on cases of tracer gas injection, as expected, there was

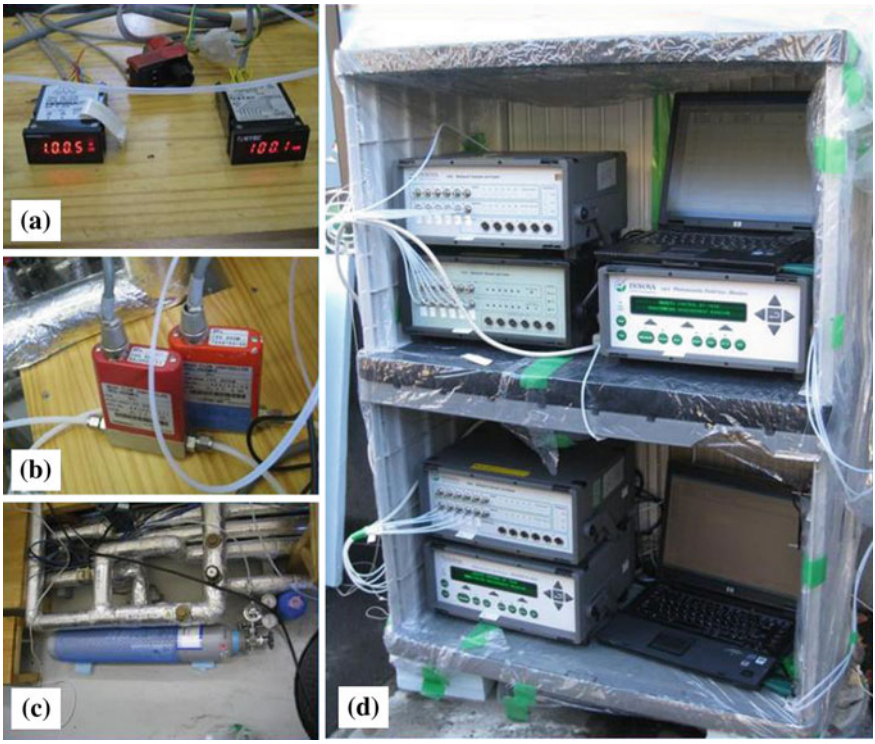

Fig. 12.4 Actual view of field measurement using tracer gas dilution method for air flow rate and leakages evaluation: **a** tracer gas flow controller; **b** tracer gas flow meter; **c** tracer gas supply tank and **d** tracer gas multiple samplers and gas analyzer with tracer gas concentration monitoring and data storage

always an increase in tracer gas concentration between the upstream and downstream where the gas was injected. Based on the presentation of tracer gas sampling points, there were sampling points that increased the tracer gas concentrations even in the other stream of air flow due to internal air leakage and air recirculation. In addition, it showed that there was an air exchange between the environment, the mechanical room and the lecture room.

12.3.2 Air Flow and Air Leakages

Figure 12.6 shows the calculated air flow and leakage rates. Based on the calculations, the air flow rates inside the system were changing from the outlet air (Point 1 and Point 2) to supply air and from the return air (Point 7 to Point 9) to exit air (Point 11 to Point 0 and Point 11 to Point 1); the same situation was occurring for the evaporative cooler primary and secondary air flow rates (Point 14 to Point 15

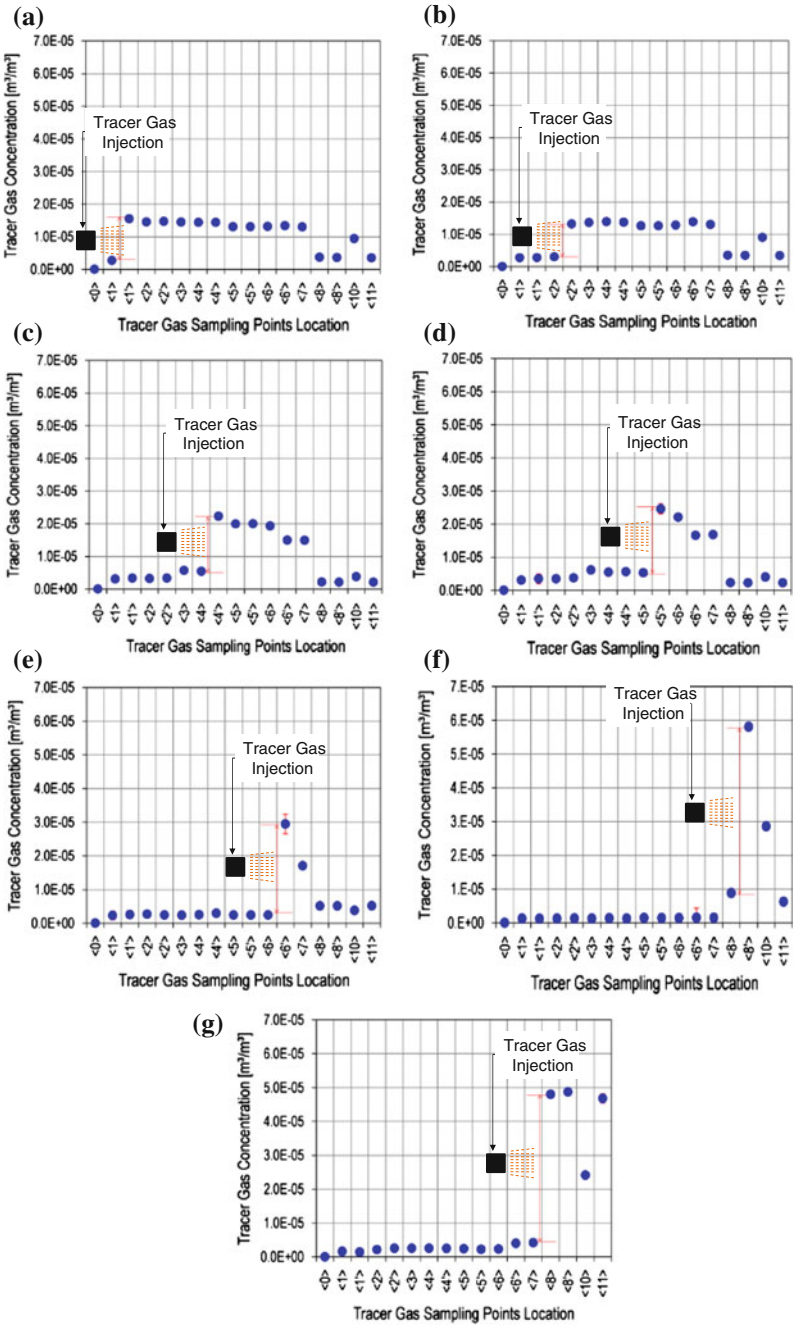

Fig. 12.5 Measured concentration of the tracer gas in different sampling points for different injection cases: **a** case 1; **b** case 2; **c** case 3; **d** case 4; **e** case 5; **f** case 6 and **g** case 7. The data were gathered for 2 h for each case with time span between cases of at least 2 h (stability time)

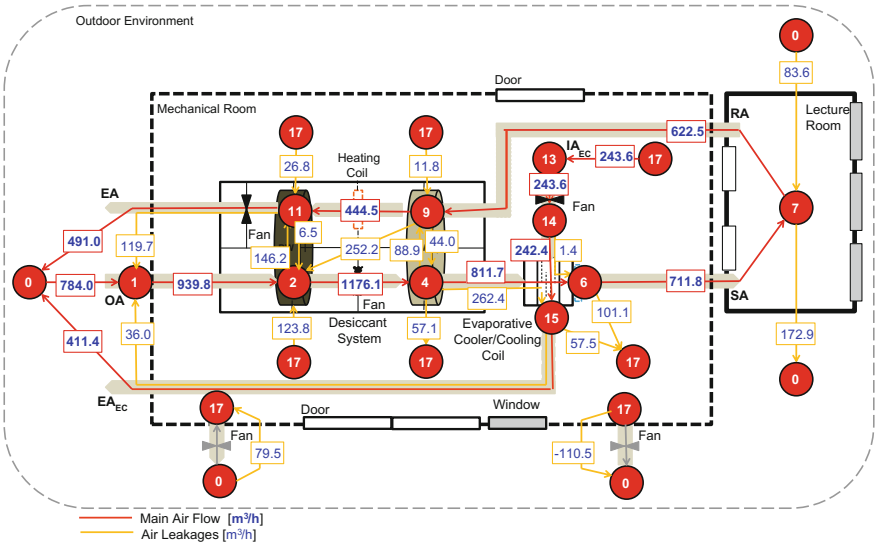

Fig. 12.6 Calculated air flow rates (*red line*) and air leakages (*orange line*) in the installed desiccant heating, ventilating and air-conditioning system. The *red line* is the intended air flow directions in the system, and the *orange line* is the detected air leakages

and Point 4 to Point 6). As presented, the outdoor air flow rate was 939.8 m^3/h, then increasing to 1176.1 m^3/h upon passing the desiccant wheel, and then decreasing to 711.8 m^3/h when supplied to the lecture room. On the other hand, the 622.5 m^3/h of return air decreased to 444.5 m^3/h when passing the heating coil and then increased after (610.7 m^3/h). There were many internal air leakages of different volumes. As expected, large air leakages were occurring from the high to the low air pressure side. An exceptional case was occurring in the evaporative cooler due to the large leakage in its elements. Furthermore, there was an exchange of air in the lecture room that might depend on the door being open or closed, or on changes of outdoor air direction and speed.

12.3.3 Flow Balances

Figure 12.7 shows the air flow rates and leakage in the desiccant wheel (Fig. 12.7a) and the heat wheel (Fig. 12.7b). Based on the calculation for the desiccant wheel, the total inlet air flow is 1687.3 m^3/h, while the total outlet flow is 1786.8 m^3/h, with a percentage difference of 5.6%. It showed that there was high air recirculation from the supply air side to the return air side in comparison with the return air side to the supply air side. The high air recirculation from the supply air side to the return air side was due to the high pressure side in the supply side rather than that of the return air side. The air recirculation from the return air side to the supply air side

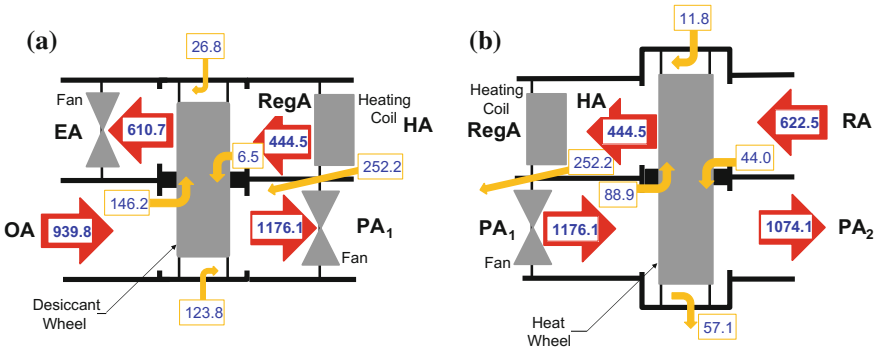

Fig. 12.7 Calculated air flow rates (*red arrow*) and air leakages (*orange arrow*): **a** desiccant wheel with total inlet flow of 1687.3 m^3/h and total outlet flow of 1786.8 m^3/h with percent difference of 5.6% and **b** heat wheel with total inlet flow of 1810.4 m^3/h and total outlet flow of 1827.9 m^3/h with percent difference of 1.0% (please see Fig. 12.6 for complete system diagram and air flow)

is most likely due to the rotation of the desiccant wheel. In the case of the heat wheel (Fig. 12.7b), there was still a high recirculation of air from the supply air side to the return air side due to the high pressure in the supply air side. The air recirculation from the return air side to the supply air side is due to the rotation of the heat wheel. For the heat wheel, the total inlet air flow was 1810.4 m^3/h, while the total outlet air flow was 1827.9 m^3/h, for a percentage difference of 1.0%. In addition, it showed that a big internal leakage from the return air side to the supply air side was happening between the heat wheel and the desiccant wheel. The high amount of leakage was determined to be due to the fabrication and installation of the parts of the desiccant wheel, fan and heating coil, and the heat wheel. Figure 12.8 shows the calculated air flow rates and leakage for the evaporative cooler (Fig. 12.8a) and the lecture room (Fig. 12.8b). For the evaporative cooler, the total inlet flow was 1317.7 m^3/h, while the total outlet flow was 1317.8 m^3/h with the difference being 0.01%. There was a large internal air leakage from the PA_2 to the EA_2 of 262.4 m^3/h. The evaporative cooler showed leakage in the mechanical room of 158.6 m^3/h. The high internal leakage of the evaporative cooler is due to the fabrication of the evaporative cooler elements. It was determined that these elements caused leakages in the two streams of air. The lecture room as shown in Fig. 12.8b has a total inlet flow of 795.4 m^3/h and an outlet flow of 795.4 m^3/h with a percentage difference of 0.0%. As presented, there was an air exchange between the room and the outdoor environment due to the opening and closing of doors, and it was affected by the changes in wind speed and direction around the lecture room. However, it is shown that there is a large air leakage from the room to the environment due to the positive pressure inside the room in comparison with the environment as the supply air flow rate is higher than the return air flow rate.

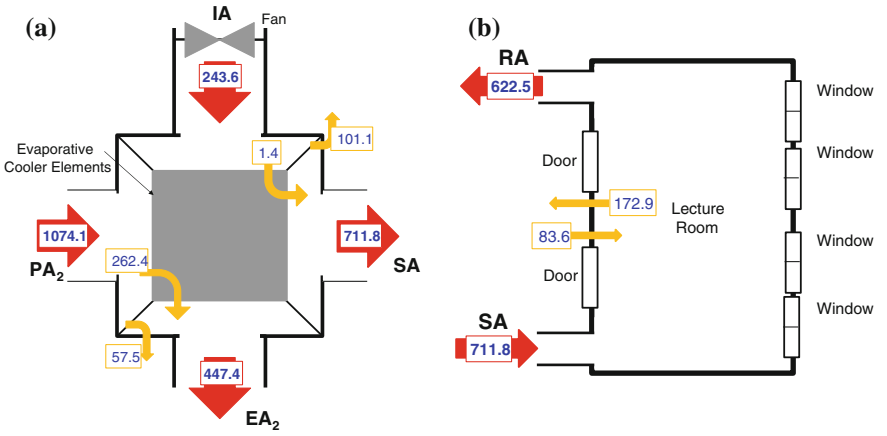

Fig. 12.8 Calculated air flow rates (*red arrow*) and air leakages (*orange arrow*): **a** evaporative cooler with total inlet flow of 1317.7 m^3/h and total outlet flow of 1317.8 m^3/h with percent difference of 0.01% and **b** lecture room with total inlet flow of 795.4 m^3/h and total outlet flow of 795.4 m^3/h with percent difference of 0.0% (please see Fig. 12.6 for complete system diagram and air flow)

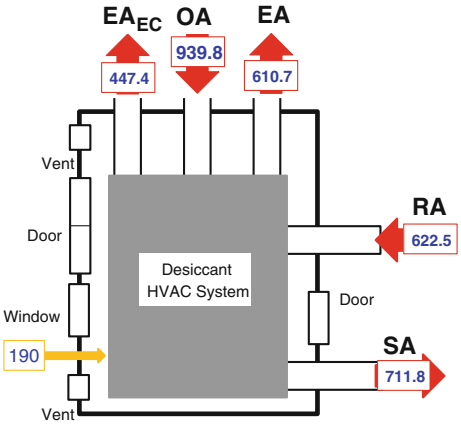

Fig. 12.9 Calculated air flow rates (*red arrow*) and air leakages (*orange arrow*) for the mechanical room of the solar thermal and heat pump supported desiccant heating, ventilating and air-conditioning system is located. The total inlet flow is 1752.2 m^3/h and total outlet flow is 1769.9 m^3/h with percent difference of 1.0% (please see Fig. 12.6 for complete system diagram and air flow)

Figure 12.9 shows the air flow rates and leakage for the mechanical room. It shows that the total inlet air flow was 1752.2 m^3/h, while the total outlet flow was 1769.9 m^3/h, with a percentage difference of 1.0%. The results show that the room air leakage was 190 m^3/h due largely to the evaporative cooler operation to support

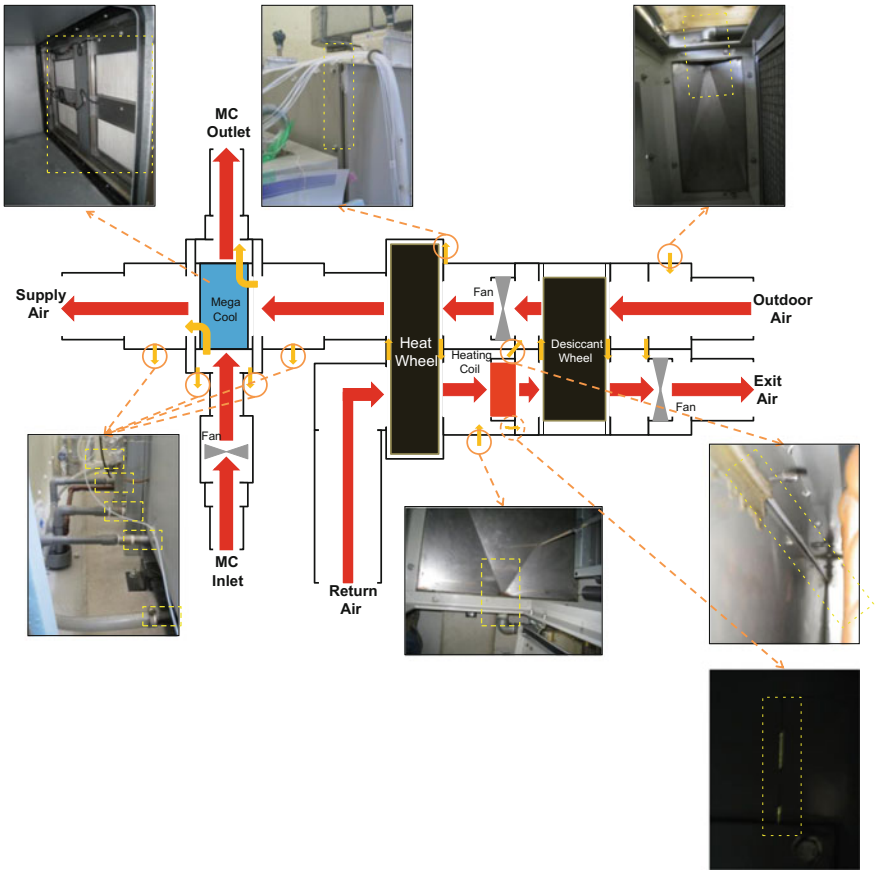

Fig. 12.10 Schematic diagram of the complete modular constructed and fabricated desiccant heating, ventilating and air-conditioning system. It shows the sources of main air leakages based on the results of tracer gas dilution method and comprehensive visual inspection with reference to tracer gas results

the secondary air flow. The evaporative cooler secondary stream of air has an air fan to support the required air flow rate to cool the primary air flow going to the room.

12.3.4 Leakage Sources

Based on the analysis of the tracer gas air flow and leakage evaluation, a physical evaluation of the system along with the lecture room and mechanical room was performed. In order to investigate the causes of air leakage, the actual investigation

of the installed DHVAC system was conducted. It shows that the system is composed of many modules and that it fits together with the complete system. For example, the desiccant wheel has one module, the heat wheel has one module, and so on. The modules are connected by nuts and bolts and using a silicon sealant. However, due to the physical size of the system, some modules are assembled on-site resulting in difficulty in testing for air leakage, even after applying sealants. Combined with the physical evaluation of the system, and analysis of the system fabrication and installation using the tracer gas method, the causes of the air leakages were determined. Figure 12.10 shows the main causes of air leakage and air recirculation. There were unexpected causes for air external air leakage and air recirculation such as the emergency water drainage pipe and the joining of the desiccant wheel module, fan and heating coil module and heat wheel module. Furthermore, the cause of leakage in the evaporative cooler was due to the installed heat transfer elements. It was also determined that the connection of modules causes some leakage between the system and the mechanical room.

12.4 Conclusions

This study shows the application of the tracer gas dilution method through multiple tracer gas injection and sampling for the diagnostic of the installed DHVAC system to determine and evaluate the actual air flow rates, air recirculation, and internal and external air leakages. Based on the application of the tracer gas dilution method, the following conclusions are drawn:

1. The air flow rates inside the installed DHVAC system varied from the outdoor air (OA) to supply air (SA) and from the return air (RA) to exit air (EA); the same situation occurred for the evaporative cooler primary and secondary air flow rates.
2. Large air leakages occurred from the high air pressure side to the low air pressure side. An exceptional case occurred in the evaporative cooler due to the large amount of leakage in its elements.
3. There is a large internal air leakage of 262.4 m^3/h from Point PA_2 to Point EA_2. The evaporative cooler has a leakage to the mechanical room of 158.6 m^3/h.
4. There is an air exchange between the room and the outdoor environment due to the opening and closing of doors which is affected by the changes in wind speed and direction in the area around the lecture room.
5. It shows that the emergency water drain pipes of the installed system contribute to external air leakage, while the incomplete sealing both internally and externally of the installed system results in air leakage.
6. A large internal air recirculation is occurring between the desiccant wheel and the heat wheel due to incomplete sealing in the boundary between the supply air side and the return air side airstreams due to the difficulty in sealing and visually checking that portion.

It was determined that the installed DHVAC system has a large unexpected internal air leakage and air recirculation due to the fabrication, assembly and installation of the emergency water drain pipe. Due to the large internal and external air leakage coupled with air recirculation, the outdoor air and exit air flow rate becomes very high to support the expected required supply air and return air flow rates for the lecture room. These air recirculation and air leakages might contribute to the poor performance of the system due to the imbalance of air flow rates. Hence, system retrofitting and repair are seriously needed to fix the problem.

Based on the study, the installed system's performance is totally different from the expected performance due to internal and external air leakage. Performance is also affected by the modular connection. Based on the results of the study, even though the system might be fully sealed with silicone sealants, duct tape, and nuts and bolts, there is no assurance that it will be free of air leakages. Therefore, based on this study, field evaluation of the HVAC system to determine its detailed and actual behavior and performance, the use of multiple injection of tracer gas, is an important component in the commissioning of the system and before the turnover to the building owner or the occupants.

References

1. Enteria N, Yoshino H, Mochida A et al (2015) Performance test of desiccant heating, ventilating and air-conditioning system by using multiple tracer gas dilution method. Int J Air-Cond 23(04):1550027
2. Enteria N, Yoshino H, Mochida A (2013) Review of the advances in open-cycle absorption air-conditioning systems. Renew Sust Energ Rev 28:265–289
3. Enteria N, Mizutani K (2011) The role of the thermally activated desiccant cooling technologies in the issue of energy and environment. Renew Sust Energ Rev 15:2095–2122
4. Ishugah FT, Wang R, Wang L, Lu Z (2014) Performance improvement of an adsorption chiller using composite adsorbent, silica gel impregnated with lithium chloride, paired with methanol as the adsorbate. Int J Air-Cond 22:1440003. doi:10.1142/S2010132514400033
5. Yadav A (2014) Analysis of desiccant wheel with purge sector for improving the performance using a mathematical model. Int J Air-Cond 22:1450004. doi:10.1142/S2010132514500047
6. Vinayak VD, Pitale AD (2015) A review on working pair used in adsorption cooling system. Int J Air-Cond 23:1530001. doi:10.1142/S2010132515300013
7. Manz H, Huber H, Helfenfinger D (2001) Impact of air leakages and short circuits in ventilation units with heat recovery on ventilation efficiency and energy requirements for heating. Energ Build 33:133–139
8. Roulet CA, Heidt FD, Foradini F, Pibiri MC (2001) Real heat recovery with air handling units. Energ Build 33:495–502
9. Cheong KW (1996) Tracer gas technology for airflow measurements in HVAC system. Int J Energ Res 20:1081–1093
10. Riffat SB, Walker J, Littler J (1988) Zone to zone tracer gas measurements: laboratory calibration and values of air flows up and down stairs in houses. In: Proceedings of 9th AIVC conference, Gent, Belgium, 12–15 Sept 1988
11. Sherman MH (1989) On the estimation of multizone ventilation rates from tracer gas measurements. Build Environ 24:355–362

12. Sandberg M, Stymne H (1989) The constant tracer flow technique. Build Environ 24:209–219
13. Sherman M (1990) A multitracer system for multizone ventilation measurement. Rev Sci Instrum 61:2457. doi:10.1063/1.1141339
14. Riffat SB (1991) Airflow rate through a heat-exchanger coil. Appl Energ 38:231–238
15. Roulet AA, Pibiri MC, Knutti R et al (2002) Effect of chemical composition on VOC transfer through rotating heat exchangers. Energ Build 34:799–807
16. Cheong KW (2001) Airflow measurements for balancing of air distribution system—tracer-gas technique as an alternative? Build Environ 36:955–964
17. Ecollab (2013) Graduate School of Environmental Studies, Tohoku University. http://www.kankyo.tohoku.ac.jp/en/ecollab.html. Accessed 18 Mar 2013
18. Roulet CA, Deschamps L, Pibiri MC et al (2000) Diagnosis of Air Handling Units, Institut de Technique du Batiment Laboratoire D'Energie Solaire et de Physique du Batiment. Ecole Polytechnique Federale de Lausanne
19. ASTM E 2029-99 (2004) Standard test method for volumetric and mass flow rate measurement in a duct using tracer gas dilution. ASTM International, PA, USA
20. Silva AR, Afonso CF (1990) Tracer gas dispersion in ducts—study of a new compact device using arrays of sonic micro jets. Energ Build 36:1131–1138
21. OSHA (1990) OSHA safety and health standards (29 CFR 1910). Occupational Safety and Health Administration, USA